Convection over an Inclined Wavy Surface in a Nanofluid Saturated Porous Medium

A Thesis Submitted to
NATIONAL INSTITUTE OF TECHNOLOGY WARANGAL, (T.S.)
for the award of the degree of
DOCTOR OF PHILOSOPHY
in
MATHEMATICS

by
P. VIJAY KUMAR
(Roll No. 701317)

under the supervision of
Dr. D. SRINIVASACHARYA

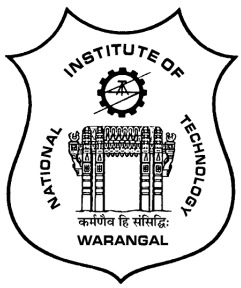

Department of Mathematics
National Institute of Technology Warangal
Telangana State, India

May 2016

Contents

[1] Case(a):Published in "**Meccanica, DOI 10.1007/s11012-015-0331-9**", Case(b):Published in "**Procedia Engineering, 127 (2015) 40–47**"

[2]Case(a):Published in "**International Journal of Numerical Methods for Heat and Fluid Flow, 25(8) (2015) 1774–1792**",
Case(b) Published in "**Journal of Nanofluids**" 5(1) (2016) 120–129

[3]Case(a):Published in "**Journal of Porous Media**",
Case(b) Communicated to "**Iranian Journal of Science and Technology**"

[4]Case(a):Published in "**International Journal of Chemical Engineering, 2015 (2015) Article ID: 927508**",

Case(b) Communicated to "**Propulsion and Power research.**"

[5]Accepted for publication in "**Computational thermal Sciences: An International Journal**"

[6]Communicated to "**International Journal of Non-linear Sciences**"

[7]Published in "**International Journal of Mining, Metallurgy and Mechanical Engineering**"

[8]Communicated to "**Open Engineering Journal**"

DECLARATION

This is to certify that the work presented in the thesis entitled **"Convection over an Inclined Wavy Surface in a Nanofluid Saturated Porous Medium"**, is a bonafide work done by me under the supervision of **Dr. D. SRINIVASACHARYA** and has not been submitted elsewhere for the award of any degree.

I declare that this written submission represents my ideas in my own words and where others' ideas or words have been included, I have adequately cited and referenced the original sources. I also declare that I have adhered to all principles of academic honesty and integrity and have not misrepresented or fabricated or falsified any idea / data / fact /source in my submission. I understand that any violation of the above will be a cause for disciplinary action by the Institute and can also evoke penal action from the sources which have thus not been properly cited or from whom proper permission has not been taken when needed.

P. Vijay Kumar

Roll No. 701317

Date:_____

C E R T I F I C A T E

This is to certify that the thesis entitled " **Convection over an Inclined Wavy Surface in a Nanofluid Saturated Porous Medium** " submitted to National Institute of Technology Warangal, for the award of the degree of ***Doctor of Philosophy***, is the bonafide research work done by **Mr. P. VIJAY KUMAR** under my supervision. The contents of this thesis have not been submitted elsewhere for the award of any degree.

Dr. D. Srinivasacharya
Associate Professor
Department of Mathematics
National Institute of Technology,
Warangal, T.S., INDIA

.

Dedicated to

My Parents

&
Sri Venkateshwara Swamy

ACKNOWLEDGEMENTS

It is a rare privilege and boon that I could associate myself for pursuing my research work with Dr. D. Srinivasacharya, Associate Professor of Mathematics, National Institute of Technology Warangal, India. I sincerely record my gratitude for his invaluable guidance and constant encouragement throughout the preparation of this thesis and his involvement and meticulous supervision while my work was in progress. With his inimitable qualities as a good teacher, he chiseled my path towards perfection. Ever since I met him, he has been a perpetual source of motivation, inspiration, encouragement and enlightenment. He is responsible for making the period of my research work as an educative and enjoyable learning experience. The thesis would not have seen the light of the day without his unrelenting support and cooperation. I deem it a privilege to have worked under his amiable guidance. My vocabulary is inadequate to express my gratitude.

I am greatly indebted to the dynamic personality, Prof. T. K. V. Iyengar (Retired Professor, NITW) for his affectionate support, encouragement and for sparing his valuable time in bringing a proper form for presentation of the results in the thesis. It is not an exaggeration to state that without his assistance and suggestions, this thesis would not have taken this form.

I am grateful to Prof. Debashis Dutta, Head, Department of Mathematics, Prof. K. N. S. Kasi Viswanadham and Prof. J. V. Ramana Murthy, Former Heads and members of Doctoral Scrutiny Committee, Department of Mathematics, for providing necessary help and support throughout the period of my research work. Also, they have given me the privilege to teach Mathematics for B.Tech course during the time of my stay at NIT, as a Research Scholar in the department.

I take this opportunity to thank Prof. Deva Pratap, member of the Doctoral Scrutiny Committee, Department of Civil Engineering for his valuable suggestions, moral support and

encouragement while my work was in progress.

I place on record my gratitude to all the faculty members of the Department of Mathematics, for their constant encouragement.

I owe my special thanks to Dr. Ch. RamReddy, Dr. K. Kaladhar, Dr. M. Krishna Prasad, Dr. M. Upendar, Dr. O. Surender (My illustrious seniors) for their support. I thank G. Madhava Rao, Ms. K. Hima Bindu, G. Venkata Suman, Ch. Venkata Rao, M. Varun Kumar, G. Nithish Kumar and my friends, who helped me during my Ph.D and all other Research Colleagues in the Department for being cooperative and also for making my stay in the NIT campus fruitful and enjoyable every moment.

I have been blessed with incessant moral support and boundless inspiration from all my family members. I thank my parents, Sri. P. Ravinder and Smt. Yashodha, brother and sister-in-law, Sri. P. Ajay Kumar and Smt. Harika, brothers B. Ranadheer, P. Rajesh, P. Suresh, P. Rakesh, sister, Ms. P. Nikitha and all other family members. Their love and affection has been motivating force behind what I am today.

. P. Vijay Kumar

A B S T R A C T

Convective heat transfer from irregular surfaces is a topic of fundamental importance due to its various enhancing heat transfer characteristics. The presence of roughness elements disturbs the flow past a flat surface and alters the heat transfer rate. Moreover, heat and mass transport characteristics about natural/mixed convection of a nanofluid saturated porous medium is very important in view of its practical applications in engineering. Nanofluids are prepared by the uniform dispersion and suspension of nanometer sized metallic particles into conventional heat transfer fluids such as water, oil, or ethylene glycol. The aim of this thesis is to study the free and mixed convection heat and nanoparticle mass transfer in a nanofluid saturated Darcy/non-Darcy porous medium in the presence of thermal radiation and thermal stratification effects. The problems considered deal with inclined wavy surface geometry.

The thesis consists of TEN chapters. Chapter 1 provides an introduction to the concepts in nanofluid, porous medium, heat and nanoparticle mass transfer and a review of the pertinent literature. Chapters 2 and 3 deal with natural and mixed convection over a semi-infinite inclined wavy surface embedded in a nanofluid saturated porous medium. Chapters 4 and 5 are extensions of chapters 2 and 3 in which thermal radiation and non-Darcy effects are studied. Chapters 6 and 7 deals with convective heat and mass transfer along an inclined wavy surface embedded in a thermally stratified nanofluid saturated porous medium. Chapters 8 and 9 are extensions of chapters 6 and 7 in which thermal radiation and non-Darcy effects are studied. In all the chapters the governing equations are transformed into a set of non-linear partial differential equations using the pseudo-similarity transformations. A local similarity and non-similarity method is used to transform the obtained partial differntial equations to a set of ordinary differntial equations. The resulting equations are linearized using the Successive Linearization Method and then solved using Chebyshev spectral collocation method. The effects of wave amplitude, angle of inclination of the wavy surface, Brownian motion parameter, thermophoresis parameter, thermal radiation parameter, non-Darcy parameter and thermal stratification parameter on the velocity, temperature, and nanoparticle volume fraction along with heat and nanoparticle mass transfer coefficients are studied.

The last chapter (Chapter - 10) gives summary and overall conclusions and scope for future work.

NOMENCLATURE

A	Angle of inclination of the wavy surface.
a	Amplitude of the wavy surface.
B	Slope of ambient temperature.
D_B	Brownian motion diffusion coefficient.
D_T	Thermophoresis diffusion coefficient.
f	Dimensionless stream function.
F_c	Forchheimer number.
g	Gravitational acceleration.
Gr	Grashof number.
k	Thermal conductivity.
K	Permeability.
K_e	Absorption coefficient.
$\tilde{K}$	Material parameter.
$\mathscr{L}$	Linear operator.
l	Characteristic length of the wavy surface.
Le	Lewis number.
$\mathscr{N}$	Non-linear operator.
N_b	Brownian motion parameter.
N_r	Nanofluid buoyancy ratio.
N_t	Thermophoresis parameter.
Nu_ξ	Local Nusselt number.
NSh_ξ	Local Nanoparticle Sherwood number.
P	Pressure.
Pe	Peclet number.
q_w, q_{np}	Heat and Nanoparticle fluxes.
R	Radiation Parameter.
Ra	Rayleigh number.
s	Reduced nanoparticle volume fraction.
S_T	Thermal Stratification Parameter.
T	Temperature.
$T_\infty(x)$	Ambient stratified temperature.
T_w	Wall temperature.
$T_{\infty,0}, T_\infty$	Ambient temperature.
U_∞	Free stream velocity.
u, v	Velocity components in x and y directions.
x, y	Coordinates along and normal to the plate.
α	Thermal diffusivity.
β	volumetric thermal expansion coefficient.

$\delta(x)$	Wavy surface.
Δ	Mixed convection parameter.
γ	Ratio between the effective heat capacity of the nanoparticle material and heat capacity of the fluid.
η	Similarity variable.
θ	Dimensionless temperature.
μ	Dynamic viscosity.
ν	Kinematic viscosity.
ξ	Non-similarity variable.
ρ_f	Density of the base fluid.
ρ_p	Density of nanoparticles.
$(\rho_c)_f$	Heat capacity of the fluid.
$(\rho_c)_p$	Effective heat capacity of the nanoparticle material.
ψ	Stream function.
ϕ	Nanoparticle volume fraction.

Subscripts

w	Wall condition.
∞	Ambient condition.

Superscript

$\prime$	Differentiation with respect to η.

Chapter 1

Introduction

1.1 Introduction

Fluid transport phenomena in porous medium refers to the processes related to and accompanied with the transport of fluid momentum, heat and mass, through the given porous medium. These processes which are encountered in many different branches of science and technology, e.g., hydrology, geomechanics, civil, petroleum, chemical and mechanical engineering, etc. are commonly subject to theoretical treatments which are based upon the methods traditionally developed in classical fluid dynamics. Over recent decades, fluid flows in porous medium have been studied both experimentally and theoretically. Convective transport in porous media has been the subject of great importance in recent years due to its wide range of applications in mechanical, chemical, and civil engineering. These applications include migration of moisture in fibrous insulation, the spreading of chemical pollutants in saturated soil, the extraction of geothermal energy, food processing and storage, geophysical systems, underground disposal of nuclear or non-nuclear waste, electro-chemistry, thermal

insulation of buildings, metallurgy, the design of pebble bed nuclear reactors, cooling system of electronic devices, etc.

Flow and heat transfer over irregular surfaces are often encountered in many engineering applications to enhance heat transfer as in cooling system of micro-electronic devices, flat-plate solar collectors and flat-plate condensers in refrigerators, and geophysical applications (e.g., flows in the earths crust), underground cable systems, electric machinery, etc. In addition, roughened surfaces could be used in the cooling of electrical and nuclear components where the wall heat flux is known. Sometimes surfaces are intentionally roughened to enhance heat transfer. The presence of roughness elements disturbs the flow past a flat surface and alters the heat transfer rate.

Moreover, engineered suspensions of nanoparticles in liquids, known recently as nanofluids, have generated considerable interest for their potential to enhance the heat transfer rate in engineering systems, while reducing, or possibly eliminating, the issues of erosion, sedimentation and clogging that plagued earlier solid-liquid mixtures with larger particles. Nanofluids can be used in a wide variety of engineering applications ranging from use in the automotive industry to the medical arena to use in power plant cooling systems as well as computers. The convection due to heated/cooled objects of various shapes under different physical conditions in a nanofluid saturated porous medium yields one of the most important scenarios for heat and mass transfer theory and thus is of considerable theoretical and practical interest

1.2 Nanofluids

Conventional heat transfer fluids like water, ethylene glycol, and oil have relatively low thermal conductivities, when compared to the thermal conductivity of solids. Hence, an innovative way of improving the thermal conductivities of fluids is to suspend small solid particles, such as millimeter- or micrometer-sized particles, into the conventional fluids. In 1904, Maxwell added millimeter- or micrometer-sized solid particles, because solids conduct

heat much better than liquids do. However, they have not been of interest for practical applications due to problems such as sedimentation, erosion, fouling and increased pressure drop of the flow channel. These problems are highly undesirable for many practical cooling applications. The recent advance in materials technology has made it possible to produce nanometer-sized particles that can overcome these problems.

A nanofluid is a term initially used by Choi [26] and refers to a base fluid with suspended solid nanoparticles in it. The thermal conductivity of nanometer sized particles is typically in the order of magnitude higher than those of the base fluids. The addition of nanoparticles to the base fluid even at low volume concentrations, results in significant increase in thermal performance. The goal of nanofluids is to achieve the highest possible thermal properties at the smallest possible concentrations (preferably $< 1\%$ by volume) by uniform dispersion and stable suspension of nanoparticles (preferably < 10nm) in host fluids. During the past decade the study of nanofluids has attracted immense enthusiasm from researchers in view of its exceptional applications in electronics, communication, computing technologies, high-power X-rays, medicine, lasers, optical devices, scientific measurement, material processing and material synthesis. Nanofluids are promising fluids for heat transfer enhancement due to their anomalously high thermal conductivity. The detailed introduction and applications of nanofluids can be seen in Das *et al.* [29].

Numerous models and methods have been proposed by different authors to study the convective flows of nanofluids. The computational studies reported in this area include two main approaches: (1) a two-phase model, in which both liquid and solid heat transfer behaviors are solved in the flow fields [116, 64] and (2) a single-phase model, in which solid particles are considered to behave as fluids, because the nanoparticles are easily fluidized [51, 106, 2]. Several issues are involved while studying the heat transfer enhancement utilizing nanofluids. These issues are like gravity, Brownian motion, layering at the interface between solid and liquid, clustering of the nanoparticles, ballistic phono transport through the particles and the friction between the fluid and the solid particles. The phenomena of sedimentation, dispersion and Brownian diffusion may coexist in the main flow of a nanofluid. In the absence of any suitable theoretical studies and experimental data in the literature to investigate these

issues, the existing macroscopic two-phase model is not applicable for analyzing nanofluids. If the main interest is focused on the heat transfer process, the modified single-phase, accounting for some of the above factors, is more convenient than the two-phase model.

Two models namely, the Tiwari-Das model [106] and Buongiorno model [10] are more frequently used by several researchers to investigate the heat transfer enhancement by very fine particles suspended in a fluid.

Tiwari-Das model

Tiwari and Das developed a model to analyze the behaviour of nanofluids by taking the volumetric fraction of nanparticles into consideration. Using this nanofluid model, the basic governing equations for the continuity, momentum and energy in laminar incompressible boundary layer flow of a nanofluid can be written as

$$\frac{\partial u}{\partial x} + \frac{\partial v}{\partial y} = 0 \tag{1.1}$$

$$\frac{\partial u}{\partial t} + u\frac{\partial u}{\partial x} + v\frac{\partial u}{\partial y} = \frac{\mu_{nf}}{\rho_{nf}}\frac{\partial^2 u}{\partial y^2} - \frac{1}{\rho_{nf}}\frac{dp}{dx} + \frac{\phi\,\rho_s\,\beta_s(1-\phi)\rho_f\,\beta_f}{\rho_{nf}}g(T - T_\infty) \tag{1.2}$$

$$\frac{\partial T}{\partial t} + u\frac{\partial T}{\partial x} + v\frac{\partial T}{\partial y} = \alpha_{nf}\frac{\partial^2 T}{\partial y^2} \tag{1.3}$$

Here u and v are the velocity components along the x and y axes, respectively, T is the temperature of the nanofluid, β_f and β_s are the thermal expansion coefficients of the base fluid and nanoparticle respectively and g is the acceleration due to gravity. Further μ_{nf} is the viscosity of the nanofluid, α_{nf} is the thermal diffusivity of the nanofluid and ρ_{nf} is the density of the nanofluid, which are given by

$$\mu_{nf} = \frac{\mu_f}{(1-\phi)^{2.5}},\ \rho_{nf} = (1-\phi)\rho_f + \phi\rho_s,\ \rho C_{p_{nf}} = (1-\phi)\rho C_{p_f} + \phi\rho C_{p_s}$$
$$\alpha_{nf} = \frac{k_{nf}}{\rho C_{p_{nf}}},\ \frac{k_{nf}}{k_f} = \frac{(k_s + 2k_f) - 2\phi(k_f - k_s)}{(k_s + 2k_f) + \phi(k_f - k_s)} \tag{1.4}$$

where ϕ is the solid volume fraction of the nanofluid, ρ_f is the density of the base fluid, ρ_s is the density of the solid particle, μ_f is the viscosity of the base fluid, k_f and k_s are the thermal conductivity of the base fluid and nanoparticle, respectively, k_{nf} is the effective thermal conductivity of the nanofluid approximated by the Maxwell-Garnett model (see Oztop and Abu-Nada [82]).

Buongiorno model

Buongiorno [10] proposed an analytical model for convective transport in nanofluids which incorporates the effects of Brownian diffusion and thermophoresis. Contrary to the Tiwari-Das model [106] that focuses on volumetric fraction of nanoparticles, Buongiorno model [10] pays more attention to Brownian motion and thermophoresis effects. Furthermore, instead of focusing on the thermophysical properties of the nanofluid, Buongiorno model focuses on explaining the heat transfer enhancement observed in convective situations. This Buongiorno model has been used in many recent works such as those of, Nield and Kuznetsov [78, 77, 79], Kuznetsov and Nield [53, 54] and Khan and Aziz [50], among others.

Brownian motion

The arbitrary motion of nanoparticles within the base fluid is called Brownian motion, and this results from continuous collisions between the nanoparticles and the molecules of the base fluid.

Thermophoresis

Particles can diffuse under the influence of a temperature gradient. This phenomenon is called thermophoresis, and is the particle equivalent of the renowned Soret effect for gaseous or liquid mixtures.

The basic governing equations of continuity, momentum, energy and nanoparticle concentration for this model are given by

$$\frac{\partial u}{\partial x} + \frac{\partial v}{\partial y} = 0 \tag{1.5}$$

$$\frac{\partial u}{\partial t} + u\frac{\partial u}{\partial x} + v\frac{\partial u}{\partial y} = \nu\frac{\partial^2 u}{\partial y^2} \tag{1.6}$$

$$\frac{\partial T}{\partial t} + u\frac{\partial T}{\partial x} + v\frac{\partial T}{\partial y} = \alpha\left(\frac{\partial^2 T}{\partial x^2} + \frac{\partial^2 T}{\partial y^2}\right) + \gamma\left[D_B\left(\frac{\partial \phi}{\partial x}\frac{\partial T}{\partial x} + \frac{\partial \phi}{\partial y}\frac{\partial T}{\partial y}\right) + \frac{D_T}{T_\infty}\left(\left(\frac{\partial T}{\partial x}\right)^2 + \left(\frac{\partial T}{\partial y}\right)^2\right)\right] \tag{1.7}$$

$$\frac{\partial \phi}{\partial t}u + \frac{\partial \phi}{\partial x} + v\frac{\partial \phi}{\partial y} = D_B\left(\frac{\partial^2 \phi}{\partial x^2} + \frac{\partial^2 \phi}{\partial y^2}\right) + \frac{D_T}{T_\infty}\left(\frac{\partial^2 T}{\partial x^2} + \frac{\partial^2 T}{\partial y^2}\right) \tag{1.8}$$

where x and y are the Cartesian coordinates measured along and normal to the surface, u and v are the velocity component along the x and y axes, T is the temperature of the nanofluid, ϕ is the nanoparticle volume fraction, ν is the kinematic viscosity of the nanofluid, α is the thermal diffusivity of the nanofluid, D_B is the Brownian diffusion coefficient, D_T is the thermophoretic diffusion coefficient, $\gamma = (\rho c)_p/(\rho c)_f$, with $(\rho c)_f$ and $(\rho c)_p$ being the heat capacity of the nanofluid and the effective heat capacity of the nanoparticle material, respectively.

1.3 Porous Medium

A porous medium may be defined as a solid matrix containing holes either connected or non-connected, dispersed within the medium in regular or random manner provided such holes occur frequently in the medium. If these pores are saturated with a fluid, then the solid matrix with the fluid is called a fluid saturated porous medium. The flow of the fluid in a saturated porous material is possible only when some of the pores are interconnected.

To study the motion of fluids through porous media, one must have sufficient understanding of the governing equations for the fluid flow through the porous media. Owing to the intricate structure of the porous medium, several models were proposed in order to explain

mathematical and physical aspects of porous media. Among these the Darcy model, and a series of its modifications, attained much acceptance. Boundary-layer assumptions were successfully applied to these models and much work over the last few decades has been done on them for a wide variety of body geometries.

Darcy Model

The governing equation for fluid motion in a vertical porous column was first given by Darcy [28] in 1856. It represents a balance of viscous force, gravitational force and pressure gradient. In mathematical form it is given as

$$V = -\frac{K}{\mu}(\nabla P - \rho\, g) \tag{1.9}$$

where V is the space averaged velocity (or Darcian velocity), K is the (intrinsic) permeability of the medium, μ is the coefficient of viscosity, P is the pressure, ρ is the density of the fluid and g is the body force per unit volume. For one-dimensional flows and for low porosity system, the above law appears to provide good agreement with experimental results. As this model does not take inertial effects into consideration, it is valid for seepage flows only i.e., for flows with low Reynolds number ($O(Re) < 1$).

Darcy-Forchheimer Model

Forchheimer, in 1901, conducted experiments and proposed that the inertial effects can be accounted for through the addition of a velocity squared term in the momentum equation. The modification to the Darcy's equation is

$$\left[1 + \frac{\rho\, c\, \sqrt{K}}{\mu}|V|\right] V = -\frac{K}{\mu}\left[\nabla P - \rho g\right], \tag{1.10}$$

where c is the dimensionless form drag coefficient and it varies with the nature of the porous medium. The coefficients of Darcy and Forchheimer terms contain both the fluid properties and the micro-structure of the porous medium. The validity of this model has been confirmed

by a number of experimental works.

Darcy-Brinkman Model

Under the assumption that the flow through an isotropic porous medium with high permeability must reduce to the viscous flow in limit, Brinkman has corrected Darcy's equation with addition of Laplace term. Brinkman felt the need to account for the viscous force exerted by a flowing fluid on a dense swarm of spherical particles embedded in a porous mass and added the term $\mu' \nabla^2 V$ to balance the pressure gradient. Here μ' is the effective viscosity given by $\mu' = \mu(1 - 2.5(1 - \epsilon))$. The validity of the Brinkman model is restricted to the high porosity medium (as confirmed by the experiments). Its governing equation is given by

$$-\left[\nabla P - \rho g\right] = \frac{\mu}{K} V - \mu' \nabla^2 V. \tag{1.11}$$

Other Models

Another model which considers both Forchheimer and Brinkman terms, is governed by the equation

$$-\nabla P = \frac{\mu}{K} V + \frac{C\,\rho\,|V|}{\sqrt{K}} V - \frac{\mu'}{\epsilon} \nabla^2 V. \tag{1.12}$$

Yet another model in which the convective term has been considered along with these two effects has also been used by researchers to study the flow of fluid in the porous medium, through the governing equation

$$\rho \frac{DV}{Dt} = -\nabla P - \frac{\mu}{K} V - \frac{C\,\rho\,|V|}{\sqrt{K}} V + \frac{\mu'}{\epsilon} \nabla^2 V. \tag{1.13}$$

Several other models are found in the literature related to porous media, the validity and limitations of these models are well discussed in Nield and Bejan [76].

1.4 Aim and Scope of the Thesis

The aim of the present thesis is to analyze some boundary layer flows arising from the convection along a semi-infinite inclined wavy surface geometry embedded in a nanofluid saturated porous medium. We study the influence of amplitude and angle of inclination of the wavy surface, thermal radiation effects, thermal stratification effects, non-Darcy parameter effects, mixed convection parameter effects, thermophoresis and Brownian motion effects on the flow characterestics, heat transfer rate and nanoparticle mass transfer rate. Buongiorno [10] model is the basis of the present study. The governing non-linear equations are linearized using Successive Linearization Method and then the resulting equations are solved using Chebyshev spectral collocation method.

Successive Linearization Method

The Successive Linearisation Method (SLM) is proposed and developed by Makukula *et al.* [60] and Motsa and Sibanda [69]. This technique has been successfully used to solve different boundary value problems in heat and mass transfer studies (Makukula *et al.* [61], Shateyi and Motsa [97] and Awad *et al.* [5]) and showed by comparison with numerical techniques that the SLM is accurate, gives rapid convergence.

To describe the basic idea behind the Successive Linearization Method (SLM), consider a non-linear boundary value problem of order n in the form

$$\mathscr{L}[u(x), u'(x), u''(x), \cdots, u^{(n)}(x)] + \mathscr{N}[u(x), u'(x), u''(x), \cdots, u^{(n)}(x)] = g(x), \quad x \in [a, b] \tag{1.14}$$

subject to the boundary conditions

$$u(a) = a_0, \qquad u(b) = b_0 \tag{1.15}$$

where $\mathscr{L}$ and $\mathscr{N}$ are linear and non-linear operators, $u(x)$ is an unknown function to be

determined and $g(x)$ is a known function.

A function $U_1(x)$ is defined as the vertical difference between the function $u(x)$ and the initial guess $u_0(x)$ *i.e.*

$$U_1(x) = u(x) - u_0(x) \quad \text{or} \quad u(x) = u_0(x) + U_1(x) \tag{1.16}$$

where $U_1(x)$ is an unknown function and $u_0(x)$ is the initial guess which is chosen to satisfy boundary conditions (1.16).

Substituting Eqn. (1.17) into Eqn. (1.15), yields

$$\begin{aligned}\mathscr{L}[U_1, U_1{}', U_1{}'', \cdots, U_1{}^{(n)}] + \mathscr{N}[U_1 + u_0, U_1{}' + u_0{}', U_1{}'' + u_0{}'', \cdots, U_1{}^{(n)} + u_0{}^{(n)}] \\ = -\mathscr{L}[u_0, u_0{}', u_0{}'', \cdots, u_0{}^{(n)}] + g(x)\end{aligned} \tag{1.17}$$

In this equation RHS is known function as $u_0(x)$ is known. Further, the above equation is non-linear in $U_1(x)$, so it may not be possible to find an exact solution. Therefore, an approximate solution is required, which is obtained by solving the linear part of the equation assuming that $U_1(x)$ and its derivatives are very small. This assumption enables to use Taylors series method to linearize the equation. Let the solution of the full Eqn. (1.18) be $U_1(x)$ and the solution of the linearized version of the Eqn. (1.18) be $u_1(x)$. Expanding Eqn. (1.18) in Taylors series and neglecting the higher order terms, we get

$$\mathscr{L}[u_1, u_1{}', u_1{}'', \cdots, u_1{}^{(n)}] + a_{0,0}u_1 + a_{1,0}u_1{}' + a_{2,0}u_1{}'' + \cdots + a_{n,0}u_1{}^{(n)} = \mathbf{R}_1(x), \tag{1.18}$$

where

$$
\begin{aligned}
a_{0,0} &= \frac{\partial N}{\partial u_1(x)}\left(u_0(x), {u_0}'(x), {u_0}''(x), \cdots, {u_0}^{(n)}(x)\right),\\
a_{1,0} &= \frac{\partial N}{\partial {u_1}'(x)}\left(u_0(x), {u_0}'(x), {u_0}''(x), \cdots, {u_0}^{(n)}(x)\right),\\
a_{2,0} &= \frac{\partial N}{\partial {u_1}''(x)}\left(u_0(x), {u_0}'(x), {u_0}''(x), \cdots, {u_0}^{(n)}(x)\right),\\
&\vdots\\
a_{n,0} &= \frac{\partial N}{\partial {u_1}^{(n)}(x)}\left(u_0(x), {u_0}'(x), {u_0}''(x), \cdots, {u_0}^{(n)}(x)\right)\\
\mathbf{R}_1(x) &= g(x) - \mathscr{L}[u_0(x), {u_0}'(x), {u_0}''(x), \cdots, {u_0}^{(n)}(x)]\\
&\quad -\mathscr{N}[u_0(x), {u_0}'(x), {u_0}''(x), \cdots, {u_0}^{(n)}(x)]
\end{aligned}
$$

Since the left hand side of Eqn. (1.19) is linear and the right hand side is known, the equation can be solved for $u_1(x)$ subject to the boundary conditions

$$u(a) = 0, \qquad u(b) = 0 \tag{1.19}$$

Assuming that the solution of the linear equation (1.19) is close to the solution of the nonlinear equation (1.18) that is $U_1(x) \approx u_1(x)$, then the first approximation of the solution (first order) is

$$u(x) \approx u_0(x) + u_1(x) \tag{1.20}$$

To improve on this solution, a function $U_2(x)$ is defined that when added to $u_1(x)$ gives $U_1(x)$

$$U_1(x) = U_2(x) + u_1(x) \tag{1.21}$$

Substitute (1.22) into equation (1.18) to give

$$
\begin{aligned}
&\mathscr{L}[U_2, {U_2}', {U_2}'', \cdots, {U_2}^{(n)}] + \mathscr{N}[U_2 + u_0 + u_1, {U_2}' + {u_0}' + {u_1}', {U_2}'' + {u_0}'' + {u_1}'', \cdots,\\
&\quad {U_2}^{(n)} + {u_0}^{(n)} + {u_1}^{(n)}] = -\mathscr{L}[u_0 + u_1, {u_0}' + {u_1}', {u_0}'' + {u_1}'', \cdots {u_0}^{(n)} + {u_0}^{(n)}] + g(x)
\end{aligned} \tag{1.22}
$$

Since $u_0(x)$ and $u_1(x)$ are known and Eqn. (1.23) is non-linear in $U_2(x)$, it may not be

possible to find an exact solution. Therefore, the equation is linearized using the Taylors series expansion and the resulting linear equation is solved. Let the solution of the linearized equation is denoted by $u_2(x)$, such that $U_2(x) \approx u_2(x)$. Taking $U_2(x) = u_2(x)$ and expanding Eqn. (1.23) for small $u_2(x)$ and its derivatives gives

$$\mathscr{L}[u_2, {u_2}', {u_2}'', ..., {u_2}^{(n)}] + a_{0,1}u_2 + a_{1,1}{u_2}' + a_{2,1}{u_2}'' + ... + a_{n,1}{u_2}^{(n)} = \mathbf{R}_2(x), \tag{1.23}$$

where

$$\begin{aligned}
a_{0,1} &= \frac{\partial N}{\partial u_2(x)}\left(u_0 + u_1, {u_0}' + {u_1}', {u_0}'' + {u_0}'', \cdots, {u_0}^{(n)} + {u_1}^{(n)}\right) \\
a_{1,1} &= \frac{\partial N}{\partial {u_2}'}\left(u_0 + u_1, {u_0}' + {u_1}', {u_0}'' + {u_0}'', \cdots, {u_0}^{(n)} + {u_1}^{(n)}\right) \\
a_{2,1} &= \frac{\partial N}{\partial {u_2}''}\left(u_0 + u_1, {u_0}' + {u_1}', {u_0}'' + {u_0}'', \cdots, {u_0}^{(n)} + {u_1}^{(n)}\right) \\
&\vdots \\
a_{n,1} &= \frac{\partial N}{\partial {u_2}^{(n)}}\left(u_0 + u_1, {u_0}' + {u_1}', {u_0}'' + {u_0}'', \cdots, {u_0}^{(n)} + {u_1}^{(n)}\right) \\
\mathbf{R}_2(x) &= g(x) - \mathscr{L}[u_0(x) + u_1(x), {u_0}'(x) + {u_1}'(x), \cdots, {u_0}^{(n)}(x) + {u_1}^{(n)}(x)] \\
&\quad -\mathscr{N}[u_0(x) + u_1(x), {u_0}'(x) + {u_1}'(x), \cdots, {u_0}^{(n)}(x) + {u_1}^{(n)}(x)]
\end{aligned}$$

After solving the equation (1.24), the second order approximation of $u(x)$ is given by

$$u(x) \approx u_0(x) + u_1(x) + u_2(x) \tag{1.24}$$

Next, $U_3(x)$ is defined such that

$$U_2(x) = U_3(x) + u_2(x) \tag{1.25}$$

Eqn. (1.26) is substituted in the non-linear equation (1.23) and the linearization process is repeated. In general, we have

$$U_i(x) = U_{i+1}(x) + u_i(x) \tag{1.26}$$

Thus, $u(x)$ is given by

$$\begin{aligned} u(x) &= U_1(x) + u_0(x) \\ &= U_2(x) + u_0(x) + u_1(x) \\ &= U_3(x) + u_0(x) + u_1(x) + u_2(x) \\ &\vdots \\ &= U_{i+1}(x) + u_0(x) + u_1(x) + u_2(x) + \cdots + u_i(x) \\ &= U_{i+1}(x) + \sum_{m=0}^{i} u_m(x) \end{aligned}$$

It is noted that when i becomes large, U_{i+1} becomes smaller. Hence, for large i, i^{th} order solution of $u(x)$ is approximated by

$$u(x) = \sum_{m=0}^{i} u_m(x) = u_i(x) + \sum_{m=0}^{i-1} u_m(x) \tag{1.27}$$

The solution $u_i(x)$ can be determined by successively linearizing original equation (1.16) starting from the initial guess $u_0(x)$ and solving the resulting linear equations for $u_i(x)$ given that the previous guess $u_{i-1}(x)$ is known. In general, the form of the linearized equation for $u_i(x)$ is given by

$$\mathscr{L}[u_i, {u_i}', {u_i}'', \cdots, {u_i}^{(n)}] + a_{0,i-1}u_i + a_{1,i-1}{u_i}' + a_{2,i-1}{u_i}'' + \cdots + a_{n,i-1}{u_i}^{(n)} = \mathbf{R}_{i-1}(x) \tag{1.28}$$

subject to the boundary conditions

$$u_i(a) = 0, \quad u_i(b) = 0 \tag{1.29}$$

where

$$
\begin{aligned}
a_{0,i-1} &= \frac{\partial N}{\partial u_i(x)}\left(\sum_{m=0}^{i-1} u_m, \sum_{m=0}^{i-1} u_m{}', \sum_{m=0}^{i-1} u_m{}'', \cdots, \sum_{m=0}^{i-1} u_m(n)\right)\\
a_{1,i-1} &= \frac{\partial N}{\partial u_i{}'(x)}\left(\sum_{m=0}^{i-1} u_m, \sum_{m=0}^{i-1} u_m{}', \sum_{m=0}^{i-1} u_m{}'', \cdots, \sum_{m=0}^{i-1} u_m(n)\right)\\
a_{2,i-1} &= \frac{\partial N}{\partial u_i{}''(x)}\left(\sum_{m=0}^{i-1} u_m, \sum_{m=0}^{i-1} u_m{}', \sum_{m=0}^{i-1} u_m{}'', \cdots, \sum_{m=0}^{i-1} u_m(n)\right)\\
&\vdots\\
a_{n,i-1} &= \frac{\partial N}{\partial u_i{}^{(n)}(x)}\left(\sum_{m=0}^{i-1} u_m, \sum_{m=0}^{i-1} u_m{}', \sum_{m=0}^{i-1} u_m{}'', \cdots, \sum_{m=0}^{i-1} u_m(n)\right)\\
\mathbf{R}_{i-1}(x) &= g(x) - \mathscr{L}[\sum_{m=0}^{i-1} u_m, \sum_{m=0}^{i-1} u_m{}', \sum_{m=0}^{i-1} u_m{}'', \cdots, \sum_{m=0}^{i-1} u_m(n)]\\
&\quad -\mathscr{N}[\sum_{m=0}^{i-1} u_m, \sum_{m=0}^{i-1} u_m{}', \sum_{m=0}^{i-1} u_m{}'', \cdots, \sum_{m=0}^{i-1} u_m(n)]
\end{aligned}
$$

The ordinary differential equation (1.29) is linear and can easily be solved using any analytical or numerical method.

Chebyshev Spectral Collocation Method

The Chebyshev spectral collocation method ([11, 31, 107]) is based on the Chebyshev polynomials defined on the interval [-1, 1]. To solve the problems using this method, first transform the domain $[a, b]$ to the domain $[-1, 1]$ by using the transformation

$$(b-a)\chi = 2x - (a+b), \;\; -1 \leq \chi \leq 1 \tag{1.30}$$

We discretize the domain [-1, 1] using the Gauss-Lobatto collocation points given by

$$\chi_j = \cos\frac{\pi j}{N}, \quad j = 0, 1, 2, ..., N \tag{1.31}$$

where N is the number of collocation points used. The function u_i is approximated at the collocation points as follows

$$u_i(\chi) = \sum_{k=0}^{N} u_i(\chi_k) T_k(\chi_j) \tag{1.32}$$

where T_k is the k^{th} Chebyshev polynomial defined by $T_k(\chi) = \cos[k\cos^{-1}\chi]$

The derivatives of the variables at the collocation points are represented as

$$\frac{d^r u_i}{dx^r} = \sum_{k=0}^{N} [\frac{2}{b-a}\mathbf{D}_{kj}]^r u_i(\chi_k), \tag{1.33}$$

where r is the order of differentiation and $\mathbf{D}$ being the Chebyshev spectral differentiation matrix whose entries are defined as ([11, 31, 107])

$$\left.\begin{aligned} &\mathbf{D}_{00} = \tfrac{2N^2+1}{6} \\ &\mathbf{D}_{jk} = \tfrac{c_j}{c_k}\tfrac{(-1)^{j+k}}{\chi_j-\chi_k}, \;\; j \neq k; \;\; j,k = 0,1,2\cdots,N, \\ &\mathbf{D}_{kk} = -\tfrac{\chi_k}{2(1-\chi_k{}^2)}, \;\; k = 1,2\cdots,N-1, \\ &\mathbf{D}_{NN} = -\tfrac{2N^2+1}{6} \end{aligned}\right\} \tag{1.34}$$

Substituting Eqns. (1.32)-(1.35) into the given equation leads to the following system of matrix equation

$$\mathbf{A}_{i-1}\mathbf{X}_i = \mathbf{R}_{i-1}, \tag{1.35}$$

in which A_{i-1} is a (N +1)×(N +1) square matrix while X_i and R_{i-1} are (N +1)× 1. After incorporating the boundary conditions, the solution of the given equation is obtained as

$$\mathbf{X}_i = \mathbf{A}_{i-1}^{-1}\mathbf{R}_{i-1} \tag{1.36}$$

1.5 Literature Review

During the past decade, the study of nanofluids has gained much interest due to its varied applications. Nanofluids are prepared by dispersing solid nanoparticles in conventional fluids such as water, oil, or ethylene glycol. Choi *et al.* [27] showed that the addition of a small amount (less than 1% by volume) of nanoparticles to conventional heat transfer liquids enhanced the thermal conductivity of the fluid. The detailed introduction and applications of nanofluids can be found in Das *et al.* [29]. Buongiorno [10] has investigated the factors which contribute to abnormal thermal conductivity increase relative to base fluids and viscosity. He developed an analytical model for convective transport in nanofluids, which takes Brownian diffusion and thermophoresis effects into account. The literature on nanofluids has been reviewed by Daungthongsuk and Wongwises [30], Trisaksri and Wongwises [108], Wang and Mujumdar [113, 114, 115], Eastman *et al.* [32], and Kakac and Pramuanjaroenkij [47], Gianluca *et al.* [35] among several others. These reviews examine in detail the work done on convective transport in nanofluids.

Natural convection in a fluid-saturated porous medium is of fundamental importance in many industrial and natural problems. Few examples of the heat transfer by natural convection can be found in geophysics and energy related engineering problems such as natural circulation in geothermal reservoirs, acquifers, porous insulations, solar power collectors, spreading of pollutants etc. Natural convection occurs due to the spatial variations in density, which is caused by the non-uniform distribution of temperature or/and concentration of a dissolved substance. The first attempt has been made by Nield [75] to analyze the stability of convective flow in horizontal layers with imposed vertical temperature and concentration gradients. A detailed review of convective heat and mass transfer in Darcy and non-Darcy porous medium can be found in Nield and Bejan [76], Ingham and Pop [44, 43], Bejan [8], Vafai [110] and Vafai and Hadim [111]. Bakier *et al.* [6] and Mahdy *et al.* [58] reported the non-similar solution for natural convection boundary layer flow past a body submerged in a fluid saturated porous medium.

Several authors investigated the natural convective heat and mass transfer over various

geometries embedded in a nanofluid saturated porous medium. The Cheng-Minkowycz problem of free convection over a vertical plate in a porous medium saturated by a nanofluid, has been investigated analytically by Nield and Kuznetsov [78]. Ahmad and Pop [4] studied the steady mixed convection boundary layer flow past a vertical flat plate embedded in a porous medium filled with nanofluids using different types of nanoparticles and the model they used for the nanofluid incorporates only the nanoparticle volume fraction parameter. A similarity solution is presented for the problem of double-diffusive free convective boundary layer flow in a porous medium saturated with a nanofluid by Nield and Kuznetsov [79]. Gorla and Chamkha [36] analyzed the natural convection flow over a horizontal plate embedded in a porous medium saturated with nanofluid. Cheng [22] studied the natural convection boundary layer flow over a truncated cone embedded in a porous medium saturated by a nanofluid with constant wall temperature and constant wall nanoparticle volume fraction. Murthy *et al.* [72] presented the influence of the prominent Soret effect on double-diffusive free convective heat and mass transfer in the boundary layer region of a semi-infinite inclined flat plate in a nanofluid saturated non-Darcy porous medium. Salari *et al.* [96] examined the heat transfer in boundary layer flow of a nanofluid past a continuous flat stretching sheet for constant surface temperature and nanoparticle volume fraction, and also for linear variation of surface temperature and nanoparticle volume fraction. Srinivasacharya and Surender [103] obtained the non-similar solution for natural convective boundary layer flow of a nanofluid past a vertical plate embedded in a doubly stratified porous medium. Chamkha *et al.* [12] studied the effect of uniform heat and nanoparticle fluxes on non-Darcy natural convection of non-Newtonian fluid along a vertical cone embedded in a porous medium filled with nanofluid.

Considerable investigations of mixed convective heat and mass transfer of a nanofluid saturated porous medium have been tackled by various authors. Mixed convection heat transfer flow in porous media has been widely studied in recent years due to its wide range of engineering applications such as chemical processing equipment, electronic device cooling, lubrication systems, solar energy collectors, food processing, heat exchangers, geothermal and hydrocarbon recovery and so on. Further, the problem of mixed convection boundary

layer flow in nanofluids has received much attention in the past. Cheng and Minkowycz [24] and Cheng [23] were the first to investigate the steady free and mixed convection flow about a vertical impermeable surface in a fluid-saturated porous medium. Later, Merkin [63] studied the mixed convection boundary layer flow on a vertical surface in a saturated porous medium. Lai [55] considered the coupled heat and mass transfer by mixed convection from a vertical plate in a saturated porous medium. Chin *et al.* [25] studied the effect of variable viscosity on mixed convection boundary layer flow over a vertical impermeable surface embedded in porous medium. Ahmad and Pop [4] obtained numerical results for the mixed convection boundary layer flow past a vertical flat plate embedded in a porous medium filled with nanofluid. Mansour *et al.* [62] carried out an experimental study of mixed convection with water-$Al_2\,O_3$ nanofluid in an inclined tube with uniform wall heat flux. Chamkha *et al.* [13] studied the effect of radiation on mixed convection over a wedge embedded in a porous medium saturated with nanofluid. Guerroudj and Kahalerras [38] adopted the Brinkman-Forchheimer extended Darcy model with the Boussinesq approximation for the mixed convection in an inclined channel with heated porous blocks. Gorla and Hossain [37] studied mixed convection boundary layer flow past a vertical cylinder in a porous medium saturated with a nanofluid. Rosca and Pop [92] studied the mixed convection stagnation point flow of a viscous fluid over a vertical flat plate subject to a heat flux condition. Rashad *et al.* [88] investigated the problem of mixed convection from a vertical surface embedded in a porous medium saturated with non-Newtonian nanofluid. Chamkha *et al.* [15] presented a boundary layer analysis for the mixed convection past a vertical wedge in a porous medium saturated with a power law type non-Newtonian nanofluid. Rosca *et al.* [91] numerically solved the problem of steady mixed convection boundary layer flow past a vertical flat plate embedded in a nanofluid saturated porous medium.

Several authors investigated the effect of thermal radiation on convective flow, heat and mass transfer from bodies of different geometries under various physical conditions due to its wide range of applications involving high temperatures such as nuclear power plant, gas turbines missiles, satellites, space vehicles and aircraft etc. Rudraiah and Sasikumar [95] reported the effects of non-Darcy and radiation on convection in porous media. Mohamma-

dien and El-Amin [65] discussed radiation effect on non-Darcy natural convection in a fluid saturated porous medium. El-Hakiem and El-Amin [33] investigated the radiation effect on non-Darcy natural convection with lateral mass transfer. Chen and Yang [17] studied the effects of thermal radiation on laminar forced and free convection along a wavy surface. Chamkha *et al.* [13] presented the non-similar solution of steady mixed convection of a nanofluid in the presence of thermal radiation. Hady *et al.* [40] reported that an increase in the thermal radiation parameter reduces the nanofluid temperature which leads to increase in the heat transfer rate. Rahman [1] numerically investigated the problem of thermal radiation and unsteady MHD flow of a nanofluid in stretching porous medium. Turkyilmazoglu and Pop [109] considered the problem of unsteady natural convection flow of some nanofluids past a vertical infinite flat plate with radiation effect. The effect of thermal radiation on boundary flow and heat transfer by non-Darcy natural convection from a vertical cylinder embedded in a porous medium saturated with nanofluids have been investigated by El-Kabeir *et al.* [34]. Agha *et al.* [3] studied the influence of thermal radiation on natural convection boundary layer flow for heat and mass transfer in a porous medium saturated by a nanofluid past a semi-infinite vertical plate, via a model in which Brownian motion and thermophoresis are taken into account. Chand and Rana [16] investigated the effect of radiation on thermal instability in a layer of nanofluid in porous medium by using Galerkin residual method and concluded that the radiation parameter has a stabilizing effect on stationary convection.

Stratification of fluid occurs due to temperature variations, concentration differences, or the presence of different fluids. The analysis of free and mixed convective flow in a doubly stratified medium is fundamentally interesting and important problem due to its broad range of applications in engineering. These applications include heat rejection into the environment such as lakes, rivers, and seas; thermal energy storage systems such as solar ponds; and heat transfer from thermal sources such as the condensers of power plants. However, the effect of double stratification on free convection in porous media has received very little attention. Tewari and Singh [105] investigated the natural convection in a thermally stratified fluid saturated porous medium. Rosmila *et al.* [93] examined the MHD free convection flow of an incompressible viscous nanofluid past a semi-infinite vertical stretching sheet in

the presence of thermal stratification. The effects of thermophoresis and Brownian motion on MHD boundary layer flow of a nanofluid in the presence of thermal stratification have been studied by Kandaswamy *et al.* [48]. Ibrahim and Makinde [42] presented a boundary layer analysis for free convection flow in a doubly stratified nanofluid over a vertical plate with uniform surface and mass flux conditions. Mahmoud and Waheed [59] investigated the problem of steady two dimensional mixed convection flow of a micropolar fluid over stretching permeable vertical surface with radiation and thermal stratification effects. Arifin *et al.* [117] performed a numerical investigation of the steady mixed convection boundary layer flow over a vertical surface embedded in a thermally stratified porous medium saturated with a nanofluid. Shezad *et al.* [98] studied the mixed convection flow of a thixotropic fluid with thermal stratification and thermal radiation effects. Srinivasacharya and Ramreddy [101] analysed the effect of double stratification on natural convection along a vertical plate embedded in a micropolar fluid in both cases of buoyancy-assisting and buoyancy-opposing flows. The problem of natural convection from a vertical plate in a thermally stratified porous medium with non-Newtonian liquid has been studied by Narayana *et al.* [73]. Recently, Srinivasacharya and Surender [103] presented the non-similar solution for natural convection boundary layer flow over a vertical plate embedded in a porous medium saturated by a nanofluid in the presence of thermal and mass stratification. They have concluded that the velocity, temperature and concentration are significantly influenced by the thermal stratification parameter. Rashad *et al.* [87] performed a numerical study to investigate the non-Darcy natural convection boundary layer flow along a vertical cylinder embedded in a thermally stratified nanofluid saturated porous medium. Rashad *et al.* [86] studied mixed convection flow of a micropolar fluid on a vertical flat plate immersed in thermally and solutally stratified medium with chemical reaction.

The study of heat and mass transfer from the irregular wavy surfaces is of fundamental importance because of its enhancing heat transfer characteristics. Irregularities in surfaces occur in many practical situations. These irregularities are encountered in several heat transfer devices such as microelectronic devices, flat plate solar collectors and flat plate condensers in refrigerators. Rees and Pop [89] investigated the problem of natural convection

from a vertical wavy surface in a non-Darcy porous medium. Hsu *et al.* [41] considered the study of mixed convection of micro polar fluids along a vertical wavy surface. Jang and Yan [46] studied the mixed convection heat and mass transfer along a vertical wavy surface. Kumar and Shalini [52] conducted a numerical study on non-Darcy free convection along a vertical wavy surface in a thermally stratified porous medium. Wang and Chen [112] obtained numerical results for the problem of mixed convection boundary layer flow on inclined wavy plate including the magnetic field effect. Cheng [18] presented numerical results of non-Darcy natural convection heat and mass transfer from a vertical wavy surface in saturated porous media using the cubic spline collocation method. Molla and Hossain [67] used Keller box method to investigate the problem of radiation effect on mixed convection laminar flow along a vertical wavy surface. Cheng [20] analyzed the coupled heat and mass transfer by natural convection near a vertical wavy surface in a non-Newtonian fluid saturated porous medium with thermal and mass stratification. Narayana and Sibanda [56] studied natural convection and mass transfer along a vertical wavy surface in a Newtonian fluid saturated Darcy porous medium by considering cross diffusion in the medium. Maria Neagu [74] studied natural convective heat and mass transfer from a vertical wavy wall with a constant surface heat and mass fluxes under the influence of thermal and mass stratification. Cheng [21] studied Soret and Dufour effects on free convection boundary layers over an inclined wavy surface in a porous medium. Mahdy and Ahmed [57] discussed the laminar free convection over a vertical wavy surface embedded in a porous medium saturated with a nanofluid. Siddiqa *et al.* [99] studied the natural convection flow with surface radiation along a vertical wavy surface.

1.6 Outline of the Thesis

The present thesis aims at presenting numerical solutions for some problems in convective heat and nanoparticle mass transfer over an inclined wavy surface embedded in a porous medium saturated with a nanofluid. The study focuses on bringing out the effects of the amplitude and angle of inclination of the wavy surface, Brownian motion, thermophoresis,

non-Darcian nature, mixed convection, thermal radiation and stratification on the characteristics of the flow field such as velocity, temperature distribution and nanoparticle volume fraction. The problems considered deal with semi-infinite inclined wavy surface geometry for the two cases: when the plate is (i) maintained at uniform wall temperature and nanoparticle volume fraction (ii) subjected to uniform heat flux and nanoparticle mass flux.

This thesis consists of TEN chapters.

Chapter - 1 is introductory in nature and gives motivation to the investigations carried out in the thesis. The basic terminology is introduced and a survey of pertinent literature is presented to exhibit the importance of the problems considered. The basic equations governing the flow, heat and nanoparticle mass transfers of nanofluid are given.

In Chapter - 2, we study the numerical solution of the steady natural convection heat and nanoparticle mass transfer along an inclined wavy surface embedded in a porous medium saturated with nanofluid. The non-dimensional velocity, temperature and nanoparticle volume fraction profiles are displayed graphically for different values of amplitude of the wavy surface, angle of inclination of the wavy surface, Brownian motion and thermophoresis parameters. In addition, the non-dimensional heat and nanoparticle mass transfer coefficients versus non-similarity variable are presented graphically for different values of pertinent flow parameters.

Chapter - 3 deals with the problem of steady, laminar mixed convection heat and nanoparticle mass transfer along an inclined wavy surface embedded in a nanofluid saturated porous medium. The effects of amplitude of the wavy surface, angle of inclination of the wavy surface, Brownian motion and thermophoresis parameters on non-dimensional velocity, temperature and nanoparticle volume fraction profiles for both aiding and opposing flows are presented graphically. The non-dimensional heat and nanoparticle mass transfer coefficients against non-similarity variable for various values of pertinent flow parameters are also analyzed through graphs.

Chapter - 4 considers the effect of radiation on natural convective heat and nanoparticle mass transfer along an inclined wavy surface in a nanofluid saturated non-Darcy porous

medium. The obtained results are exhibited graphically to demonstrate the influence of radiation, non-Darcy, amplitude of the wavy surface, angle of inclination of the wavy surface, Brownian motion and thermophoresis parameters on the dimensionless velocity, wall temperature and nanoparticle volume fraction. Further, the effect of the physical parameters on non-dimensional heat and nanoparticle mass transfer coefficients versus non-similarity variable are discussed and displayed through graphs.

In Chapter - 5, an attempt has been made to study the steady, mixed convection heat and nanoparticle mass transfer along an inclined wavy surface in a nanofluid saturated non-Darcy porous medium with radiation effect. The effects of non-Darcy, radiation, amplitude of the wavy surface, angle of inclination of the wavy surface, Brownian motion and thermophoresis parameters on non-dimensional velocity, temperature and nanoparticle volume fraction for both aiding and opposing flows are examined. Also, heat and nanoparticle mass transfer coefficients against non-similarity variable are illustrated through graphs for various values of radiation, non-Darcy, amplitude, angle of inclination, Brownian motion and thermophoresis parameters.

In all the above chapters (2 - 5), two types (cases) of boundary conditions for the temperature and nanoparticle volume fraction on the inclined wavy surface are considered. In the first type of boundary condition, it is assumed that the wall temperature and nanoparticle volume fraction are kept uniform on the wavy plate. The second type of boundary condition involves the imposition of uniform constant heat and nanoparticle mass flux on the wavy plate. In both the cases, the usual conditions of no slip on velocity component are prescribed.

Chapter - 6 reports the effect of thermal stratification on steady, natural convective heat and nanoparticle mass transfer along an inclined wavy surface in a porous medium saturated with nanofluid. The obtained results are exhibited graphically to illustrate the effects of thermal stratification, Brownian motion, thermophoresis parameters, amplitude and angle of inclination of the wavy surface on the dimensionless velocity, temperature, nanoparticle volume fraction. Further, the influence of the physical parameters on non-dimensional heat and nanoparticle mass transfer coefficients against non-similarity variable are discussed graphically.

Chapter - 7 presents a steady, mixed convection heat and nanoparticle mass transfer along an inclined wavy surface in a nanofluid saturated porous medium under the influence of thermal stratification. The effects of amplitude and angle of inclination of the wavy surface, Brownian motion, thermophoresis and thermal stratification parameters on non-dimensional velocity, temperature and nanoparticle volume fraction for both aiding and opposing flows are depicted through graphs. Also, heat and nanoparticle mass transfer coefficients against non-similarity variable are analyzed through graphs for various values of thermal stratification parameter, Brownian motion parameter, thermophoresis parameter, amplitude and angle of inclination of the wavy surface.

Chapter - 8 deals with the effect of radiation and thermal stratification on steady, natural convective heat and nanoparticle mass transfer along an inclined wavy surface in a non-Darcy porous medium saturated with nanofluid. Numerical Solutions for non-dimensional velocity, temperature and nanoparticle volume fraction, heat and nanoparticle mass transfer are computed. The effects of non - Darcy, radiation, amplitude and angle of inclination of the wavy surface, Brownian motion, thermophoresis and thermal stratification parameters on the non-dimensional velocity, temperature and nanoparticle volume fraction, heat and nanoparticle mass transfer are presented graphically.

In Chapter - 9, the analysis of steady, mixed convective heat and nanoparticle mass transfer along an inclined wavy surface in a non-Darcy porous medium saturated by nanofluid with thermal radiation and thermal stratification effects has been carried out. The obtained results are displayed graphically to explore the effects of non - Darcy, Brownian motion, thermophoresis, thermal radiation, thermal stratification parameters, amplitude and angle of inclination of the wavy surface on the dimensionless velocity, temperature, nanoparticle volume fraction for both aiding and opposing flows. Further, the influence of the physical parameters on non-dimensional heat and nanoparticle mass transfer coefficients against non-similarity variable are discussed graphically.

In all the above chapters (2 - 9), the non-linear governing equations and their associated boundary conditions are initially cast into dimensionless forms by pseudo-similarity variables. The resulting system of non-similar equations are transformed into ordinary differential

equations using local similarity and non-similarity method and then solved numerically by using Successive Linearization Method. Using this method the non-linear boundary layer equations reduce to a system of linear differential equations. The Chebyshev pseudo spectral method is then used to transform the iterative sequence of linearized differential equations into a system of linear algebraic equations which are converted into a matrix system. The obtained results are compared against previously published work wherever possible on special cases of the problem and are found to be in good agreement.

In Chapter - 10, the main conclusions of the earlier chapters are recorded and the directions in which further investigations may be carried out are indicated.

List of references is given at the end of the thesis. The references are arranged in alphabetical order.

Considerable part of the work in the thesis is published/accepted for publication in journals. The remaining part is communicated for publications. The details are presented below.

List of papers published

1. "Numerical solution to natural convection over an inclined wavy surface embedded in a porous medium saturated with a nanofluid", *Meccanica*, DOI 10.1007/s11012-015-0331-9.

2. "Mixed convection over an inclined wavy surface embedded in a nanofluid saturated porous medium", *International Journal of Numerical methods for Heat and Fluid Flow*, Vol. 25(8) (2015), pp.1774–1792.

3. "Radiation effect on natural convection over an inclined wavy surface embedded in a non-Darcy porous medium saturated with a nanofluid", *Journal of porous Media*, Vol. 18(8) (2015), pp.777–789.

4. "Mixed convection over an inclined wavy surface in a nanofluid saturated non-Darcy porous medium with radiation effect", *International Journal of Chemical Engineering*, Vol. 2015, **Article ID:** 927508, 15 pages, (2015), doi:10.1155/2015/927508.

5. "Effect of thermal radiation and stratification on natural convection over an inclined wavy surface in a nanofluid saturated porous medium", *International Journal of Mining, Metallurgy & Mechanical Engineering*, Vol.3(1) (2015), pp.1–6.

6. "Free convection of a nanofluid over an inclined wavy surface embedded in a porous medium with wall heat flux", *Procedia Engineering.* Vol.127 (2015), pp.40–47.

7. "Mixed convection along an inclined wavy surface in a nanofluid saturated porous medium with wall heat flux", *Journal of Nanofluids* Vol.5(1) (2016), pp.120–129.

List of papers accepted

8. "Natural convection over an inclined wavy surface embedded in a thermally stratified porous medium saturated with a nanofluid", Accepted for publication in *Computational Thermal Sciences.*

List of papers communicated

9. "Mixed convection over an inclined wavy surface embedded in a thermally stratified porous medium saturated with a nanofluid", Communicated to *International Journal of Non-Linear Sciences.*

10. "Effects of thermal radiation and thermal stratification on mixed convection over an inclined wavy surface embedded in a non-Darcy porous medium saturated with a nanofluid", Communicated to *Open Engineering Journal.*

11. "Free convection over an inclined wavy surface embedded in a nanofluid saturated non-Darcy porous medium with thermal radiation and wall heat flux", Communicated to *Iranian Journal of Science and Tecnology, Transactions of Mechanical Engneering.*

12. "Effect of thermal radiation on mixed convection of a nanofluid from an inclined wavy surface embedded in a non-Darcy porous medium with wall heat flux", Communicated to *Propulsion and Power Research.*

Chapter 2

Natural convection over an inclined wavy surface in a nanofluid saturated porous medium [1]

2.1 Introduction

As mentioned in Chapter 1, Natural convection is a very important mechanism that is operative in a variety of environments from cooling electronic circuit boards in computers to causing large scale circulation in the atmosphere as well as in lakes and oceans that influences the weather. It is caused by the action of density gradients in conjunction with a gravitational field. Natural convection in a fluid-saturated porous medium may be met in geophysical, geothermal and industrial applications, such as the migration of moisture through air contained in fibrous insulations, grain storage installations, and the dispersion of chemical contaminants through water-saturated soil. For an exhaustive discussion of the natural convection, the reader is referred the book by Bejan [8]. Khan and Aziz [49] studied the double-diffusive natural convection from a vertical plate in a porous medium saturated

[1] Case(a):Published in "**Meccanica, DOI 10.1007/s11012-015-0331-9**", Case(b):Published in "**Procedia Engineering, 127 (2015) 40–47**"

with a binary base fluid containing nanoparticles. Haddad *et al.* [39] studied the significance of the effect of Brownian motion and thermophoresis parameters on natural convection of nanofluids. Noghrehabadi *et al.* [81] examined the natural convection heat and mass transfer of nanofluids past a vertical plate in a saturated Darcy porous medium, where the plate is subject to surface heat and nanoparticle fluxes.

The study of heat and mass transfer from the irregular wavy surfaces is of primary importance because of its enhancing heat transfer characteristics. Tashtoush and Al-Odat [104] numerically investigated the effect of magnetic field on forced convection heat and fluid flow along a wavy surface with prescribed heat flux. Molla *et al.* [66] studied the natural convection boundary layer flow along a vertical wavy surface with uniform surface heat flux. Rahman *et al.* [84] studied natural convection flow along a vertical wavy cone with uniform surface heat flux.

The preceding literature reveals that the problem of free convection of nanofluid along an inclined wavy surface embedded in a porous medium has not been considered so far. Hence, the aim of this chapter is to explore the effects of amplitude, angle of inclination of the wavy plate to the horizontal, Brownian motion and thermophoresis on natural convection in Darcy porous medium saturated with nanofluid. Using pseudo-similarity variables, the non-linear, non-homogeneous governing partial differential equations and their associated boundary conditions are converted into non-dimensional form. The reduced system of non-similar equations is solved numerically using Successive Linearization Method ([68], [5]).

2.2 Mathematical Formulation

Consider a natural convection flow along a semi-infinite inclined wavy surface embedded in a nanofluid saturated porous medium. The x coordinate is taken along the wavy plate and the y coordinate is measured normal to the wavy plate, while the origin of the reference system is considered at the leading edge of the wavy plate. The physical model and coordinate

system is shown in Fig. 2.1. The wavy surface is described by

$$y = \delta(x) = a \sin(\pi x/l)$$

where a is the amplitude of the wavy surface and $2l$ is the characteristic length of the wavy surface. The following assumptions are made to formulate the present problem.

1. The flow is steady, laminar, incompressible and two-dimensional.
2. The porous medium is homogeneous and isotropic (i.e., uniform with a constant porosity and permeability).
3. The fluid has constant properties except the density in the buoyancy term of the balance of momentum equation.
4. The wavy plate is inclined at an angle A ($0^o \leq A \leq 90^o$) to the horizontal. The inclination angle is 0^o for horizontal plate, 90^o for vertical plate and $0^o < A < 90^o$ for inclined plate.
5. The temperature and the nanoparticle concentration of the ambient medium are T_∞ and ϕ_∞.
6. The Boussinesq and boundary-layer approximations are applicable.

With the above assumptions, the governing equations for flow are given by [10, 53]

$$\frac{\partial u}{\partial x} + \frac{\partial v}{\partial y} = 0, \tag{2.1}$$

$$\begin{aligned} \frac{\partial u}{\partial y} - \frac{\partial v}{\partial x} = {} & \frac{(1-\phi_\infty)\rho_{f_\infty}\beta\, K\, g}{\mu}\left(\frac{\partial T}{\partial y}\sin A - \frac{\partial T}{\partial x}\cos A\right) \\ & - \frac{(\rho_p - \rho_{f_\infty})\, K\, g}{\mu}\left(\frac{\partial \phi}{\partial y}\sin A - \frac{\partial \phi}{\partial x}\cos A\right), \end{aligned} \tag{2.2}$$

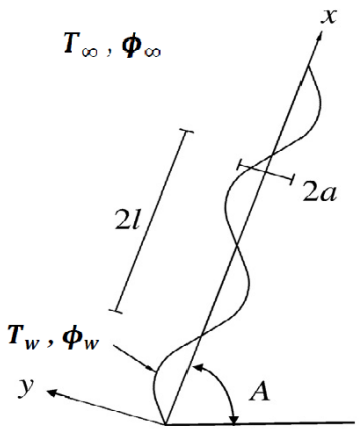

Figure 2.1: Physical model

$$u\frac{\partial T}{\partial x}+v\frac{\partial T}{\partial y}=\alpha\left(\frac{\partial^2 T}{\partial x^2}+\frac{\partial^2 T}{\partial y^2}\right)+\gamma\left[D_B\left(\frac{\partial\phi}{\partial x}\frac{\partial T}{\partial x}+\frac{\partial\phi}{\partial y}\frac{\partial T}{\partial y}\right)+\frac{D_T}{T_\infty}\left(\left(\frac{\partial T}{\partial x}\right)^2+\left(\frac{\partial T}{\partial y}\right)^2\right)\right], \tag{2.3}$$

$$u\frac{\partial\phi}{\partial x}+v\frac{\partial\phi}{\partial y}=D_B\left(\frac{\partial^2\phi}{\partial x^2}+\frac{\partial^2\phi}{\partial y^2}\right)+\frac{D_T}{T_\infty}\left(\frac{\partial^2 T}{\partial x^2}+\frac{\partial^2 T}{\partial y^2}\right), \tag{2.4}$$

where u and v are the velocity components in the x and y directions, respectively, T is the temperature, ϕ is the nanoparticle concentration, g is the acceleration due to gravity, K is the permeability, ρ_{f_∞} is the the density of the base fluid at far field, ρ_p is the density of the particles, $\alpha = k/(\rho c)_f$ is the thermal diffusivity of the fluid, k is the thermal conductivity, β is the volumetric thermal expansion coefficient of the nanofluid, μ is the dynamic viscosity of the fluid, D_B is the Brownian diffusion coefficient, D_T is the thermophoresis diffusion coefficient and γ is the ratio between the effective heat capacity of the nanoparticle material and heat capacity of the fluid (i.e. $\gamma = (\rho c)_p/(\rho c)_f$).

In this chapter, two types (cases) of boundary conditions for the temperature and nanoparticle concentration on the semi-infinite inclined wavy surface are considered. In the first type (case a), the wavy plate is subject to uniform wall temperature and nanoparticle volume fraction. In the second type (case b), the wavy plate is subject to uniform heat and nanoparticle mass fluxes.

2.2.1 Case(a): Uniform Wall Temperature and Nanoparticle Volume Fraction

Let uniform wall temperature T_w and nanoparticle volume fraction ϕ_w be prescribed on the inclined wavy surface. These values are assumed to be greater than the ambient temperature T_∞ and nanoparticle volume fraction ϕ_∞ at any arbitrary reference point in the medium (inside the boundary layer). Hence, the boundary conditions are

$$v = 0, \quad T = T_w, \quad \phi = \phi_w, \quad \text{at} \quad y = \delta(x), \tag{2.5a}$$

$$u = 0, \quad T \to T_\infty, \quad \phi \to \phi_\infty \quad \text{as} \quad y \to \infty, \tag{2.5b}$$

where the subscripts w and ∞ indicate the conditions at the wall and at the outer edge of the boundary layer respectively.

Introducing the stream function ψ by

$$u = \frac{\partial \psi}{\partial y}, \quad v = -\frac{\partial \psi}{\partial x} \tag{2.6}$$

and the following non-dimensional variables

$$\left.\begin{aligned} \xi = \frac{x}{L}, \quad \eta = \frac{(y/l - \delta)\, Ra^{1/2}}{\xi^{1/2}\,(1+\dot{\delta}^2)}, \quad \psi = \alpha Ra^{1/2} \xi^{1/2} f(\eta), \\ \theta = \frac{T - T_\infty}{T_w - T_\infty}, \\ s = \frac{\phi - \phi_\infty}{\phi_w - \phi_\infty}, \end{aligned}\right\} \tag{2.7}$$

into Eqns. (2.1) - (2.4) and letting $Ra \to \infty$ (i.e., boundary layer approximation), we obtain the following boundary layer equations:

$$f'' = (\sin A + \dot{\delta} \cos A)\,(\theta' - N_r s')\,, \tag{2.8}$$

$$\theta'' + \frac{1}{2} f\theta' + N_b s'\theta' + N_t \theta'^2 = 0, \tag{2.9}$$

$$s'' + \frac{1}{2} Le f s' + \frac{N_t}{N_b}\theta'' = 0, \tag{2.10}$$

where the prime denotes differentiation with respect to η, $Ra = \dfrac{(1-\phi_\infty)\rho_{f_\infty}\beta\, K\, g\,(T_w - T_\infty) l}{\mu\alpha}$ is the Rayleigh number, $N_r = \dfrac{(\rho_p - \rho_{f_\infty})(\phi_w - \phi_\infty)}{\rho_{f_\infty}\beta(T_w - T_\infty)(1-\phi_\infty)}$ is the buoyancy ratio, $N_b = \dfrac{\gamma D_B(\phi_w - \phi_\infty)}{\alpha}$ is the Brownian motion parameter, $N_t = \dfrac{\gamma D_T(T_w - T_\infty)}{\alpha T_\infty}$ is the thermoporesis parameter and $Le = \dfrac{\alpha}{D_B}$ is the Lewis number respectively.

The boundary conditions (2.5) in terms of f, θ and s become

$$f = 0, \quad \theta = 1, \quad s = 1, \quad \text{at} \quad \eta = 0 \tag{2.11a}$$

$$f' = 0, \quad \theta \to 0, \quad s \to 0 \quad \text{as} \quad \eta \to \infty, \tag{2.11b}$$

The heat and nanoparticle mass transfer from the wavy surface are given by

$$q_w = -kn.\nabla T, \tag{2.12a}$$

$$q_{np} = -D_B n.\nabla\phi. \tag{2.12b}$$

The local Nusselt number $\left(= \dfrac{q_w\, x}{k(T_w - T_\infty)}\right)$ and the local nanoparticle Sherwood number $\left(= \dfrac{q_{np}\, x}{D_B(\phi_w - \phi_\infty)}\right)$ are given by

$$\frac{Nu_x}{\sqrt{Ra_x}} = -\sqrt{\frac{1}{1+\dot{\delta}^2}}\left(\frac{\partial\theta}{\partial\eta}\right)_{\eta=0}, \tag{2.13a}$$

$$\frac{NSh_x}{\sqrt{Ra_x}} = -\sqrt{\frac{1}{1+\dot{\delta}^2}}\left(\frac{\partial s}{\partial\eta}\right)_{\eta=0}. \tag{2.13b}$$

Method of Solution

Eqns. (2.8) - (2.10) along with the boundary conditions (2.11) were solved numerically using the Successive Linearisation Method (SLM) [68, 5]. Using this method the non-linear boundary layer equations reduce to a system of linear differential equations. The Chebyshev pseudo spectral method is then used to transform the iterative sequence of linearized differential equations into a system of linear algebraic equations which are converted into a matrix system.

In this method we assume that the independent vector $\boldsymbol{\Upsilon}(\eta) = [f(\eta), \theta(\eta), s(\eta)]$ can be expressed as

$$\boldsymbol{\Upsilon}(\eta) = \boldsymbol{\Upsilon}_i(\eta) + \sum_{n=0}^{i-1} \boldsymbol{\Upsilon}_n(\eta) \tag{2.14}$$

where $\boldsymbol{\Upsilon}_i(\eta)$, $(i = 1, 2, 3, ...)$ are unknown functions and $\boldsymbol{\Upsilon}_n(\eta)$ are the approximations which are obtained by recursively solving the linear part of the system of equations that results from substituting (2.14) in (2.8) - (2.10).

The initial approximation $\boldsymbol{\Upsilon}_0(\eta)$ is chosen such that they satisfy the boundary conditions (2.5). Therefore $\boldsymbol{\Upsilon}_0(\eta) = [1 - e^{-\eta}, \quad e^{-\eta}, \quad e^{-\eta}]$. The subsequent solutions f_i, θ_i, s_i ,$i \geq 1$ are obtained by successively solving the following linearized form of the equations which are obtained by substituting Eqn. (2.14) in the governing equations (2.8) - (2.10).

$$f_i'' + a_{1,i-1}\theta_i' + a_{2,i-1}s_i' = r_{1,i-1} \tag{2.15}$$

$$\theta_i'' + b_{1,i-1}\theta_i' + b_{2,i-1}s_i' + b_{3,i-1}f_i = r_{2,i-1} \tag{2.16}$$

$$s_i'' + c_{1,i-1}s_i' + c_{2,i-1}\theta_i'' + c_{3,i-1}f_i = r_{3,i-1} \tag{2.17}$$

where

$$a_{1,i-1} = -(\sin A + \dot{\delta}\cos A), \quad a_{2,i-1} = N_r(\sin A + \dot{\delta}\cos A)$$
$$b_{1,i-1} = \frac{1}{2}\sum_{n=0}^{i-1} f_n + N_b \sum_{n=0}^{i-1} {s_n}' + 2N_t \sum_{n=0}^{i-1} {\theta_n}', \; b_{2,i-1} = N_b \sum_{n=0}^{i-1} {\theta_n}', \; b_{3,i-1} = \frac{1}{2}\sum_{n=0}^{i-1} {\theta_n}'$$
$$c_{1,i-1} = \frac{1}{2}Le\sum_{n=0}^{i-1} f_n, \; c_{2,i-1} = \frac{N_t}{N_b}, \; c_{3,i-1} = \frac{1}{2}Le\sum_{n=0}^{i-1} {s_n}'$$
$$r_{1,i-1} = -\sum_{n=0}^{i-1} {f_n}'' + (\sin A + \dot{\delta}\cos A)\sum_{n=0}^{i-1} {\theta_n}' - (\sin A + \dot{\delta}\cos A)N_r \sum_{n=0}^{i-1} {s_n}'$$
$$r_{2,i-1} = -\sum_{n=0}^{i-1} {\theta_n}'' - \frac{1}{2}\sum_{n=0}^{i-1} f_n \sum_{n=0}^{i-1} {\theta_n}' - N_b \sum_{n=0}^{i-1} {s_n}' \sum_{n=0}^{i-1} {\theta_n}' - N_t \sum_{n=0}^{i-1} {\theta_n}' \sum_{n=0}^{i-1} {\theta_n}'$$
$$r_{3,i-1} = -\sum_{n=0}^{i-1} {s_n}'' - \frac{1}{2}\sum_{n=0}^{i-1} f_n \sum_{n=0}^{i-1} {s_n}' - \frac{N_t}{N_b}\sum_{n=0}^{i-1} {\theta_n}''$$

The boundary conditions reduce to

$$f_i(0) = {f_i}'(\infty) = 0, \quad \theta_i(0) = \theta_i(\infty) = s_i(0) = s_i(\infty) = 0 \tag{2.18}$$

The approximate solution for $\boldsymbol{\Upsilon}(\eta)$ is then obtained as

$$\boldsymbol{\Upsilon}(\eta) \approx \sum_{m=0}^{M} \boldsymbol{\Upsilon}_m(\eta) \tag{2.19}$$

where M is the order of SLM approximation. Eqns. (2.15) - (2.17) are solved using the Chebyshev spectral collocation method [11]. The unknown functions are approximated by the Chebyshev interpolating polynomials in such a way that they are collocated at the Gauss-Lobatto points defined as

$$\chi_j = \cos\frac{\pi j}{N}, \quad j = 0, 1, 2, ..., N \tag{2.20}$$

where N is the number of collocation points used. The physical region $[0, \infty)$ is transformed into the region [-1, 1] using the domain truncation technique in which the problem is solved

on the interval [0, L] instead of $[0, \infty)$. This leads to the mapping

$$\frac{\eta}{L} = \frac{\chi + 1}{2}, \quad -1 \leq \chi \leq 1 \tag{2.21}$$

where L is a scaling parameter used to invoke the boundary condition at infinity. The function $\boldsymbol{\Upsilon}(\eta)$ is approximated at the collocation points by

$$\boldsymbol{\Upsilon}_i(\chi) = \sum_{k=0}^{N} \boldsymbol{\Upsilon}_i(\chi_k) T_k(\chi_j), \quad j = 0, 1, 2, ..., N \tag{2.22}$$

where T_k is the k^{th} Chebyshev polynomial defined by $T_k(\chi) = \cos[k\cos^{-1}\chi]$.

The derivatives of the variables at the collocation points are represented as

$$\frac{d^r}{d\eta^r}\boldsymbol{\Upsilon}_i(\chi) = \sum_{k=0}^{N} \mathbf{D}_{kj}^r \boldsymbol{\Upsilon}_i(\chi_k), \quad j = 0, 1, 2, ..., N. \tag{2.23}$$

where r is the order of differentiation and $\mathbf{D} = \frac{2}{L}\mathscr{D}$, $\mathscr{D}$ being the Chebyshev spectral differentiation matrix. Substituting Eqs. (2.21) - (2.23) into Eqs. (2.15) - (2.17) leads to the following matrix equation

$$\mathbf{A}_{i-1}\mathbf{X}_i = \mathbf{R}_{i-1}, \tag{2.24}$$

subject to the boundary conditions

$$f_i(\chi_N) = 0, \quad \sum_{k=0}^{N} \mathbf{D}_{0k} f_i(\chi_k) = 0 \tag{2.25}$$

$$\theta_i(\chi_N) = \theta_i(\chi_0) = s_i(\chi_N) = s_i(\chi_0) = 0 \tag{2.26}$$

In Eqn. (2.24), $\mathbf{A}_{i-1}$ is a (3N + 3)×(3N + 3) square matrix and $\mathbf{X}_i$ and $\mathbf{R}_{i-1}$ are (3N + 3)×1 column vectors defined by

$$\mathbf{A}_{i-1} = \begin{bmatrix} A_{11} & A_{12} & A_{13} \\ A_{21} & A_{22} & A_{23} \\ A_{31} & A_{32} & A_{33} \end{bmatrix}, \quad \mathbf{X}_i = \begin{bmatrix} \mathbf{F}_i \\ \boldsymbol{\Theta}_i \\ \boldsymbol{\Phi}_i \end{bmatrix}, \quad \mathbf{R}_{i-1} = \begin{bmatrix} \mathbf{r}_{1,i-1} \\ \mathbf{r}_{2,i-1} \\ \mathbf{r}_{3,i-1} \end{bmatrix} \tag{2.27}$$

where

$$\mathbf{F}_i = [f_i(\chi_0), f_i(\chi_1), ..., f_i(\chi_{N-1}), f_i(\chi_N)]^T,$$
$$\mathbf{\Theta}_i = [\theta_i(\chi_0), \theta_i(\chi_1), ..., \theta_i(\chi_{N-1}), \theta_i(\chi_N)]^T,$$
$$\mathbf{\Phi}_i = [s_i(\chi_0), s_i(\chi_1), ..., s_i(\chi_{N-1}), s_i(\chi_N)]^T,$$
$$\mathbf{r}_{1,i-1} = [r_{1,i-1}(\chi_0), r_{1,i-1}(\chi_1), ..., r_{1,i-1}(\chi_{N-1}), r_{1,i-1}(\chi_N)]^T$$
$$\mathbf{r}_{2,i-1} = [r_{2,i-1}(\chi_0), r_{2,i-1}(\chi_1), ..., r_{2,i-1}(\chi_{N-1}), r_{2,i-1}(\chi_N)]^T$$
$$\mathbf{r}_{3,i-1} = [r_{3,i-1}(\chi_0), r_{3,i-1}(\chi_1), ..., r_{3,i-1}(\chi_{N-1}), r_{3,i-1}(\chi_N)]^T$$
$$A_{11} = \mathbf{D}^2, \quad A_{12} = a_{1,i-1}\mathbf{D}, \quad A_{13} = a_{2,i-1}\mathbf{D}$$
$$A_{21} = b_{3,i-1}\mathbf{I}, \quad A_{22} = \mathbf{D}^2 + b_{1,i-1}\mathbf{D}, \quad A_{23} = b_{2,i-1}\mathbf{D}$$
$$A_{31} = c_{3,i-1}\mathbf{I}, \quad A_{32} = c_{2,i-1}\mathbf{D}^2, \quad A_{33} = \mathbf{D}^2 + c_{1,i-1}\mathbf{D}$$

Here $\mathbf{I}$ is an identity matrix of size (N +1)×(N +1). After modifying the matrix system (2.24) to incorporate boundary conditions (2.25) - (2.26), the solution is obtained as

$$\mathbf{X}_i = \mathbf{A}_{i-1}^{-1}\mathbf{R}_{i-1} \tag{2.28}$$

Results and Discussion

We have computed the solutions for the dimensionless velocity, temperature and nanoparticle volume fraction functions and heat and nanoparticle mass transfer rates and the results are shown graphically in Figs. 2.2 - 2.7. The effects of angle of inclination (A), Brownian motion parameter (N_b), thermophoresis parameter (N_t) and amplitude (a) of the wavy surface are discussed hereunder. The choice of values for N_r, N_t and N_b is based on those values utilized by Nield and Kuznetsov [78] for the case with the isothermal wall boundary condition.

Table. 2.1 shows the comparison of the results of the local Nusselt number $Nu_x/\sqrt{Ra_x}$ for fixed values of $A = \pi/2$, $a = 0$, with the results obtained by Bejan and Khair [9]. It is shown that these two results are in excellent agreement.

Figure. 2.2 shows the effect of the amplitude of the wavy surface on velocity, temperature and nanoparticle volume fraction distributions. It is observed that increasing the amplitude a of the wavy surface increases the velocity near the plate and decreases away from the plate,

whereas the temperature and nanoparticle volume fraction decreases.

The effect of the angle of inclination of the wavy surface on velocity, temperature and nanoparticle volume fraction is plotted in Fig. 2.3. The similarity equations for the limiting cases of the horizontal and vertical plates are recovered from the transformed equations by setting $A = 0^o$ and $A = 90^o$, respectively. It is noted from Fig. 2.3 that as A increases, the velocity increases near the plate and decreases away from the plate but the temperature and nanoparticle volume fraction decrease within the boundary layer region. When the surface is vertical, the smallest temperature and nanoparticle volume fraction distributions are observed, whereas they are largest for the horizontal surface.

Figure. 2.4 displays the effect of Brownian motion parameter N_b on dimensionless velocity, temperature and nanoparticle fraction. It is interesting to note that an increase in the intensity of Brownian motion parameter produces an enhancement in the fluid velocity within the momentum boundary layer which causes an increase in the diffusion of the nanoparticles into the the fluid. This results an increase in velocity and temperature of the fluid as shown in Fig. 2.4(a) and 2.4(b). Increasing the Brownian motion parameter tends to reduce the nanoparticle volume fraction as shown in Fig. 2.4(c). This is due to increase in difference between the nanoparticle volume fractions at the wall and the ambient.

Figure. 2.5 shows the effect of thermophoresis parameter N_t on dimensionless velocity, temperature and nanoparticle fraction of the fluid. It is observed that an increase in the thermophoresis parameter tends to increase the maximum stream wise velocity, temperature and nanoparticle volume fraction of the fluid. This is due to the fact that increase in thermophoresis parameter increases the thermophoresis force, which tends to move particles from the hot zone to the cold zone, which results in the increase in nanoparticle concentration, as seen in 2.5(c). Furthermore, increase in the thermophoresis parameter increases the nanoparticle diffusion into the fluid which increases the magnitude of the dimensionless temperature, as shown in 2.5(b).

The variation of heat and nanoparticle mass transfer rates for various values of the wave amplitude a and angle of inclination A is displayed in Fig. 2.6. Figs. 2.6(a) and 2.6(b)

shows the effect of wave amplitude on the local Nusselt and nanoparticle Sherwood number. It is found that an enhancement in wavy amplitude reduces the local heat and nanoparticle mass transfer rates as compared with the limiting case of a smooth surface. It is noticed that the maximum value of the local heat transfer rate is located at ξ =1, 2, 3, 4 and 5 and its minimum value is located at ξ =0.5, 1.5, 2.5, 3.5 and 4.5. In general, we conclude that the surface becomes more roughened for increasing values of amplitude of the wavy surface. Figs. 2.6(c) and 2.6(d) displays the variation of heat and nanoparticle mass transfer rates for various values of the angle of inclination A. It is observed that an increase in the angle of inclination increases the buoyancy force and assists the flow, leading to an increase in the heat and nanoparticle mass transfer rates. The maximum values of the dimensionless heat and nanoparticle mass transfer rates are observed when the surface is vertical; in which case, the buoyancy force is at its maximum.

The effect of Brownian motion parameter N_b and thermoporesis parameter N_t on the heat and nanoparticle mass transfer rates is presented in Fig. 2.7. Figs. 2.7(a) and 2.7(c) depict that the dimensionless heat transfer rate decreases with increase in both the Browinian motion and thermophoresis parameters. An increase in the value of Brownian motion parameter enhances the nanoparticle volume fraction transfer rate, as shown in Fig. 2.7(b). It is seen from Fig. 2.7(d) that the nanoparticle mass transfer rate decreases with an increase in the thermophoresis parameter. As Brownian motion is proportional to the volumetric fraction of nanoparticles in the direction from high to low concentration, and the thermophoresis is proportional to the temperature gradient from hot to cold. Hence, we conclude that the effect of the combination of Brownian motion and thermophoresis is to reduce the value of Nusselt number.

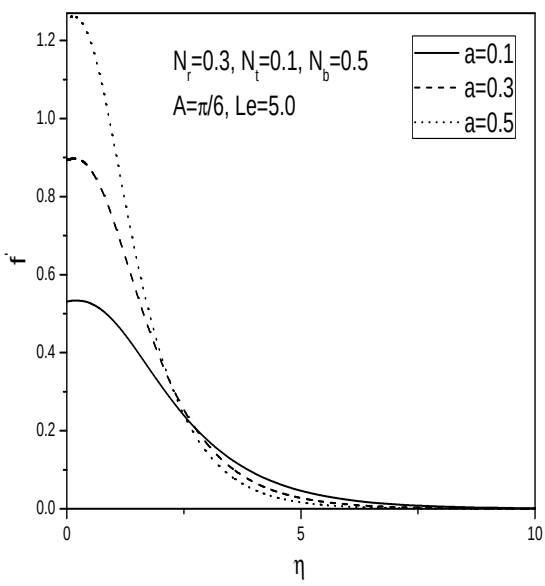

(a)

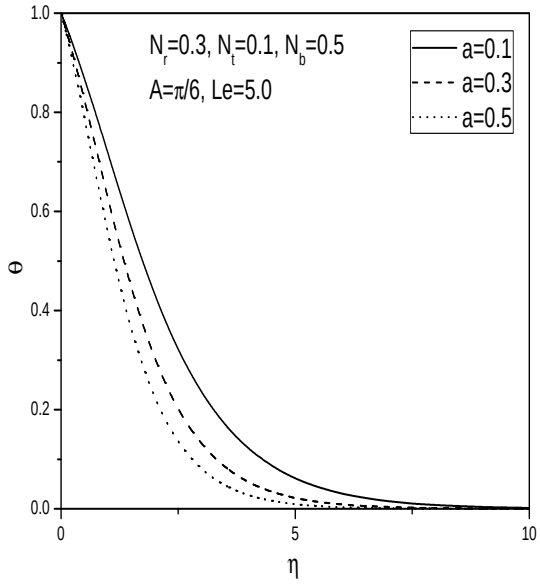

(b)

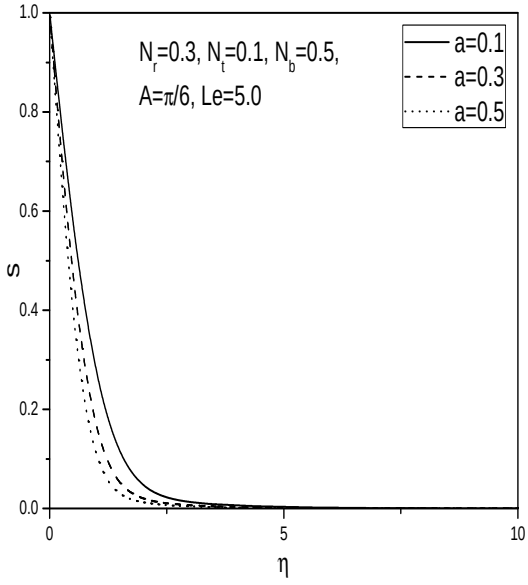

(c)

Figure 2.2: (a) Velocity, (b) temperature and (c) nanoparticle volume fraction profiles for various values of amplitude of the wavy surface a.

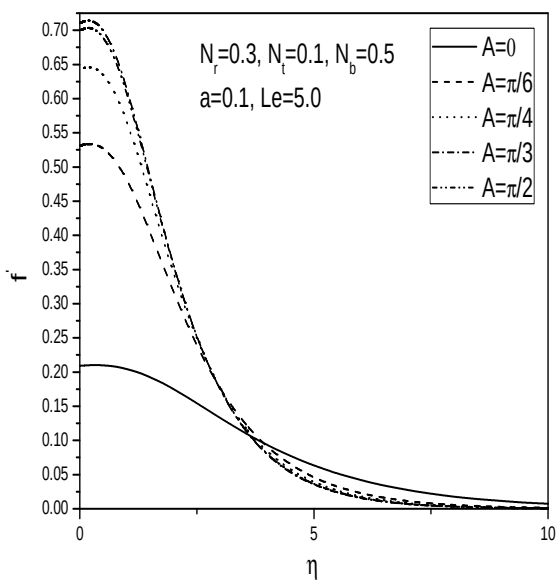

(a)

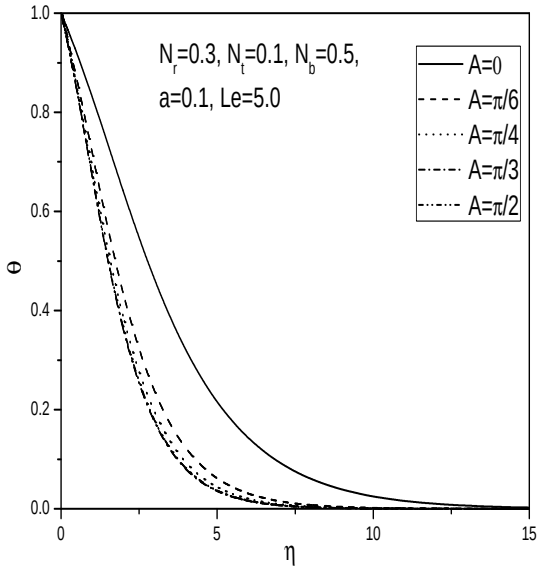

(b)

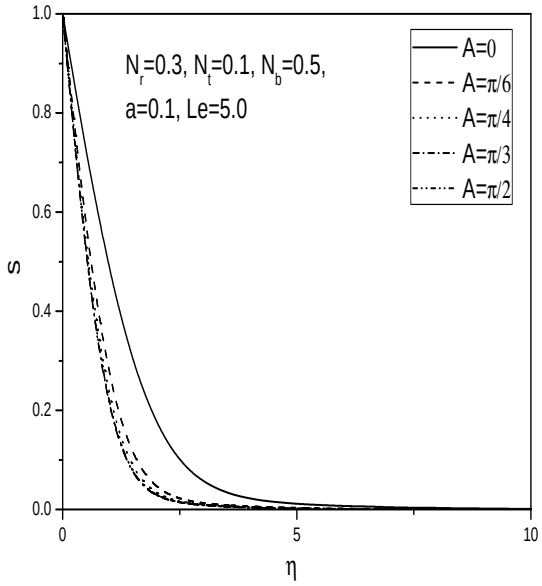

(c)

Figure 2.3: (a) Velocity, (b) temperature and (c) nanoparticle volume fraction profiles for various values of angle of inclination A.

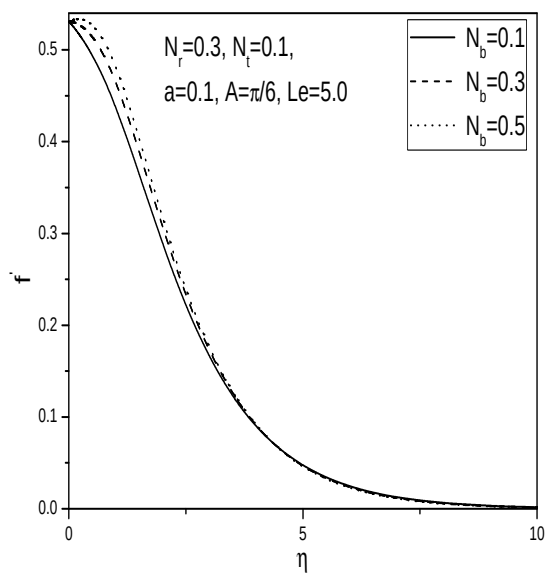

(a)

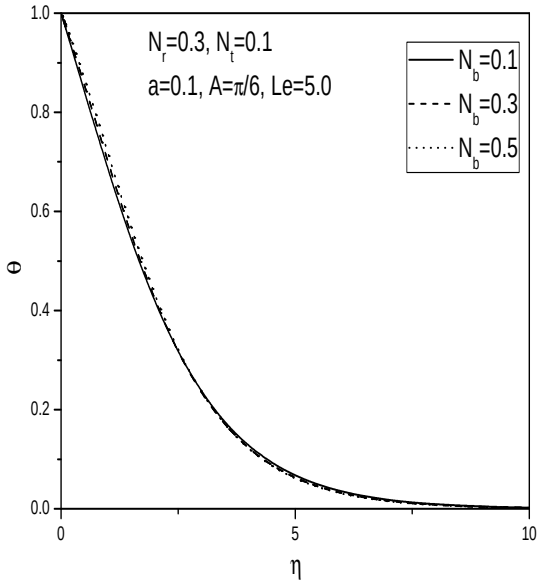

(b)

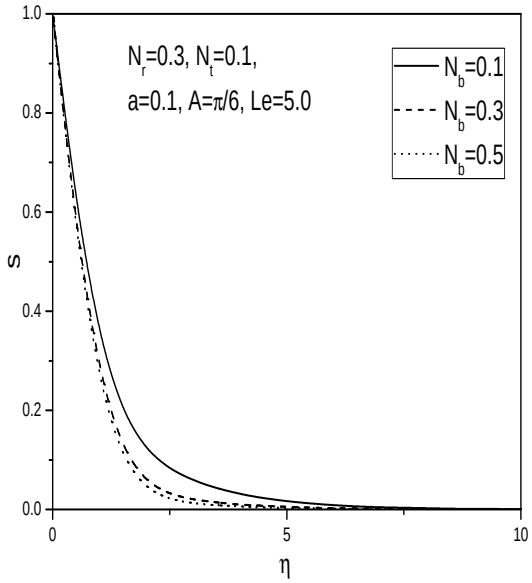

(c)

Figure 2.4: (a) Velocity, (b) temperature and (c) nanoparticle volume fraction profiles for various values of Brownian motion parameer N_b.

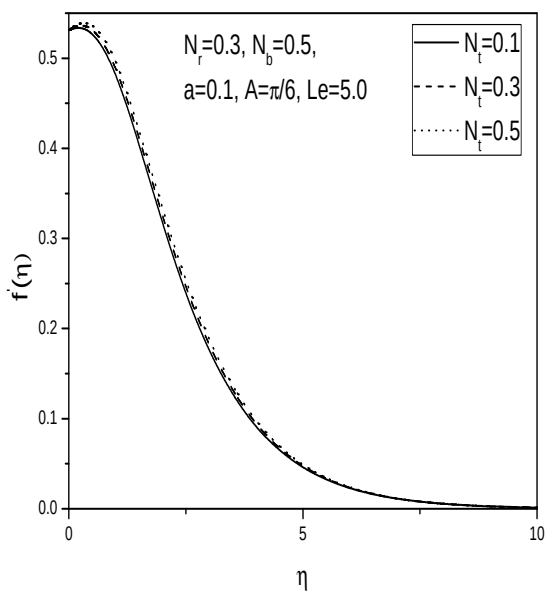

(a)

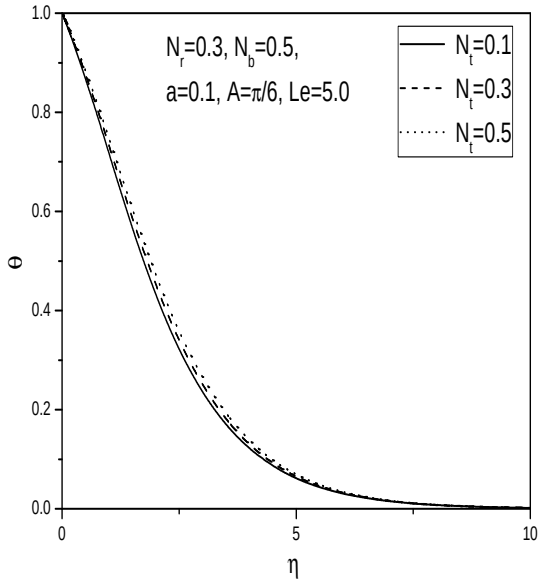

(b)

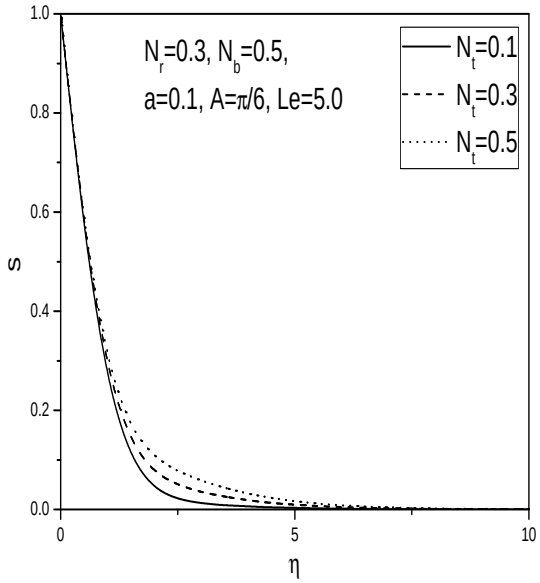

(c)

Figure 2.5: (a) Velocity, (b) temperature and (c) nanoparticle volume fraction profiles for various values of thermophoresis parameter N_t.

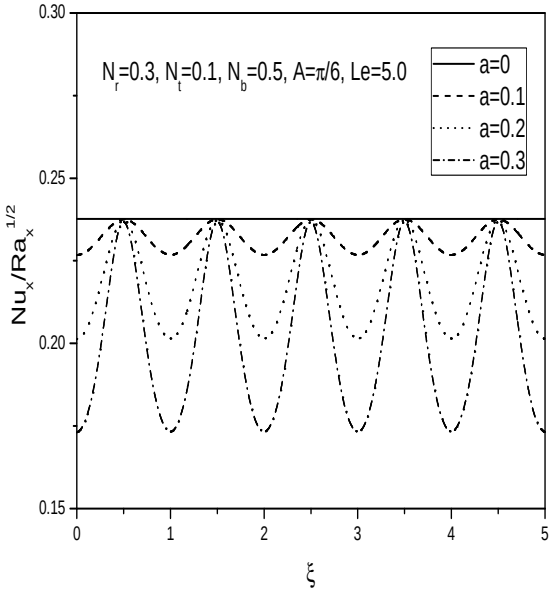

(a)

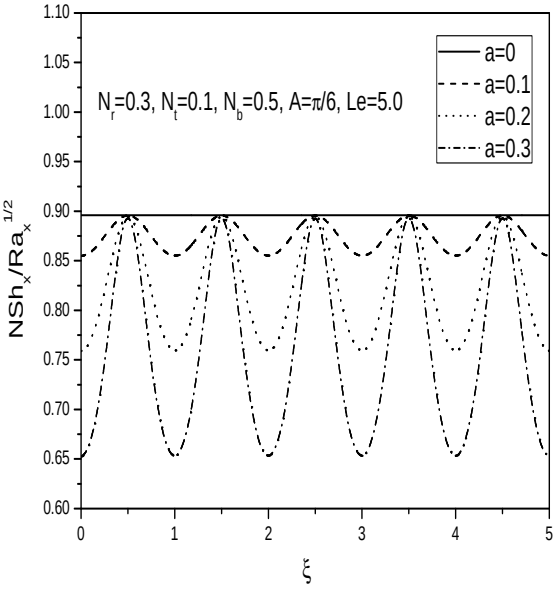

(b)

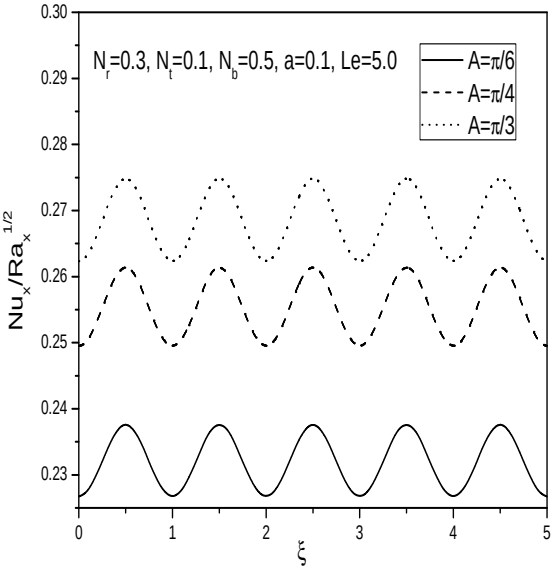

(c)

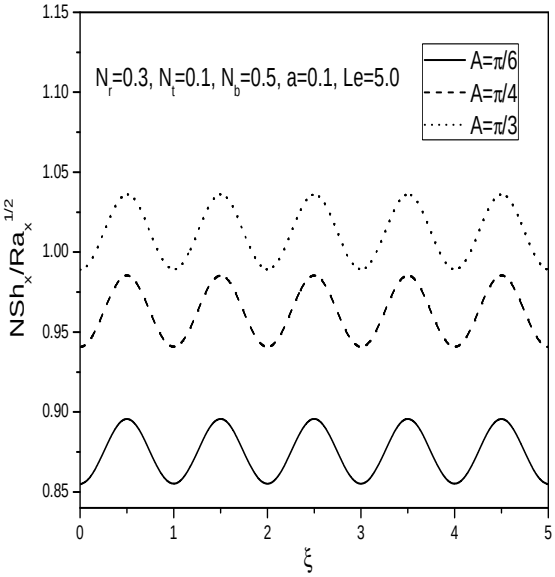

(d)

Figure 2.6: Variation of (a) heat, (b) nanoparticle mass transfer coefficients with wave amplitude a and (c) heat, (d) nanoparticle mass transfer coefficients with angle of inclination A.

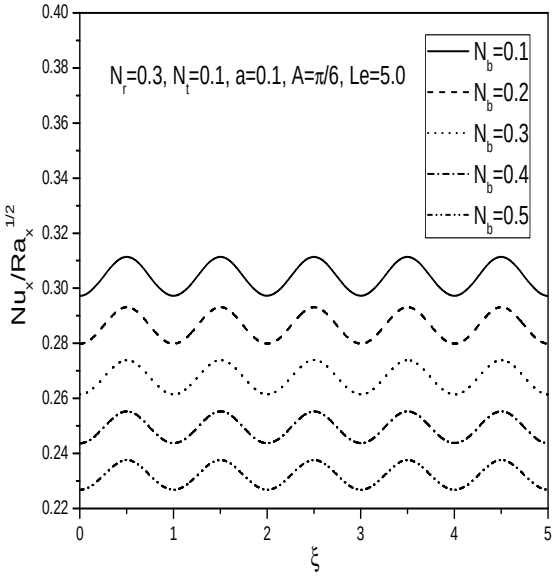

(a)

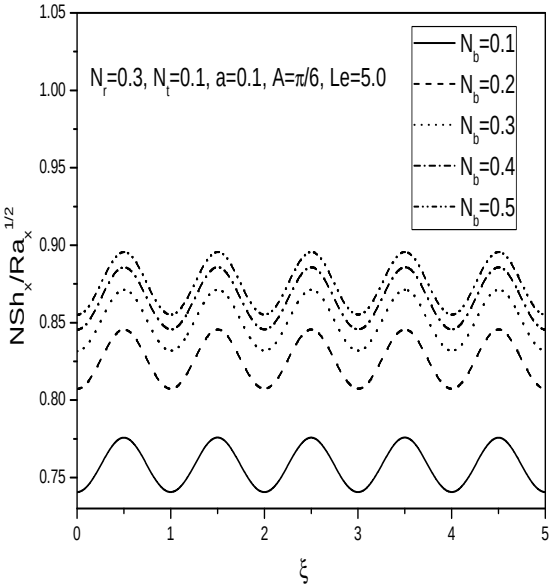

(b)

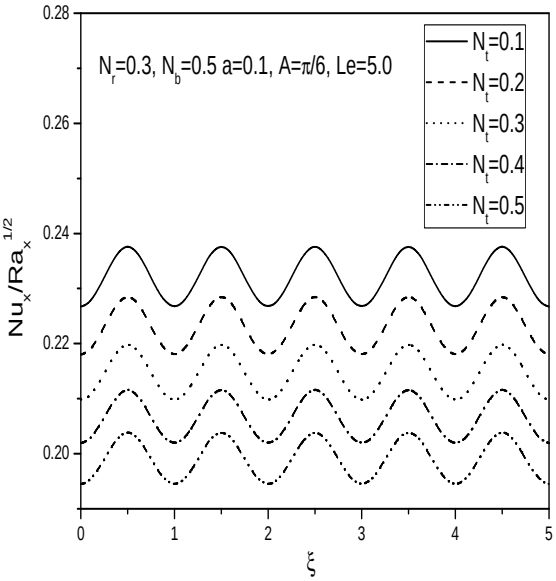

(c)

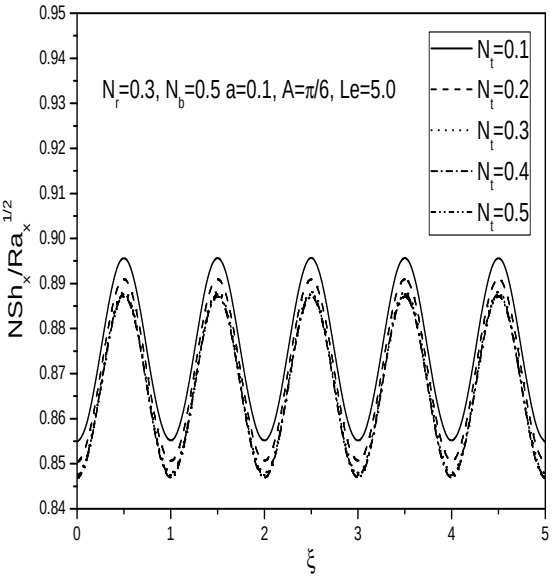

(d)

Figure 2.7: Variation of (a) heat and (b) nanoparticle mass transfer coefficients with Brownian motion parameter N_b and (c) heat, (d) nanoparticle mass transfer coefficients with thermophoresis parameter N_t.

Table 2.1: Comparison of $Nu_x/\sqrt{Ra_x}$ by the present method and Bejan and Khair [9] for fixed values of $A = \frac{\pi}{2}$, $a = 0$, $\xi = 0$.

N_r	Le	Bejan & Khair[9]	Present
-1	4	0.559	0.55849933
-1	6	0.541	0.54076461
-1	8	0.529	0.52943958
-4	4	0.798	0.79754849
-4	6	0.742	0.74229679
-4	8	0.707	0.706508651

2.2.2 Case(b): Uniform Wall Heat and Nanoparticle Mass Flux

Let a uniform and constant heat flux q_w and uniform nanoparticle mass flux q_{np} be prescribed on the wavy surface. The steady natural convection boundary layer flow is governed by Eqns. (2.1) to (2.4) and the boundary conditions are given by

$$v = 0,\ q_w = -k(n.\nabla T),\ q_{np} = D_B(n.\nabla\phi) \text{ at } \quad y = \delta(x), \tag{2.29a}$$

$$u = 0, \quad T \to T_\infty, \quad \phi \to \phi_\infty \quad \text{as} \quad y \to \infty. \tag{2.29b}$$

Substituting the stream function ψ and introducing the following non-dimensional variables

$$\left.\begin{aligned} \xi = \frac{x}{L}, \quad \eta = \frac{(y/l - \delta)\, Ra^{1/3}}{\xi^{1/3}\,(1+\dot{\delta}^2)}, \quad \psi = \alpha\, Ra^{1/3}\, \xi^{2/3}\, f(\xi,\eta), \\ T - T_\infty = \frac{q_w\, l}{k} \xi^{1/3} Ra^{-1/3}\, \theta(\xi,\eta), \\ \phi - \phi_\infty = \frac{q_{np} l}{D_B} \xi^{1/3} Ra^{-1/3}\, s(\xi,\eta), \end{aligned}\right\} \tag{2.30}$$

in to Eqns. (2.1) - (2.4) and letting $Ra \to \infty$ (i.e., boundary layer approximation), we obtain the following boundary layer equations

$$f'' = (\sin A + \dot{\delta}\cos A)\,(\theta' - N_r s') \tag{2.31}$$

$$\theta'' + \frac{2}{3} f\theta' - \frac{1}{3} f'\theta + \xi^{1/3}\, N_b s'\theta' + \xi^{1/3}\, N_t \theta'^2 = \xi \left(f' \frac{\partial \theta}{\partial \xi} - \theta' \frac{\partial f}{\partial \xi} \right) \tag{2.32}$$

$$s'' + \frac{2}{3} Le\, f\, s' - \frac{1}{3} Le\, f'\, s + \frac{N_t}{N_b}\theta'' = Le\xi \left(f' \frac{\partial s}{\partial \xi} - s' \frac{\partial f}{\partial \xi} \right) \tag{2.33}$$

where $Ra = \dfrac{(1-\phi_\infty)\rho_{f_\infty}\beta\, K\, g\, q_w\, l^2}{\mu\, k\, \alpha}$ is the Rayleigh number, $N_r = \dfrac{(\rho_p - \rho_{f_\infty})k\, q_{np}}{(1-\phi_\infty)\,\rho_{f_\infty}\beta\, q_w\, D_B}$ is the buoyancy ratio, $N_b = \dfrac{\gamma\, q_{np}\, l}{\alpha}\, Ra^{-1/3}$ is the Brownian motion parameter, $N_t = \dfrac{\gamma D_T\, q_w\, l}{\alpha T_\infty\, k} Ra^{-1/3}$ is the thermophoresis parameter and $Le = \dfrac{\alpha}{D_B}$ is the Lewis number respectively.

The boundary conditions (2.29) in terms of f, θ and s becomes

$$2f + 3\xi \left(\frac{\partial f}{\partial \xi} \right)_{\eta=0} = 0, \quad \theta' = -\sqrt{1+\dot{\delta}^2}, \quad s' = -\sqrt{1+\dot{\delta}^2}, \quad \text{at} \quad \eta = 0 \tag{2.34a}$$

$$f' \to 0, \quad \theta \to 0, \quad s \to 0 \quad \text{as} \quad \eta \to \infty. \tag{2.34b}$$

The non-dimensional local Nusselt number Nu_ξ and the local nanoparticle Sherwood number NSh_ξ are given by

$$\frac{Nu_\xi}{{Ra_\xi}^{1/3}} = \frac{\xi^{1/3}}{\theta(\xi, 0)}, \tag{2.35a}$$

$$\frac{NSh_\xi}{{Ra_\xi}^{1/3}} = \frac{\xi^{1/3}}{s(\xi, 0)}. \tag{2.35b}$$

Method of Solution

To solve the system of Eqns. (2.31) - (2.33) along with the boundary conditions (2.34), a local similarity and non-similarity method [24, 100] has been applied. The boundary value problems obtained from this method are linearized by the Successive Linearisation Method and then solved using Chebyshev spectral collocation method.

The local similarity and non-similarity method includes three levels of truncations which are explained as follows

In the first level of truncation, the terms accompanied by $\xi \frac{\partial}{\partial \xi}$ are assumed to be very

small. This is particularly true when $\xi << 1$. Thus the terms with $\xi\frac{\partial}{\partial\xi}$ in Eqns. (2.31) - (2.33) can be neglected to get the following system of equations.

$$f'' = (\sin A + \dot{\delta}\cos A)(\theta' - N_r s') \tag{2.36}$$

$$\theta'' + \frac{2}{3}f\theta' - \frac{1}{3}f'\theta + \xi^{1/3}N_b s'\theta' + \xi^{1/3}N_t\theta'^2 = 0 \tag{2.37}$$

$$s'' + \frac{2}{3}Le\, f\, s' - \frac{1}{3}Le\, f'\, s + \frac{N_t}{N_b}\theta'' = 0 \tag{2.38}$$

The associated boundary conditions are

$$f = 0, \quad \theta' = -\sqrt{1+\dot{\delta}^2}, \quad s' = -\sqrt{1+\dot{\delta}^2} \quad \eta = 0 \tag{2.39a}$$

$$f' = 0, \quad \theta \to 0, \quad s \to 0 \quad \text{as} \quad \eta \to \infty, \tag{2.39b}$$

For the second level of truncation we introduce $g = \frac{\partial f}{\partial\xi}$, $h = \frac{\partial\theta}{\partial\xi}$ and $k = \frac{\partial s}{\partial\xi}$ and recover the neglected terms at the first level of truncation. Thus the governing equations at the second level reduce to

$$f'' = (\sin A + \dot{\delta}\cos A)(\theta' - N_r s') \tag{2.40}$$

$$\theta'' + \frac{2}{3}f\theta' - \frac{1}{3}f'\theta + \xi^{1/3}N_b s'\theta' + \xi^{1/3}N_t\theta'^2 = \xi(f'h - \theta' g) \tag{2.41}$$

$$s'' + \frac{2}{3}Le\, f\, s' - \frac{1}{3}Le\, f'\, s + \frac{N_t}{N_b}\theta'' = Le\xi(f'k - s'g) \tag{2.42}$$

The associated boundary conditions are

$$2f + 3\xi g = 0, \quad \theta' = -\sqrt{1+\dot{\delta}^2}, \quad s' = -\sqrt{1+\dot{\delta}^2} \quad \eta = 0 \tag{2.43a}$$

$$f' = 0, \quad \theta \to 0, \quad s \to 0 \quad \text{as} \quad \eta \to \infty, \tag{2.43b}$$

At the third level of truncation we differentiate Eqns. (2.40) - (2.43) with respect to ξ and neglect the terms $\frac{\partial g}{\partial\xi}$, $\frac{\partial h}{\partial\xi}$ and $\frac{\partial k}{\partial\xi}$ to get the following system of equations

$$g'' = (\ddot{\delta}\cos A)(\theta' - N_r s') + (\sin A + \dot{\delta}\cos A)(h' - N_r k') \tag{2.44}$$

$$h'' + \frac{5}{3}g\theta' + \frac{2}{3}fh' - \frac{1}{3}g'\theta - \frac{4}{3}f'h + \frac{1}{3}N_b\xi^{-2/3}s'\theta' + N_b\xi^{1/3}(k'\theta' + s'h') + \frac{1}{3}N_t\xi^{-2/3}\theta'^2 + 2N_t\xi^{1/3}\theta'h' - \xi(g'h - h'g) = 0 \quad (2.45)$$

$$k'' + \frac{5}{3}Legs' + \frac{2}{3}Lefk' - \frac{1}{3}Leg's - \frac{4}{3}Lef'k + \frac{N_t}{N_b}h'' - Le\xi(g'k - k'g) = 0 \quad (2.46)$$

The associated boundary conditions are

$$g = 0, \quad h' = -\frac{\dot{\delta}\ddot{\delta}}{\sqrt{1+\dot{\delta}^2}}, \quad k' = -\frac{\dot{\delta}\ddot{\delta}}{\sqrt{1+\dot{\delta}^2}}, \quad \text{at} \quad \eta = 0 \quad (2.47a)$$

$$g' = 0, \quad h \to 0, \quad k \to 0 \quad \text{as} \quad \eta \to \infty, \quad (2.47b)$$

The set of differential equations (2.40) - (2.42) and (2.44) - (2.46) together with the boundary conditions (2.43) and (2.47) are now solved using Successive Linearisation Method([68, 5]). Proceeding same as in the case (a), we obtain the following matrix equation

$$\mathbf{A}_{i-1}\mathbf{X}_i = \mathbf{R}_{i-1}, \quad (2.48)$$

In Eq. (2.48), $\mathbf{A}_{i-1}$ is a (6N + 6)×(6N + 6) square matrix and $\mathbf{X}_i$ and $\mathbf{R}_{i-1}$ are (6N + 6)×1 column vectors defined by

$$\mathbf{A}_{i-1} = \begin{bmatrix} A_{11} & A_{12} & A_{13} & A_{14} & A_{15} & A_{16} \\ A_{21} & A_{22} & A_{23} & A_{24} & A_{25} & A_{26} \\ A_{31} & A_{32} & A_{33} & A_{34} & A_{35} & A_{36} \\ A_{41} & A_{42} & A_{43} & A_{44} & A_{45} & A_{46} \\ A_{51} & A_{52} & A_{53} & A_{54} & A_{55} & A_{56} \\ A_{61} & A_{62} & A_{63} & A_{64} & A_{65} & A_{66} \end{bmatrix}, \quad \mathbf{X}_i = \begin{bmatrix} \mathbf{F}_i \\ \boldsymbol{\Theta}_i \\ \boldsymbol{\Phi}_i \\ \mathbf{G}_i \\ \mathbf{H}_i \\ \mathbf{K}_i \end{bmatrix}, \quad \mathbf{R}_{i-1} = \begin{bmatrix} \mathbf{r}_{1,i-1} \\ \mathbf{r}_{2,i-1} \\ \mathbf{r}_{3,i-1} \\ \mathbf{r}_{4,i-1} \\ \mathbf{r}_{5,i-1} \\ \mathbf{r}_{6,i-1} \end{bmatrix} \quad (2.49)$$

where

$\mathbf{F}_i = [f_i(\chi_0), f_i(\chi_1), ..., f_i(\chi_{N-1}), f_i(\chi_N)]^T$, $\mathbf{\Theta_i} = [\theta_i(\chi_0), \theta_i(\chi_1), ..., \theta_i(\chi_{N-1}), \theta_i(\chi_N)]^T$,
$\mathbf{\Phi_i} = [s_i(\chi_0), s_i(\chi_1), ..., s_i(\chi_{N-1}), s_i(\chi_N)]^T$, $\mathbf{G}_i = [g_i(\chi_0), g_i(\chi_1), ..., g_i(\chi_{N-1}), g_i(\chi_N)]^T$,
$\mathbf{H}_i = [h_i(\chi_0), h_i(\chi_1), ..., h_i(\chi_{N-1}), h_i(\chi_N)]^T$, $\mathbf{K}_i = [k_i(\chi_0), k_i(\chi_1), ..., k_i(\chi_{N-1}), k_i(\chi_N)]^T$,
$\mathbf{r}_{j,i-1} = [r_{j,i-1}(\chi_0), r_{j,i-1}(\chi_1), \cdots, r_{j,i-1}(\chi_{N-1}), r_{j,i-1}(\chi_N)]^T, j = 1, 2, 3, 4, 5, 6$
$A_{11} = \mathbf{D}^2,\ A_{12} = a_{1,i-1}\mathbf{D},\ A_{13} = a_{2,i-1}\mathbf{D},\ A_{14} = \mathbf{0},\ A_{15} = \mathbf{0},\ A_{16} = \mathbf{0}$
$A_{21} = b_{3,i-1}\mathbf{D} + b_{4,i-1}\mathbf{I},\ A_{22} = \mathbf{D}^2 + b_{1,i-1}\mathbf{D} + b_{2,i-1}\mathbf{I},\ A_{23} = b_{5,i-1}\mathbf{D},\ A_{24} = b_{6,i-1}\mathbf{I},$
$A_{25} = b_{7,i-1}\mathbf{I},\ A_{26} = \mathbf{0},\ A_{31} = c_{3,i-1}\mathbf{D} + c_{4,i-1}\mathbf{I},\ A_{32} = c_{5,i-1}\mathbf{D}^2,$
$A_{33} = \mathbf{D}^2 + c_{1,i-1}\mathbf{D} + c_{2,i-1}\mathbf{I},\ A_{34} = c_{6,i-1}\mathbf{I},\ A_{35} = \mathbf{0},\ A_{36} = c_{7,i-1}\mathbf{I},\ A_{41} = \mathbf{0},$
$A_{42} = d_{1,i-1}\mathbf{D},\ A_{43} = d_{2,i-1}\mathbf{D},\ A_{44} = \mathbf{D}^2,\ A_{45} = d_{3,i-1}\mathbf{D},\ A_{46} = d_{4,i-1}\mathbf{D},$
$A_{51} = l_{3,i-1}\mathbf{D} + l_{4,i-1}\mathbf{I},\ A_{52} = l_{5,i-1}\mathbf{D} + l_{6,i-1}\mathbf{I},\ A_{53} = l_{7,i-1}\mathbf{D}$
$A_{54} = l_{8,i-1}\mathbf{D} + l_{9,i-1}\mathbf{I},\ A_{55} = \mathbf{D}^2 + l_{1,i-1}\mathbf{D} + l_{2,i-1}\mathbf{I},\ A_{56} = l_{10,i-1}\mathbf{D},$
$A_{61} = m_{3,i-1}\mathbf{D} + m_{4,i-1}I,\ A_{62} = \mathbf{0},\ A_{63} = m_{5,i-1}\mathbf{D} + m_{6,i-1}\mathbf{I}$
$A_{64} = m_{7,i-1}\mathbf{D} + m_{8,i-1}\mathbf{I},\ A_{65} = m_{9,i-1}\mathbf{D}^2,\ A_{66} = \mathbf{D}^2 + m_{1,i-1}\mathbf{D} + m_{2,i-1}\mathbf{I}$

where $\mathbf{I}$ is an identity matrix of size (N +1)×(N +1). After modifying the matrix system (2.48) to incorporate boundary conditions, the solution is obtained as

$$\mathbf{X}_i = \mathbf{A}_{i-1}^{-1}\mathbf{R}_{i-1} \tag{2.50}$$

Results and Discussion

The solutions for dimensionless heat and nanoparticle mass transfer rates are computed and presented graphically in Figs. 2.8 and 2.9. The effects of angle of inclination (A), Brownian motion parameter (N_b), thermophoresis parameter (N_t) and amplitude (a) of the wavy surface have been discussed.

The effect of the amplitude and angle of inclination of the wavy surface on the Nusselt and nanoparticle Sherwood number is plotted in Fig. 2.8. It is observed from Figs. 2.8(a) and 2.8(b) that an enhancement in wavy amplitude increases the local heat and nanoparticle

mass transfer rates as compared with the limiting case of a smooth surface. The variation of heat and nanoparticle mass transfer rates for various values of the angle of inclination A is displayed in Figs. 2.8(c) and 2.8(d). It is found that increasing the angle of inclination increases the buoyancy force and assist the flow, leading to an increase in the heat and nanoparticle mass transfer rates. The maximum values of the dimensionless heat and nanoparticle mass transfer rates are observed when the surface is vertical; in which case, the buoyancy force is at its maximum.

Fig. 2.9 displays the effect of Brownian motion and thermophoresis parameters on the heat and nanoparticle mass transfer rates. Fig. 2.9(a) depicts that the dimensionless heat transfer rate decreases with increase in the Browinian motion parameter. An increase in the value of Brownian motion parameter enhances the nanoparticle volume fraction transfer rate, as shown in Fig. 2.9(b). It is seen from Fig. 2.9(c) that the heat transfer rate decreases with increase in the thermophoresis parameter. The effect of thermophoresis number on nanoparticle mass transfer is to increase the nanoparticle Sherwood number which can be seen from Fig. 2.9(d).

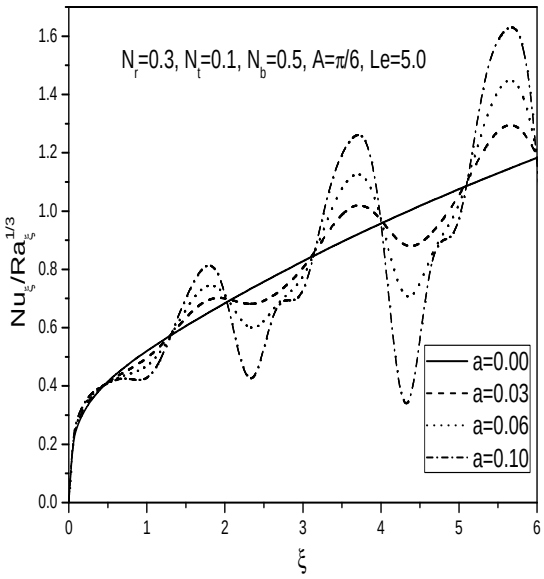

(a)

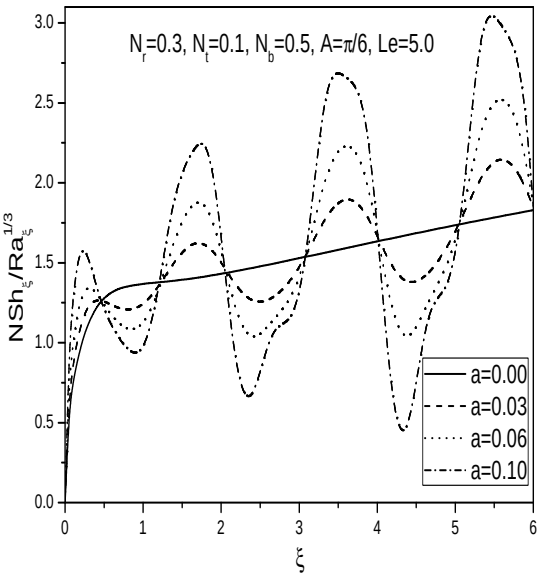

(b)

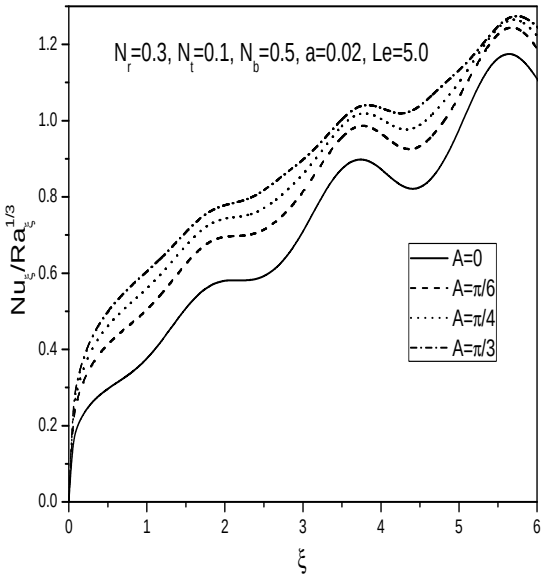

(c)

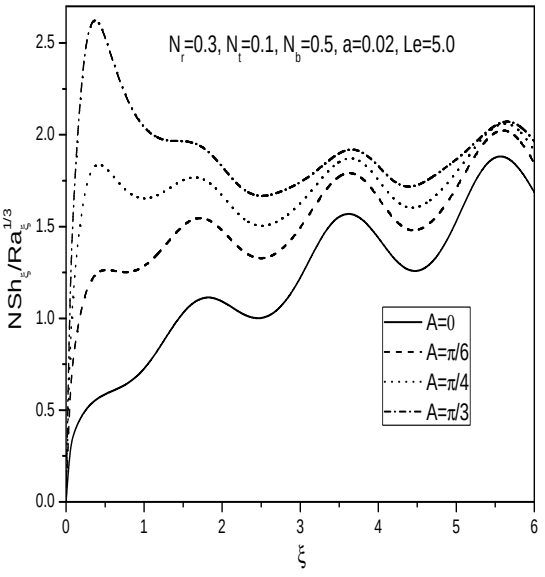

(d)

Figure 2.8: Variation of (a) heat, (b) nanoparticle mass transfer coefficients with wave amplitude a and (c) heat, (d)nanoparticle mass transfer coefficients with angle of inclination A.

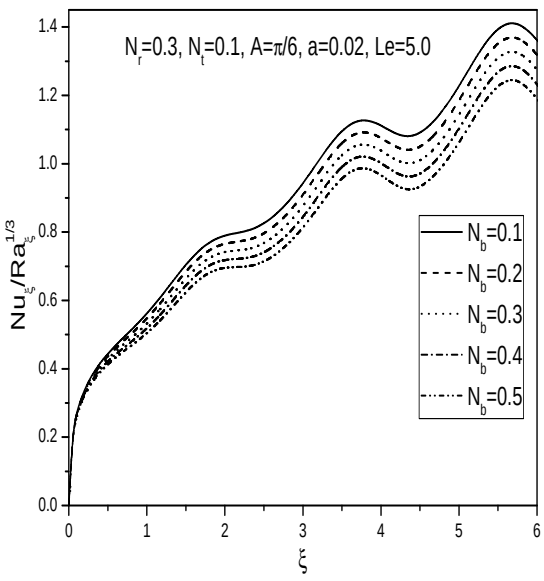

(a)

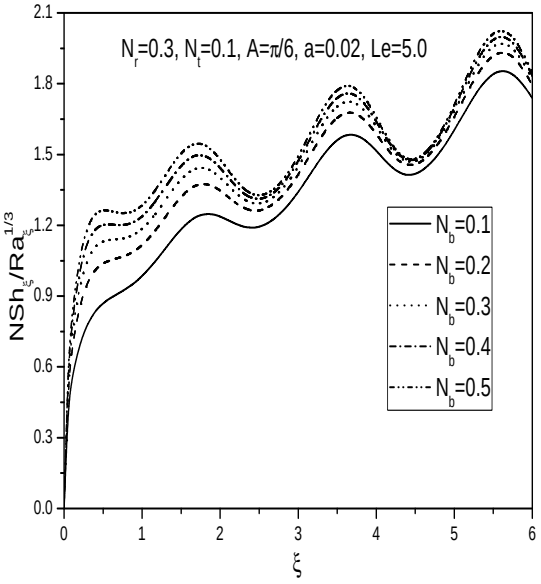

(b)

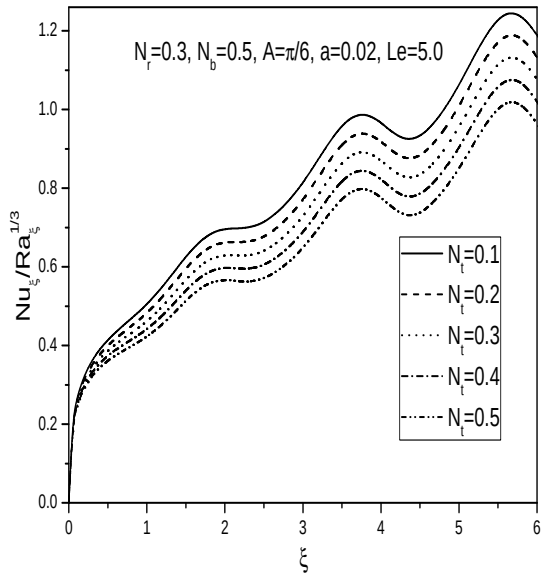

(c)

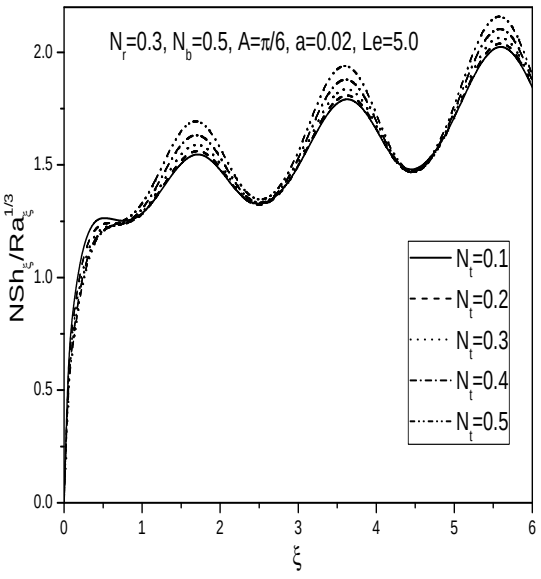

(d)

Figure 2.9: Variation of (a) heat, (b) nanoparticle mass transfer coefficients with Brownian motion parameter N_b and (c) heat, (d)nanoparticle mass transfer coefficients with thermophoresis parameter N_t.

2.3 Conclusions

In this chapter, we studied the problem of natural convection heat and nanoparticle mass transfer over an inclined wavy surface embedded in a porous medium saturated with nanofluid with (a) uniform wall temperature and nanoparticle volume fraction conditions and (b)uniform and constant heat and nanoparticle mass flux conditions. From this analysis, the following conclusions can be drawn for both the cases (a) and (b):

An increase in the Brownian motion parameter N_b, increases the velocity, temperature and local nanoparticle mass transfer coefficient but reduces the nanoparticle volume fraction and local heat transfer coefficient. A higher value of the thermoporesis parameter N_t leads to higher velocity, temperature and nanoparticle volume fraction but lower local heat transfer coefficient and no effect is seen on nanoparticle mass transfer coefficient. The effect of the amplitude of the wavy surface is to reduce the local heat transfer and local nanoparticle mass transfer coefficients for case (a) but enhances in case (b). The influence of the angle of inclination of the wavy surface to the horizontal is to enhance the velocity and local heat and nanoparticle mass transfer rate but to reduce the temperature and nanoparticle volume fraction of the fluid.

Chapter 3

Mixed convection over an inclined wavy surface in a nanofluid saturated porous medium [1]

3.1 Introduction

Mixed convective heat and mass transfer problems are used in a wide range of industrial and engineering applications that include heat exchangers, nuclear reactors, thermal insulation systems, electronic device cooling, oil separation from sand by steam, packed bed chemical reactors, underground disposal of nuclear waste materials and food storage. Several authors studied the mixed convective transport in the boundary layer flow past different geometries submerged in a porous medium subject to various effects ([70, 41, 67, 14, 80, 90, 103]).

Conventional heat transfer fluids such as water and oil are poor heat transfer fluids. So as to improve the thermal conductivity of these fluids, nanosized particles are being suspended in them. Nanofluids are used in the production of nano structured materials for cleaning

[1] Case(a):Published in "**International Journal of Numerical Methods for Heat and Fluid Flow, 25(8) (2015) 1774–1792**",
Case(b) Published in "**Journal of Nanofluids**" 5(1) (2016) 120–129

oil from surfaces due to their exceptional wetting and spreading behavior. Nanofluids are used as coolant in heat exchangers, electronic cooling system (flat plate) and radiators. Moreover, the study of heat transfer from irregular surfaces (wavy surfaces) is a problem of fundamental importance. Irregularities in surfaces occur in many practical situations which enhances the heat transfer characteristics. These irregularities encounter in several heat transfer devices such as microelectronic devices, flat plate solar collectors and flat plate condensers in refrigerators.

In this chapter we consider the mixed convective heat and nanoparticle mass transfer over an inclined wavy surface in a nanofluid saturated porous medium for both the cases of aiding and opposing flows. The presence of Brownian motion and thermophoresis effects is taken into account. The influence of pertinent parameters on physical quantities for both aiding and opposing flows are examined numerically and shown through graphs.

3.2 Mathematical Formulation

Consider the steady laminar incompressible mixed convective two-dimensional boundary layer flow along a semi-infinite inclined wavy surface embedded in a nanofluid saturated Darcy porous medium with uniform stream U_∞ in the ambient medium. The wavy plate is inclined at an angle A ($0^o \leq A \leq 90^o$) to the horizontal. Choose the coordinate system so that x-axis is along the wavy plate and y-axis is normal to the plate. The physical model and coordinate system are as shown in 2.1.

Using the same assumptions made in chapter-2, the governing equations of the flow are

$$\frac{\partial u}{\partial x} + \frac{\partial v}{\partial y} = 0, \tag{3.1}$$

$$\begin{aligned}\frac{\partial u}{\partial y} - \frac{\partial v}{\partial x} = &\frac{(1-\phi_\infty)\rho_{f_\infty}\beta\, K\, g}{\mu}\left(\frac{\partial T}{\partial y}\sin A - \frac{\partial T}{\partial x}\cos A\right)\\ &-\frac{(\rho_p - \rho_{f_\infty})\, K\, g}{\mu}\left(\frac{\partial \phi}{\partial y}\sin A - \frac{\partial \phi}{\partial x}\cos A\right),\end{aligned} \tag{3.2}$$

$$u\frac{\partial T}{\partial x}+v\frac{\partial T}{\partial y}=\alpha\left(\frac{\partial^2 T}{\partial x^2}+\frac{\partial^2 T}{\partial y^2}\right)+\gamma\left[D_B\left(\frac{\partial\phi}{\partial x}\frac{\partial T}{\partial x}+\frac{\partial\phi}{\partial y}\frac{\partial T}{\partial y}\right)+\frac{D_T}{T_\infty}\left(\left(\frac{\partial T}{\partial x}\right)^2+\left(\frac{\partial T}{\partial y}\right)^2\right)\right], \tag{3.3}$$

$$u\frac{\partial\phi}{\partial x}+v\frac{\partial\phi}{\partial y}=D_B\left(\frac{\partial^2\phi}{\partial x^2}+\frac{\partial^2\phi}{\partial y^2}\right)+\frac{D_T}{T_\infty}\left(\frac{\partial^2 T}{\partial x^2}+\frac{\partial^2 T}{\partial y^2}\right), \tag{3.4}$$

In this chapter, we have solved the problem subject to two types of boundary conditions, given in the previous chapter.

3.2.1 Case(a): Uniform Wall Temperature and Nanoparticle Volume Fraction

Let uniform wall temperature T_w and nanoparticle volume fraction ϕ_w are prescribed on the wavy surface. These values are assumed to be greater than the ambient temperature T_∞ and nanoparticle volume fraction ϕ_∞ at any arbitrary reference point in the medium (inside the boundary layer). Hence, the boundary conditions are

$$v=0,\quad T=T_w,\quad \phi=\phi_w,\quad \text{at}\quad y=\delta(x), \tag{3.5a}$$

$$u=U_\infty,\quad T\to T_\infty,\quad \phi\to\phi_\infty\quad \text{as}\quad y\to\infty, \tag{3.5b}$$

where the subscripts w, and ∞ indicate the conditions at the wall and at the outer edge of the boundary layer respectively.

Introducing the stream function ψ in Eqns. (3.2) - (3.4) and then using the following

non-dimensional variables

$$\left.\begin{aligned} \xi = \tfrac{x}{L}, \quad \eta = \frac{(y/l-\delta)\,Pe^{1/2}}{\xi^{1/2}\,(1+\dot{\delta}^2)}, \quad \psi = U_\infty l Pe^{-1/2}\xi^{1/2} f(\eta), \\ \theta = \frac{T-T_\infty}{T_w-T_\infty}, \\ s = \frac{\phi-\phi_\infty}{\phi_w-\phi_\infty}, \end{aligned}\right\} \tag{3.6}$$

we obtain the following system of ordinary differential equations

$$f'' = \Delta(\sin A + \dot{\delta}\cos A)\,(\theta' - N_r s')\,, \tag{3.7}$$

$$\theta'' + \frac{1}{2} f\theta' + N_b s'\theta' + N_t \theta'^2 = 0, \tag{3.8}$$

$$s'' + \frac{1}{2} Le f s' + \frac{N_t}{N_b}\theta'' = 0, \tag{3.9}$$

where $\Delta = \frac{Ra}{Pe}$ is mixed convection parameter, $Pe = \frac{U_\infty L}{\alpha}$ is the Peclet number.

The boundary conditions (3.5) in terms of f, θ and s becomes

$$f = 0, \quad \theta = 1, \quad s = 1, \quad \text{at} \quad \eta = 0, \tag{3.10a}$$

$$f' = 1, \quad \theta \to 0, \quad s \to 0 \quad \text{as} \quad \eta \to \infty. \tag{3.10b}$$

The local Nusselt number and the local nanoparticle Sherwood number are given by

$$\frac{Nu_x}{{Pe_x}^{1/2}} = -\sqrt{\frac{1}{1+\dot{\delta}^2}}\left(\frac{\partial\theta}{\partial\eta}\right)_{\eta=0}, \tag{3.11a}$$

$$\frac{NSh_x}{{Pe_x}^{1/2}} = -\sqrt{\frac{1}{1+\dot{\delta}^2}}\left(\frac{\partial s}{\partial\eta}\right)_{\eta=0}. \tag{3.11b}$$

Method of Solution

The system of Eqns. (3.7) - (3.9) along with the boundary conditions (3.10) were solved numerically using the Successive Linearisation Method (SLM) ([68, 5]). Using this method the non linear boundary layer equations reduce to a system of linear differential equations. The Chebyshev pseudo spectral method is then used to transform the iterative sequence of linearized differential equations into a system of linear algebraic equations which are converted into a matrix system as described in detail in Chapter-2. Proceeding same as in the chapter-2, we obtain the following matrix equation

$$\mathbf{A}_{i-1}\mathbf{X}_i = \mathbf{R}_{i-1}, \tag{3.12}$$

subject to the boundary conditions

$$f_i(\chi_N) = 0, \quad \sum_{k=0}^{N} \mathbf{D}_{0k} f_i(\chi_k) = 0 \tag{3.13}$$

$$\theta_i(\chi_N) = \theta_i(\chi_0) = s_i(\chi_N) = s_i(\chi_0) = 0 \tag{3.14}$$

In Eqn. (3.12), $\mathbf{A}_{i-1}$ is a (3N + 3)×(3N + 3) square matrix and $\mathbf{X}_i$ and $\mathbf{R}_{i-1}$ are (3N + 3)×1 column vectors defined by

$$\mathbf{A}_{i-1} = \begin{bmatrix} A_{11} & A_{12} & A_{13} \\ A_{21} & A_{22} & A_{23} \\ A_{31} & A_{32} & A_{33} \end{bmatrix}, \quad \mathbf{X}_i = \begin{bmatrix} \mathbf{F}_i \\ \mathbf{\Theta}_i \\ \mathbf{\Phi}_i \end{bmatrix}, \quad \mathbf{R}_i = \begin{bmatrix} \mathbf{r}_{1,i-1} \\ \mathbf{r}_{2,i-1} \\ \mathbf{r}_{3,i-1} \end{bmatrix} \tag{3.15}$$

where

$$\mathbf{F}_i = [f_i(\chi_0), f_i(\chi_1), ..., f_i(\chi_{N-1}), f_i(\chi_N)]^T,$$
$$\mathbf{\Theta}_i = [\theta_i(\chi_0), \theta_i(\chi_1), ..., \theta_i(\chi_{N-1}), \theta_i(\chi_N)]^T,$$
$$\mathbf{\Phi}_i = [s_i(\chi_0), s_i(\chi_1), ..., s_i(\chi_{N-1}), s_i(\chi_N)]^T,$$
$$\mathbf{r}_{1,i-1} = [r_{1,i-1}(\chi_0), r_{1,i-1}(\chi_1), ..., r_{1,i-1}(\chi_{N-1}), r_{1,i-1}(\chi_N)]^T$$
$$\mathbf{r}_{2,i-1} = [r_{2,i-1}(\chi_0), r_{2,i-1}(\chi_1), ..., r_{2,i-1}(\chi_{N-1}), r_{2,i-1}(\chi_N)]^T$$
$$\mathbf{r}_{3,i-1} = [r_{3,i-1}(\chi_0), r_{3,i-1}(\chi_1), ..., r_{3,i-1}(\chi_{N-1}), r_{3,i-1}(\chi_N)]^T$$
$$A_{11} = \mathbf{D}^2, \quad A_{12} = a_{1,i-1}\mathbf{D}, \quad A_{13} = a_{2,i-1}\mathbf{D}$$
$$A_{21} = b_{3,i-1}\mathbf{I}, \quad A_{22} = \mathbf{D}^2 + b_{1,i-1}\mathbf{D}, \quad A_{23} = b_{2,i-1}\mathbf{D}$$
$$A_{31} = c_{3,i-1}\mathbf{I}, \quad A_{32} = c_{2,i-1}\mathbf{D}^2, \quad A_{33} = \mathbf{D}^2 + c_{1,i-1}\mathbf{D}$$

Here $\mathbf{I}$ is an identity matrix of size (N +1)×(N +1). After modifying the matrix system (3.12) to incorporate boundary conditions (3.13) - (3.14), the solution is obtained as

$$\mathbf{X}_i = \mathbf{A}_{i-1}^{-1}\mathbf{R}_{i-1} \tag{3.16}$$

Results and Discussion

Solutions for the dimensionless velocity, temperature and nanoparticle volume fraction functions, heat and nanoparticle mass transfer rates for aiding and opposing flows have been computed and displayed graphically in Figs. 3.1 - 3.6. The effects of angle of inclination A, Brownian motion parameter N_b, thermophoresis parameter N_t and amplitude a of the wave surface for both aiding and opposing flows have been discussed.

In order to assess the accuracy of our method, we have compared our results with those of Cheng [23] for fixed values of $a = 0, A = \pi/2, N_r = 0, N_t = 0, Le = 0.0, N_b \to 0$ with the variation of mixed convection parameter Δ for both aiding and opposing flows. The comparison in the above case is found to be in good agreement, as shown in Tables 3.1 and 3.2.

Figure 3.1 depicts the effect of the amplitude of the wavy surface on velocity, temperature and nanoparticle volume fraction distributions. It is observed that as a increases, velocity

Table 3.1: Comparison of $-\theta'(0)$ calculated by the present method and that of Cheng [23] for fixed values of $a = 0, A = \pi/2, N_r = 0, N_t = 0, Le = 0.0, N_b \to 0$ with the variation of mixed convection parameter Δ for the case of aiding flow

	$-\theta'(0)$	
Δ	Cheng [23]	Present
0.0	0.5641	0.56413
0.5	0.6473	0.64733
1.0	0.7205	0.72052
3.0	0.9574	0.95747
10.0	1.516	1.51596
20.0	2.066	2.06615

Table 3.2: Comparison of $-\theta'(0)$ calculated by the present method and that of Cheng [23] for fixed values of $a = 0, A = \pi/2, N_r = 0, N_t = 0, Le = 0.0, N_b \to 0$ with the variation of mixed convection parameter Δ for the case of opposing flow

	$-\theta'(0)$	
Δ	Cheng [23]	Present
-0.2	0.5269	0.52691089
-0.4	0.4865	0.48653284
-0.6	0.442	0.44202064
-0.8	0.3916	0.39166292
-1.0	0.332	0.33202116

increases near the plate and decreases away from the plate in the case of aiding flow while in the case of opposing flow, velocity decreases near the plate and increases away from the plate. But the temperature and nanoparticle volume fraction decrease for aiding flow and increase for opposing flow.

The variation of non-dimensional velocity, temperature and nanoparticle volume fraction profiles with η for different values of angle of inclination A is illustrated in Fig. 3.2. It is observed from Fig. 3.2(a) that the velocity increases near the plate and decreases away from the plate for aiding flow whereas the velocity decreases near the plate and increases away from the plate for opposing flow with increase in the values of the angle of inclination A. From Fig. 3.2(b) and 3.2(c), it is clear that the temperature and nanoparticle volume fraction decrease within the boundary layer region for the aiding flow and increase for opposing flow. When the surface is vertical, the smallest temperature and nanoparticle volume fraction distributions are observed for aiding flow whereas largest temperature and nanoparticle volume fraction distributions are observed for opposing flow. For the horizontal surface, largest temperature and nanoparticle volume fraction distributions are observed for aiding flow whereas smallest temperature and nanoparticle volume fraction distributions are observed for opposing flow.

Figures 3.3 and 3.4 show the distributions of the dimensionless velocity component, temperature and nanoparticle volume fraction for different values of Brownian motion parameter N_b and thermophoresis parameter N_t. It is observed that an increase in the intensity of Brownian motion parameter produces an enhancement in the fluid velocity within the momentum boundary layer thus enhancing the fluid flow in the case of aiding flow but reduces in the case of opposing flow as shown in Fig. 3.3(a). Fig. 3.4(a) depicts that an increase in the thermophoresis parameter tends to increase the maximum stream wise velocity, thus assisting the fluid flow in the case of aiding flow but reduces in the case of opposing flow. Fig. 3.3(b) shows that as the Brownian motion parameter increases, the temperature of the fluid in the boundary layer increases for both aiding and opposing flows. Moreover, the temperature increases in both the cases (i.e. aiding and opposing flows) with an increase in the thermophoresis parameter, as shown in Fig. 3.4(b). Increase in the Brownian motion parameter tends to reduce the nanoparticle volume fraction for both aiding and opposing

flows as shown in Fig. 3.3(c). However, the reverse trend is observed in case of thermophoresis parameter, i.e. an increase in the value of the thermophoresis parameter enhances the nanoparticle volume fraction for both aiding and opposing flows as shown in Fig. 3.4(c).

The effect of wave amplitude a on the local heat and nanoparticle mass transfer is shown in Figs. 3.5(a) and 3.5(b). This figure reveals that an enhancement in wave amplitude causes smaller fluctuations in the heat and nanoparticle transfer rates for both aiding and opposing flows. In general, we conclude that the surface becomes more roughened for increasing values of amplitude of the wavy surface.

The variation of heat and nanoparticle mass transfer rates with the angle of inclination A is displayed in Figs. 3.5(c) and 3.5(d). This figure shows that increasing the angle of inclination increases the buoyancy force and assists the flow, leading to an increase in the heat and nanoparticle mass transfer rates in the case of aiding flow whereas a reverse trend is observed in the case of opposing flow.

Figure 3.6 presents the effects of Brownian motion parameter N_b and thermophoresis parameter N_t on the heat and nanoparticle mass transfer rates. The dimensionless heat transfer rate decreases with increase in the Brownian motion parameter and thermophoresis parameter for both aiding and opposing flows as shown in Figs. 3.6(a) and 3.6(c). An increase in the value of the Brownian motion parameter enhances the nanoparticle mass transfer rate, as shown in Fig. 3.6(b). The effect of thermophoresis number on the nanoparticle mass transfer is negligible as depicted in Fig. 3.6(d).

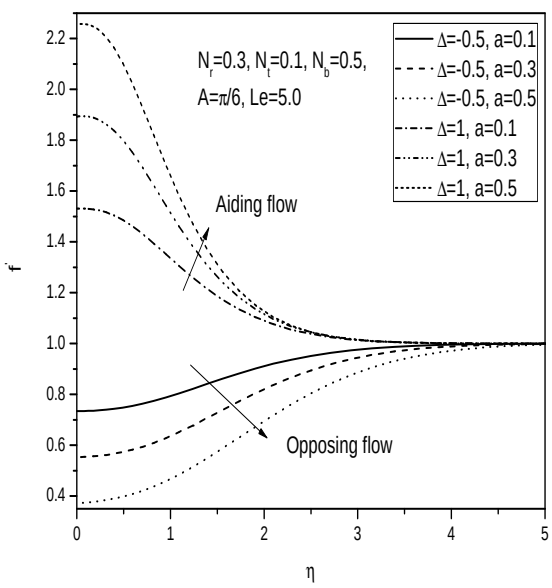

(a)

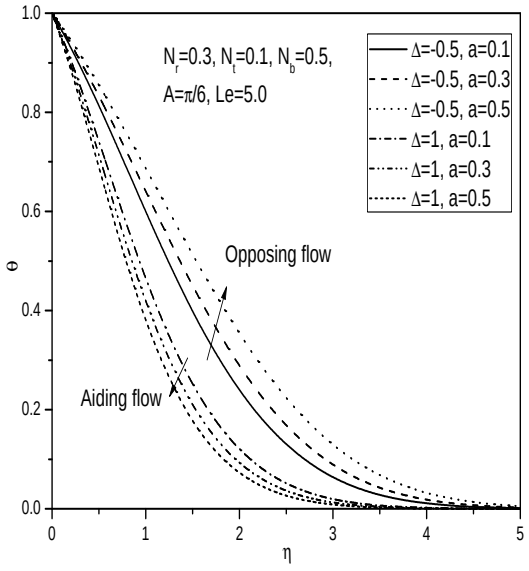

(b)

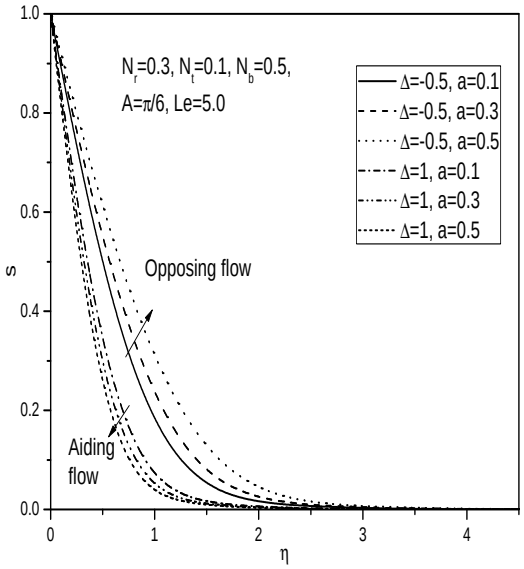

(c)

Figure 3.1: (a) Velocity, (b) temperature and (c) nanoparticle volume fraction profiles for various values of wave amplitude a.

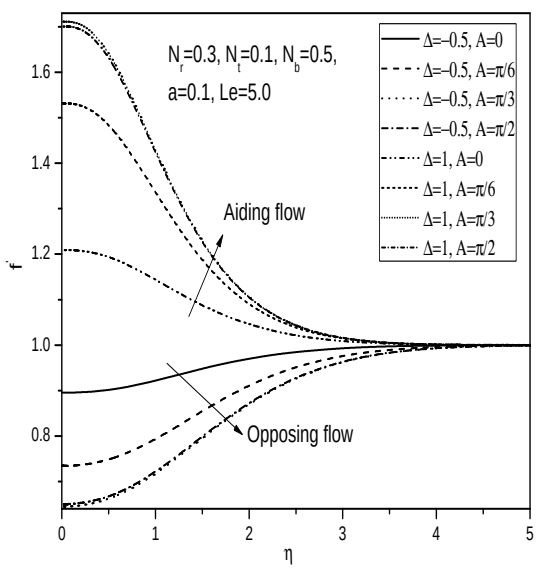

(a)

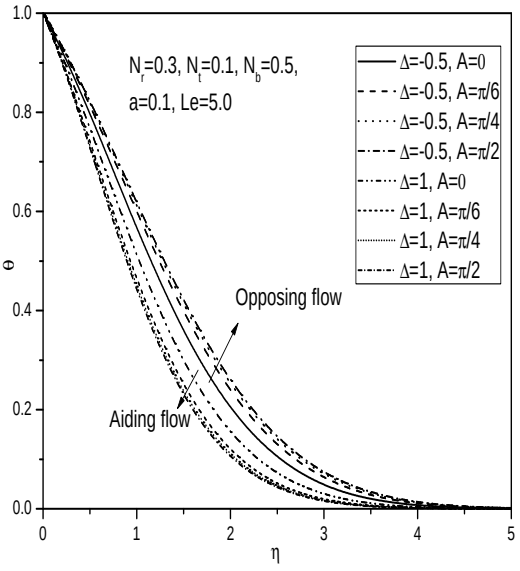

(b)

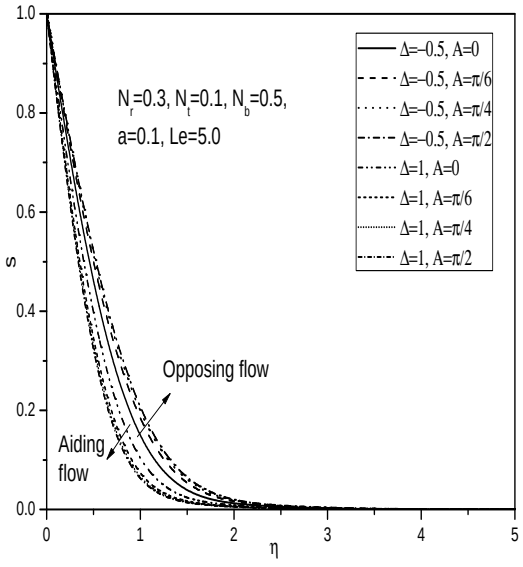

(c)

Figure 3.2: (a) Velocity, (b) temperature and (c) nanoparticle volume fraction profiles for various values of angle of inclination A.

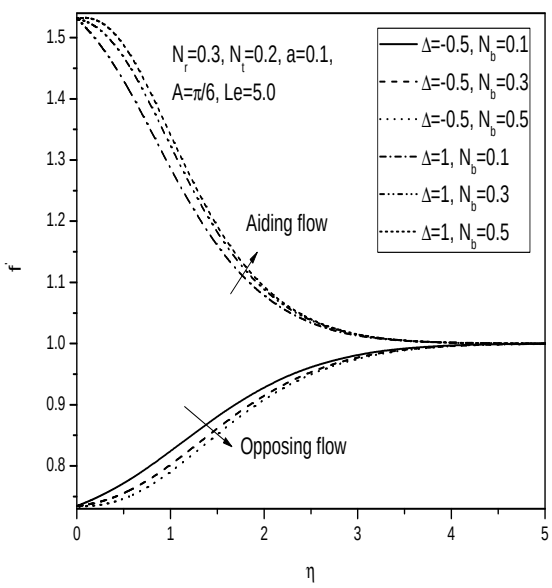

(a)

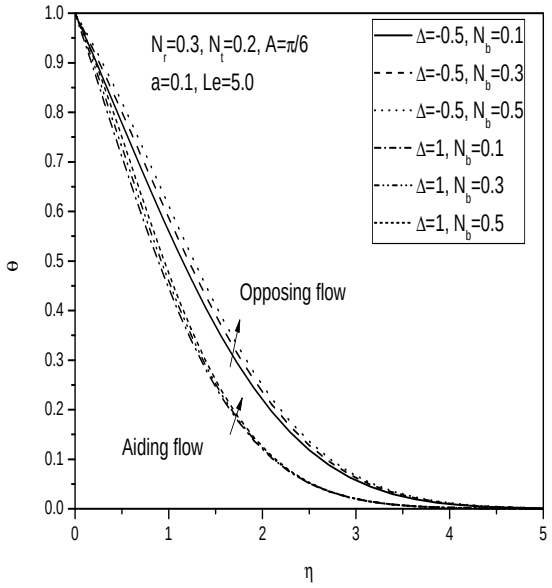

(b)

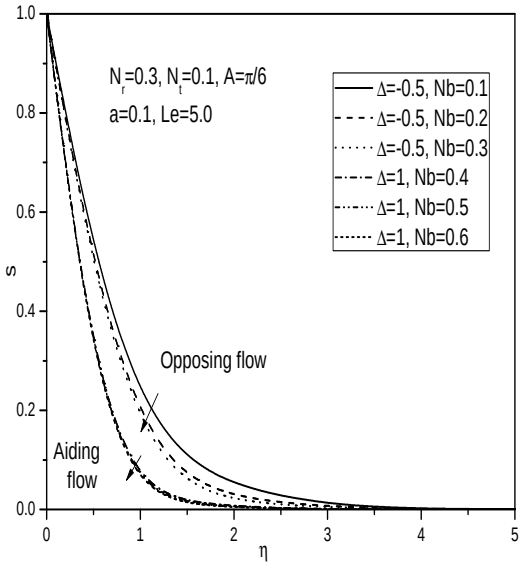

(c)

Figure 3.3: (a) Velocity, (b) temperature and (c) nanoparticle volume fraction profiles for various values of Brownian motion parameter N_b.

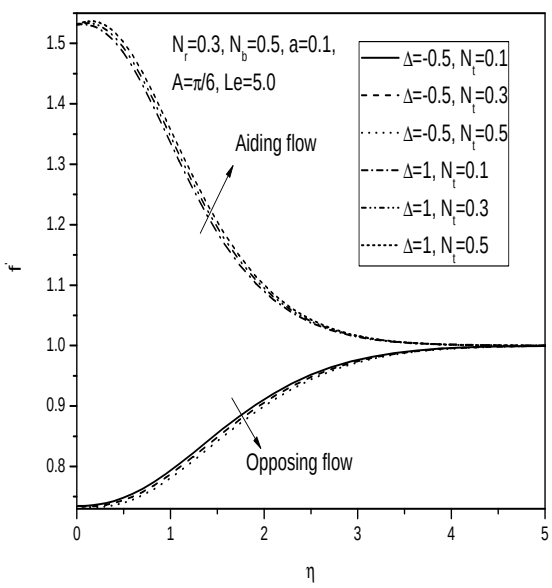

(a)

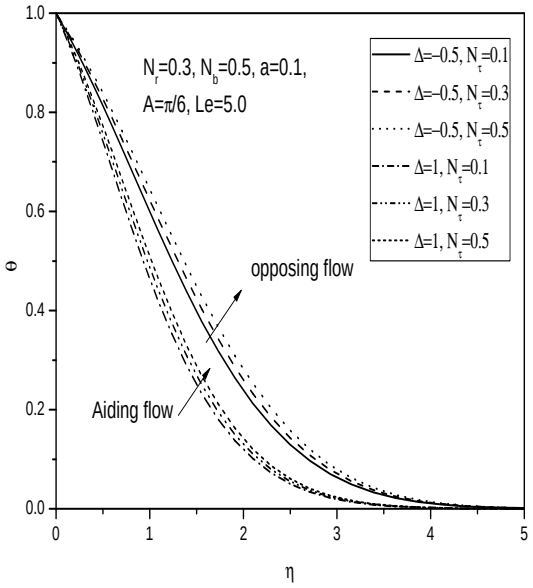

(b)

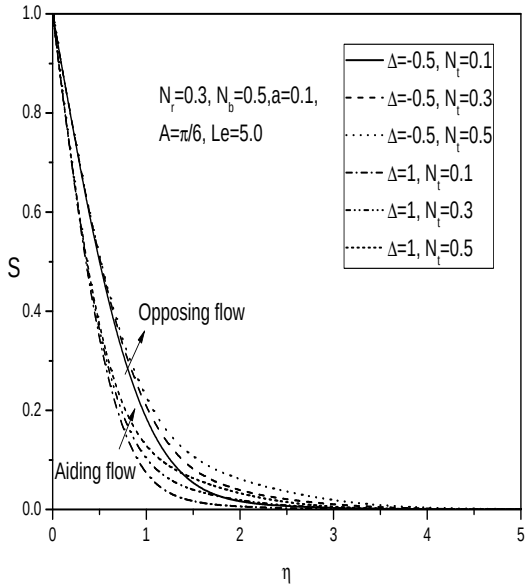

(c)

Figure 3.4: (a) Velocity, (b) temperature and (c) nanoparticle volume fraction profiles for various values of thermophoresis parameter N_t.

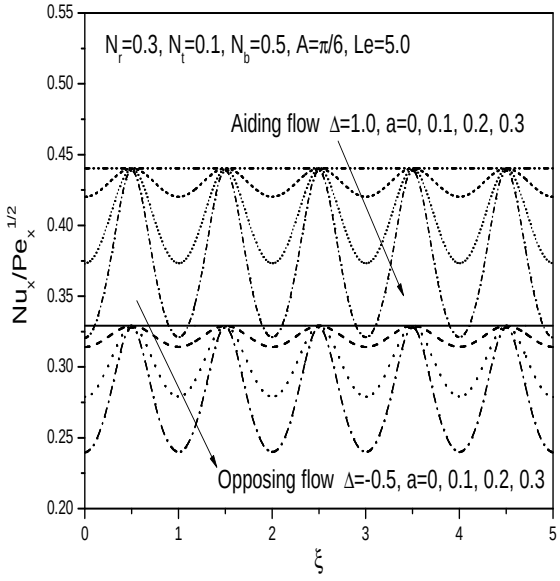

(a)

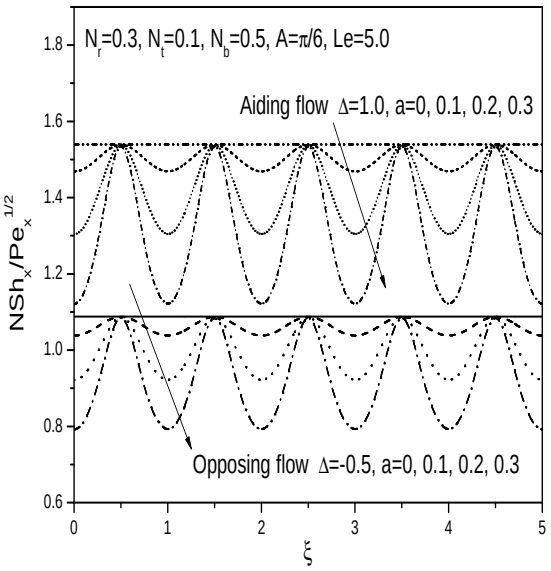

(b)

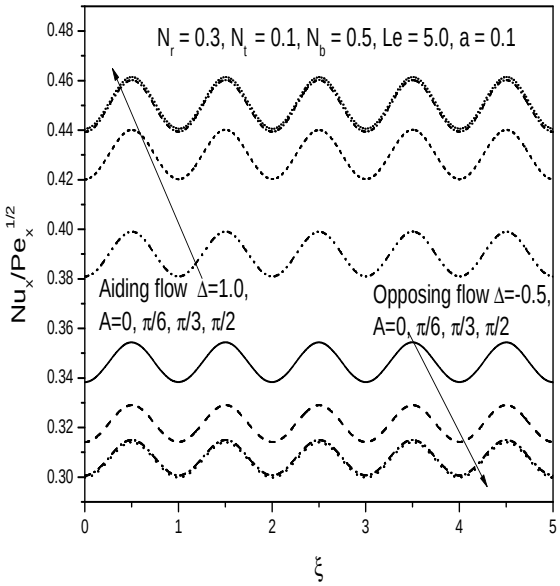

(c)

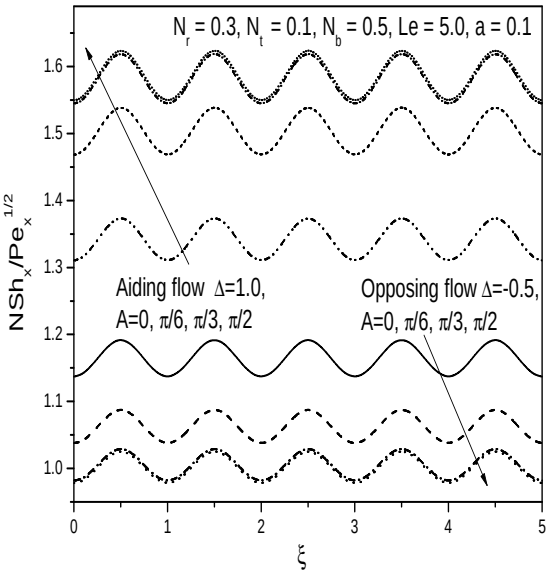

(d)

Figure 3.5: Variation of (a) heat, (b)nanoparticle mass transfer coefficients with wave amplitude a and (c) heat, (d)nanoparticle mass transfer coefficients with angle of inclination A.

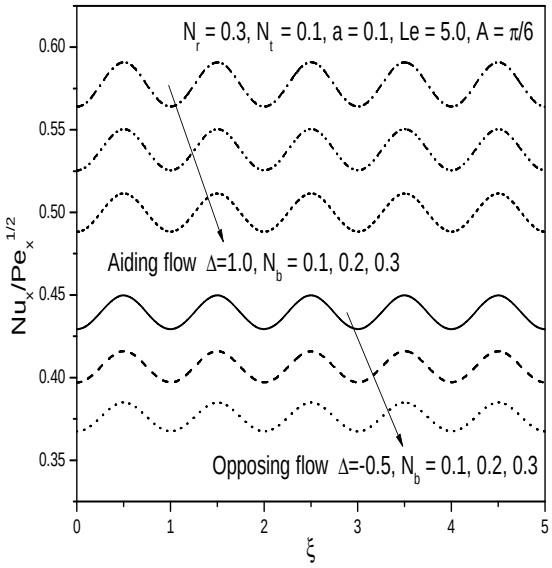

(a)

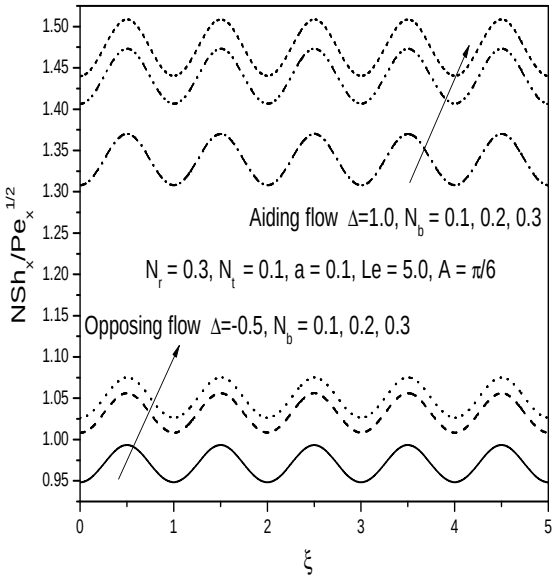

(b)

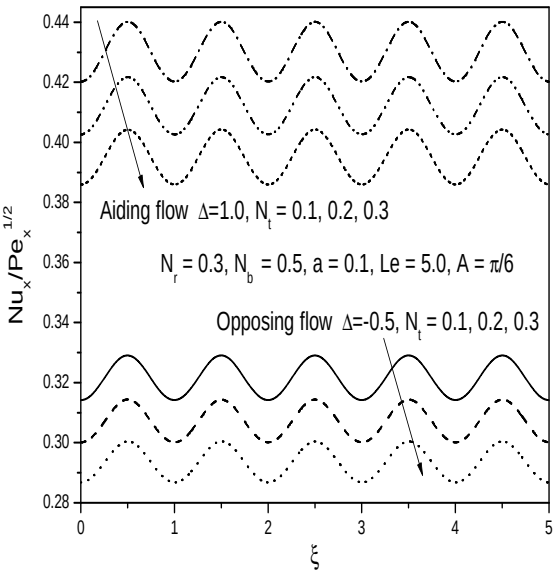

(c)

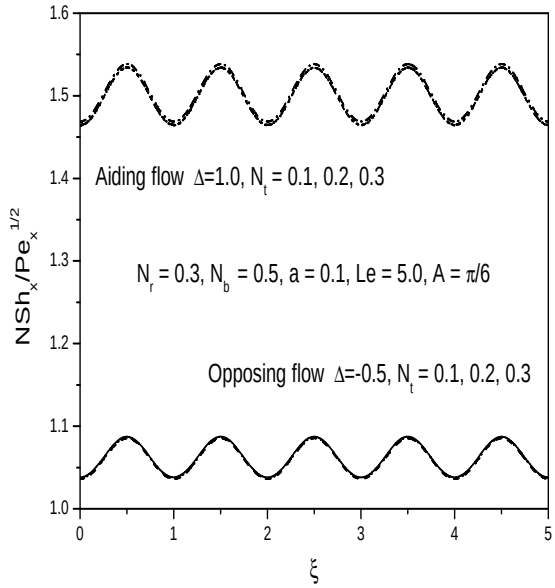

(d)

Figure 3.6: Variation of (a) heat, (b)nanoparticle mass transfer coefficients with Brownian motion parameter N_b and (c) heat, (d)nanoparticle mass transfer coefficients with thermophoresis parameter N_t.

3.2.2 Case(b): Uniform Wall Heat and Nanoparticle Mass Flux

Assume that the plate is maintained at uniform and constant heat and nanoparticle mass fluxes q_w and q_{np} respectively. The steady mixed convection boundary layer flow is governed by Eqs. (3.1) to (3.4) and the boundary conditions are given by

$$v = 0, q_w = -k(n.\nabla T),\ q_{np} = -D_B(n.\nabla\phi) \text{ at } y = 0 \tag{3.17a}$$

$$u = U_\infty,\ T \to T_\infty,\ \phi \to \phi_\infty \text{ as } y \to \infty \tag{3.17b}$$

Substituting the stream function ψ and introducing the following non-dimensional variables in Eqns. (3.1) - (3.4)

$$\left.\begin{aligned} \xi = \tfrac{x}{L}, \quad \eta = \frac{(y/l-\delta)\,Pe^{1/3}}{\xi^{1/3}\,(1+\dot{\delta}^2)}, \quad \psi = U_\infty l\, Pe^{-2/3}\xi^{2/3} f(\xi,\eta), \\ T - T_\infty = \frac{q_w\, l}{k}\,\xi^{1/3}\,Pe^{-1/3}\,\theta(\xi,\eta), \quad \phi - \phi_\infty = \frac{q_{np}\, l}{D_B}\,\xi^{1/3}\,Pe^{-1/3}\,s(\xi,\eta), \end{aligned}\right\} \tag{3.18}$$

we get the following system of non-linear partial differential equations

$$f''' = \Delta\left(\sin A + \dot{\delta}\cos A\right)\left(\theta' - N_r s'\right), \tag{3.19}$$

$$\theta'' + \frac{2}{3} f\theta' - \frac{1}{3} f'\theta + \xi^{1/3}\, N_b s'\theta' + \xi^{1/3}\, N_t \theta'^2 = \xi\left(f'\frac{\partial\theta}{\partial\xi} - \theta'\frac{\partial f}{\partial\xi}\right), \tag{3.20}$$

$$s'' + \frac{2}{3} Le\, f\, s' - \frac{1}{3} Le\, f'\, s + \frac{N_t}{N_b}\theta'' = Le\xi\left(f'\frac{\partial s}{\partial\xi} - s'\frac{\partial f}{\partial\xi}\right), \tag{3.21}$$

The boundary conditions (3.17) in terms of f, θ and s becomes

$$2f + 3\xi\left(\frac{\partial f}{\partial\xi}\right)_{\eta=0} = 0, \quad \theta' = -\sqrt{1+\dot{\delta}^2}, \quad \phi' = -\sqrt{1+\dot{\delta}^2}, \tag{3.22a}$$

$$f' \to 1, \quad \theta \to 0, \quad \phi \to 0. \tag{3.22b}$$

The non-dimensional local Nusselt number Nu_ξ and the local nanoparticle Sherwood number

NSh_ξ are given by

$$\frac{Nu_\xi}{{Pe_\xi}^{1/3}} = \frac{\xi^{1/3}}{\theta(\xi,0)}, \tag{3.23a}$$

$$\frac{NSh_\xi}{{Pe_\xi}^{1/3}} = \frac{\xi^{1/3}}{s(\xi,0)}. \tag{3.23b}$$

Method of Solution

To solve the system of Eqns. (3.19) - (3.21) along with the boundary conditions (3.22), a local similarity and non-similarity method [24, 100] has been applied. The boundary value problems obtained from this method are linearized by the Successive Linearisation Method and then solved using Chebyshev spectral collocation method as explained in detail in chapter-2. Proceeding same as in chapter-2, we obtain the following matrix equation

$$\mathbf{A}_{i-1}\mathbf{X}_i = \mathbf{R}_{i-1}, \tag{3.24}$$

In Eqn. (3.24), $\mathbf{A}_{i-1}$ is a (6N + 6)×(6N + 6) square matrix and $\mathbf{X}_i$ and $\mathbf{R}_{i-1}$ are (6N + 6)×1 column vectors defined by

$$\mathbf{A}_{i-1} = \begin{bmatrix} A_{11} & A_{12} & A_{13} & A_{14} & A_{15} & A_{16} \\ A_{21} & A_{22} & A_{23} & A_{24} & A_{25} & A_{26} \\ A_{31} & A_{32} & A_{33} & A_{34} & A_{35} & A_{36} \\ A_{41} & A_{42} & A_{43} & A_{44} & A_{45} & A_{46} \\ A_{51} & A_{52} & A_{53} & A_{54} & A_{55} & A_{56} \\ A_{61} & A_{62} & A_{63} & A_{64} & A_{65} & A_{66} \end{bmatrix}, \quad \mathbf{X}_i = \begin{bmatrix} \mathbf{F}_i \\ \boldsymbol{\Theta_i} \\ \boldsymbol{\Phi_i} \\ \mathbf{G}_i \\ \mathbf{H}_i \\ \mathbf{K}_i \end{bmatrix}, \quad \mathbf{R}_{i-1} = \begin{bmatrix} \mathbf{r}_{1,i-1} \\ \mathbf{r}_{2,i-1} \\ \mathbf{r}_{3,i-1} \\ \mathbf{r}_{4,i-1} \\ \mathbf{r}_{5,i-1} \\ \mathbf{r}_{6,i-1} \end{bmatrix} \tag{3.25}$$

where

$$\mathbf{F}_i = [f_i(\chi_0), f_i(\chi_1), ..., f_i(\chi_{N-1}), f_i(\chi_N)]^T,\ \mathbf{\Theta_i} = [\theta_i(\chi_0), \theta_i(\chi_1), ..., \theta_i(\chi_{N-1}), \theta_i(\chi_N)]^T,$$
$$\mathbf{\Phi_i} = [s_i(\chi_0), s_i(\chi_1), ..., s_i(\chi_{N-1}), s_i(\chi_N)]^T,\ \mathbf{G}_i = [g_i(\chi_0), g_i(\chi_1), ..., g_i(\chi_{N-1}), g_i(\chi_N)]^T,$$
$$\mathbf{H}_i = [h_i(\chi_0), h_i(\chi_1), ..., h_i(\chi_{N-1}), h_i(\chi_N)]^T,\ \mathbf{K}_i = [k_i(\chi_0), k_i(\chi_1), ..., k_i(\chi_{N-1}), k_i(\chi_N)]^T,$$
$$\mathbf{r}_{j,i-1} = [r_{j,i-1}(\chi_0), r_{j,i-1}(\chi_1), \cdots, r_{j,i-1}(\chi_{N-1}), r_{j,i-1}(\chi_N)]^T, j = 1, 2, 3, 4, 5, 6$$
$$A_{11} = \mathbf{D}^2,\ A_{12} = a_{1,i-1}\mathbf{D},\ A_{13} = a_{2,i-1}\mathbf{D},\ A_{14} = \mathbf{0},\ A_{15} = \mathbf{0},\ A_{16} = \mathbf{0}$$
$$A_{21} = b_{3,i-1}\mathbf{D} + b_{4,i-1}\mathbf{I},\ A_{22} = \mathbf{D}^2 + b_{1,i-1}\mathbf{D} + b_{2,i-1}\mathbf{I},\ A_{23} = b_{5,i-1}\mathbf{D},\ A_{24} = b_{6,i-1}\mathbf{I},$$
$$A_{25} = b_{7,i-1}\mathbf{I},\ A_{26} = \mathbf{0},\ A_{31} = c_{3,i-1}\mathbf{D} + c_{4,i-1}\mathbf{I},\ A_{32} = c_{5,i-1}\mathbf{D}^2,$$
$$A_{33} = \mathbf{D}^2 + c_{1,i-1}\mathbf{D} + c_{2,i-1}\mathbf{I},\ A_{34} = c_{6,i-1}\mathbf{I},\ A_{35} = \mathbf{0},\ A_{36} = c_{7,i-1}\mathbf{I},\ A_{41} = \mathbf{0},$$
$$A_{42} = d_{1,i-1}\mathbf{D},\ A_{43} = d_{2,i-1}\mathbf{D},\ A_{44} = \mathbf{D}^2,\ A_{45} = d_{3,i-1}\mathbf{D},\ A_{46} = d_{4,i-1}\mathbf{D},$$
$$A_{51} = l_{3,i-1}\mathbf{D} + l_{4,i-1}\mathbf{I},\ A_{52} = l_{5,i-1}\mathbf{D} + l_{6,i-1}\mathbf{I},\ A_{53} = l_{7,i-1}\mathbf{D}$$
$$A_{54} = l_{8,i-1}\mathbf{D} + l_{9,i-1}\mathbf{I},\ A_{55} = \mathbf{D}^2 + l_{1,i-1}\mathbf{D} + l_{2,i-1}\mathbf{I},\ A_{56} = l_{10,i-1}\mathbf{D},$$
$$A_{61} = m_{3,i-1}\mathbf{D} + m_{4,i-1}I,\ A_{62} = \mathbf{0},\ A_{63} = m_{5,i-1}\mathbf{D} + m_{6,i-1}\mathbf{I}$$
$$A_{64} = m_{7,i-1}\mathbf{D} + m_{8,i-1}\mathbf{I},\ A_{65} = m_{9,i-1}\mathbf{D}^2,\ A_{66} = \mathbf{D}^2 + m_{1,i-1}\mathbf{D} + m_{2,i-1}\mathbf{I}$$

Here $\mathbf{I}$ is an identity matrix of size (N +1)×(N +1). After modifying the matrix system (3.24) to incorporate boundary conditions, the solution is obtained as

$$\mathbf{X}_i = \mathbf{A}_{i-1}^{-1}\mathbf{R}_{i-1} \tag{3.26}$$

Results and Discussion

The numerical solution for dimensionless velocity, temperature and nanoparticle volume fraction functions and heat and nanoparticle mass transfer rates are computed and presented graphically for both aiding and opposing flows in Figs. 3.7 - 3.18. The effects of angle of inclination A, Brownian motion parameter N_b, thermophoresis parameter N_t and amplitude a of the wavy surface on the flow, heat and nanoparticle mass transfer rates have been discussed.

The effect of amplitude a of the wavy surface on the velocity, temperature and nanopar-

ticle volume fraction for both aiding and opposing flows respectively are plotted in Fig. 3.7. It is observed that as a increases, velocity increases but the temperature and nanoparticle volume fraction decreases for aiding flow. In contrast, for opposing flow it is observed that the velocity decreases and the temperature and nanoparticle volume fraction of the fluid flow increase.

Figure 3.8 displays the effect of angle of inclination A on the velocity, temperature and nanoparticle volume fraction for both aiding and opposing flows respectively. The equations for the limiting cases of the horizontal and vertical plates are recovered from the transformed equations by setting $A = 0^o$ and $A = 90^o$, respectively. It is noted from Fig. 3.8 that the velocity increases near the plate but the temperature and nanoparticle volume fraction decrease within the boundary layer region for the aiding flow whereas velocity reduces but the temperature and nanoparticle volume fraction increase for opposing flow with increase in the values of angle of inclination.

The dimensionless velocity, temperature, and nanoparticle fraction for different values of Brownian motion parameter and thermophoresis parameter are displayed in Figs. 3.9 and 3.10. It is seen that an increase in the value of Brownian motion parameter increases the fluid velocity within the momentum boundary layer thus enhancing the fluid flow in the case of aiding flow whereas the velocity of the fluid flow decreases in the case of opposing flow, as shown in Fig 3.9(a). Fig 3.10(a) depicts that an increase in the thermophoresis parameter tends to increase the maximum stream wise velocity, thus assisting the fluid flow in the case of aiding flow, while the velocity of the fluid flow decreases in the case of opposing flow. Fig 3.9(b) shows that as the Brownian motion parameter increases, the temperature of the fluid in the boundary layer increases for both aiding and opposing flows. Moreover, the temperature increases in both the cases of aiding and opposing flows with an increase in the thermophoresis parameter, as shown in Fig 3.10(b). Increase in the Brownian motion parameter tends to reduce the nanoparticle volume fraction for both aiding and opposing flows as shown in Fig 3.9(c). An increase in the value of the thermophoresis parameter enhances the nanoparticle volume fraction for both aiding and opposing flows as shown in Fig 3.10(c).

The effect of the wave amplitude on the local Nusselt number $Nu_\xi/Pe_\xi{}^{1/3}$ and nanoparticle Sherwood number $NSh_\xi/Pe_\xi{}^{1/3}$ for both aiding and opposing flows is plotted in Figs 3.11 and 3.12. It is observed that an enhancement in wavy amplitude increases the local heat transfer and nanoparticle mass transfer rates for both aiding and opposing flows.

The variation of heat and nanoparticle mass transfer rates for various values of the angle of inclination A is displayed in Figs. 3.13 and 3.14. It is noticed that increasing the angle of inclination increases the buoyancy force and assists the flow, leading to an increase in the heat and nanoparticle mass transfer rates in the case of aiding flow whereas a reverse trend is seen in the case of opposing flow. The minimum value of the dimensionless heat transfer rate is observed when the surface is vertical.

The effect of Brownian motion parameter N_b on the heat and nanoparticle mass transfer rates is plotted in Figs. 3.15 and 3.16. It is observed that the local heat transfer rate decreases with increase in the Browinian motion parameter N_b for both aiding and opposing flows as shown in Fig. 3.15. Increasing the Brownian motion parameter enhances the nanoparticle mass transfer rate for both aiding and opposing flows as shown in Fig. 3.16

Figures 3.17 and 3.18 display the effect of local Nusselt number $Nu_\xi/Pe_\xi{}^{1/3}$ and nanoparticle Sherwood number $NSh_\xi/Pe_\xi{}^{1/3}$ on the thermophoresis parameter N_t for both aiding and opposing flows. It is seen that the heat and nanoparticle mass transfer rates decrease with increase in the value of thermophoresis parameter N_t for both aiding and opposing flows. Brownian motion is proportional to the volumetric fraction of nanoparticles in the direction from high to low concentration, whereas the thermophoresis is proportional to the temperature gradient from hot to cold. Hence, we conclude that the effect of the combination of Brownian motion and thermophoresis is to reduce the rate of heat transfer.

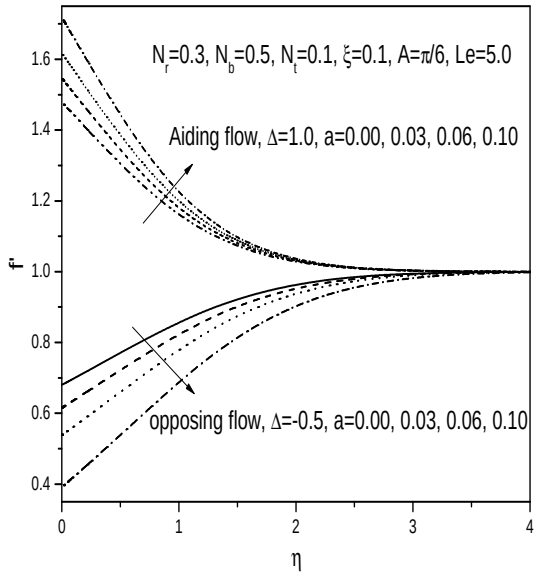

(a)

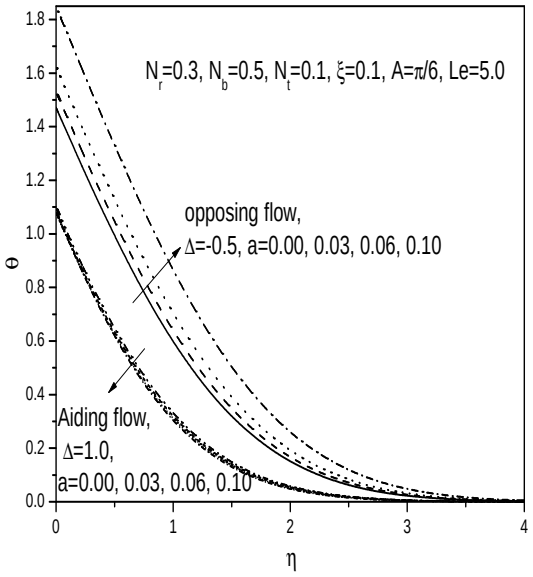

(b)

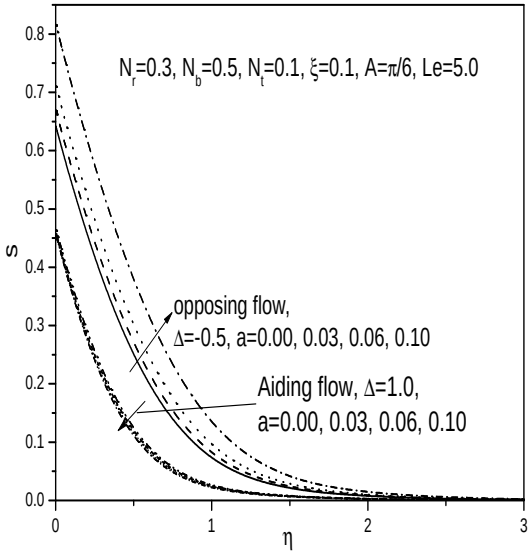

(c)

Figure 3.7: (a) Velocity, (b) temperature and (c) nanoparticle volume fraction profiles for various values of wave amplitude a.

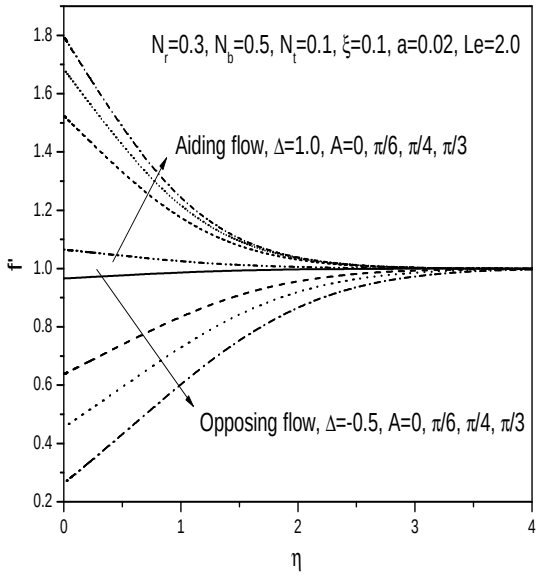

(a)

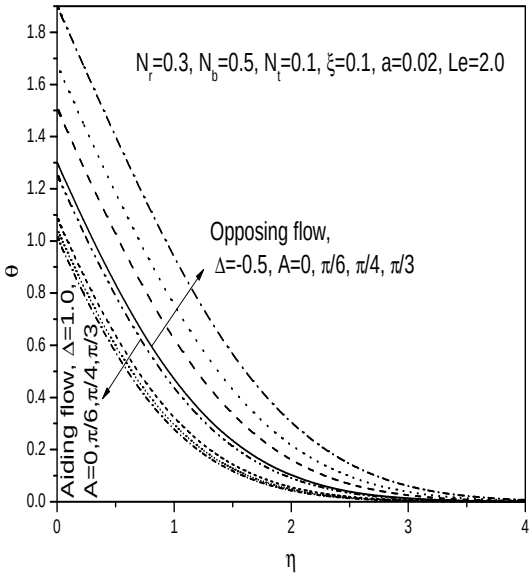

(b)

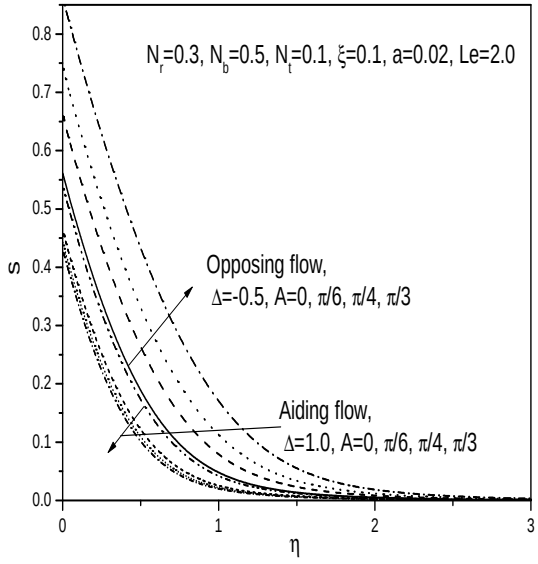

(c)

Figure 3.8: (a) Velocity, (b) temperature and (c) nanoparticle volume fraction profiles for various values of angle of inclination A.

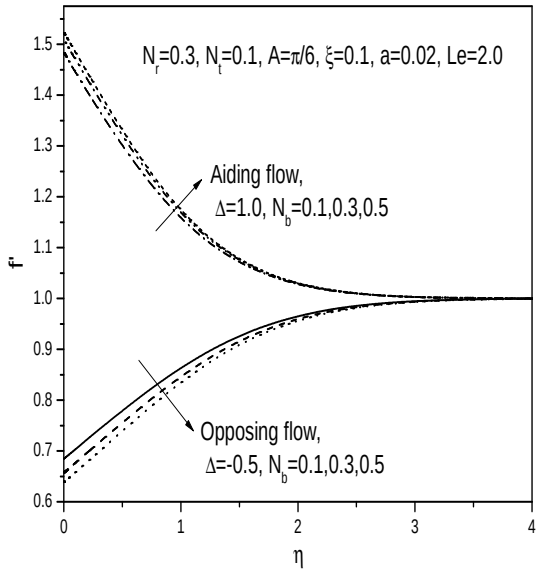

(a)

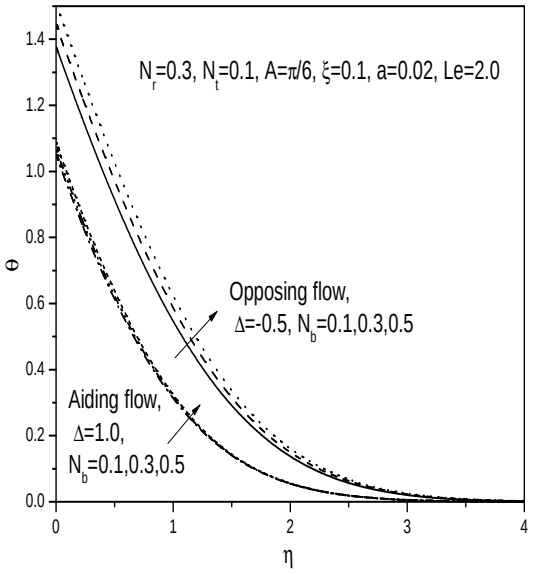

(b)

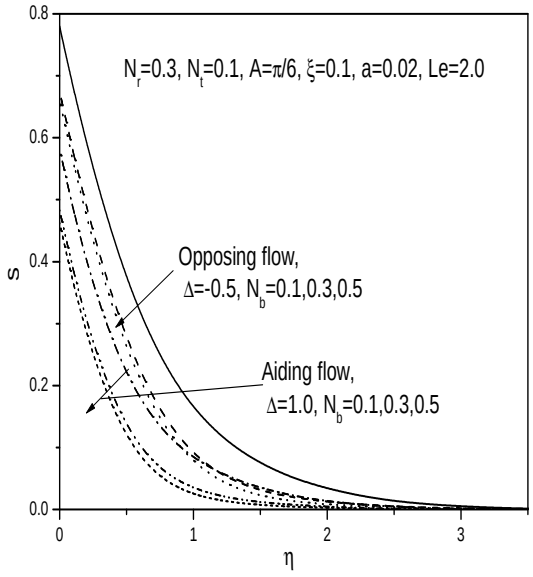

(c)

Figure 3.9: (a) Velocity, (b) temperature and (c) nanoparticle volume fraction profiles for various values of Brownian motion parameter N_b.

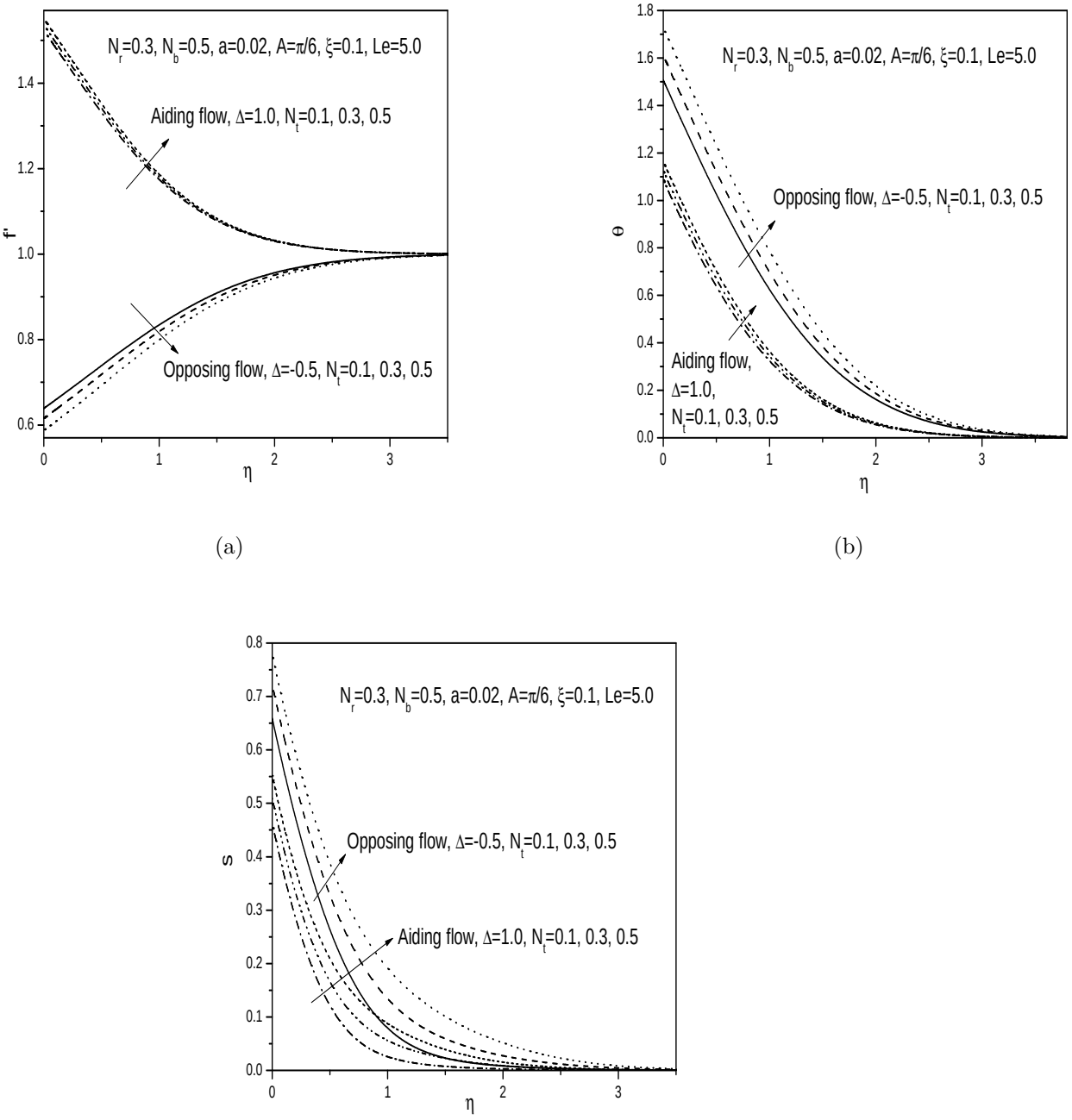

Figure 3.10: (a) Velocity, (b) temperature and (c) nanoparticle volume fraction profiles for various values of thermophoresis parameter N_t.

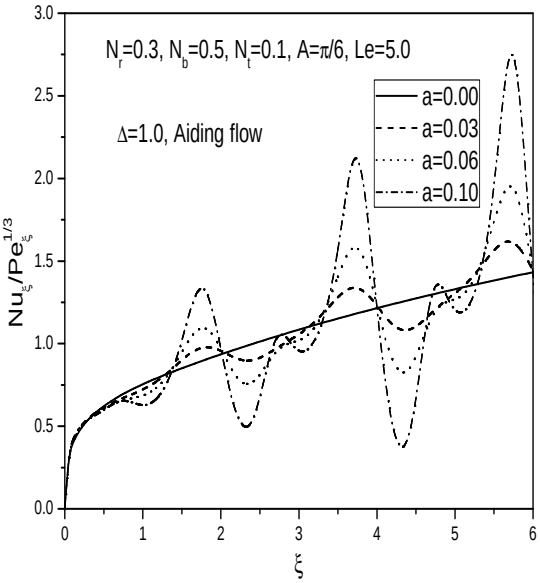

(a)

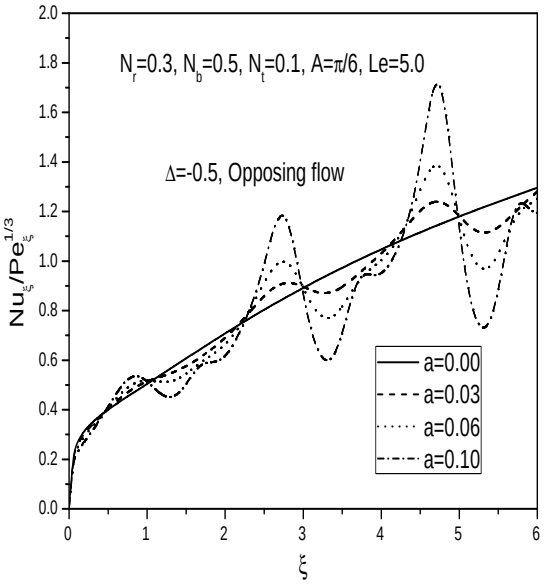

(b)

Figure 3.11: Variation of heat transfer coefficient with wave amplitude a for both (a) Aiding and (b) Opposing flows.

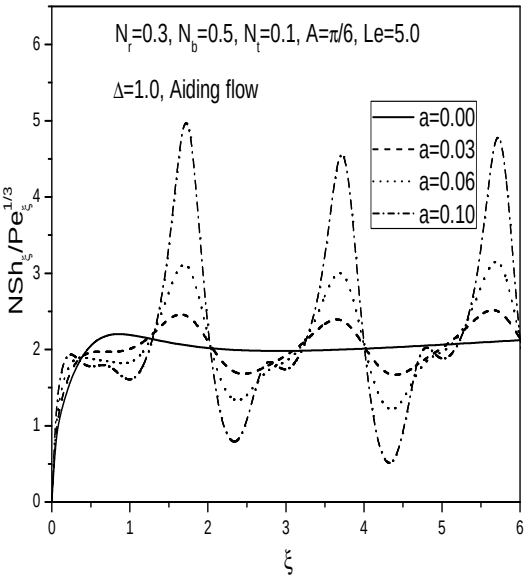

(a)

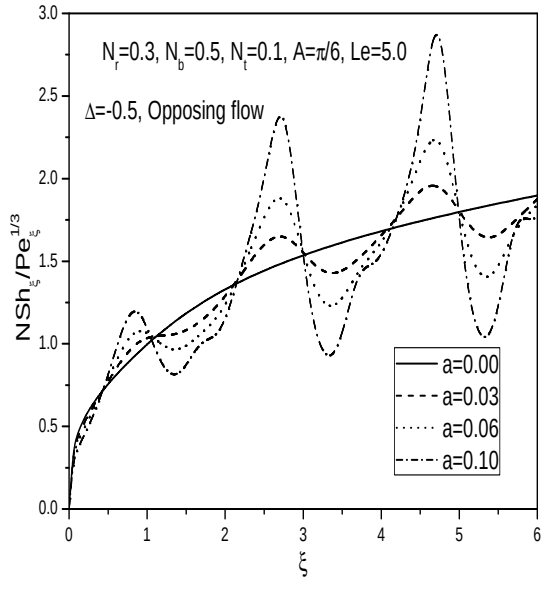

(b)

Figure 3.12: Variation of nanoparticle mass transfer coefficient with wave amplitude a for both (a) Aiding and (b) Opposing flows.

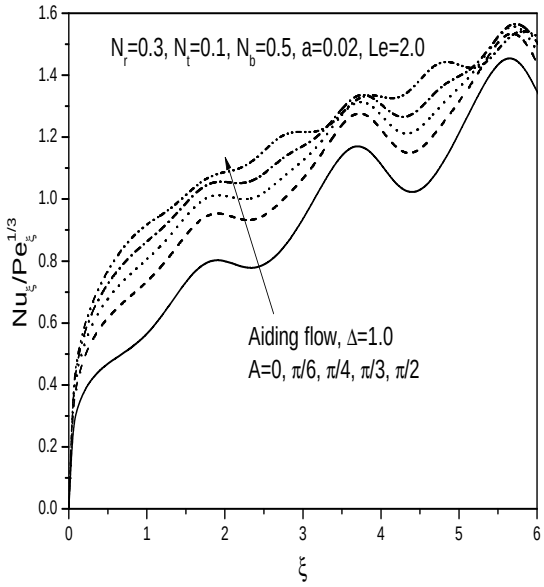

(a)

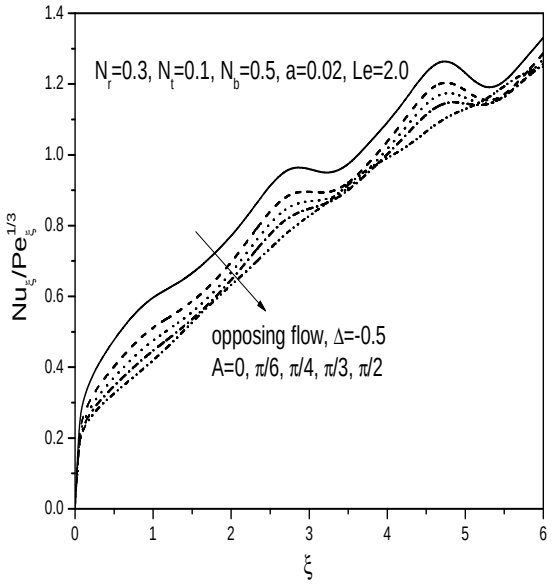

(b)

Figure 3.13: Variation of heat transfer coefficient with angle of inclination A for both (a) Aiding and (b) Opposing flows.

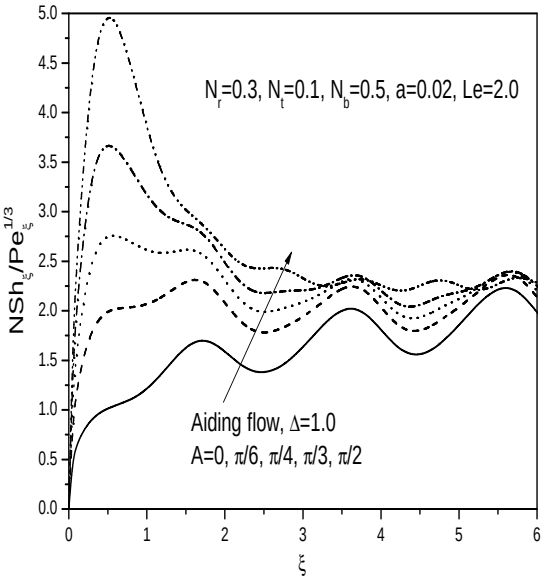

(a)

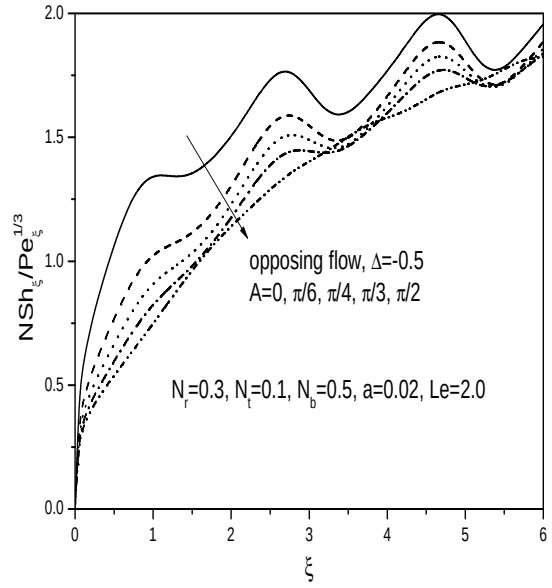

(b)

Figure 3.14: Variation of nanoparticle mass transfer coefficient with angle of inclination A for both (a) Aiding and (b) Opposing flows.

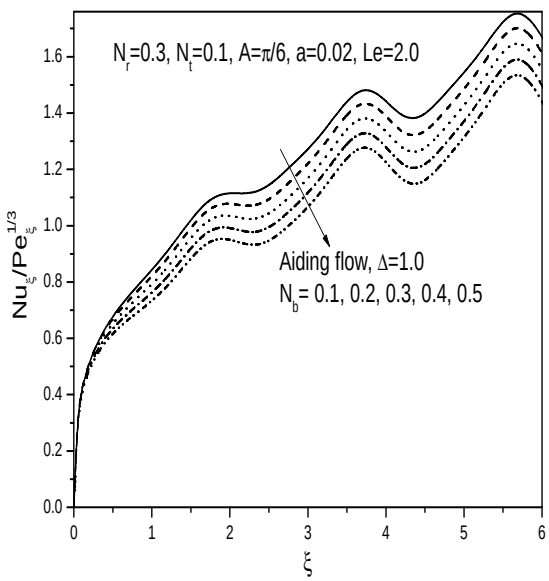

(a)

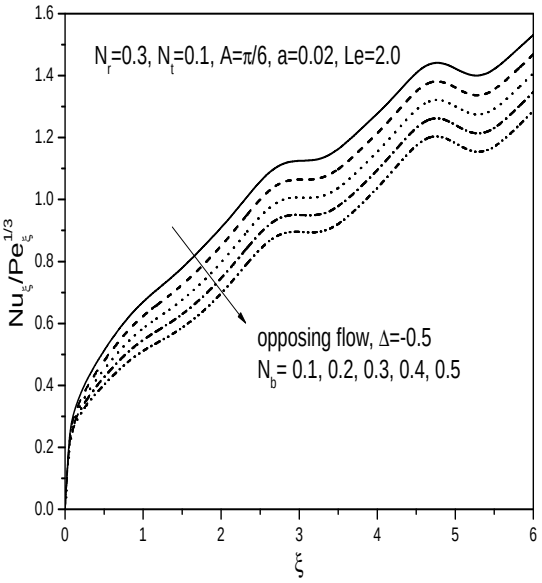

(b)

Figure 3.15: Variation of heat transfer coefficient with Brownian motion Parameter N_b for both (a) Aiding and (b) Opposing flows.

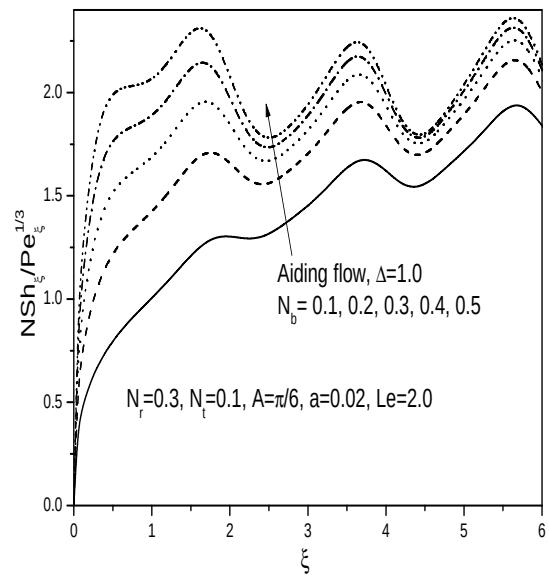

(a)

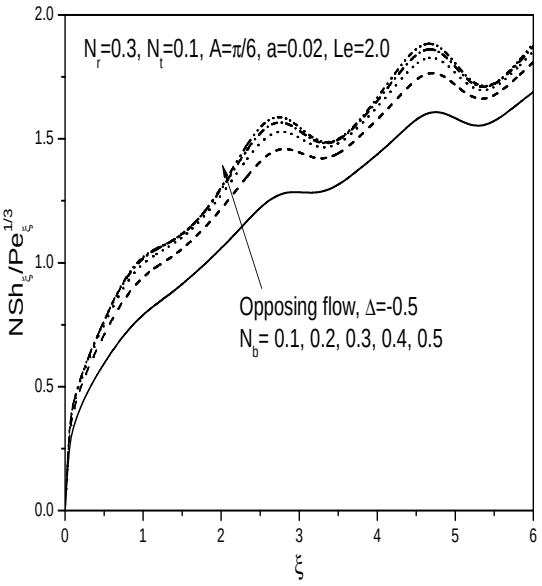

(b)

Figure 3.16: Variation of nanoparticle mass transfer coefficient with Brownian motion Parameter N_b for both (a) Aiding and (b) Opposing flows.

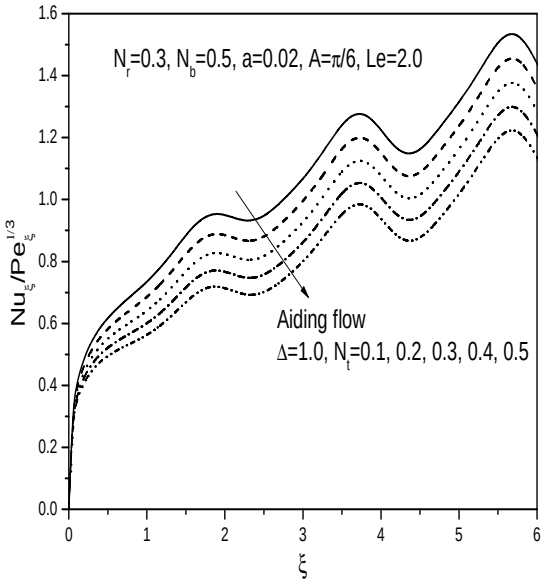

(a)

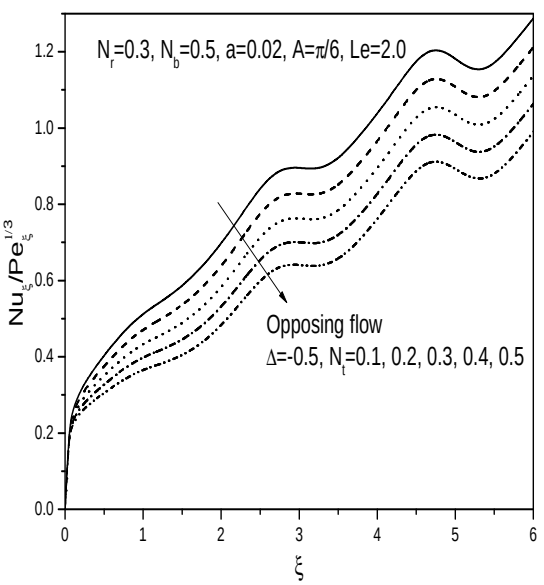

(b)

Figure 3.17: Variation of heat transfer coefficient with thermophoresis Parameter N_t for both (a) Aiding and (b) Opposing flows.

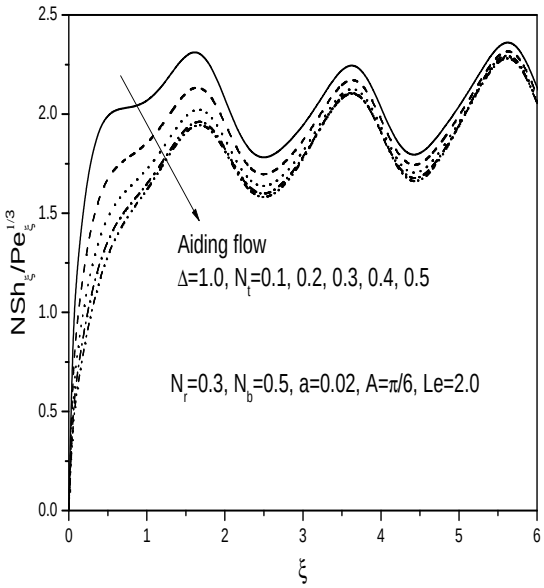

(a)

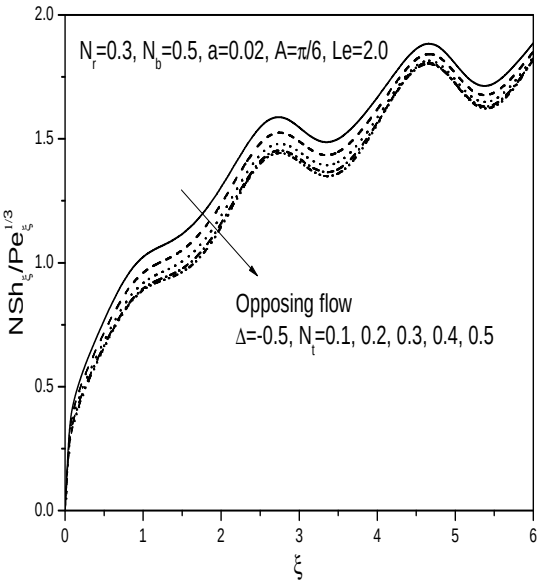

(b)

Figure 3.18: Variation of nanoparticle mass transfer coefficient with thermophoresis Parameter N_t for both (a) Aiding and (b) Opposing flows.

3.3 Conclusions

In this Chapter, Mixed convection heat and nanoparticle mass transfer over an inclined wavy surface embedded in a porous medium saturated with nanofluid subject to (a) uniform wall temperature and nanoparticle volume fraction conditions and (b)uniform and constant heat flux and nanoparticle mass flux conditions has been analyzed. From this analysis, the following conclusions are drawn for both the cases (a) and (b).

An increase in the Brownian motion parameter N_b, increases the velocity, temperature and local nanoparticle mass transfer coefficient for aiding flow, but reduces the nanoparticle volume fraction and local heat transfer coefficient for both aiding and opposing flows. A higher value of the thermophoresis parameter N_t leads to higher temperatures and nanoparticle volume fraction for both aiding and opposing flows, but an increase in velocity for aiding flow and decrease in velocity for opposing flow is observed. Moreover, lower local heat transfer coefficient for both aiding and opposing flows is observed. The effect of the amplitude of the wavy surface is to increase the velocity but to reduce the temperature and nanoparticle volume fraction for aiding flow and a reverse trend is observed for opposing flow. The local heat transfer coefficient and local nanoparticle mass transfer coefficient reduces for both aiding and opposing flows for case (a) and a reverse trend is seen in case (b). The influence of the angle of inclination of the wavy surface to the horizontal is to enhance the velocity and local heat and nanoparticle mass transfer coefficients but to reduce the temperature, nanoparticle volume fraction for aiding flow and to increase these in the case of opposing flow.

Chapter 4

Radiation effect on natural convection over an inclined wavy surface embedded in a non-Darcy porous medium saturated with a nanofluid [1]

4.1 Introduction

Natural convection in a fluid-saturated porous medium is of fundamental importance in many industrial and natural problems. Most of the researches have been carried out on natural convection in porous medium under the assumption of Darcy law model. However, this model is valid only for slow flows through porous matrix. For fluid flows with high velocity, we must consider the non-Darcy model that considers the effect of fluid inertia as well as viscous diffusion. In many practical situations the porous medium is bounded by an impermeable wall, has higher flow rates, and reveals non-uniform porosity distribution near the wall region, making Darcy law inapplicable. To model the real physical situation

[1] Case(a):Published in "**Journal of Porous Media**",
Case(b) Communicated to "**Iranian Journal of Science and Technology**"

better, it is therefore necessary to include the non-Darcy terms in the analysis of convective transport in a porous medium. Non-Darcy models are the extensions of the classical Darcy formulation to incorporate inertial drag effects, vorticity diffusion, and combinations of these effects. The Darcy-Forchheimer (non-Darcy) model is an extension of the classical Darcy model obtained by adding a velocity squared term in the momentum equation to account for the inertial effects.

A few studies have been reported in the literature to study the effect of the radiation on natural convection in a nanofluid saturated porous medium. The effect of thermal radiation on flow and heat transfer processes is of major importance in the design of many advanced energy conversion systems operating at high temperature. Thermal radiation within such systems occur because of the emission by the hot walls and working fluid. Several investigations have been carried out on natural convection under the influence of thermal radiation. It is really important to study the effect of thermal radiation due to its relevance to various applications involving high temperatures such as nuclear power plant, gas turbines missiles, satellites, space vehicles and aircrafts etc.

In this chapter, we obtain the numerical solutions for the problem of natural convection over an inclined wavy surface embedded in a nanofluid saturated non-Darcy porous medium. The Rosseland approximation is considered to study the effect of radiation. A wavy to flat plate transformation is employed to convert the wavy surface to flat surface. The governing partial differential equations are transformed to non-linear ordinary differential equations and solved using Successive Linearization Method. The influence of pertinent parameters on physical quantities are examined and the results are exhibited through graphs.

4.2 Mathematical Formulation

We consider a steady, laminar, incompressible and two-dimensional boundary layer free convection flow along a semi-infinite inclined wavy surface embedded in a nanofluid saturated non-Darcy porous medium in the presence of radiation effect. The porous medium

is considered to be homogeneous and isotropic (i.e. uniform with a constant porosity and permeability). The fluid has constant properties except the density in the buoyancy term of the balance of momentum equation. The fluid flow is moderate, so the pressure drop is proportional to the linear combination of fluid velocity and the square of velocity (Forchheimer flow model is considered). The fluid is considered to be a gray, absorbing emitting radiation but non-scattering medium. The wavy surface is described by

$$y = \delta(x) = a\sin(\pi x/l)$$

where a is the amplitude of the wavy surface, and $2l$ is the characteristic length of the wavy surface. The wavy surface is maintained at constant temperature T_w and constant nanoparticle volume fraction ϕ_w which are higher than the porous medium temperature T_∞ and nanoparticle volume fraction ϕ_∞ sufficiently far from the wavy surface.

The governing equations for this problem under the laminar boundary layer assumptions, Boussinesq approximation and by using the Darcy-Forchheimer model are given by

$$\frac{\partial u}{\partial x} + \frac{\partial v}{\partial y} = 0, \tag{4.1}$$

$$\left(1 + \frac{\tilde{K}}{\nu}\sqrt{u^2+v^2}\right)\left[\frac{\partial u}{\partial y} - \frac{\partial v}{\partial x}\right] + \frac{\tilde{K}}{\nu\sqrt{u^2+v^2}}\left[u^2\frac{\partial u}{\partial y} + uv\left(\frac{\partial v}{\partial y} - \frac{\partial u}{\partial x}\right) - v^2\frac{\partial v}{\partial x}\right] =$$
$$\frac{(1-\phi_\infty)\rho_{f_\infty}\beta\, K\, g}{\mu}\left(\frac{\partial T}{\partial y}\sin A - \frac{\partial T}{\partial x}\cos A\right) - \frac{(\rho_p - \rho_{f_\infty})\, K\, g}{\mu}\left(\frac{\partial \phi}{\partial y}\sin A - \frac{\partial \phi}{\partial x}\cos A\right), \tag{4.2}$$

$$u\frac{\partial T}{\partial x} + v\frac{\partial T}{\partial y} = \alpha\left(\frac{\partial^2 T}{\partial x^2} + \frac{\partial^2 T}{\partial y^2}\right) + \gamma\left[D_B\left(\frac{\partial \phi}{\partial x}\frac{\partial T}{\partial x} + \frac{\partial \phi}{\partial y}\frac{\partial T}{\partial y}\right) + \frac{D_T}{T_\infty}\left(\left(\frac{\partial T}{\partial x}\right)^2 + \left(\frac{\partial T}{\partial y}\right)^2\right)\right]$$
$$+\frac{16\,\sigma\, T_\infty^3}{3\, K_e}\left(\frac{\partial^2 T}{\partial x^2} + \frac{\partial^2 T}{\partial y^2}\right), \tag{4.3}$$

$$u\frac{\partial \phi}{\partial x} + v\frac{\partial \phi}{\partial y} = D_B\left(\frac{\partial^2 \phi}{\partial x^2} + \frac{\partial^2 \phi}{\partial y^2}\right) + \frac{D_T}{T_\infty}\left(\frac{\partial^2 T}{\partial x^2} + \frac{\partial^2 T}{\partial y^2}\right), \tag{4.4}$$

where $\tilde{K}$ is a material parameter which is a measure of inertia impedance of the matrix to account for non-Darcian inertial effects and q_r is the radiative heat flux. If $\tilde{K} = 0$, the flow becomes Darcian flow. The last term in Eqn. (4.3) is due to radiation effect.

Two types (cases) of boundary conditions for the temperature and nanoparticle volume fraction on inclined wavy plate are presented in this chapter. In case(a), the plate is maintained at uniform wall temperature and nanoparticle volume fraction. In case(b), the plate is subjected to a uniform and constant heat and nanoparticle mass fluxes.

4.2.1 Case(a): Uniform Wall Temperature and Nanoparticle Volume Fraction

Assume that the wavy plate is subject to uniform wall temperature and nanoparticle volume fraction T_w and ϕ_w respectively. These values are assumed to be greater than the ambient temperature T_∞ and nanoparticle volume fraction ϕ_∞ at any arbitrary reference point in the medium (inside the boundary layer). Therefore, the boundary conditions are given by (2.5)

Introducing the stream function ψ in Eqns. (4.1) - (4.4) and then making use of the non-dimensional variables given in (2.7), we get the following system of non-linear ordinary differential equations

$$f'' + 2Gr(1+\dot{\delta}^2)^{-1/2} f' f'' = (\sin A + \dot{\delta}\cos A)\,(\theta' - N_r s')\,, \tag{4.5}$$

$$\left(1 + \frac{4R}{3}\right)\theta'' + \frac{1}{2} f\theta' + N_b s'\theta' + N_t \theta'^2 = 0, \tag{4.6}$$

$$s'' + \frac{1}{2} Le f s' + \frac{N_t}{N_b}\theta'' = 0 \tag{4.7}$$

where $Gr = \dfrac{(1-\phi_\infty)\beta\, K\, \tilde{K}\, g\,(T_w - T_\infty)}{\nu^2}$ is the Grashof number and $R = \dfrac{4\,\sigma\, {T_\infty}^3}{K\, K_e}$ is the Radiation parameter.

The boundary conditions (2.5) in terms of f, θ and s are given by (2.11).

The non-dimensional heat and nanoparticle mass transfer rates are given by

$$\frac{Nu_\xi}{{Ra_\xi}^{1/2}} = -\left(1+\frac{4R}{3}\right)\sqrt{\frac{1}{1+\dot{\delta}^2}}\left(\frac{\partial\theta}{\partial\eta}\right)_{\eta=0}, \tag{4.8a}$$

$$\frac{NSh_\xi}{{Ra_\xi}^{1/2}} = -\sqrt{\frac{1}{1+\dot{\delta}^2}}\left(\frac{\partial s}{\partial\eta}\right)_{\eta=0}. \tag{4.8b}$$

Method of Solution

The transformed governing equations (4.5) to (4.7) with the boundary conditions (2.11) are solved numerically using Successive Linearization Method along with Chebyshev spectral collocation method. The detailed descreption of the method can be seen in chapter-2. Proceeding as in chapter-2, we obtain the following matrix equation

$$\mathbf{A}_{i-1}\mathbf{X}_i = \mathbf{R}_{i-1}, \tag{4.9}$$

subject to the boundary conditions

$$f_i(\chi_N) = 0, \quad \sum_{k=0}^{N}\mathbf{D}_{0k}f_i(\chi_k) = 0 \tag{4.10}$$

$$\theta_i(\chi_N) = \theta_i(\chi_0) = s_i(\chi_N) = s_i(\chi_0) = 0 \tag{4.11}$$

In Eqn. (4.9), $\mathbf{A}_{i-1}$ is a (3N + 3)×(3N + 3) square matrix and $\mathbf{X}_i$ and $\mathbf{R}_{i-1}$ are (3N + 3)×1 column vectors defined by

$$\mathbf{A}_{i-1} = \begin{bmatrix} A_{11} & A_{12} & A_{13} \\ A_{21} & A_{22} & A_{23} \\ A_{31} & A_{32} & A_{33} \end{bmatrix}, \quad \mathbf{X}_i = \begin{bmatrix} \mathbf{F}_i \\ \mathbf{\Theta_i} \\ \mathbf{\Phi_i} \end{bmatrix}, \quad \mathbf{R}_{i-1} = \begin{bmatrix} \mathbf{r}_{1,i-1} \\ \mathbf{r}_{2,i-1} \\ \mathbf{r}_{3,i-1} \end{bmatrix} \tag{4.12}$$

where

$$\mathbf{F}_i = [f_i(\chi_0), f_i(\chi_1), ..., f_i(\chi_{N-1}), f_i(\chi_N)]^T,$$
$$\mathbf{\Theta}_i = [\theta_i(\chi_0), \theta_i(\chi_1), ..., \theta_i(\chi_{N-1}), \theta_i(\chi_N)]^T,$$
$$\mathbf{\Phi}_i = [s_i(\chi_0), s_i(\chi_1), ..., s_i(\chi_{N-1}), s_i(\chi_N)]^T,$$
$$\mathbf{r}_{1,i-1} = [r_{1,i-1}(\chi_0), r_{1,i-1}(\chi_1), ..., r_{1,i-1}(\chi_{N-1}), r_{1,i-1}(\chi_N)]^T$$
$$\mathbf{r}_{2,i-1} = [r_{2,i-1}(\chi_0), r_{2,i-1}(\chi_1), ..., r_{2,i-1}(\chi_{N-1}), r_{2,i-1}(\chi_N)]^T$$
$$\mathbf{r}_{3,i-1} = [r_{3,i-1}(\chi_0), r_{3,i-1}(\chi_1), ..., r_{3,i-1}(\chi_{N-1}), r_{3,i-1}(\chi_N)]^T$$
$$A_{11} = a_{1,i-1}\mathbf{D}^2 + a_{2,i-1}\mathbf{D}, \quad A_{12} = a_{3,i-1}\mathbf{D}, \quad A_{13} = a_{4,i-1}\mathbf{D}$$
$$A_{21} = b_{4,i-1}\mathbf{I}, \quad A_{22} = b_{1,i-1}\mathbf{D}^2 + b_{2,i-1}\mathbf{D}, \quad A_{23} = b_{3,i-1}\mathbf{D}$$
$$A_{31} = c_{3,i-1}\mathbf{I}, \quad A_{32} = c_{2,i-1}\mathbf{D}^2, \quad A_{33} = \mathbf{D}^2 + c_{1,i-1}\mathbf{D}$$

Here $a_{k,i-1}$, $b_{l,i-1}$, $c_{l,i-1}$ $(k = 1, 2)$ and $(l = 1, 2, 3)$ are diagonal matrices of size (N+1)×(N+1) and $\mathbf{I}$ is an identity matrix of size (N +1)×(N +1). After modifying the matrix system (4.9) to incorporate boundary conditions (4.10) - (4.11), the solution is obtained as

$$\mathbf{X}_i = \mathbf{A}_{i-1}^{-1}\mathbf{R}_{i-1} \tag{4.13}$$

Results and Discussion

In order to assess the accuracy of our method, we have compared our results with those of Bejan and Khair [83] for fixed values of $A = \frac{\pi}{2}$, $a = 0$, $\xi = 0$, $Gr = 0$, $R = 0$ with the variation of N_r and Le. The comparison in the above case is found to be in good agreement, as shown in Table 4.1.

The effect of the amplitude of the wavy surface on velocity, temperature and nanoparticle volume fraction is plotted in Fig. 4.1. It is noticed that as a increases, the velocity increases near the plate and decreases away from the plate but the temperature and nanoparticle volume fraction decrease within the boundary layer region.

Fig. 4.2 shows the effect of the angle of inclination of the wavy surface on velocity, temperature and nanoparticle volume fraction. It is observed that as A increases, the velocity increases near the plate and decreases away from the plate but the temperature and

Table 4.1: Comparison of $Nu_\xi/\sqrt{Ra_\xi}$ and $NSh_\xi/\sqrt{Ra_\xi}$ for various values of N_r and Le calculated by the present method with $A = \frac{\pi}{2}$, $a = 0$, $\xi = 0$, $Gr = 0$, $R = 0$ and that of Bejan and Khair [9].

		$Nu_\xi/\sqrt{Ra_\xi}$		$NSh_\xi/\sqrt{Ra_\xi}$	
N_r	Le	Bejan and Khair [9]	Present	Bejan and Khair [9]	Present
-3	6	0.683	0.68337284	2.286	2.28633713
-3	8	0.655	0.65480116	2.652	2.65158112
-3	10	0.634	0.63445699	2.973	2.97299942
-2	6	0.618	0.61746121	2.009	2.00890316
-2	8	0.597	0.59691786	2.332	2.33244761
-2	10	0.582	0.58231077	2.617	2.61712295

nanoparticle volume fraction decrease within the boundary layer region. When the surface is vertical, the smallest temperature and nanoparticle volume fraction distributions are observed. While for the horizontal surface, largest temperature and nanoparticle volume fraction distributions are observed.

Figure 4.3 presents the variation of non-dimensional velocity, temperature and nanoparticle volume fraction with variation of Grashof number Gr. It is clear from Fig. 4.3(a) that velocity of the fluid decreases near the plate and then increases away from the plate with the increase of Grashof number. It is observed from Figs. 4.3(b) and 4.3(c) that the temperature and nanoparticle volume fraction of the fluid increases with increase of the Grashof number.

The effect of radiation R on non dimensional velocity, temperature and nanoparticle volume fraction is displayed in Fig. 4.4. It is observed from Figs. 4.4(a) and 4.4(b) that the velocity and temperature increase with increase in the value of radiation parameter. It is noticed from Fig. 4.4(c) that the nanoparticle volume fraction reduces with increase in the value of radiation parameter.

The variation of heat and nanoparticle mass transfer rates for various values of the amplitude a is displayed in Figs. 4.5(a) and 4.5(b). This figure shows that increasing the amplitude decreases the buoyancy force and retards the flow, leading to a decrease in the heat and nanoparticle mass transfer rates. Therefore, the heat and nanoparticle mass transfer

rates are at a lower level when this effect is considered. The influence of angle of inclination of the wavy surface on the local heat and nanoparticle mass transfer rates is shown in Figs. 4.5(c) and 4.5(d). It is observed that increase in the angle of inclination A enhances the local heat and nanoparticle mass transfer rates.

The effect of Brownian motion parameter N_b and thermophoresis parameter N_t on the local heat and nanoparticle mass transfer rates is presented in Figs. 4.6(a) and 4.6(b). As observed from the previous chapters that the dimensionless heat transfer rate decreases with increase in both the Brownian motion parameter and thermophoresis parameter as indicated by Fig. 4.6(a). An increase in the value of Brownian motion parameter enhances the nanoparticle mass transfer rate but increase in the thermophoresis parameter reduces the nanoparticle mass transfer rate. This is seen in Fig. 4.6(b).

Figures 4.6(c) and 4.6(d) display the streamwise distribution of Nusselt and nanoparticle Sherwood numbers for different values of radiation parameter R and Grashof number Gr. It is seen that the heat transfer rate increases with increase in the radiation parameter but decreases with increase in the Grashof number. The effect of radiation parameter and Grashof number on nanoparticle mass transfer is depicted in Fig. 4.6(d) which shows that increase in the value of Grashof number reduces the nanoparticle mass transfer rate but increase in the value of radiation parameter enhances the nanoparticle Sherwood number.

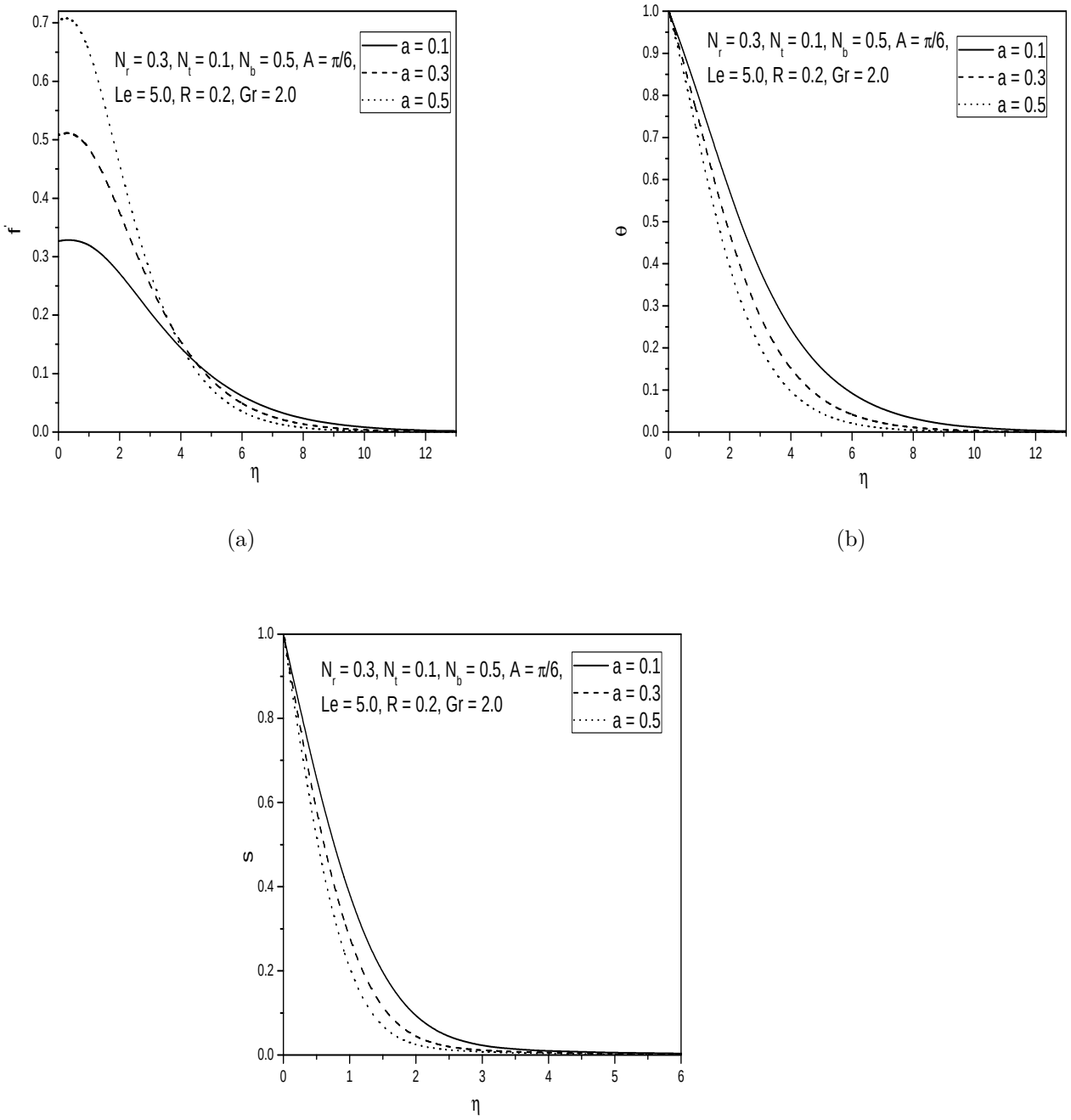

(a)

(b)

(c)

Figure 4.1: (a) Velocity, (b) temperature and (c) nanoparticle volume fraction profiles for various values of wave amplitude a.

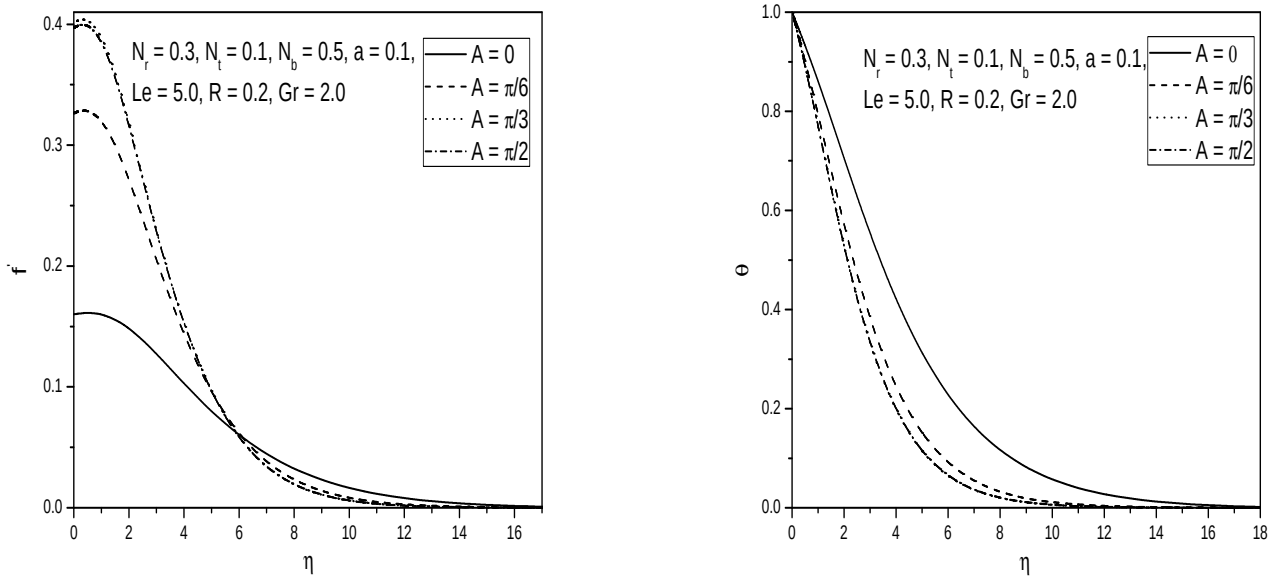

(a)

(b)

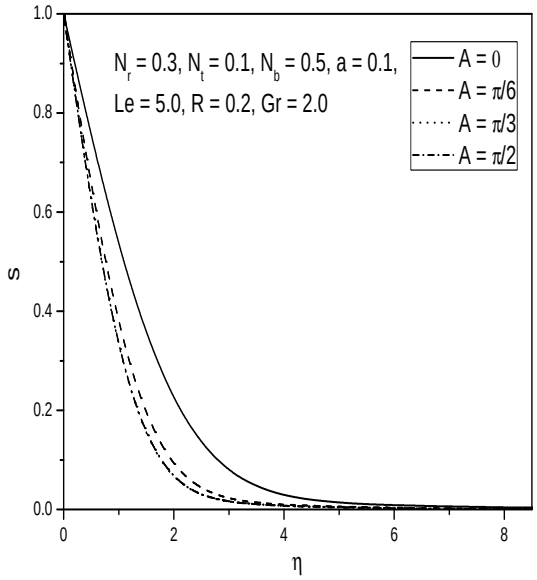

(c)

Figure 4.2: (a) Velocity, (b) temperature and (c) nanoparticle volume fraction profiles for various values of angle of inclination A.

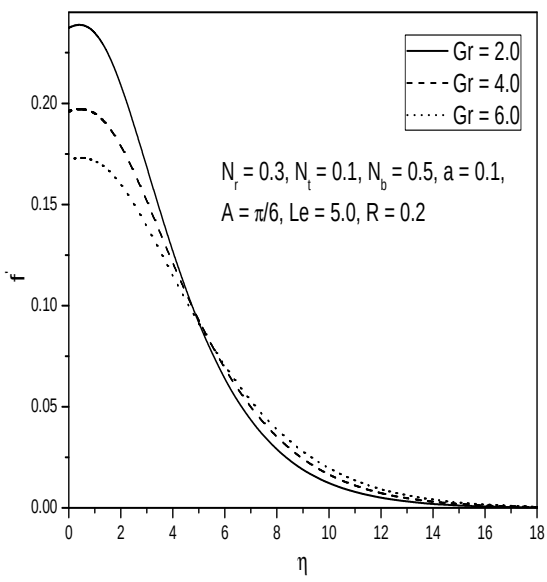

(a)

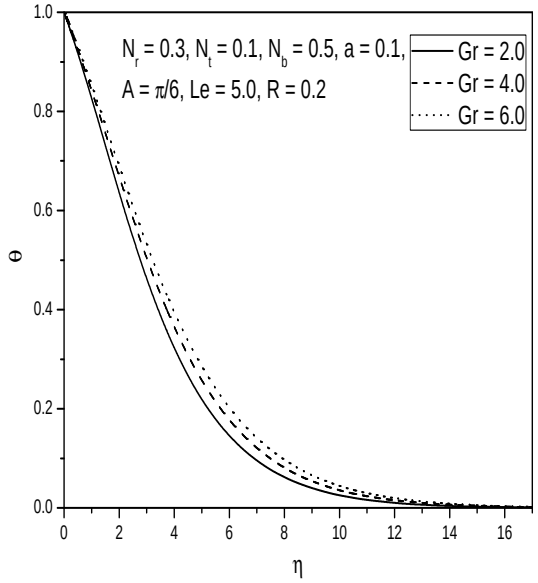

(b)

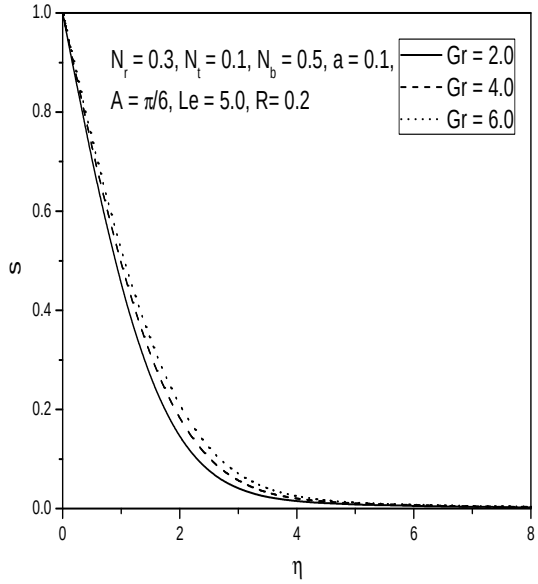

(c)

Figure 4.3: (a) Velocity, (b) temperature and (c) nanoparticle volume fraction profiles for various values of Grashof number Gr.

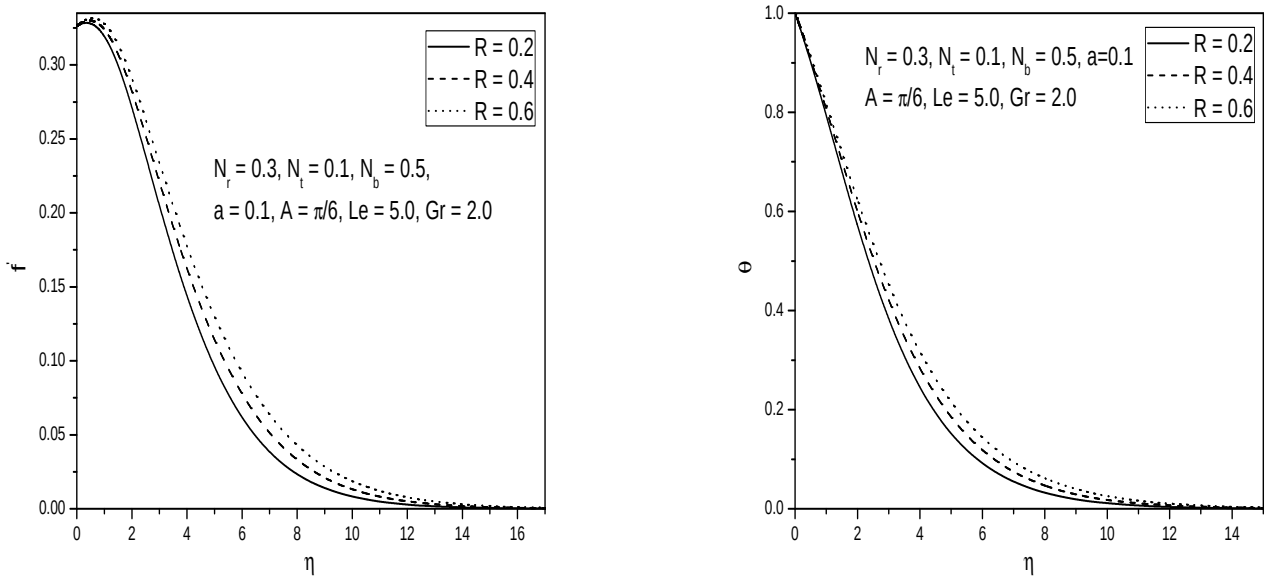

(a)

(b)

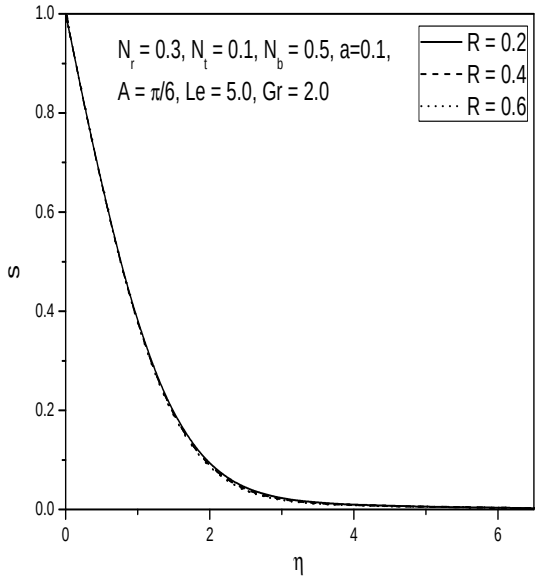

(c)

Figure 4.4: (a) Velocity, (b) temperature and (c) nanoparticle volume fraction profiles for various values of radiation parameter R.

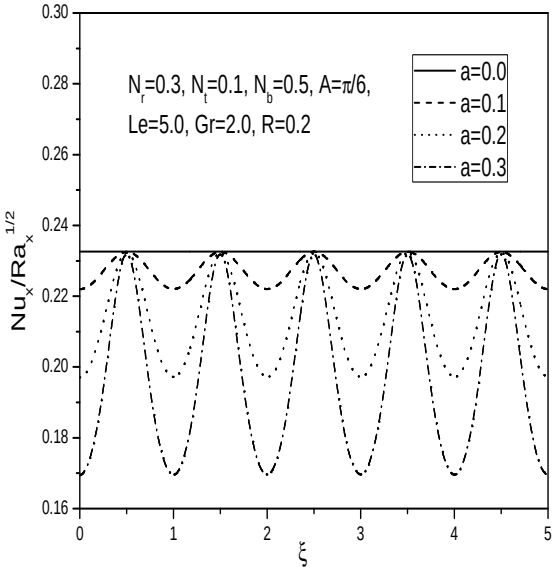

(a)

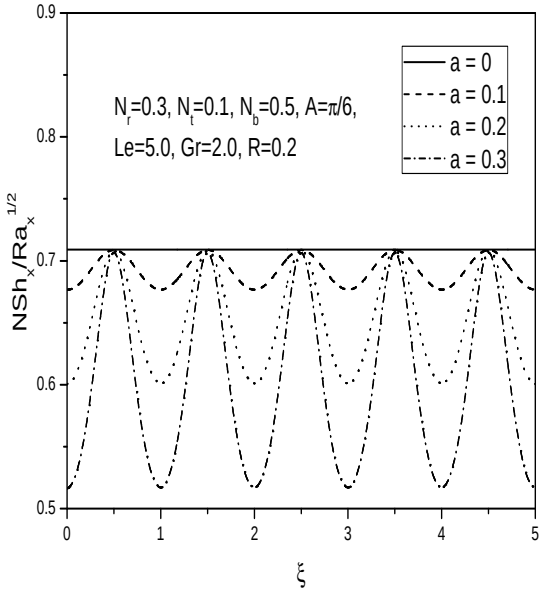

(b)

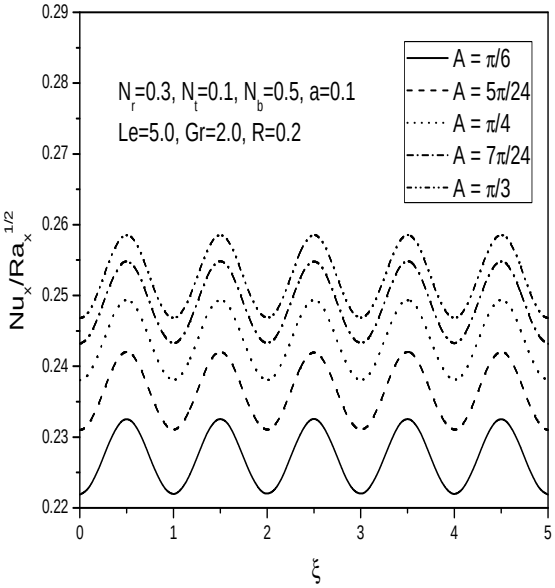

(c)

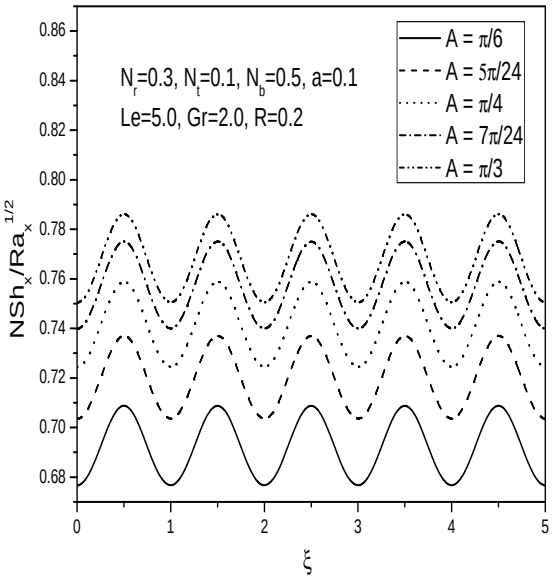

(d)

Figure 4.5: Variation of (a) heat, (b) nanoparticle mass transfer coefficients with wave amplitude a and (c) heat, (d) nanoparticle mass transfer coefficients with angle of inclination A.

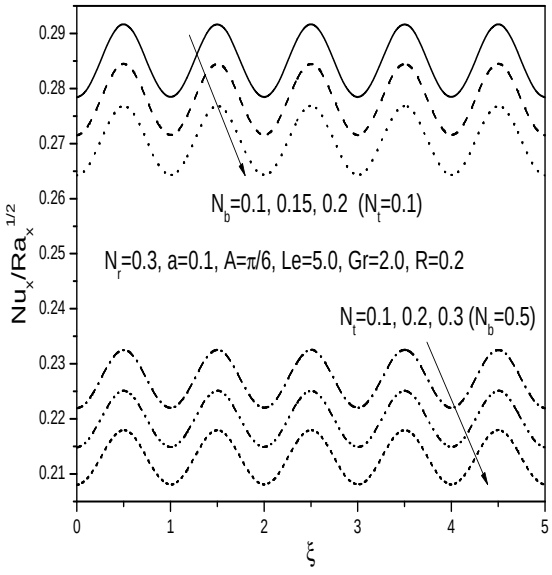

(a)

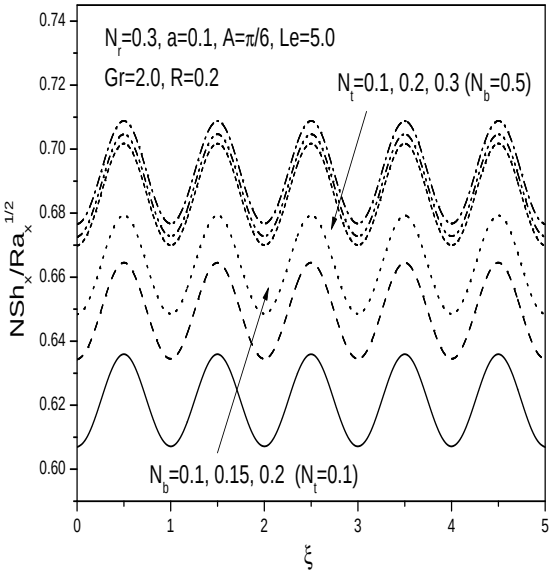

(b)

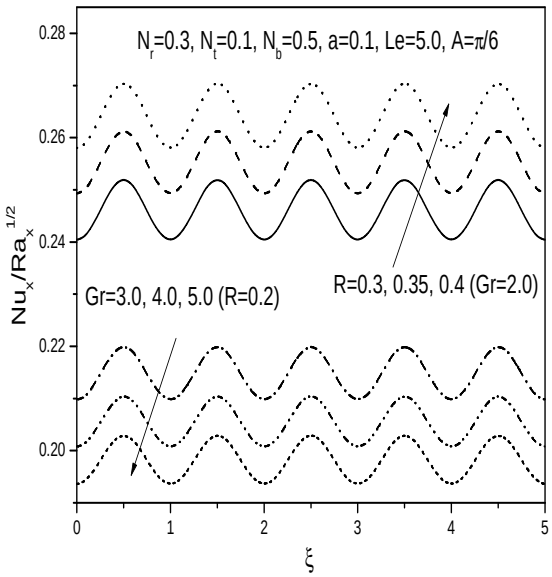

(c)

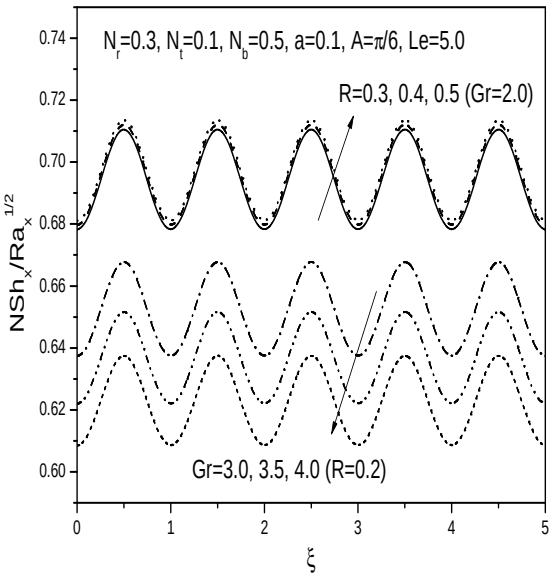

(d)

Figure 4.6: Variation of (a) heat, (b) nanoparticle mass transfer coefficients with Brownian motion and thermophoresis parameters (c) heat, (d) nanoparticle mass transfer coefficients with Grashof number and radiation parameters.

4.2.2 Case(b): Uniform Wall Heat and Nanoparticle Mass Flux

Assume that the plate is maintained at uniform and constant heat and nanoparticle mass fluxes q_w and q_{np} respectively. The steady natural convection boundary layer flow is governed by Eqns. (4.1) to (4.4) and the boundary conditions are given by

$$v = 0, \quad q_w = -k(n.\nabla T) + n.q_r, \quad q_{np} = D_B(n.\nabla\phi) \quad \text{at} \quad y = 0, \tag{4.14a}$$

$$u = 0, \quad T \to T_\infty, \quad \phi \to \phi_\infty \quad \text{as} \quad y \to \infty. \tag{4.14b}$$

Substituting the stream function ψ in Eqns. (4.1) - (4.4), and introducing the following non-dimensional variables

$$\left.\begin{aligned} \xi = \frac{x}{L}, \quad \eta = \frac{(y/l - \delta)\, Ra^{1/3}}{\xi^{1/3}\,(1+\dot{\delta}^2)}, \quad \psi = \alpha\, Ra^{1/3}\, \xi^{2/3}\, f(\xi,\eta), \\ T - T_\infty = \frac{q_w\, l}{k} \xi^{1/3} Ra^{-1/3}\, \theta(\xi,\eta), \\ \phi - \phi_\infty = \frac{q_{np} l}{D_B} \xi^{1/3} Ra^{-1/3}\, s(\xi,\eta), \; Gr^* = Gr\, Ra^{-1/3} \end{aligned}\right\} \tag{4.15}$$

we obtain the following system of nonlinear ordinary differential equations

$$f'' + 2Gr^*\xi^{1/3}(1+\dot{\delta}^2)^{-1/2} f' f'' = (\sin A + \dot{\delta}\cos A)\,(\theta' - N_r s')\,, \tag{4.16}$$

$$\left(1 + \frac{4R}{3}\right)\theta'' + \frac{2}{3} f\theta' - \frac{1}{3} f'\theta + \xi^{1/3}\, N_b s'\theta' + \xi^{1/3}\, N_t \theta'^2 = \xi\left(f'\frac{\partial\theta}{\partial\xi} - \theta'\frac{\partial f}{\partial\xi}\right), \tag{4.17}$$

$$s'' + \frac{2}{3} Le\, f\, s' - \frac{1}{3} Le\, f'\, s + \frac{N_t}{N_b}\theta'' = Le\xi\left(f'\frac{\partial s}{\partial\xi} - s'\frac{\partial f}{\partial\xi}\right), \tag{4.18}$$

The boundary conditions (4.14) in terms of f, θ and s are given by

$$2f + 3\xi \left(\frac{\partial f}{\partial \xi}\right)_{\eta=0} = 0, \quad \theta' = -\frac{3}{3+4\,R}\sqrt{1+\dot{\delta}^2}, \quad s' = -\sqrt{1+\dot{\delta}^2}, \tag{4.19a}$$

$$f' \to 0, \quad \theta \to 0, \quad s \to 0. \tag{4.19b}$$

and the non-dimensional heat and nanoparticle mass transfer rates are given by

$$\frac{Nu_\xi}{{Ra_\xi}^{1/3}} = \frac{\xi^{1/3}}{\theta(\xi,0)}, \tag{4.20a}$$

$$\frac{NSh_\xi}{{Ra_\xi}^{1/3}} = \frac{\xi^{1/3}}{s(\xi,0)}. \tag{4.20b}$$

Method of Solution

The transformed governing equations (4.16) to (4.18) with the boundary conditions (4.19) are solved using a local similarity and non-similarity method. The resulting boundary layer equations are linearized using Successive linearization Method and then solved using Chebyshev spectral collocation method same as in the previous chapters. Proceeding same as in previous chapters, we obtain the following matrix equation

$$\mathbf{A}_{i-1}\mathbf{X}_i = \mathbf{R}_{i-1}, \tag{4.21}$$

In Eqn. (4.21), $\mathbf{A}_{i-1}$ is a (6N + 6)×(6N + 6) square matrix and $\mathbf{X}_i$ and $\mathbf{R}_{i-1}$ are (6N + 6)×1 column vectors defined by

$$\mathbf{A}_{i-1} = \begin{bmatrix} A_{11} & A_{12} & A_{13} & A_{14} & A_{15} & A_{16} \\ A_{21} & A_{22} & A_{23} & A_{24} & A_{25} & A_{26} \\ A_{31} & A_{32} & A_{33} & A_{34} & A_{35} & A_{36} \\ A_{41} & A_{42} & A_{43} & A_{44} & A_{45} & A_{46} \\ A_{51} & A_{52} & A_{53} & A_{54} & A_{55} & A_{56} \\ A_{61} & A_{62} & A_{63} & A_{64} & A_{65} & A_{66} \end{bmatrix}, \quad \mathbf{X}_i = \begin{bmatrix} \mathbf{F}_i \\ \boldsymbol{\Theta_i} \\ \boldsymbol{\Phi_i} \\ \mathbf{G}_i \\ \mathbf{H}_i \\ \mathbf{K}_i \end{bmatrix}, \quad \mathbf{R}_{i-1} = \begin{bmatrix} \mathbf{r}_{1,i-1} \\ \mathbf{r}_{2,i-1} \\ \mathbf{r}_{3,i-1} \\ \mathbf{r}_{4,i-1} \\ \mathbf{r}_{5,i-1} \\ \mathbf{r}_{6,i-1} \end{bmatrix} \tag{4.22}$$

where

$\mathbf{F}_i = [f_i(\chi_0), f_i(\chi_1), ..., f_i(\chi_{N-1}), f_i(\chi_N)]^T$, $\mathbf{\Theta_i} = [\theta_i(\chi_0), \theta_i(\chi_1), ..., \theta_i(\chi_{N-1}), \theta_i(\chi_N)]^T$,
$\mathbf{\Phi_i} = [s_i(\chi_0), s_i(\chi_1), ..., s_i(\chi_{N-1}), s_i(\chi_N)]^T$, $\mathbf{G}_i = [g_i(\chi_0), g_i(\chi_1), ..., g_i(\chi_{N-1}), g_i(\chi_N)]^T$,
$\mathbf{H}_i = [h_i(\chi_0), h_i(\chi_1), ..., h_i(\chi_{N-1}), h_i(\chi_N)]^T$, $\mathbf{K}_i = [k_i(\chi_0), k_i(\chi_1), ..., k_i(\chi_{N-1}), k_i(\chi_N)]^T$,
$\mathbf{r}_{j,i-1} = [r_{j,i-1}(\chi_0), r_{j,i-1}(\chi_1), \cdots, r_{j,i-1}(\chi_{N-1}), r_{j,i-1}(\chi_N)]^T, j = 1, 2, 3, 4, 5, 6$
$A_{11} = a_{1,i-1}\mathbf{D}^2 + a_{2,i-1}\mathbf{D},\ A_{12} = a_{3,i-1}\mathbf{D},\ A_{13} = a_{4,i-1}\mathbf{D},\ A_{14} = \mathbf{0},\ A_{15} = \mathbf{0},\ A_{16} = \mathbf{0}$
$A_{21} = b_{4,i-1}\mathbf{D} + b_{5,i-1}\mathbf{I},\ A_{22} = b_{1,i-1}\mathbf{D}^2 + b_{2,i-1}\mathbf{D} + b_{3,i-1}\mathbf{I},\ A_{23} = b_{6,i-1}\mathbf{D},$
$A_{24} = b_{7,i-1}\mathbf{I},\ A_{25} = b_{8,i-1}\mathbf{I},\ A_{26} = \mathbf{0},\ A_{31} = c_{3,i-1}\mathbf{D} + c_{4,i-1}\mathbf{I},\ A_{32} = c_{5,i-1}\mathbf{D}^2,$
$A_{33} = \mathbf{D}^2 + c_{1,i-1}\mathbf{D} + c_{2,i-1}\mathbf{I},\ A_{34} = c_{6,i-1}\mathbf{I},\ A_{35} = \mathbf{0},\ A_{36} = c_{7,i-1}\mathbf{I},$
$A_{41} = d_{3,i-1}\mathbf{D}^2 + d_{4,i-1}\mathbf{D},\ A_{42} = d_{5,i-1}\mathbf{D},\ A_{43} = d_{6,i-1}\mathbf{D},\ A_{44} = d_{1,i-1}\mathbf{D}^2 + d_{2,i-1}\mathbf{D},$
$A_{45} = d_{7,i-1}\mathbf{D},\ A_{46} = d_{8,i-1}\mathbf{D},\ A_{51} = l_{4,i-1}\mathbf{D} + l_{5,i-1}\mathbf{I}, A_{52} = l_{6,i-1}\mathbf{D} + l_{7,i-1}\mathbf{I},$
$A_{53} = l_{8,i-1}\mathbf{D}\ A_{54} = l_{9,i-1}\mathbf{D} + l_{10,i-1}\mathbf{I},\ A_{55} = l_{1,i-1}\mathbf{D}^2 + l_{2,i-1}\mathbf{D} + l_{3,i-1}\mathbf{I},$
$A_{56} = l_{11,i-1}\mathbf{D},\ A_{61} = m_{3,i-1}\mathbf{D} + m_{4,i-1}I,\ A_{62} = \mathbf{0},\ A_{63} = m_{5,i-1}\mathbf{D} + m_{6,i-1}\mathbf{I}$
$A_{64} = m_{7,i-1}\mathbf{D} + m_{8,i-1}\mathbf{I},\ A_{65} = m_{9,i-1}\mathbf{D}^2,\ A_{66} = \mathbf{D}^2 + m_{1,i-1}\mathbf{D} + m_{2,i-1}\mathbf{I}$

Here $a_{k,i-1}$, $b_{k,i-1}$, $c_{k,i-1}$,$d_{k,i-1}$, $l_{k,i-1}$, $m_{k,i-1}$ are diagonal matrices of size (N+1)×(N+1) and $\mathbf{I}$ is an identity matrix of size (N +1)×(N +1). After modifying the matrix system (4.21) to incorporate boundary conditions, the solution is obtained as

$$\mathbf{X}_i = \mathbf{A}_{i-1}^{-1}\mathbf{R}_{i-1} \tag{4.23}$$

Results and Discussion

Numerical solutions for dimensionless heat and nanoparticle mass transfer rates with variation of pertinent parameters are computed and presented graphically in Figs. 4.7 - 4.9.

Figures 4.7(a) and 4.7(b) show the effect of wave amplitude on the Nusselt and nanoparticle Sherwood number. It is observed that an enhancement in wavy amplitude increases the local heat and nanoparticle mass transfer rates as compared with the limiting case of a smooth surface. In general, we conclude that increasing the amplitude a leads to a larger fluc-

tuation of the local Nusselt number and nanoparticle sherwood number with the streamwise coordinate ξ.

The effect of angle of inclination A on the heat and nanoparticle mass transfer rates is displayed in Figs. 4.7(c) and 4.7(d). This figure shows that increasing the angle of inclination increases the buoyancy force and assists the flow, leading to an increase in the heat and nanoparticle mass transfer rates. The maximum values of the dimensionless heat and nanoparticle mass transfer rates are observed when the surface is vertical; in which case, the buoyancy force is at its maximum.

Figures. 4.8(a) and 4.8(b) display the effect of Brownian motion parameter N_b on the heat and nanoparticle mass transfer rates. Fig. 4.8(a) depicts that the dimensionless heat transfer rate decreases with an increase in the Browinian motion parameter. An increase in the value of Brownian motion parameter enhances the nanoparticle mass transfer rate, as shown in Fig. 4.8(b). Figs. 4.8(c) and 4.8(d) depict the streamwise distribution of Nusselt and nanoparticle Sherwood numbers for different values of thermophoresis parameter N_t. It is noticed that the heat and nanoparticle mass transfer rates decrease with the increase in the thermophoresis parameter. Since, Brownian motion is proportional to the volumetric fraction of nanoparticles in the direction from high to low concentration, whereas the thermophoresis is proportional to the temperature gradient from hot to cold, we conclude that the effect of Brownian motion and thermophoresis is to reduce the value of non-dimensional heat transfer rate.

The variation of heat and nanoparticle mass transfer rates for different values of Grashof number Gr is plotted in Figs. 4.9(a) and 4.9(b). It is seen that the heat and nanoparticle mass transfer rates decrease with increase in the value of Grashof number. The effect of radiation parameter on the heat and nanoparticle mass transfer is depicted in Figs. 4.9(c) and 4.9(d) which shows that increase in the value of radiation parameter enhances the heat and nanoparticle mass transfer rates. This is due to the fact that an increase in the radiation parameter for given K and T_∞ means a decrease in the Rosseland radiation absorptivity K_e. Hence, the divergence of radiative heat flux q_r increases as K_e decreases. Therefore, the rate of radiative heat transferred to the fluid increases, and consequently the fluid temperature

and heat transfer increases.

4.3 Conclusions

In this chapter, we have investigated the problem of steady, laminar natural convection boundary layer flow over a semi-infinite inclined wavy plate embedded in a nanofluid saturated non-Darcy porous medium in the presence of radiation effect with (a) uniform wall temperature and nanoparticle volume fraction conditions and (b)uniform and constant heat and nanoparticle mass flux conditions. From this analysis, the following conclusions are drawn for both the cases (a) and (b).

An increase in the value of radiation parameter R increases the velocity, temperature, heat and nanoparticle mass transfer rates but reduces the nanoparticle volume fraction of the fluid. The influence of Grashof number Gr is to reduce the velocity, heat transfer rate and nanoparticle mass transfer rate near the plate and to increase the temperature and nanoparticle volume fraction of the fluid. An increase in the amplitude a of the wavy surface enhances the velocity near the plate and reduces the temperature, nanoparticle volume fraction, heat transfer, and nanoparticle mass transfer rates. The effect of angle of inclination A of the wavy surface is to increase the velocity, heat transfer and nanoparticle mass transfer and to reduce the temperature and nanoparticle volume fraction.

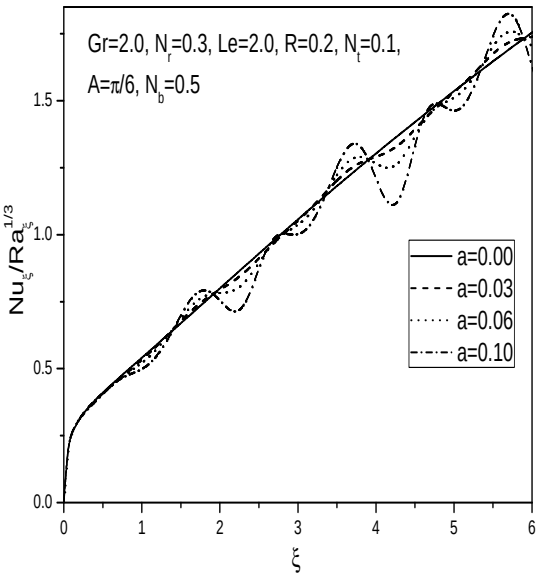

(a)

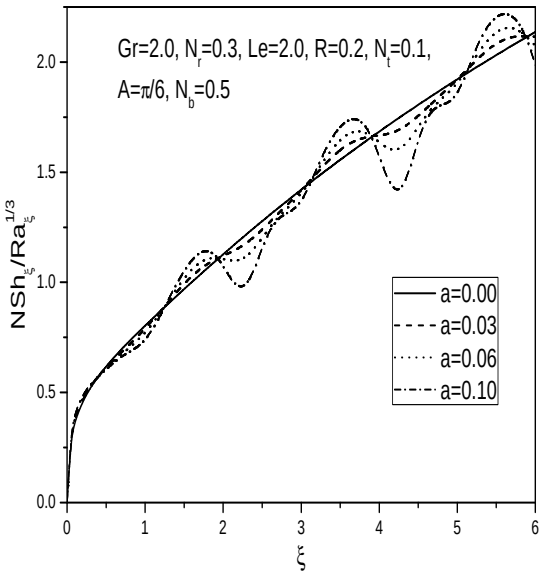

(b)

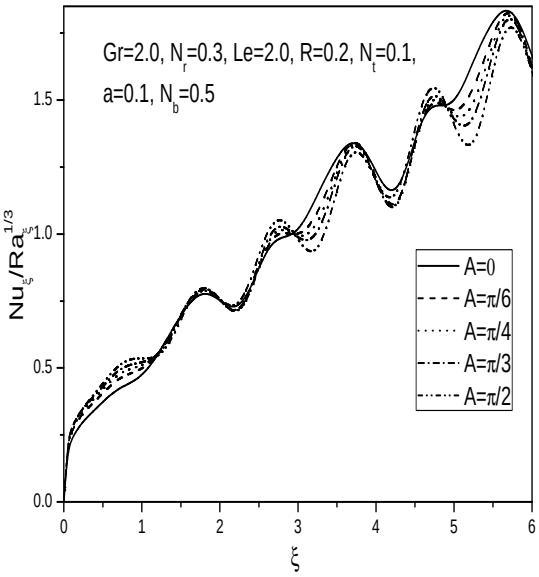

(c)

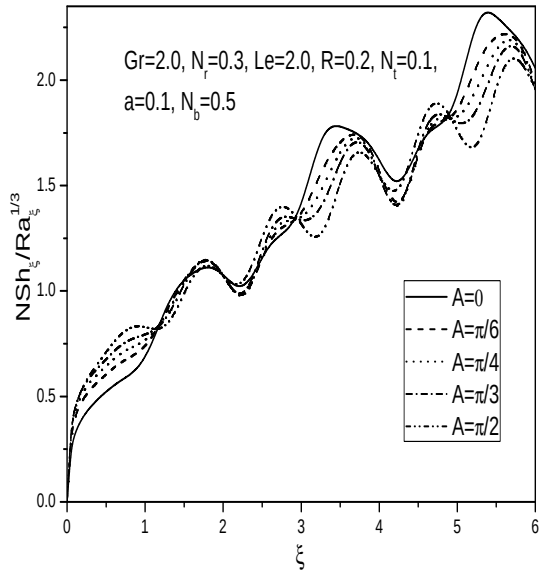

(d)

Figure 4.7: Variation of (a) heat, (b) nanoparticle mass transfer coefficients with wave amplitude a and (c) heat, (d) nanoparticle mass transfer coefficients with angle of inclination A.

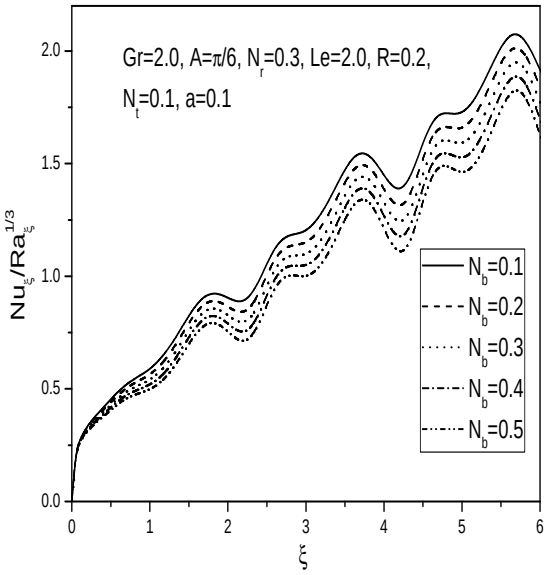

(a)

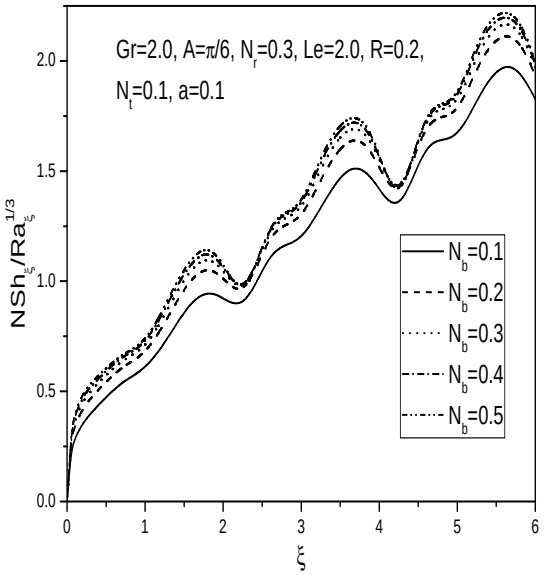

(b)

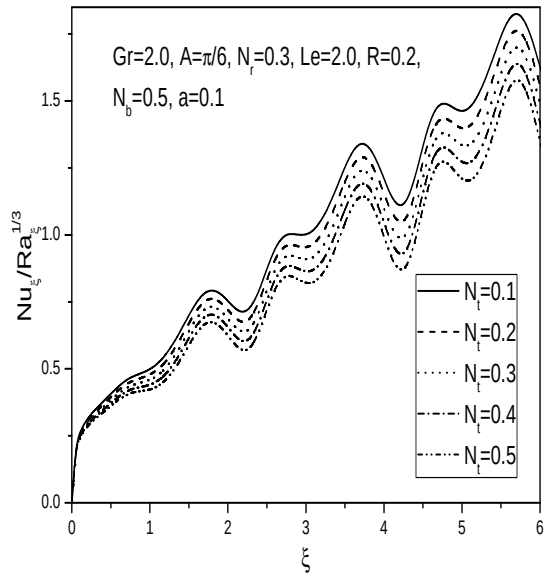

(c)

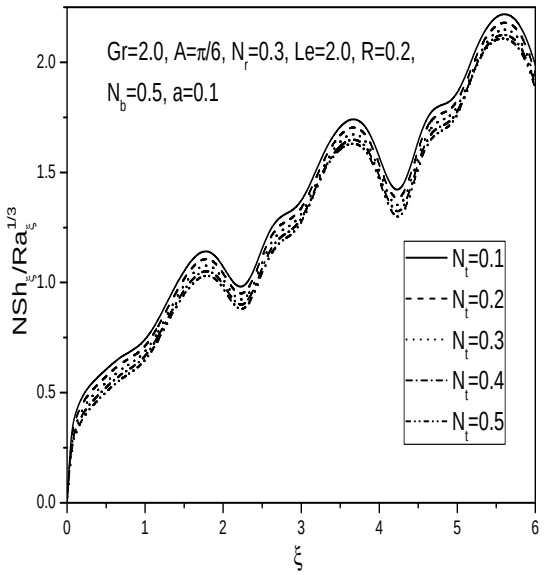

(d)

Figure 4.8: Variation of (a) heat, (b) nanoparticle mass transfer coefficients with Brownian motion parameter N_b and (c) heat, (d) nanoparticle mass transfer coefficients with thermophoresis parameter N_t.

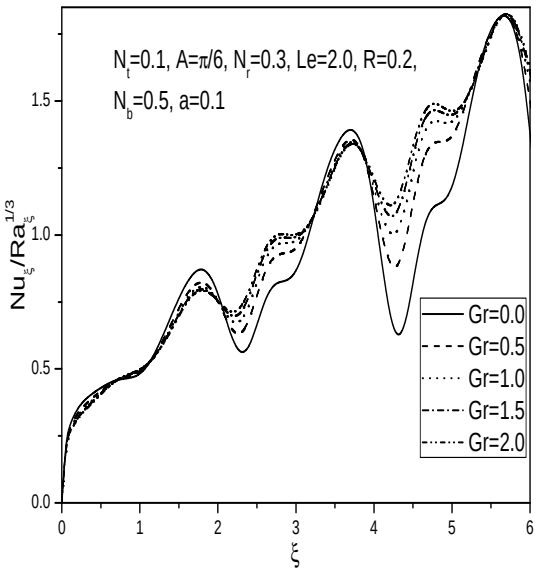

(a)

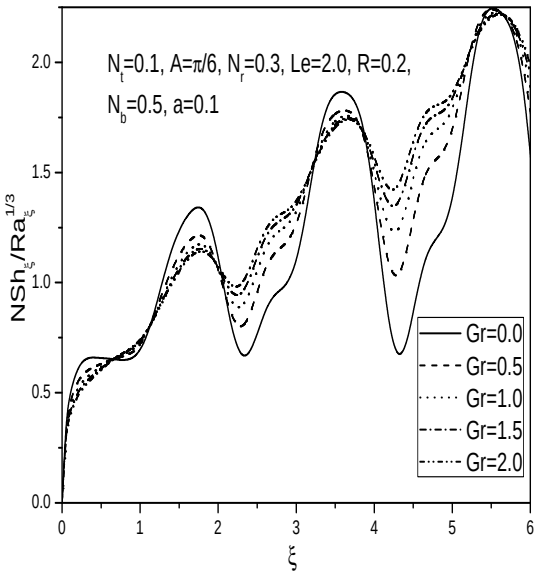

(b)

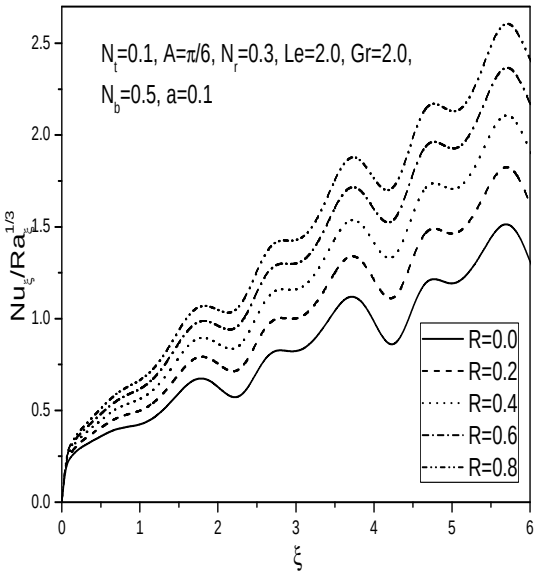

(c)

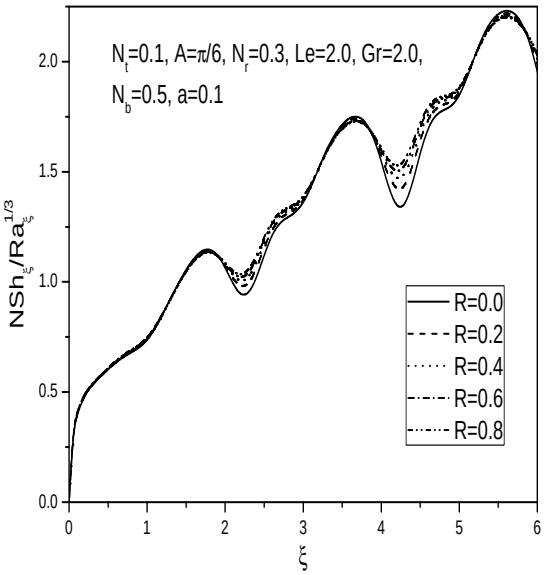

(d)

Figure 4.9: Variation of (a) heat, (b) nanoparticle mass transfer coefficients with Grashof number Gr and (c) heat, (d) nanoparticle mass transfer coefficients with radiation parameter.

Chapter 5

Mixed convection over an inclined wavy surface in a nanofluid saturated non-Darcy porous medium with radiation effect [1]

5.1 Introduction

In the previous chapter we have studied the natural convection flow of a nanofluid over an inclined wavy surface in the presence of radiation effect. In this chapter we undertake the analysis of mixed convection flow of nanofluid over an inclined wavy surface in the presence of radiation effect. Considerable work has been reported in the literature focusing on the problem of mixed convection of nanofluid along various geometries embedded in porous medium. Radiation effect on mixed convection gained importance in the context of many industrial applications involving high temperatures such as gas turbines, nuclear power plant and various propulsion engines for aircraft, missiles, satellites, and space technology.

[1] Case(a):Published in "**International Journal of Chemical Engineering, 2015 (2015) Article ID: 927508**",
Case(b) Communicated to "**Propulsion and Power research.**"

Chamkha *et al.* [13] presented the non-similar solution of steady mixed convection of a nanofluid in the presence of thermal radiation. Chamkha *et al.* [14] investigated the effect of thermal radiation on mixed convection about a cone embedded in a porous medium filled with a nanofluid. Yazdi *et al.* [118] considered the problem of two dimensional mixed convection MHD boundary layer stagnation point flow over a stretching vertical plate in porous medium filled with a nanofluid in the presence of thermal radiation.

The objective of the present chapter is to obtain the numerical solution for the problem of mixed convection over an inclined wavy surface immersed in a porous medium filled with nanofluid. A Rosseland approximation is considered to study the effect of radiation. The influence of pertinent parameters on physical quantities are examined numerically and shown through graphs.

5.2 Mathematical Formulation

A steady, laminar, incompressible, two-dimensional mixed convective flow of a nanofluid with uniform velocity U_∞, temperature T_∞ and nanoparticle volume fraction ϕ_∞ along a semi infinite inclined wavy surface in a non-Darcy porous medium with radiation effect is considered. The porous medium is considered to be homogeneous and isotropic and the fluid has constant properties except the density in the buoyancy term of the balance of momentum equation. The fluid is considered to be a gray, absorbing emitting radiation but non-scattering medium.

The physical model and the coordinate system are shown in Fig. 2.1. By employing laminar boundary layer flow assumptions, Boussinesq approximation and using the Darcy-Forchheimer model, the governing equations for flow are given by

$$\frac{\partial u}{\partial x}+\frac{\partial v}{\partial y}=0, \tag{5.1}$$

$$\left(1+\frac{\tilde{K}}{\nu}\sqrt{u^2+v^2}\right)\left[\frac{\partial u}{\partial y}-\frac{\partial v}{\partial x}\right]+\frac{\tilde{K}}{\nu\sqrt{u^2+v^2}}\left[u^2\frac{\partial u}{\partial y}+uv\left(\frac{\partial v}{\partial y}-\frac{\partial u}{\partial x}\right)-v^2\frac{\partial v}{\partial x}\right]=$$
$$\frac{(1-\phi_\infty)\rho_{f_\infty}\beta\,K\,g}{\mu}\left(\frac{\partial T}{\partial y}\sin A-\frac{\partial T}{\partial x}\cos A\right)-\frac{(\rho_p-\rho_{f_\infty})\,K\,g}{\mu}\left(\frac{\partial \phi}{\partial y}\sin A-\frac{\partial \phi}{\partial x}\cos A\right), \tag{5.2}$$

$$u\frac{\partial T}{\partial x}+v\frac{\partial T}{\partial y}=\alpha\left(\frac{\partial^2 T}{\partial x^2}+\frac{\partial^2 T}{\partial y^2}\right)+\gamma\left[D_B\left(\frac{\partial \phi}{\partial x}\frac{\partial T}{\partial x}+\frac{\partial \phi}{\partial y}\frac{\partial T}{\partial y}\right)+\frac{D_T}{T_\infty}\left(\left(\frac{\partial T}{\partial x}\right)^2+\left(\frac{\partial T}{\partial y}\right)^2\right)\right]$$
$$+\frac{16\,\sigma\,T_\infty^3}{3\,K_e}\left(\frac{\partial^2 T}{\partial x^2}+\frac{\partial^2 T}{\partial y^2}\right), \tag{5.3}$$

$$u\frac{\partial \phi}{\partial x}+v\frac{\partial \phi}{\partial y}=D_B\left(\frac{\partial^2 \phi}{\partial x^2}+\frac{\partial^2 \phi}{\partial y^2}\right)+\frac{D_T}{T_\infty}\left(\frac{\partial^2 T}{\partial x^2}+\frac{\partial^2 T}{\partial y^2}\right), \tag{5.4}$$

Here in this chapter also, we have considered two types (cases) of boundary conditions for the temperature and nanoparticle volume fraction on the semi-infinite inclined wavy plate as seen in previous chapters. In case(a), the plate is maintained at uniform wall temperature and nanoparticle volume fraction. In case(b), the plate is subjected to a uniform and constant heat and nanoparticle mass fluxes.

5.2.1 Case(a): Uniform Wall Temperature and Nanoparticle Volume Fraction

Assume that the wavy plate is subject to uniform wall temperature and nanoparticle volume fraction T_w and ϕ_w respectively. These values are assumed to be greater than the ambient temperature T_∞ and nanoparticle volume fraction ϕ_∞ at any arbitrary reference point in the medium (inside the boundary layer). Hence, the boundary conditions are given by (3.5).

Introducing stream function ψ in Eqns. (5.1) - (5.4) and then using the non-dimensional variables given in (3.6), we get the following system of non-linear ordinary differential equations

$$f'' + 2F_c(1+\dot{\delta}^2)^{-1/2} f' f'' = \Delta(\sin A + \dot{\delta}\cos A)\left(\theta' - N_r s'\right), \tag{5.5}$$

$$\left(1+\frac{4R}{3}\right)\theta'' + \frac{1}{2} f\theta' + N_b s'\theta' + N_t \theta'^2 = 0, \tag{5.6}$$

$$s'' + \frac{1}{2} Le f s' + \frac{N_t}{N_b}\theta'' = 0, \tag{5.7}$$

where $F_c = \dfrac{\tilde{K}\, U_\infty}{\nu}$ is the non-Darcy parameter and $R = \dfrac{4\,\sigma\, {T_\infty}^3}{K\, K_e}$ is the Radiation parameter.

The boundary conditions (3.5) in terms of f, θ and s are given by (3.10).
The non-dimensional heat and nanoparticle mass transfer rates are given by

$$\frac{Nu_x}{\sqrt{Pe_x}} = -\left(1+\frac{4R}{3}\right)\sqrt{\frac{1}{1+\dot{\delta}^2}}\left(\frac{\partial\theta}{\partial\eta}\right)_{\eta=0}, \tag{5.8a}$$

$$\frac{NSh_x}{\sqrt{Pe_x}} = -\sqrt{\frac{1}{1+\dot{\delta}^2}}\left(\frac{\partial s}{\partial\eta}\right)_{\eta=0}. \tag{5.8b}$$

Method of Solution

Equations (5.5) - (5.7) with the boundary conditions (3.10) are solved numerically using Successive Linearization Method along with Chebyshev spectral collocation method as described in detail in previous chapters. Proceeding same as in previous chapters we obtain the following matrix equation

$$\mathbf{A}_{i-1}\mathbf{X}_i = \mathbf{R}_{i-1}, \tag{5.9}$$

subject to the boundary conditions

$$f_i(\chi_N) = 0, \quad \sum_{k=0}^{N} \mathbf{D}_{0k} f_i(\chi_k) = 0 \tag{5.10}$$

$$\theta_i(\chi_N) = \theta_i(\chi_0) = s_i(\chi_N) = s_i(\chi_0) = 0 \tag{5.11}$$

In Eqn. (5.9), $\mathbf{A}_{i-1}$ is a (3N + 3)×(3N + 3) square matrix and $\mathbf{X}_i$ and $\mathbf{R}_{i-1}$ are (3N + 3)×1 column vectors defined by

$$\mathbf{A}_{i-1} = \begin{bmatrix} A_{11} & A_{12} & A_{13} \\ A_{21} & A_{22} & A_{23} \\ A_{31} & A_{32} & A_{33} \end{bmatrix}, \quad \mathbf{X}_i = \begin{bmatrix} \mathbf{F}_i \\ \mathbf{\Theta}_i \\ \mathbf{\Phi}_i \end{bmatrix}, \quad \mathbf{R}_{i-1} = \begin{bmatrix} \mathbf{r}_{1,i-1} \\ \mathbf{r}_{2,i-1} \\ \mathbf{r}_{3,i-1} \end{bmatrix} \tag{5.12}$$

where

$$\mathbf{F}_i = [f_i(\chi_0), f_i(\chi_1), ..., f_i(\chi_{N-1}), f_i(\chi_N)]^T,$$
$$\mathbf{\Theta}_i = [\theta_i(\chi_0), \theta_i(\chi_1), ..., \theta_i(\chi_{N-1}), \theta_i(\chi_N)]^T,$$
$$\mathbf{\Phi}_i = [s_i(\chi_0), s_i(\chi_1), ..., s_i(\chi_{N-1}), s_i(\chi_N)]^T,$$
$$\mathbf{r}_{1,i-1} = [r_{1,i-1}(\chi_0), r_{1,i-1}(\chi_1), ..., r_{1,i-1}(\chi_{N-1}), r_{1,i-1}(\chi_N)]^T$$
$$\mathbf{r}_{2,i-1} = [r_{2,i-1}(\chi_0), r_{2,i-1}(\chi_1), ..., r_{2,i-1}(\chi_{N-1}), r_{2,i-1}(\chi_N)]^T$$
$$\mathbf{r}_{3,i-1} = [r_{3,i-1}(\chi_0), r_{3,i-1}(\chi_1), ..., r_{3,i-1}(\chi_{N-1}), r_{3,i-1}(\chi_N)]^T$$
$$A_{11} = a_{1,i-1}\mathbf{D}^2 + a_{2,i-1}\mathbf{D}, \quad A_{12} = a_{3,i-1}\mathbf{D}, \quad A_{13} = a_{4,i-1}\mathbf{D}$$
$$A_{21} = b_{4,i-1}\mathbf{I}, \quad A_{22} = b_{1,i-1}\mathbf{D}^2 + b_{2,i-1}\mathbf{D}, \quad A_{23} = b_{3,i-1}\mathbf{D}$$
$$A_{31} = c_{3,i-1}\mathbf{I}, \quad A_{32} = c_{2,i-1}\mathbf{D}^2, \quad A_{33} = \mathbf{D}^2 + c_{1,i-1}\mathbf{D}$$

Here $a_{k,i-1}$, $b_{l,i-1}$, $c_{l,i-1}$ $(k = 1, 2)$ and $(l = 1, 2, 3)$ are diagonal matrices of size (N+1)×(N+1) and $\mathbf{I}$ is an identity matrix of size (N +1)×(N +1). After modifying the matrix system (5.9) to incorporate boundary conditions (5.10) - (5.11), the solution is obtained as

$$\mathbf{X}_i = \mathbf{A}_{i-1}^{-1}\mathbf{R}_{i-1} \tag{5.13}$$

Results and Discussion

In order to validate the numerical procedure generated, the results of the present problem have been compared with work of Cheng [23] as a special case by taking $A = \frac{\pi}{2}$, $a = 0$, $\xi = 0$, $N_r = 0$, $N_t = 0$, $N_b \to 0$, $Le = 0$, $F_c = 0$, $R = 0$ and found that they are in good agreement,

Table 5.1: Comparison of values of $-\theta'(0)$ for aiding and opposing flows by the present method and Cheng [23] for fixed values of $A = \frac{\pi}{2}$, $a = 0$, $\xi = 0$, $N_r = 0$, $N_t = 0$, $N_b \to 0$, $Le = 0$, $R = 0$.

	Aiding Flow			Opposing Flow	
Δ	Cheng [23]	Present	Δ	Cheng [23]	Present
0	0.5641	0.56415775	-0.2	0.5269	0.52691089
0.5	0.6473	0.64736510	-0.4	0.4865	0.48653284
1	0.7205	0.72055401	-0.6	0.442	0.44202064
3	0.9574	0.95744512	-0.8	0.3916	0.39166292
10	1.516	1.51623967	-1.0	0.332	0.33202116
20	2.066	2.066			

as shown in Table. (5.1).

The effects of radiation R, non-Darcy parameter F_c, angle of inclination A, Brownian motion parameter N_b, thermophoresis parameter N_t and amplitude a of the wavy surface on the dimensionless velocity, temperature, nanoparticle volume fraction functions and heat and nanoparticle mass transfer rates are presented graphically in Figs. 5.1 - 5.7.

Fig. 5.1 shows the effect of the amplitude of the wavy surface on velocity, temperature and nanoparticle volume fraction distributions. It is observed that as a increases, velocity increases near the plate and decreases away from the plate, whereas the temperature and nanoparticle volume fraction decrease for aiding flow and the reverse trend is observed in the case of opposing flow.

The effect of the angle of inclination of the wavy surface on velocity, temperature and nanoparticle volume fraction is plotted in Fig. 5.2. Here again as observed in previous chapters, we note that as A increases, the velocity increases near the plate and decreases away from the plate for aiding flow whereas the velocity decreases near the plate and increases away from the plate for opposing flow. But the temperature and nanoparticle volume fraction decrease within the boundary layer region for the aiding flow and increase for the opposing flow. When the surface is vertical, the smallest temperature and nanoparticle volume fraction distributions are observed for aiding flow whereas largest temperature and nanoparticle volume fraction distributions are observed for opposing flow. For the horizontal surface,

largest temperature and nanoparticle volume fraction distributions are observed for aiding flow. Smallest temperature and nanoparticle volume fraction distributions are observed for opposing flow.

Fig. 5.3 displays the effect of non-Darcy parameter on the dimensionless velocity, temperature and nanoparticle volume fraction. Fig. 5.3(a) shows that an increase in non-Darcy parameter reduces velocity for aiding flow. Since F_c represents the inertial drag, an increase in the non-Darcy parameter increases the resistance to the flow and so a decrease in the fluid velocity is expected. Here $F_c = 0$ represents the case where the flow is Darcian. The velocity is maximum in this case due to the total absence of inertial drag. In case of opposing flow the velocity is increasing with the increase in the non-Darcy parameter. An increase in F_c, increases temperature values for aiding flow, since as the fluid is decelerated, energy is dissipated as heat and serves to increase temperatures. As such the temperature is minimised for the lowest value of F_c and maximised for the highest value of F_c as shown in Fig. 5.3(b). Further it is noticed that increase in F_c decreases the temperature for opposing flow. From Fig. 5.3(c), it is observed that the nanoparticle volume fraction increases for aiding flow and decreases in the case of opposing flow.

The variation of velocity, temperature and nanoparticle volume fraction on radiation parameter R is shown in Fig. 5.4. Fig. 5.4(a) reveals that an increase in the radiation parameter increases the velocity for aiding flow and reduces for the case of opposing flow. Increase in radiation parameter enhances the temperature for both aiding and opposing flows as shown in Fig. 5.4(b). We observe a negligible effect of radiation on nanoparticle volume fraction as shown in Fig. 5.4(c). These results can be explained by the fact that an increase in the radiation parameter ($R = \frac{4\sigma {T_\infty}^3}{K K_e}$) for a given K and T_∞ means a decrease in the Rosseland radiation absorptivity K_e. Hence, the divergence of radiative heat flux q_r increases as K_e decreases. Therefore, the rate of radiative heat transferred to the fluid increases, and consequently the fluid temperature increases and simultaneously the velocity of the fluid also increases.

Figure 5.5 shows the effect of amplitude and angle of inclination of the wavy surface on the Nusselt and nanoparticle Sherwood number. It reveals that an increase in the wave

amplitude reduces the local heat and nanoparticle mass transfer for both aiding and opposing flows as shown in Figs. 5.5(a) and 5.5(b). In general, we conclude that increasing the wave amplitude makes the surface more roughened. The variation of heat and nanoparticle mass transfer rates for various values of the angle of inclination A is displayed in Figs. 5.5(c) and 5.5(d). It is seen that an increase in the angle of inclination increases the buoyancy force and assists the flow, leading to an increase in the heat and nanoparticle mass transfer rates for aiding flow whereas reverse trend is observed in the case of opposing flow. The minimum values of the dimensionless heat and nanoparticle mass transfer rates are observed when the surface is horizontal; in which case, the buoyancy force is at its maximum. Therefore, the heat and nanoparticle mass transfer rates are at a lower level when this effect is considered.

The effect of Brownian motion parameter N_b on the heat and nanoparticle mass transfer rates is presented in Figs. 5.6(a) and 5.6(b). Fig. 5.6(a) depicts that the dimensionless heat transfer rate decreases with an increase in the Brownian motion parameter for both aiding and opposing flows. An increase in the value of Brownian motion parameter enhances the nanoparticle volume fraction transfer rate for both aiding and opposing flows, as shown in Fig. 5.6(b). Figs. 5.6(c) and 5.6(d) depict the streamwise distribution of Nusselt and nanoparticle Sherwood numbers for different values of thermophoresis parameter N_t. It is revealed that the heat and nanoparticle mass transfer rate reduce with an increase in the thermophoresis parameter for both aiding and opposing flows.

Figures 5.7(a) and 5.7(b) display the effect of non-Darcy parameter F_c on the Nusselt and nanoparticle Sherwood number. It is observed that in the case of aiding flow, the heat and nanoparticle mass transfer reduces with increase in the value of non-Darcy parameter and a reverse trend is observed in the case of opposing flow. The effect of radiation R on the heat and nanoparticle mass transfer is illustrated in Figs. 5.7(c) and 5.7(d). It is noticed from Fig. 5.7(c) that increase in the radiation parameter increases the heat transfer rate for both aiding and opposing flows. And a negligible effect of radiation on nanoparticle mass transfer is seen through Fig. 5.7(d).

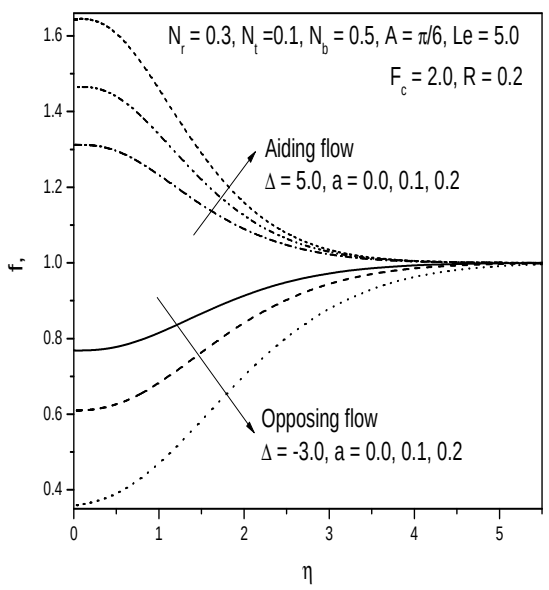

(a)

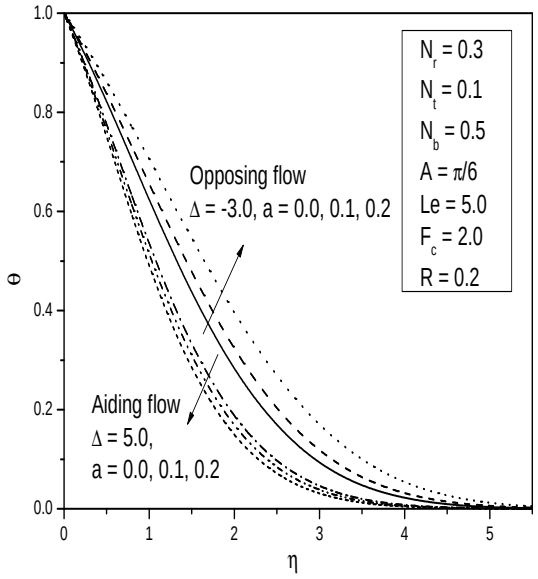

(b)

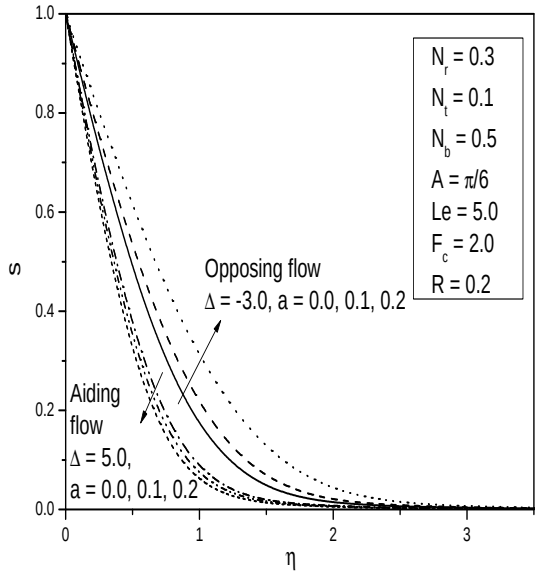

(c)

Figure 5.1: (a) Velocity, (b) temperature and (c) nanoparticle volume fraction profiles for various values of wave amplitude a.

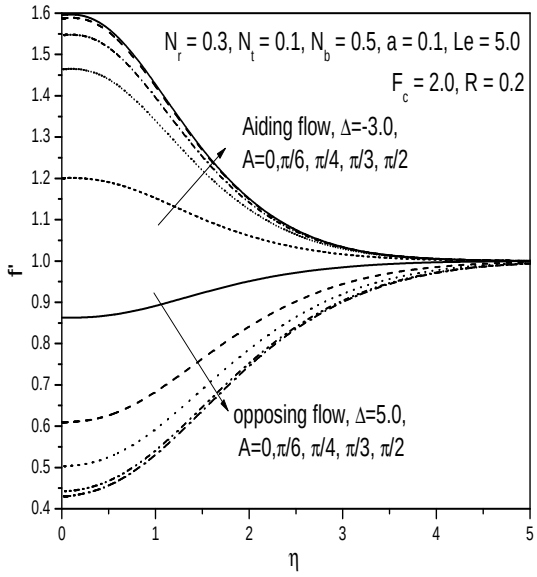

(a)

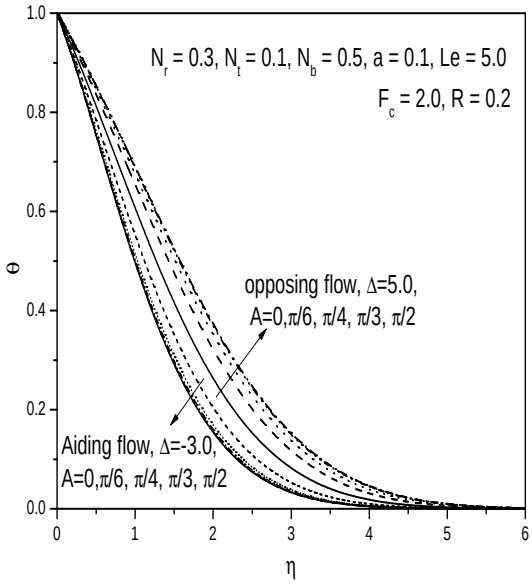

(b)

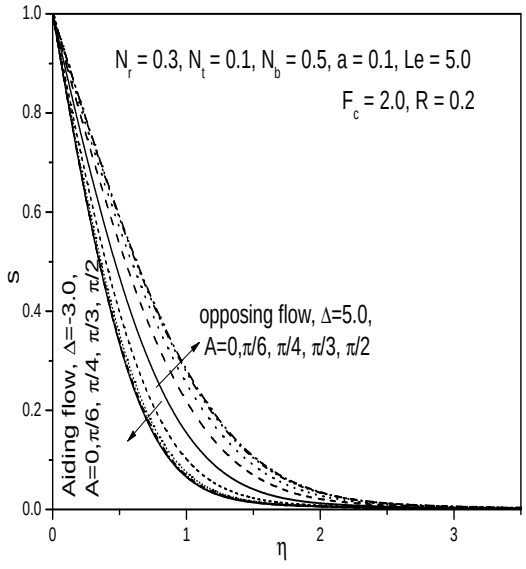

(c)

Figure 5.2: (a) Velocity, (b) temperature and (c) nanoparticle volume fraction profiles for various values of angle of inclination A.

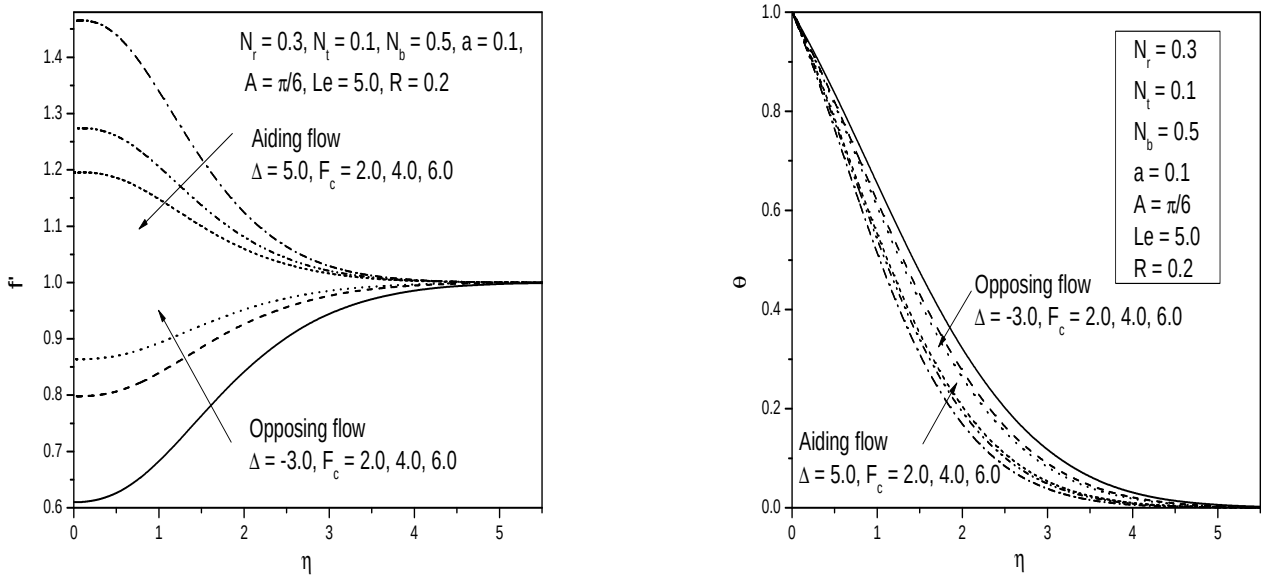

(a) (b)

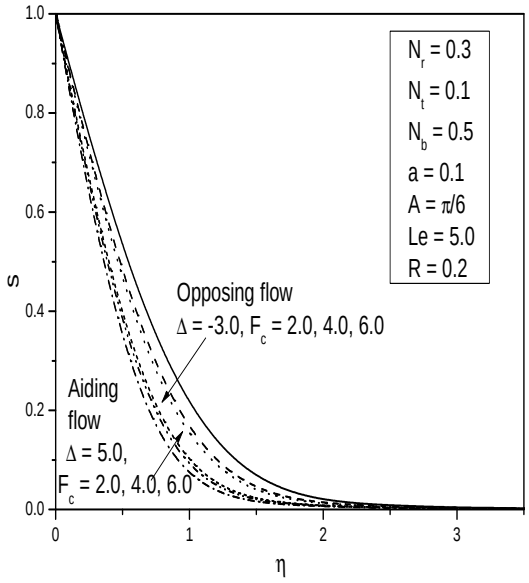

(c)

Figure 5.3: (a) Velocity, (b) temperature and (c) nanoparticle volume fraction profiles for various values of non-Darcy parameter F_c.

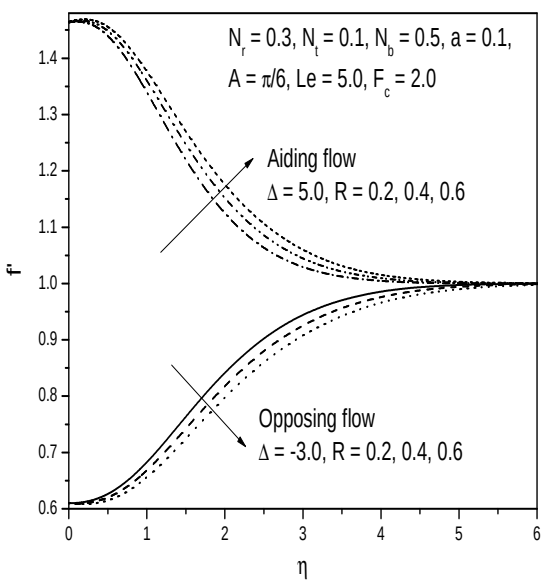

(a)

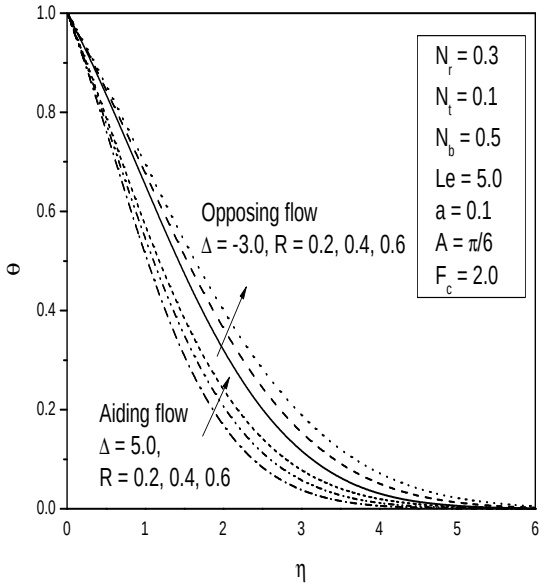

(b)

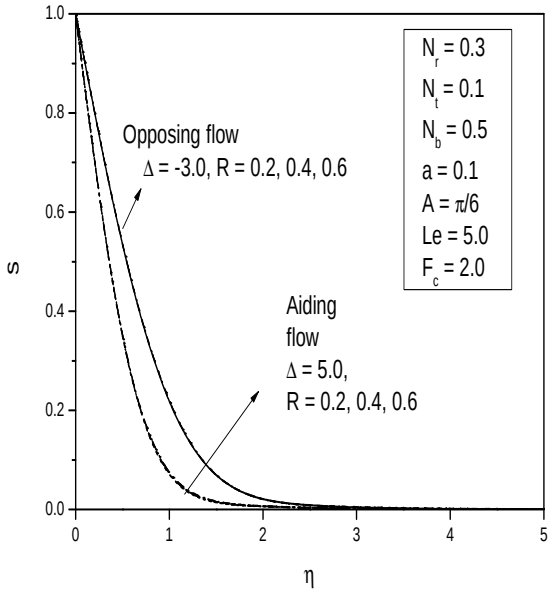

(c)

Figure 5.4: (a) Velocity, (b) temperature and (c) nanoparticle volume fraction profiles for various values of radiation parameter R.

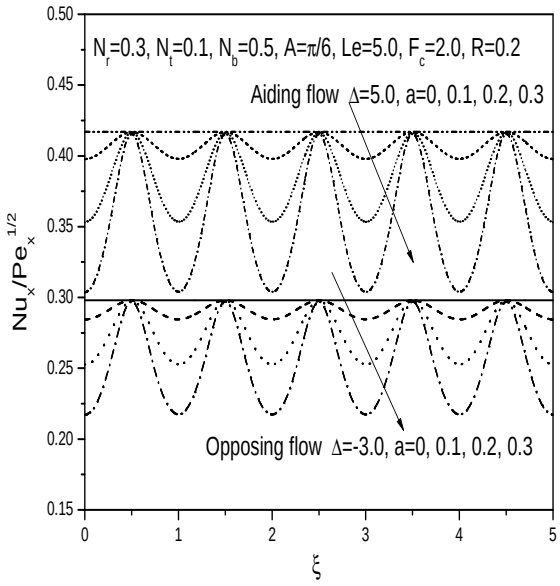

(a)

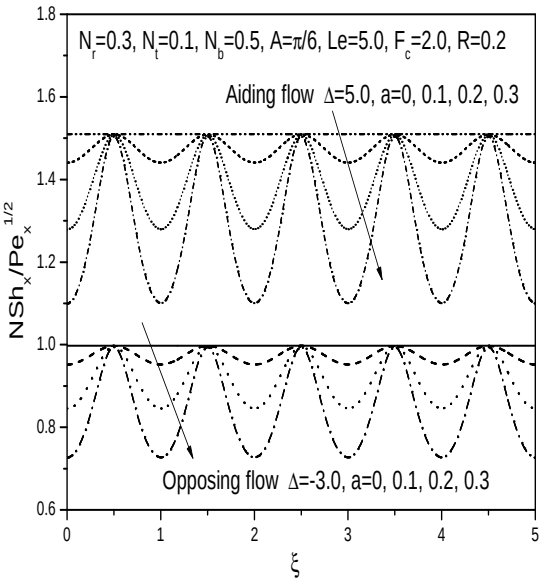

(b)

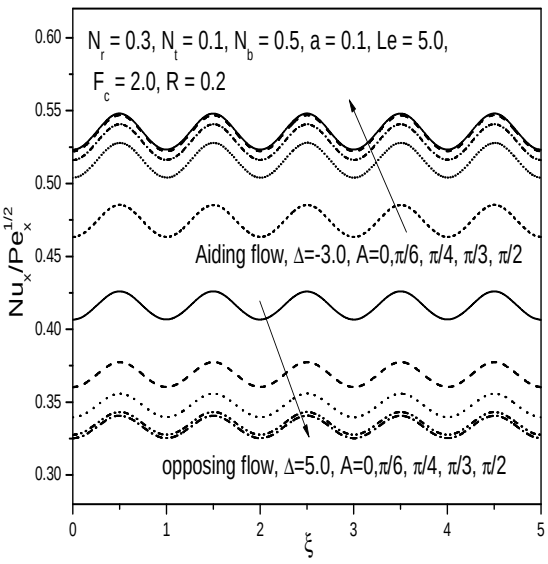

(c)

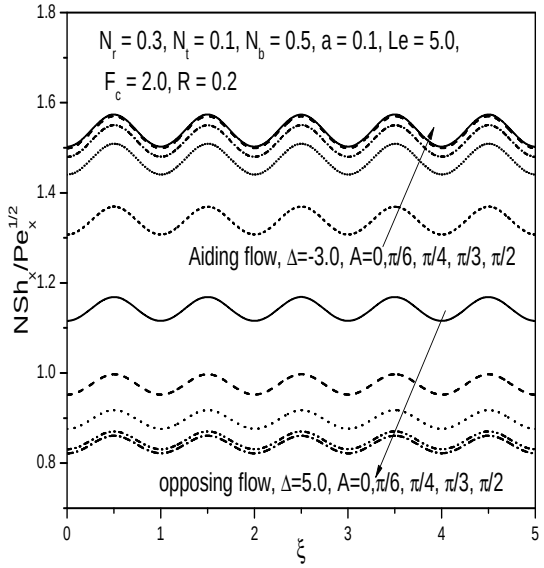

(d)

Figure 5.5: Variation of (a) heat, (b) nanoparticle mass transfer coefficients with wave amplitude and (c) heat, (d) nanoparticle mass transfer coefficients with angle of inclination.

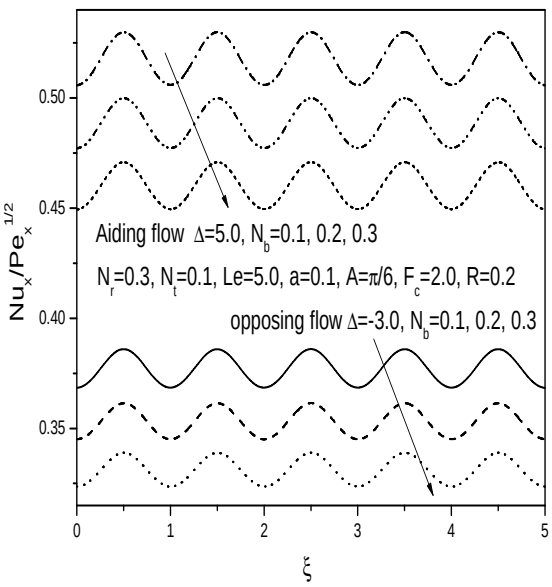

(a)

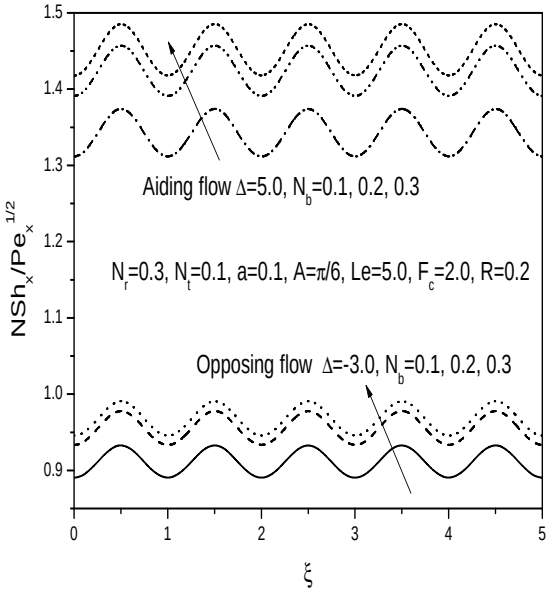

(b)

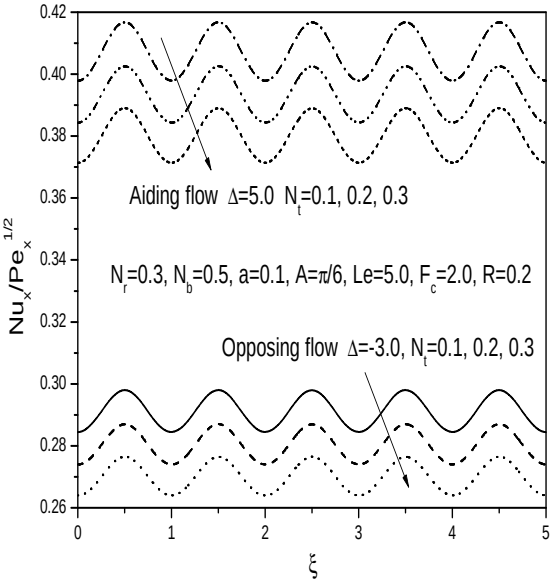

(c)

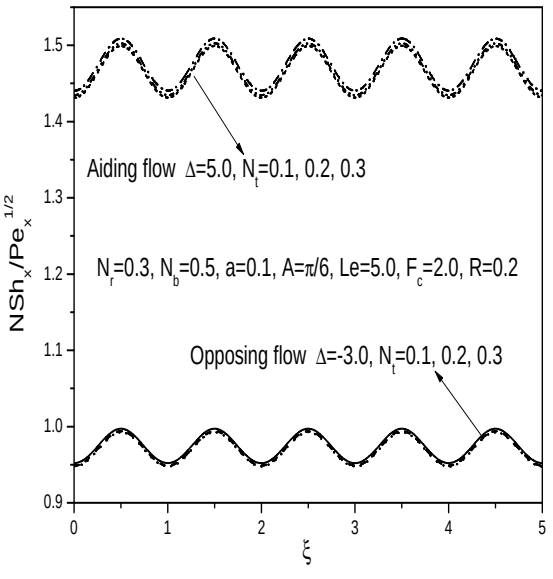

(d)

Figure 5.6: Variation of (a) heat, (b) nanoparticle mass transfer coefficients with Brownian motion parameter and (c) heat, (d) nanoparticle mass transfer coefficients with thermophoresis parameter.

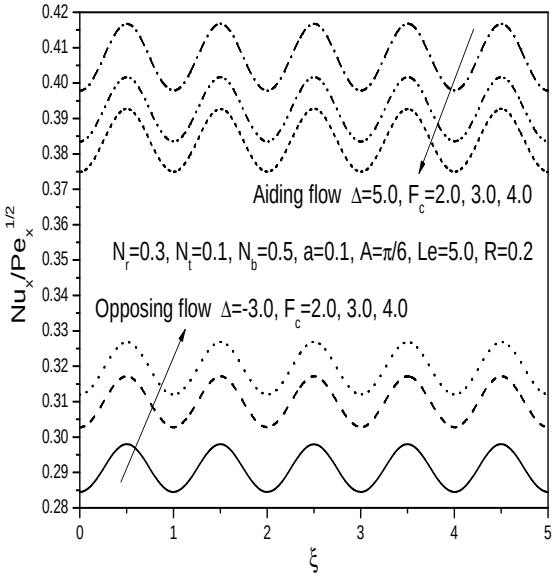

(a)

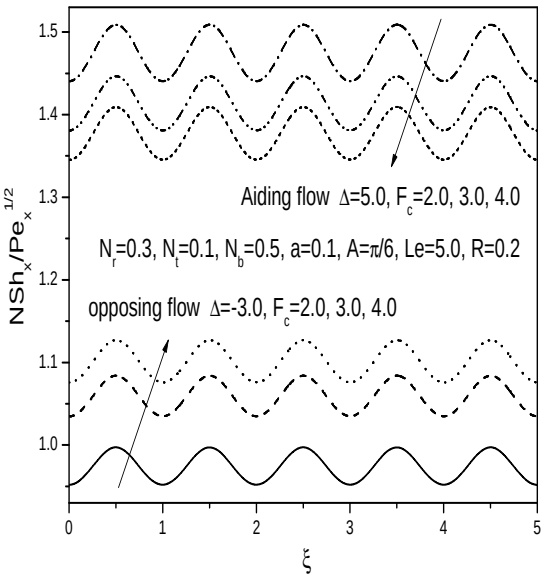

(b)

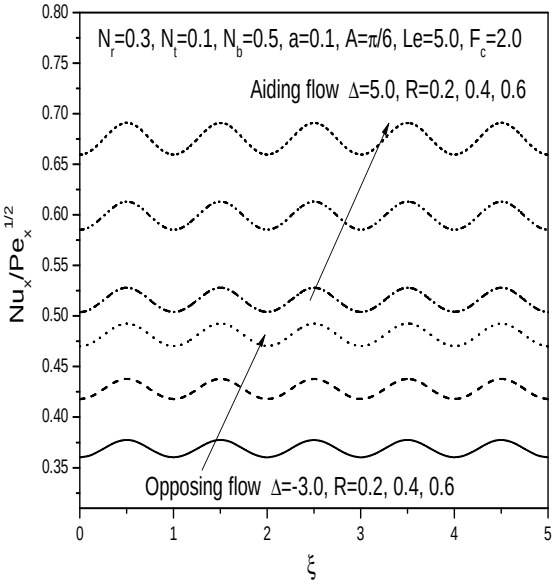

(c)

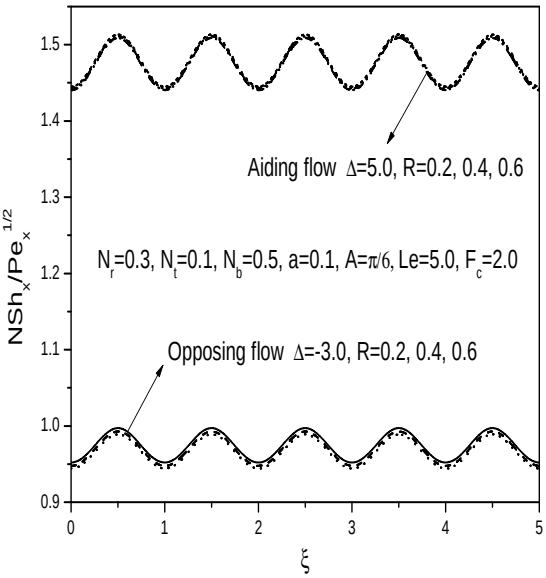

(d)

Figure 5.7: Variation of (a) heat, (b) nanoparticle mass transfer coefficients with non-Darcy parameter and (c) heat, (d) nanoparticle mass transfer coefficients with radiation parameter.

5.2.2 Case(b): Uniform Wall Heat and Nanoparticle Mass Flux

Assume that the wavy plate is maintained at uniform and constant heat and nanoparticle mass fluxes q_w and q_{np} respectively. The steady mixed convection boundary layer flow is governed by Eqns. (5.1) to (5.4) and the present boundary conditions are given by

$$v = 0, \quad q_w = -k(n.\nabla T) + n.q_r, \quad q_{np} = D_B(n.\nabla\phi) \quad \text{at} \quad y = 0, \tag{5.14a}$$

$$u = U_\infty, \quad T \to T_\infty, \quad \phi \to \phi_\infty \quad \text{as} \quad y \to \infty. \tag{5.14b}$$

Substituting the stream function ψ in Eqns. (5.1) - (5.4), and introducing the non-dimensional variables given in (3.18) including $F_c{}^* = F_c\, Pe^{-1/3}$, we get the following system of non-linear partial differential equations

$$f'' + 2F_c{}^*\xi^{1/3}(1+\dot{\delta}^2)^{-1/2} f' f'' = \Delta(\sin A + \dot{\delta}\cos A)\,(\theta' - N_r s')\,, \tag{5.15}$$

$$\left(1 + \frac{4R}{3}\right)\theta'' + \frac{2}{3} f\theta' - \frac{1}{3} f'\theta + \xi^{1/3}\, N_b s'\theta' + \xi^{1/3}\, N_t \theta'^2 = \xi\left(f'\frac{\partial\theta}{\partial\xi} - \theta'\frac{\partial f}{\partial\xi}\right), \tag{5.16}$$

$$s'' + \frac{2}{3} Le\, f\, s' - \frac{1}{3} Le\, f'\, s + \frac{N_t}{N_b}\theta'' = Le\xi\left(f'\frac{\partial s}{\partial\xi} - s'\frac{\partial f}{\partial\xi}\right), \tag{5.17}$$

where $F_c = \dfrac{\tilde{K}\, U_\infty}{\nu}$ is the non-Darcy parameter and $R = \dfrac{4\,\sigma\, {T_\infty}^3}{K\, K_e}$ is the Radiation parameter. The boundary conditions (5.14) in terms of f, θ and s are given by

$$2f + 3\xi\left(\frac{\partial f}{\partial\xi}\right)_{\eta=0} = 0, \quad \theta' = -\frac{3}{3+4\,R}\sqrt{1+\dot{\delta}^2}, \quad s' = -\sqrt{1+\dot{\delta}^2}, \tag{5.18a}$$

$$f' \to 1, \quad \theta \to 0, \quad s \to 0. \tag{5.18b}$$

The non-dimensional heat and nanoparticle mass transfer rates are respectively given by

$$\frac{Nu_\xi}{{Pe_\xi}^{1/3}} = \frac{\xi^{1/3}}{\theta(\xi,0)}, \tag{5.19a}$$

$$\frac{NSh_\xi}{{Pe_\xi}^{1/3}} = \frac{\xi^{1/3}}{s(\xi,0)}. \tag{5.19b}$$

Method of Solution

A local similarity and non-similarity method has been applied to solve the system of Eqns. (5.15) - (5.17) along with the boundary conditions (5.18). The boundary value problems obtained from this method are linearized by the Successive Linearisation Method and then solved using Chebyshev spectral collocation method as explained in detail in previous chapters. Proceeding same as in previous chapters, we obtain the following matrix equation

$$\mathbf{A}_{i-1}\mathbf{X}_i = \mathbf{R}_{i-1}, \tag{5.20}$$

In Eqn. (5.20), $\mathbf{A}_{i-1}$ is a (6N + 6)×(6N + 6) square matrix and $\mathbf{X}_i$ and $\mathbf{R}_{i-1}$ are (6N + 6)×1 column vectors defined by

$$\mathbf{A}_{i-1} = \begin{bmatrix} A_{11} & A_{12} & A_{13} & A_{14} & A_{15} & A_{16} \\ A_{21} & A_{22} & A_{23} & A_{24} & A_{25} & A_{26} \\ A_{31} & A_{32} & A_{33} & A_{34} & A_{35} & A_{36} \\ A_{41} & A_{42} & A_{43} & A_{44} & A_{45} & A_{46} \\ A_{51} & A_{52} & A_{53} & A_{54} & A_{55} & A_{56} \\ A_{61} & A_{62} & A_{63} & A_{64} & A_{65} & A_{66} \end{bmatrix}, \quad \mathbf{X}_i = \begin{bmatrix} \mathbf{F}_i \\ \boldsymbol{\Theta}_{\boldsymbol{i}} \\ \boldsymbol{\Phi}_{\boldsymbol{i}} \\ \mathbf{G}_i \\ \mathbf{H}_i \\ \mathbf{K}_i \end{bmatrix}, \quad \mathbf{R}_{i-1} = \begin{bmatrix} \mathbf{r}_{1,i-1} \\ \mathbf{r}_{2,i-1} \\ \mathbf{r}_{3,i-1} \\ \mathbf{r}_{4,i-1} \\ \mathbf{r}_{5,i-1} \\ \mathbf{r}_{6,i-1} \end{bmatrix} \tag{5.21}$$

where

$\mathbf{F}_i = [f_i(\chi_0), f_i(\chi_1), ..., f_i(\chi_{N-1}), f_i(\chi_N)]^T$, $\mathbf{\Theta_i} = [\theta_i(\chi_0), \theta_i(\chi_1), ..., \theta_i(\chi_{N-1}), \theta_i(\chi_N)]^T$,
$\mathbf{\Phi_i} = [s_i(\chi_0), s_i(\chi_1), ..., s_i(\chi_{N-1}), s_i(\chi_N)]^T$, $\mathbf{G}_i = [g_i(\chi_0), g_i(\chi_1), ..., g_i(\chi_{N-1}), g_i(\chi_N)]^T$,
$\mathbf{H}_i = [h_i(\chi_0), h_i(\chi_1), ..., h_i(\chi_{N-1}), h_i(\chi_N)]^T$, $\mathbf{K}_i = [k_i(\chi_0), k_i(\chi_1), ..., k_i(\chi_{N-1}), k_i(\chi_N)]^T$,
$\mathbf{r}_{j,i-1} = [r_{j,i-1}(\chi_0), r_{j,i-1}(\chi_1), \cdots, r_{j,i-1}(\chi_{N-1}), r_{j,i-1}(\chi_N)]^T, j = 1, 2, 3, 4, 5, 6$
$A_{11} = a_{1,i-1}\mathbf{D}^2 + a_{2,i-1}\mathbf{D},\ A_{12} = a_{3,i-1}\mathbf{D},\ A_{13} = a_{4,i-1}\mathbf{D},\ A_{14} = \mathbf{0},\ A_{15} = \mathbf{0},\ A_{16} = \mathbf{0}$
$A_{21} = b_{4,i-1}\mathbf{D} + b_{5,i-1}\mathbf{I},\ A_{22} = b_{1,i-1}\mathbf{D}^2 + b_{2,i-1}\mathbf{D} + b_{3,i-1}\mathbf{I},\ A_{23} = b_{6,i-1}\mathbf{D},$
$A_{24} = b_{7,i-1}\mathbf{I},\ A_{25} = b_{8,i-1}\mathbf{I},\ A_{26} = \mathbf{0},\ A_{31} = c_{3,i-1}\mathbf{D} + c_{4,i-1}\mathbf{I},\ A_{32} = c_{5,i-1}\mathbf{D}^2,$
$A_{33} = \mathbf{D}^2 + c_{1,i-1}\mathbf{D} + c_{2,i-1}\mathbf{I},\ A_{34} = c_{6,i-1}\mathbf{I},\ A_{35} = \mathbf{0},\ A_{36} = c_{7,i-1}\mathbf{I},$
$A_{41} = d_{3,i-1}\mathbf{D}^2 + d_{4,i-1}\mathbf{D},\ A_{42} = d_{5,i-1}\mathbf{D},\ A_{43} = d_{6,i-1}\mathbf{D},\ A_{44} = d_{1,i-1}\mathbf{D}^2 + d_{2,i-1}\mathbf{D},$
$A_{45} = d_{7,i-1}\mathbf{D},\ A_{46} = d_{8,i-1}\mathbf{D},\ A_{51} = l_{4,i-1}\mathbf{D} + l_{5,i-1}\mathbf{I}, A_{52} = l_{6,i-1}\mathbf{D} + l_{7,i-1}\mathbf{I},$
$A_{53} = l_{8,i-1}\mathbf{D},\ A_{54} = l_{9,i-1}\mathbf{D} + l_{10,i-1}\mathbf{I},\ A_{55} = l_{1,i-1}\mathbf{D}^2 + l_{2,i-1}\mathbf{D} + l_{3,i-1}\mathbf{I},$
$A_{56} = l_{11,i-1}\mathbf{D},\ A_{61} = m_{3,i-1}\mathbf{D} + m_{4,i-1}I,\ A_{62} = \mathbf{0},\ A_{63} = m_{5,i-1}\mathbf{D} + m_{6,i-1}\mathbf{I}$
$A_{64} = m_{7,i-1}\mathbf{D} + m_{8,i-1}\mathbf{I},\ A_{65} = m_{9,i-1}\mathbf{D}^2,\ A_{66} = \mathbf{D}^2 + m_{1,i-1}\mathbf{D} + m_{2,i-1}\mathbf{I}$

Here $a_{k,i-1}$, $b_{k,i-1}$, $c_{k,i-1}$,$d_{k,i-1}$, $l_{k,i-1}$, $m_{k,i-1}$ are diagonal matrices of size (N+1)×(N+1) and $\mathbf{I}$ is an identity matrix of size (N +1)×(N +1). After modifying the matrix system (5.20) to incorporate boundary conditions, the solution is obtained as

$$\mathbf{X}_i = \mathbf{A}_{i-1}^{-1}\mathbf{R}_{i-1} \tag{5.22}$$

Results and Discussion

The effects of non-Darcy parameter F_c, radiation parameter R, amplitude a of the wavy surface, angle of inclination A, Brownian motion parameter N_b and thermophoresis parameter N_t on the heat and nanopareticle mass transfer rates have been displayed in Figs. 5.8 - 5.19.

The effect of wave amplitude on the heat and nanoparticle mass transfer rates is shown in Figs. 5.8 and 5.9. It is observed that an increase in the wave amplitude increases the local heat and nanoparticle mass transfer for both aiding and opposing flows. In general, we

conclude that increasing the wave amplitude makes the surface more roughened.

The variation of heat and nanoparticle mass transfer rates for various values of the angle of inclination A is displayed in Figs. 5.10 and 5.11. It is shown that an increase in the angle of inclination increases the buoyancy force and assists the flow, leading to an increase in the heat and nanoparticle mass transfer rates for aiding flow while reverse trend is observed in the case of opposing flow. The minimum values of the dimensionless heat and nanoparticle mass transfer rates are observed when the surface is horizontal; in which case, the buoyancy force is at its maximum. Therefore, the heat and nanoparticle mass transfer rates are at a lower level when this effect is considered ($A \neq 0$).

Figs. 5.12 and 5.13 present the effect of Brownian motion parameter N_b on the heat and nanoparticle mass transfer rates. Fig. 5.12 depicts that the dimensionless heat transfer rate decreases with increase in the Brownian motion parameter for both aiding and opposing flows. An increase in the value of Brownian motion parameter enhances the nanoparticle mass transfer rate for both aiding and opposing flows, as shown in Fig. 5.13. The streamwise distribution of Nusselt and nanoparticle Sherwood numbers for different values of thermophoresis parameter N_t is plotted in Figs. 5.14 and 5.15. It is depicted that the heat and nanoparticle mass transfer rates reduce with an increase in the thermophoresis parameter for both the cases of aiding and opposing flows.

Figs. 5.16 and 5.17 display the effect of non-Darcy parameter F_c on the Nusselt and nanoparticle Sherwood number. It is revealed that the heat and nanoparticle mass transfer reduces with increase in the value of non-Darcy parameter in both the cases of aiding and opposing flows. The effect of radiation R on the heat and nanoparticle mass transfer is illustrated in Figs. 5.18 and 5.19. It is noticed that increase in the radiation parameter increases the heat and nanoparticle mass transfer rates for both aiding and opposing flows.

5.3 Conclusions

In this Chapter, the problem of mixed convection in a nanofluid along an inclined wavy surface embedded in a non-Darcy porous medium with radiation effect with (a) uniform wall temperature and nanoparticle concentration conditions and (b)uniform and constant heat and nanoparticle mass flux conditions has been investigated. From this investigation, the following conclusions are drawn for cases (a) and (b).

The effect of non-Darcy parameter is to reduce the velocity, local heat and nanoparticle mass transfer for aiding flow and to increase in the case of opposing flow while the temperature and nanoparticle volume fraction increases for aiding flow and reduces for opposing flow. The influence of radiation is to enhance the velocity and temperature for aiding flow and to reduce these in the case of opposing flow. For both aiding and opposing flows, the local heat transfer enhances and a negligible effect on nanoparticle volume fraction and nanoparticle mass transfer rates is observed. An increase in the wave amplitude enhances the velocity for aiding flow but reduces for opposing flow whereas the temperature, nanoparticle volume fraction reduces for aiding flow and increases for opposing flow. The local heat and nanoparticle mass transfer rates are increased for both aiding and opposing flows. The effect of angle of inclination is to increase the velocity, local heat and nanoparticle mass transfer for aiding flow and a reverse trend is observed in the case of opposing flow. Moreover, the temperature and nanoparticle volume fraction reduce for aiding flow and increase these for opposing flow.

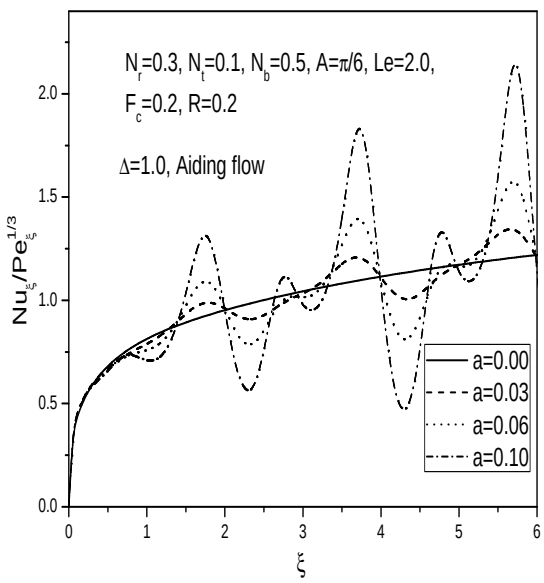

(a)

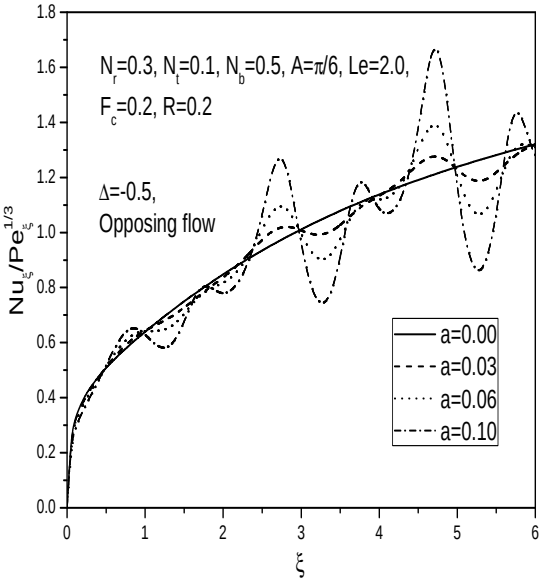

(b)

Figure 5.8: Variation of heat transfer coefficient with wave amplitude a for both (a) Aiding and (b) Opposing flows.

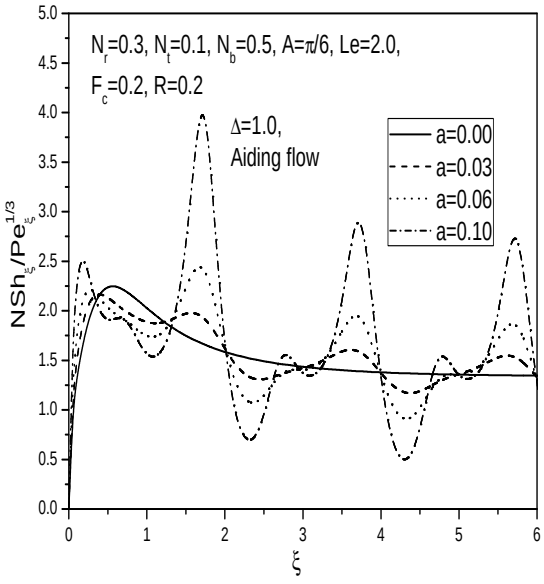

(a)

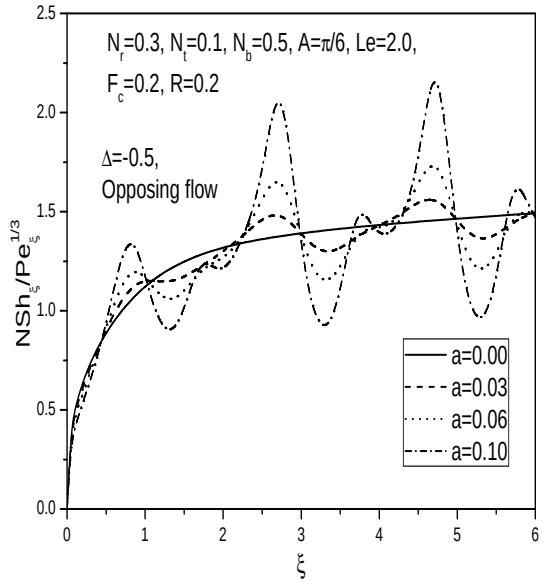

(b)

Figure 5.9: Variation of nanoparticle mass transfer coefficient with wave amplitude a for both (a) Aiding and (b) Opposing flows.

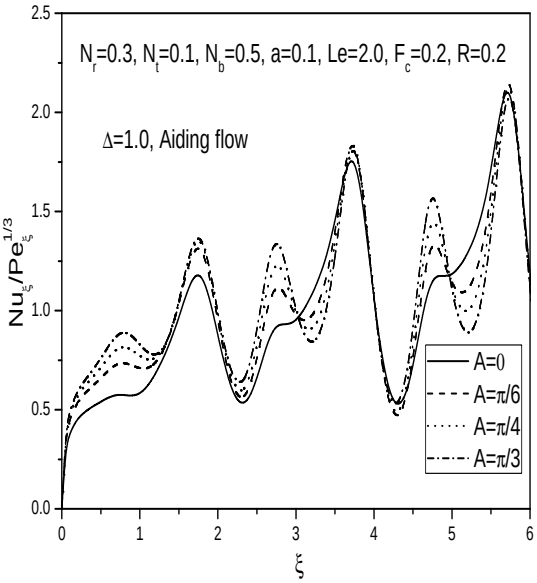

(a)

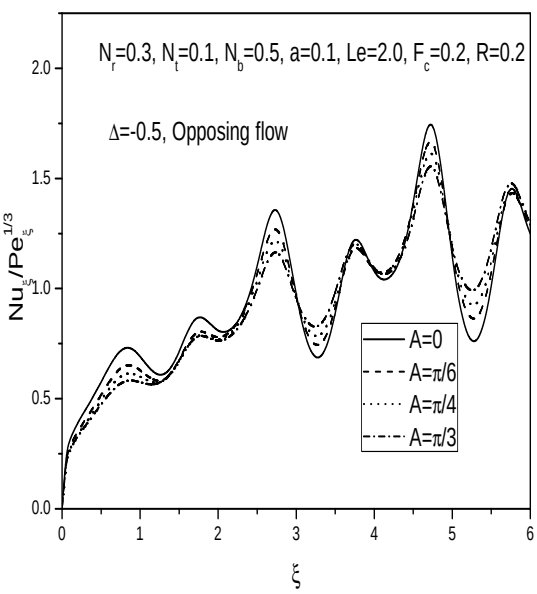

(b)

Figure 5.10: Variation of heat transfer coefficient with angle of inclination A for both (a) Aiding and (b) Opposing flows.

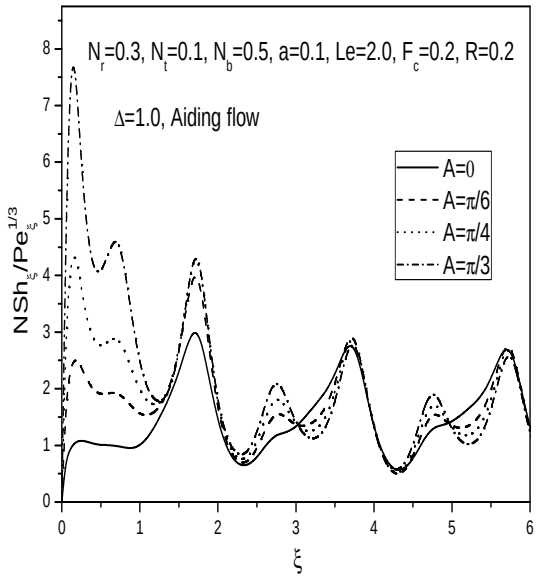

(a)

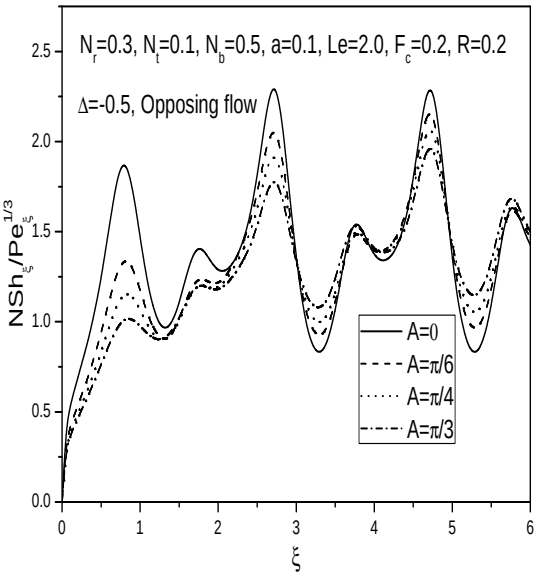

(b)

Figure 5.11: Variation of nanoparticle mass transfer coefficient with angle of inclination A for both (a) Aiding and (b) Opposing flows.

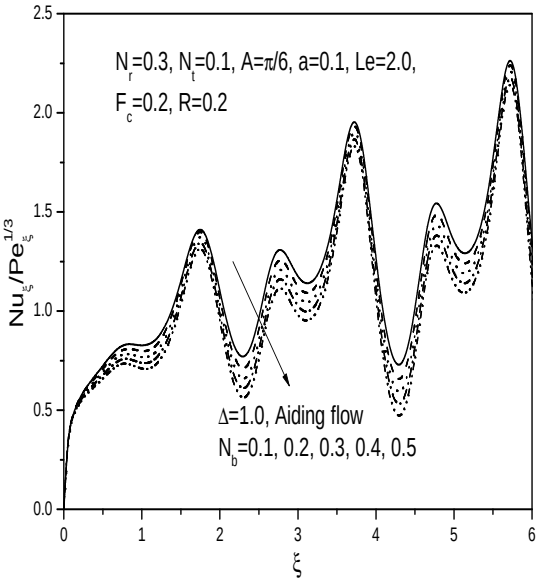

(a)

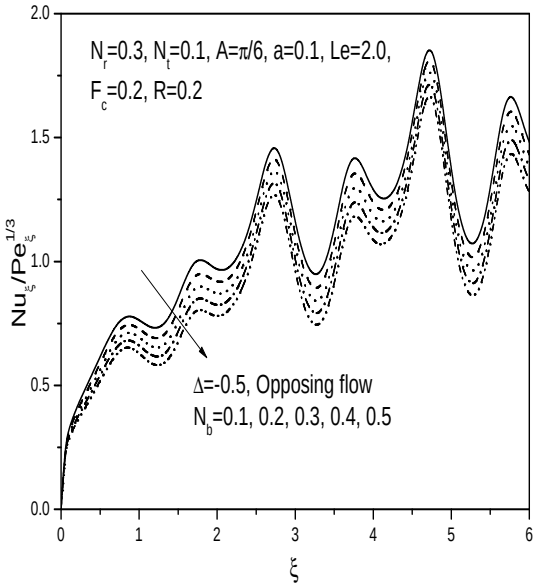

(b)

Figure 5.12: Variation of heat transfer coefficient with Brownian motion parameter N_b for both (a) Aiding and (b) Opposing flows.

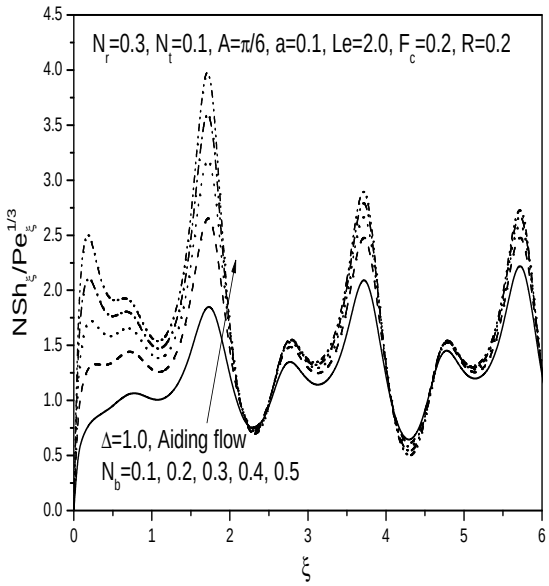

(a)

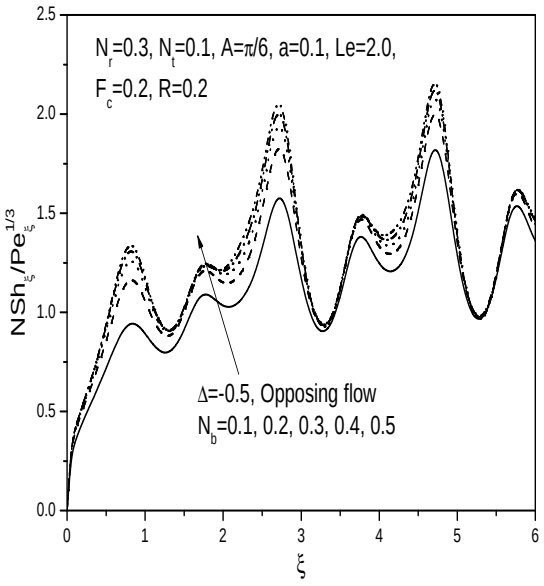

(b)

Figure 5.13: Variation of nanoparticle mass transfer coefficient with Brownian motion parameter N_b for both (a) Aiding and (b) Opposing flows.

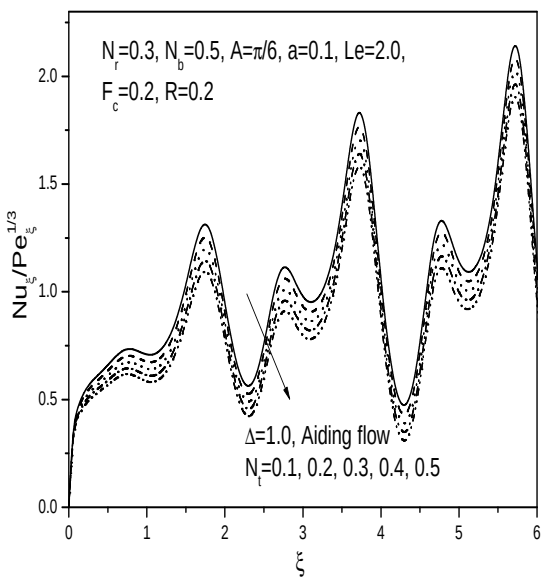

(a)

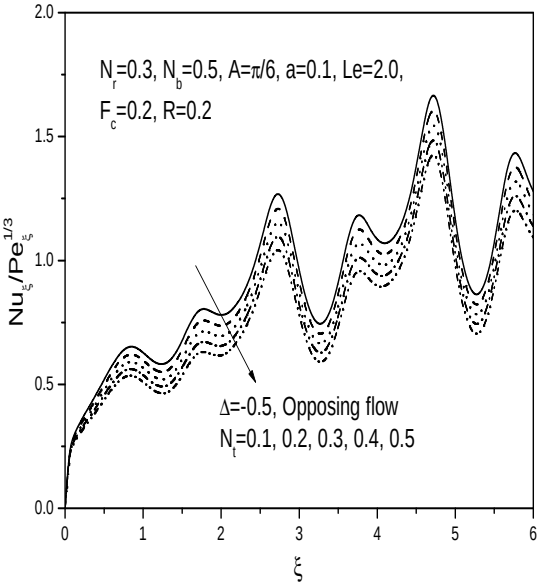

(b)

Figure 5.14: Variation of heat transfer coefficient with thermophoresis parameter N_t for both (a) Aiding and (b) Opposing flows.

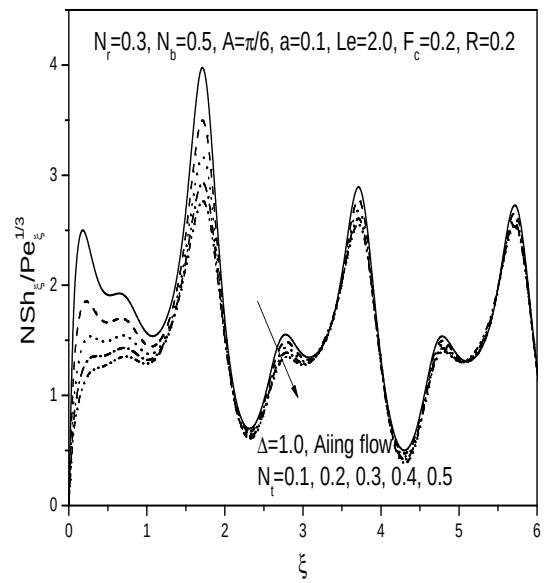

(a)

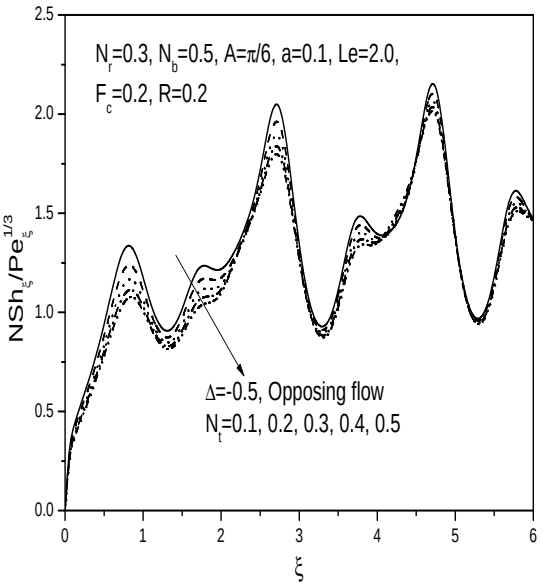

(b)

Figure 5.15: Variation of nanoparticle mass transfer coefficient with thermophoresis parameter N_t for both (a) Aiding and (b) Opposing flows.

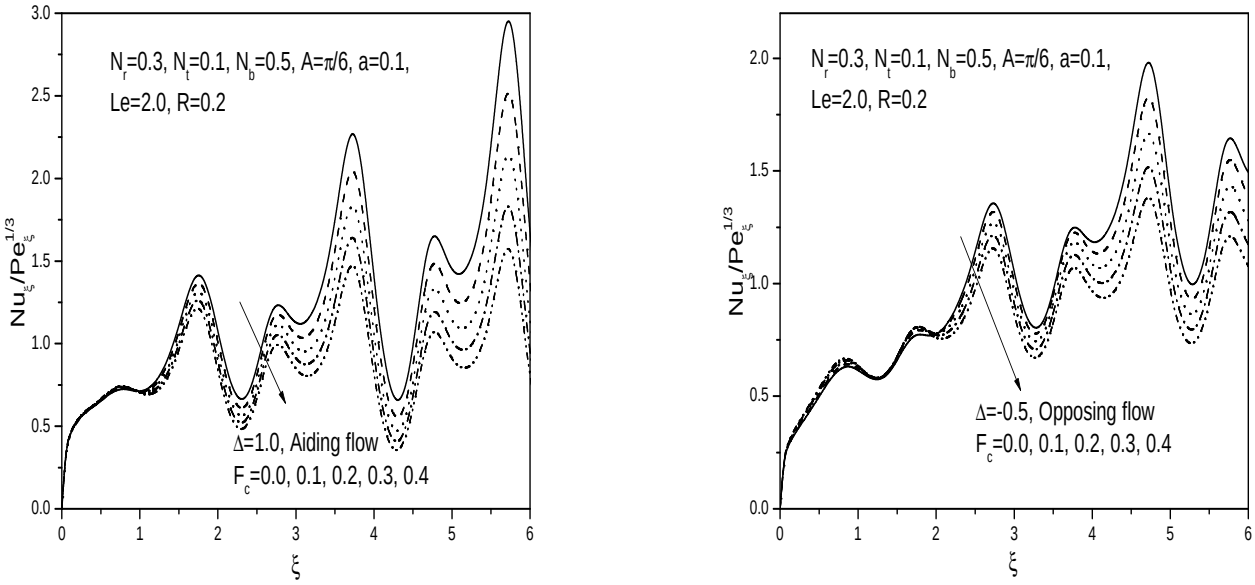

(a) (b)

Figure 5.16: Variation of heat transfer coefficient with non-Darcy parameter F_c for both (a) Aiding and (b) Opposing flows.

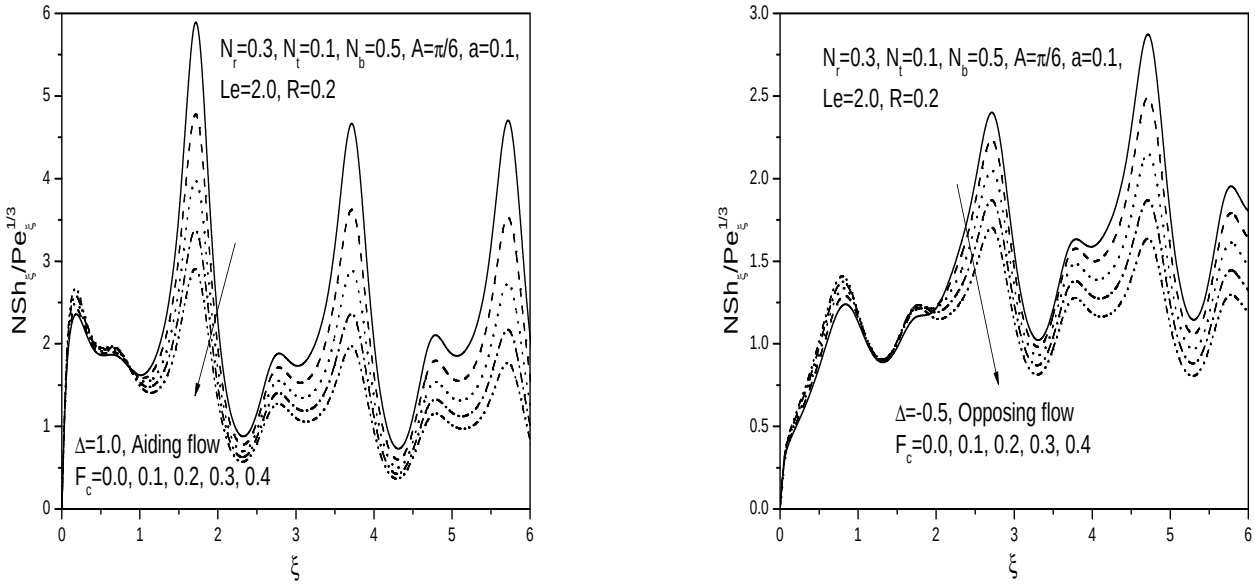

(a) (b)

Figure 5.17: Variation of nanoparticle mass transfer coefficient with non-Darcy parameter F_c for both (a) Aiding and (b) Opposing flows.

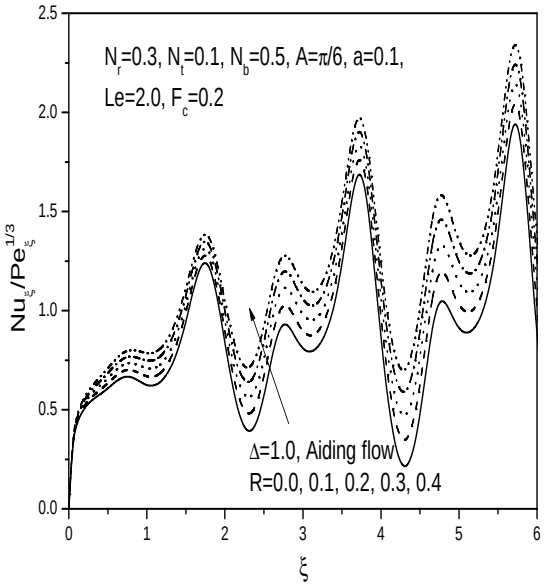

(a)

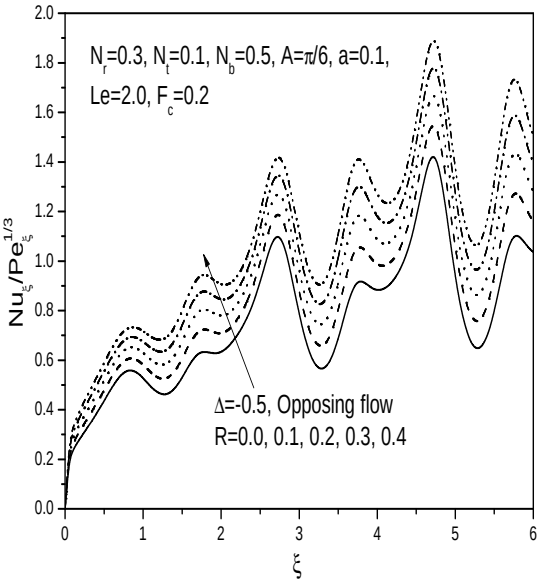

(b)

Figure 5.18: Variation of heat transfer coefficient with radiation parameter R for both (a) Aiding and (b) Opposing flows.

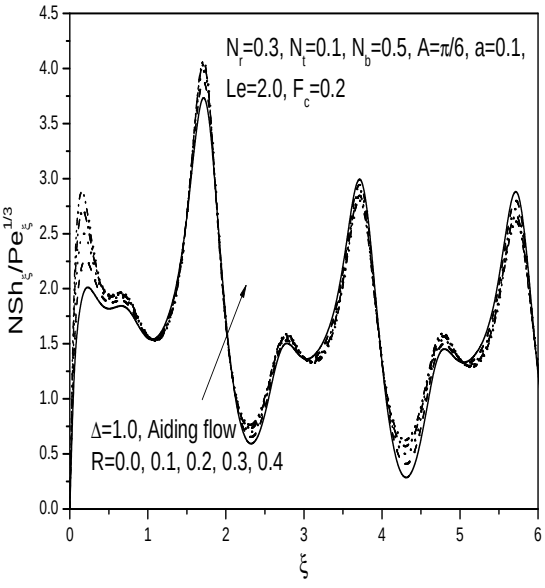

(a)

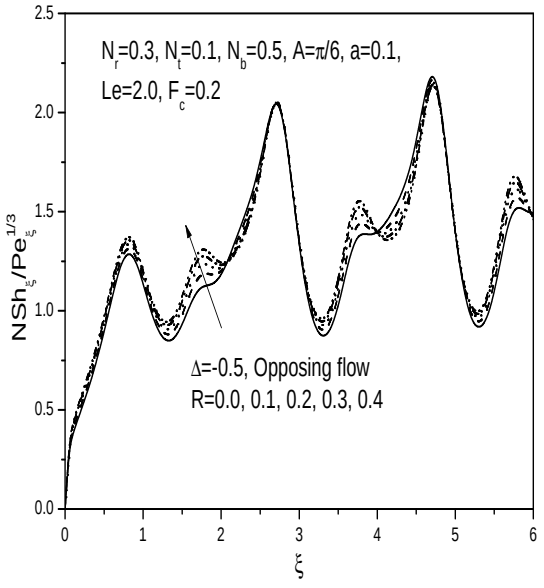

(b)

Figure 5.19: Variation of nanoparticle mass transfer coefficient with radiation parameter R for both (a) Aiding and (b) Opposing flows.

Chapter 6

Effect of thermal stratification on natural convection over an inclined wavy surface embedded in a porous medium saturated with a nanofluid [1]

6.1 Introduction

In practical situations, where heat and mass transfer mechanism run in parallel, particularly in porous media applications, it is worth analyzing the effect of thermal stratification on natural convective heat and mass transfer in porous medium. For example, the temperature stratification and concentration differences of hydrogen and oxygen in lakes and ponds is one instance that needs examination, as this may directly affect the growth rate of all cultured species. Also, the analysis of thermal stratification is important for solar engineering because higher energy efficiency can be achieved with better stratification. Some of the authors have explored the importance of convective transport in doubly stratified porous media due to its application in various fields. Based on their results, the scientists have shown that

[1] Accepted for publication in "**Computational thermal Sciences: An International Journal**"

thermal stratification in energy storage may considerably increase system performance. An exhaustive discussion of the natural convection in a thermallly stratified porous medium can be found in the literature.

The study of heat and mass transfer from the irregular wavy surfaces is of fundamental importance because of its enhancing heat transfer characteristics. Rathish kumar and Shalini [52] investigated the effect of thermal stratification on free convection along a vertical wavy surface and showed that thermal stratification decreases the local Nusselt number along the wavy wall as one moves away from the leading edge. Cheng [19] analyzed the effect of thermal and mass stratification on double diffusion from a vertical frustum of a wavy cone in porous media saturated with power law fluid. Cheng [20] studied the coupled heat and mass transfer by natural convection near a vertical wavy surface in a non-Newtonian fluid saturated porous medium with thermal and mass stratification.

A Survey of earlier studies on convective transport in porous media reveals that the problem of free convection of nanofluid over an inclined wavy surface in a thermally stratified porous medium is not considered so far. The aim of the present chapter is to consider the influence of thermal stratification on natural convection over an inclined wavy surface in a porous medium saturated with a nanofluid. The effects of pertinent parameters on physical quantities are studied and the results are displayed graphically.

6.2 Mathematical Formulation

Consider the steady natural convection boundary layer flow over an inclined wavy surface embedded in a porous medium saturated with a nanofluid. The x coordinate is taken along the wavy plate and the y coordinate is measured normal to the plate, while the origin of the reference system is considered at the leading edge of the wavy plate. The ambient medium is assumed to be linearly stratified with respect to temperature in the form $T_\infty(x) = T_{\infty,0} + Bx$, where B is a constant which is varied to alter the intensity of stratification in the medium. The values of T_w and ϕ_w are assumed to be greater than the ambient temperature $T_{\infty,0}$ and

nanoparticle concentration ϕ_∞ at any arbitrary reference point in the medium (inside the boundary layer). The porous medium is assumed to be uniform and isotropic and is in local thermal equilibrium with the fluid. The fluid properties are assumed to be constant except for density variations in the buoyancy force term.

Making use of the Boussinesq and standard boundary layer approximations, the governing equations for the conservation of mass, momentum, energy and nanoparticle volume fraction within the boundary layer near the wavy plate are

$$\frac{\partial u}{\partial x} + \frac{\partial v}{\partial y} = 0, \tag{6.1}$$

$$\begin{aligned}\frac{\partial u}{\partial y} - \frac{\partial v}{\partial x} = \frac{(1-\phi_\infty)\rho_{f_\infty}\beta\, K\, g}{\mu}\left(\frac{\partial T}{\partial y}\sin A - \frac{\partial T}{\partial x}\cos A\right) \\ -\frac{(\rho_p - \rho_{f_\infty})\, K\, g}{\mu}\left(\frac{\partial \phi}{\partial y}\sin A - \frac{\partial \phi}{\partial x}\cos A\right),\end{aligned} \tag{6.2}$$

$$\begin{aligned}u\frac{\partial T}{\partial x} + v\frac{\partial T}{\partial y} = \alpha\left(\frac{\partial^2 T}{\partial x^2} + \frac{\partial^2 T}{\partial y^2}\right) + \gamma\left[D_B\left(\frac{\partial \phi}{\partial x}\frac{\partial T}{\partial x} + \frac{\partial \phi}{\partial y}\frac{\partial T}{\partial y}\right)\right. \\ \left. + \frac{D_T}{T_\infty}\left(\left(\frac{\partial T}{\partial x}\right)^2 + \left(\frac{\partial T}{\partial y}\right)^2\right)\right],\end{aligned} \tag{6.3}$$

$$u\frac{\partial \phi}{\partial x} + v\frac{\partial \phi}{\partial y} = D_B\left(\frac{\partial^2 \phi}{\partial x^2} + \frac{\partial^2 \phi}{\partial y^2}\right) + \frac{D_T}{T_\infty}\left(\frac{\partial^2 T}{\partial x^2} + \frac{\partial^2 T}{\partial y^2}\right), \tag{6.4}$$

We study the problem with the condition that the plate is maintained at uniform wall temperature and nanoparticle volume fraction. Here we do not consider the other case (i,e. imposition of uniform and constant heat and nanoparticle mass flux on the wavy surface) as the results are analogous to the previous chapters.

Boundary Conditions

Assume that the semi-infinite inclined wavy plate is subject to uniform wall temperature and nanoparticle volume fraction T_w and ϕ_w, respectively. Hence, the boundary conditions are

$$v = 0,\ T = T_w,\ \phi = \phi_w \text{ at } y = 0 \tag{6.5a}$$

$$u \to 0,\ T \to T_\infty(x),\ \phi \to \phi_\infty \text{ as } y \to \infty, \tag{6.5b}$$

Introducing the stream function ψ in Eqns. (6.1) - (6.4) and then using the following non-dimensional variables

$$\left.\begin{aligned} \xi = \frac{x}{l},\quad \eta = \frac{(y/l-\delta)\,Ra^{1/2}}{\xi^{1/2}\,(1+\dot{\delta}^2)},\quad \psi = \alpha Ra^{1/2}\xi^{1/2} f(\xi,\eta), \\ T - T_\infty(x) = (T_w - T_{\infty,0})\theta(\xi,\eta) \\ \phi - \phi_\infty = (\phi_w - \phi_\infty)\, s(\xi,\eta), \end{aligned}\right\} \tag{6.6}$$

we get the following system of non-linear partial differential equations

$$f'' = (\sin A + \dot{\delta}\cos A)\,(\theta' - N_r s')\,, \tag{6.7}$$

$$\theta'' + \frac{1}{2} f\theta' + N_b s'\theta' + N_t \theta'^2 = \xi\left(S_T f' + f'\frac{\partial\theta}{\partial\xi} - \theta'\frac{\partial f}{\partial\xi}\right), \tag{6.8}$$

$$s'' + \frac{1}{2} Lef s' + \frac{N_t}{N_b}\theta'' = Le\xi\left(f'\frac{\partial s}{\partial\xi} - s'\frac{\partial f}{\partial\xi}\right), \tag{6.9}$$

where $S_T = \dfrac{Bl}{T_w - T_{\infty,0}}$ is the thermal stratification parameter.

The boundary conditions (6.5) in terms of f, θ and s becomes

$$f + 2\xi \left(\frac{\partial f}{\partial \xi}\right)_{\eta=0} = 0, \quad \theta = 1 - S_T \xi, \quad s = 1, \quad \text{at} \quad \eta = 0 \tag{6.10a}$$

$$f' = 0, \quad \theta \to 0, \quad s \to 0 \quad \text{as} \quad \eta \to \infty \tag{6.10b}$$

The heat and nanoparticle fluxes from the wavy plate are given by

$$q_w = -kn.\nabla T, \tag{6.11a}$$

$$q_{np} = -D_B\, n.\nabla \phi. \tag{6.11b}$$

The non dimensional rate of heat transfer, called the Nusselt number $Nu_\xi = \dfrac{q_w\, x}{k\,(T_w\, -\, T_{\infty,0})}$ and the rate of nanoparticle transfer, called nanoparticle Sherwood number $NSh_\xi = \dfrac{q_{np}\, x}{D_B\,(\phi_w - \phi_\infty)}$ are given by

$$\frac{Nu_\xi}{\sqrt{Ra_\xi}} = -\frac{\theta'(\xi, 0)}{(1 - S_T\xi)(1 + \dot{\delta}^2)^{1/2}}, \tag{6.12a}$$

$$\frac{NSh_\xi}{\sqrt{Ra_\xi}} = -\frac{s'(\xi, 0)}{(1 + \dot{\delta}^2)^{1/2}}. \tag{6.12b}$$

Method of Solution

A local Similarity and non-Similarity method is used to solve the non-linear boundary value problems (6.7) - (6.9) subject to the boundary conditions (6.10) to convert them to a sequence of ordinary differential equations and then the Successive Linearization Method along with Chebyshev spetral collocation method is used to solve the resulting system of equations. Proceeding same as in previous chapters we obtain the following matrix equation

$$\mathbf{A}_{i-1}\mathbf{X}_i = \mathbf{R}_{i-1}, \tag{6.13}$$

In Eqn. (6.13), $\mathbf{A}_{i-1}$ is a (6N + 6)×(6N + 6) square matrix and $\mathbf{X}_i$ and $\mathbf{R}_{i-1}$ are (6N + 6)×1 column vectors defined by

$$\mathbf{A}_{i-1} = \begin{bmatrix} A_{11} & A_{12} & A_{13} & A_{14} & A_{15} & A_{16} \\ A_{21} & A_{22} & A_{23} & A_{24} & A_{25} & A_{26} \\ A_{31} & A_{32} & A_{33} & A_{34} & A_{35} & A_{36} \\ A_{41} & A_{42} & A_{43} & A_{44} & A_{45} & A_{46} \\ A_{51} & A_{52} & A_{53} & A_{54} & A_{55} & A_{56} \\ A_{61} & A_{62} & A_{63} & A_{64} & A_{65} & A_{66} \end{bmatrix}, \quad \mathbf{X}_i = \begin{bmatrix} \mathbf{F}_i \\ \mathbf{\Theta}_i \\ \mathbf{\Phi}_i \\ \mathbf{G}_i \\ \mathbf{H}_i \\ \mathbf{K}_i \end{bmatrix}, \quad \mathbf{R}_{i-1} = \begin{bmatrix} \mathbf{r}_{1,i-1} \\ \mathbf{r}_{2,i-1} \\ \mathbf{r}_{3,i-1} \\ \mathbf{r}_{4,i-1} \\ \mathbf{r}_{5,i-1} \\ \mathbf{r}_{6,i-1} \end{bmatrix} \tag{6.14}$$

where

$\mathbf{F}_i = [f_i(\chi_0), f_i(\chi_1), ..., f_i(\chi_{N-1}), f_i(\chi_N)]^T$, $\mathbf{\Theta_i} = [\theta_i(\chi_0), \theta_i(\chi_1), ..., \theta_i(\chi_{N-1}), \theta_i(\chi_N)]^T$,
$\mathbf{\Phi_i} = [s_i(\chi_0), s_i(\chi_1), ..., s_i(\chi_{N-1}), s_i(\chi_N)]^T$, $\mathbf{G}_i = [g_i(\chi_0), g_i(\chi_1), ..., g_i(\chi_{N-1}), g_i(\chi_N)]^T$,
$\mathbf{H}_i = [h_i(\chi_0), h_i(\chi_1), ..., h_i(\chi_{N-1}), h_i(\chi_N)]^T$, $\mathbf{K}_i = [k_i(\chi_0), k_i(\chi_1), ..., k_i(\chi_{N-1}), k_i(\chi_N)]^T$,
$\mathbf{r}_{j,i-1} = [r_{j,i-1}(\chi_0), r_{j,i-1}(\chi_1), \cdots, r_{j,i-1}(\chi_{N-1}), r_{j,i-1}(\chi_N)]^T, j = 1, 2, 3, 4, 5, 6$
$A_{11} = \mathbf{D}^2,\ A_{12} = a_{1,i-1}\mathbf{D},\ A_{13} = a_{2,i-1}\mathbf{D}\ A_{14} = \mathbf{0},\ A_{15} = \mathbf{0},\ A_{16} = \mathbf{0}$
$A_{21} = b_{2,i-1}\mathbf{D} + b_{3,i-1}\mathbf{I},\ A_{22} = \mathbf{D}^2 + b_{1,i-1}\mathbf{D},\ A_{23} = b_{4,i-1}\mathbf{D},\ A_{24} = b_{5,i-1}\mathbf{I},$
$A_{25} = b_{6,i-1}\mathbf{I},\ A_{26} = \mathbf{0},\ A_{31} = c_{2,i-1}\mathbf{D} + c_{3,i-1}\mathbf{I},\ A_{32} = c_{4,i-1}\mathbf{D}^2,\ A_{33} = \mathbf{D}^2 + c_{1,i-1}\mathbf{D},$
$A_{34} = c_{5,i-1}\mathbf{I},\ A_{35} = \mathbf{0},\ A_{36} = c_{6,i-1}\mathbf{I},\ A_{41} = \mathbf{0},\ A_{42} = d_{1,i-1}\mathbf{D},\ A_{43} = d_{2,i-1}\mathbf{D},$
$A_{44} = \mathbf{D}^2,\ A_{45} = d_{3,i-1}\mathbf{D},\ A_{46} = d_{4,i-1}\mathbf{D},\ A_{51} = l_{3,i-1}\mathbf{D} + l_{4,i-1}\mathbf{I},\ A_{52} = l_{5,i-1}\mathbf{D},$
$A_{53} = l_{6,i-1}\mathbf{D},\ A_{54} = l_{7,i-1}\mathbf{D} + l_{8,i-1}\mathbf{I},\ A_{55} = \mathbf{D}^2 + l_{1,i-1}\mathbf{D} + l_{2,i-1}I,\ A_{56} = l_{9,i-1}\mathbf{D}$
$A_{61} = m_{3,i-1}\mathbf{D} + m_{4,i-1}\mathbf{I},\ A_{62} = \mathbf{0},\ A_{63} = m_{5,i-1}\mathbf{D},\ A_{64} = m_{6,i-1}\mathbf{D} + m_{7,i-1}\mathbf{I},$
$A_{65} = m_{8,i-1}\mathbf{D}^2,\ A_{66} = \mathbf{D}^2 + m_{1,i-1}\mathbf{D} + m_{2,i-1}\mathbf{I}$

Here $a_{k,i-1}$, $b_{k,i-1}$, $c_{k,i-1}$,$d_{k,i-1}$, $l_{k,i-1}$, $m_{k,i-1}$ are diagonal matrices of size (N+1)×(N+1) and $\mathbf{I}$ is an identity matrix of size (N +1)×(N +1). After modifying the matrix system (6.13) to incorporate boundary conditions, the solution is obtained as

$$\mathbf{X}_i = \mathbf{A}_{i-1}^{-1}\mathbf{R}_{i-1} \tag{6.15}$$

Results and Discussion

Figures 6.1 - 6.5 display the effects of thermal stratification, angle of inclination, Brownian motion parameter, thermophoresis parameter and amplitude of the wavy surface on the flow, heat and nanoparticle mass transfer of the fluid.

The effect of amplitude and the angle of inclination of the wavy surface on velocity, temperature and nanoparticle volume fraction is plotted in Figs. 6.1 and 6.2. It is observed from Fig. 6.1 that as a increases, velocity increases near the plate and decreases away from the plate, whereas the temperature and nanoparticle volume fraction decreases with increasing values of amplitude. It is noted from Fig. 6.2 that as A increases, the velocity increases near the plate and decreases away from the plate but the temperature and nanoparticle volume fraction decrease within the boundary layer region. When the surface is vertical, the smallest temperature and nanoparticle volume fraction distributions are observed, whereas they are largest for the horizontal surface.

Fig. 6.3 shows the effect of thermal stratification on velocity, temperature and nanoparticle volume fraction distributions. It is noticed that increase in thermal stratification parameter diminishes the effective convective potential between the heated plate and the ambient fluid in the medium. This factor causes a decrease in the buoyancy force, which decelerates the velocity of the flow. Also it is observed that increase in the thermal stratification parameter S_T reduces the temperature of the fluid but increases the nanoparticle volume fraction of the fluid flow.

The effect of the wave amplitude on the local Nusselt and nanoparticle Sherwood number is plotted in Figs. 6.4(a) and 6.4(b). It is seen that an enhancement in wavy amplitude decreases the local heat and nanoparticle mass transfer rates. In general, we conclude that the surface becomes more roughened for increasing values of amplitude of the wavy surface.

The variation of heat and nanoparticle mass transfer rates for various values of the angle of inclination A and thermal stratification parameter S_T is displayed in Figs. 6.4(c) and 6.4(d). It is observed that increasing the angle of inclination increases the buoyancy

force and assists the flow, leading to an increase in the heat and nanoparticle mass transfer rates. But, increasing the thermal stratification parameter S_T decreases both the heat and nanoparticle mass transfer rates.

In Fig. 6.5, the effect of Brownian motion parameter N_b and thermophoresis parameter N_t on the heat and nanoparticle mass transfer rates is presented. The dimensionless heat transfer rate decreases with increasing values of Brownian motion and thermophoresis parameter whereas the nanoparticle mass transfer rate increases with increasing values of Brownian motion parameter and decreases with increasing values of thermophoresis parameter as observed in the earlier chapters.

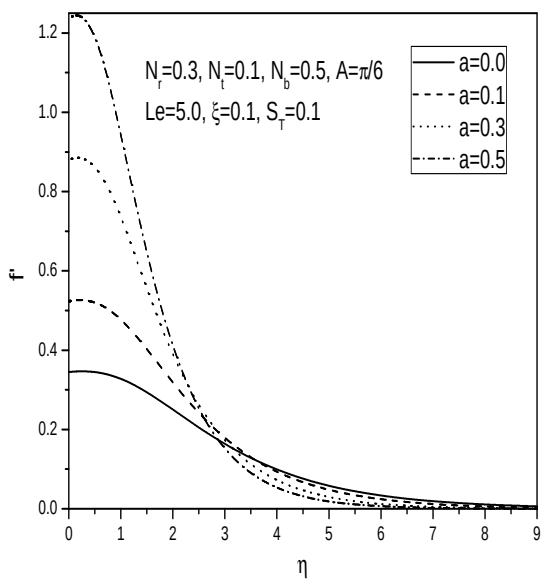

(a)

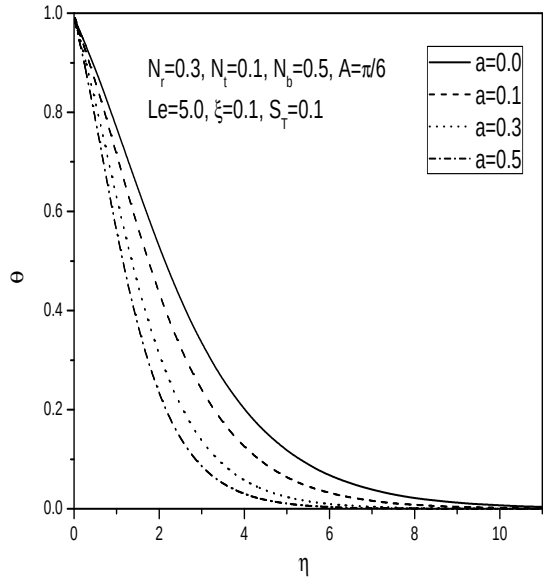

(b)

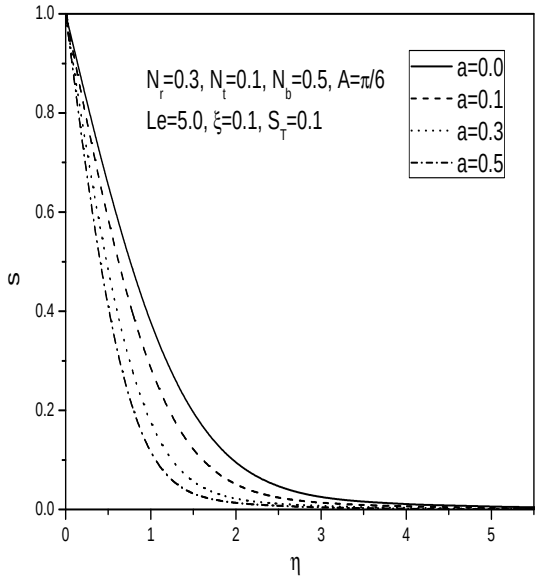

(c)

Figure 6.1: Variation of (a) velocity, (b) temperature and (c) nanoparticle volume fraction profiles with wave amplitude a.

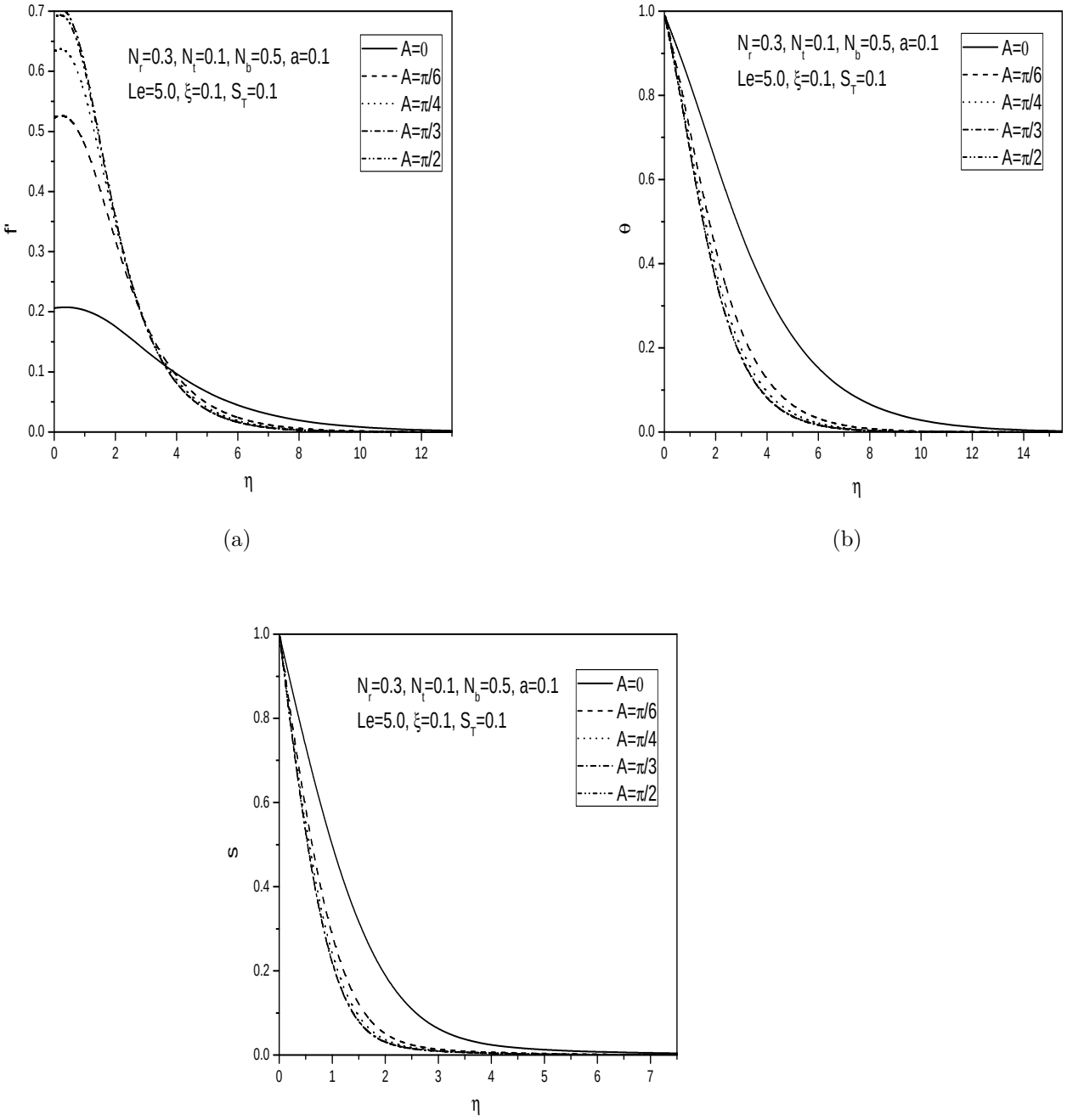

Figure 6.2: Variation of (a) velocity, (b) temperature and (c) nanoparticle volume fraction profiles with angle of inclination A.

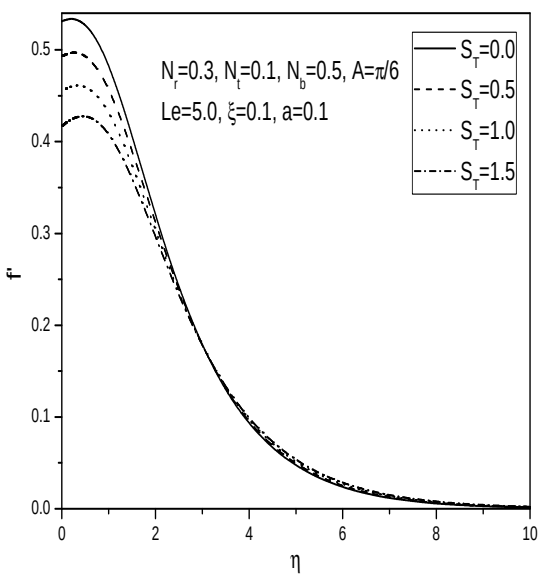

(a)

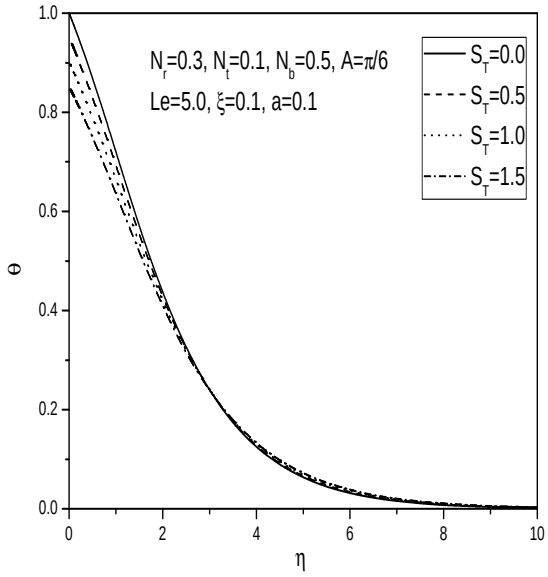

(b)

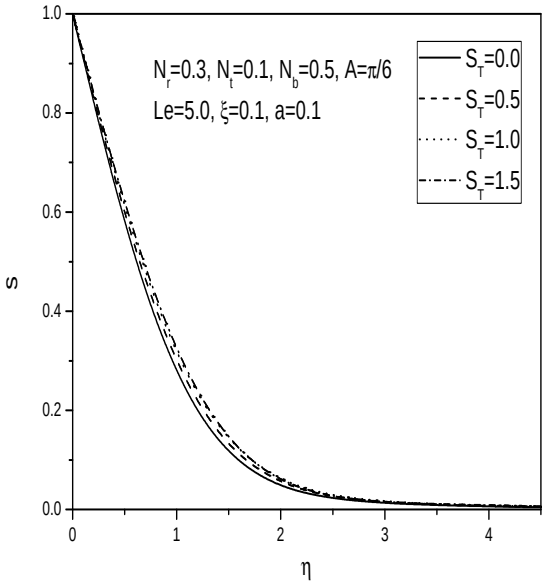

(c)

Figure 6.3: Variation of (a) velocity, (b) temperature and (c) nanoparticle volume fraction profiles with thermal stratification parameter S_T.

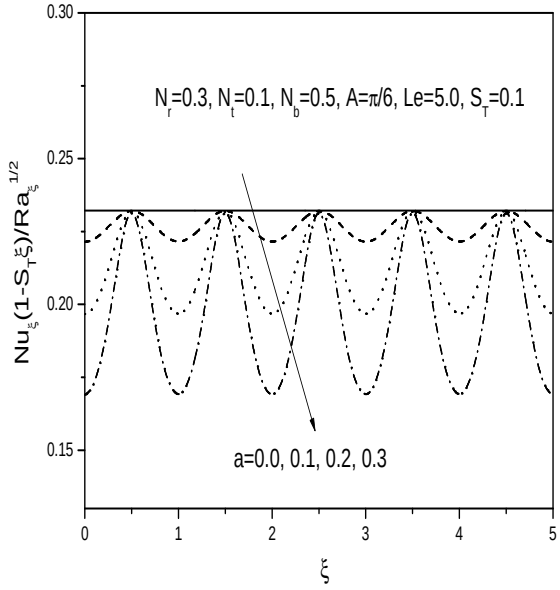

(a)

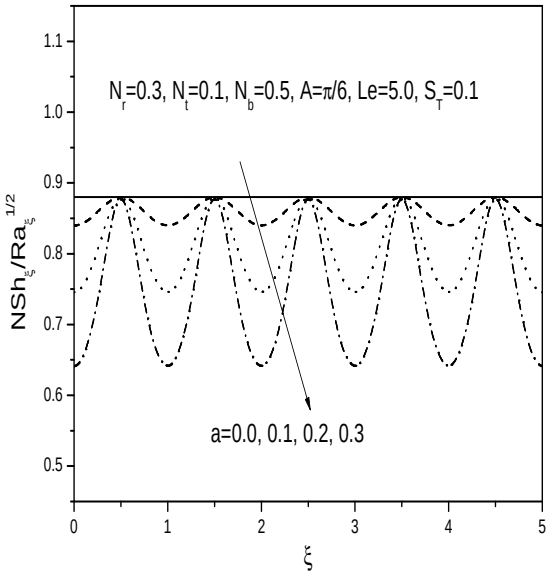

(b)

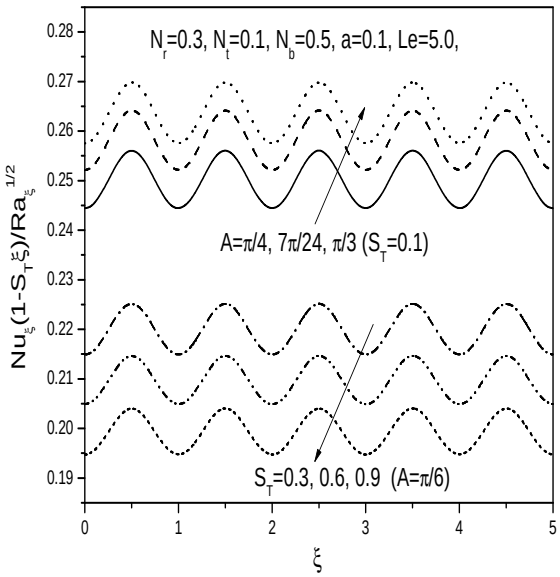

(c)

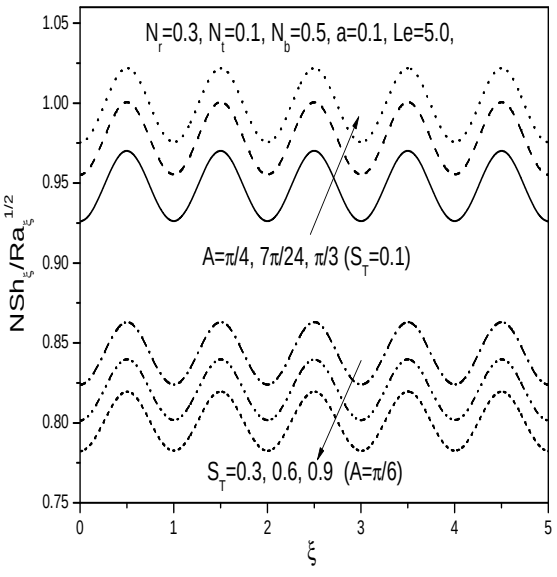

(d)

Figure 6.4: Variation of (a) heat and (b) nanoparticle mass transfer rates with wave amplitude a and (c) heat and (d) nanoparticle mass transfer rates with angle of inclination A and thermal stratification parameter S_T.

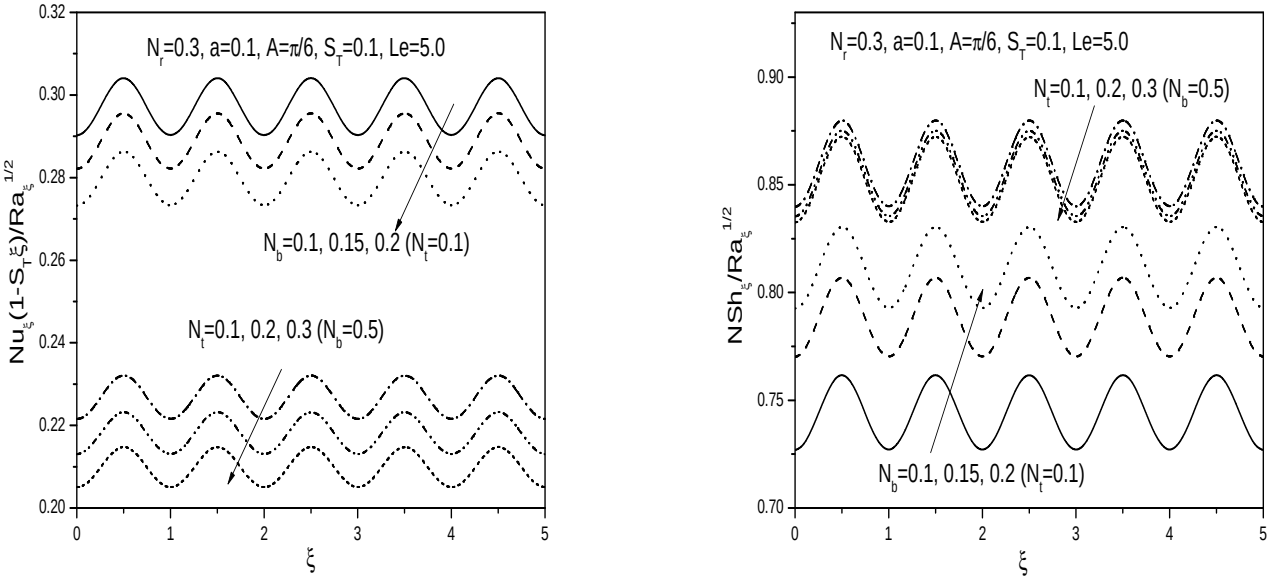

(a) (b)

Figure 6.5: Variation of (a) heat and (b) nanoparticle mass transfer rates with Brownian motion parameter N_b and thermophoresis parameter N_t.

6.3 Conclusions

In this chapter, we analyzed the problem of natural convection heat and nanoparticle mass transfer over an inclined wavy surface embedded in a thermally stratified porous medium saturated with nanofluid subject to uniform wall temperature and nanoparticle volume fraction conditions. From this analysis, the following conclusions are drawn.

Increase in the value of thermal stratification parameter reduces the velocity, temperature, local heat and nanoparticle mass transfer rates but enhances the nanoparticle volume fraction of the fluid. The effect of amplitude a of the wavy surface was found to enhance the velocity near the plate and to reduce the temperature, nanoparticle volume fraction, and local heat transfer and nanoparticle mass transfer coefficients. The influence of the angle of inclination A of the wavy surface to the horizontal is to enhance the velocity, local heat transfer and nanoparticle mass transfer rates, but to reduce the temperature and nanoparticle volume fraction of the fluid flow.

Chapter 7

Effect of thermal stratification on mixed convection over an inclined wavy surface embedded in a porous medium saturated with a nanofluid [1]

7.1 Introduction

In Chapter-6, we studied the influence of thermal stratification on natural convection flow of a nanofluid past an inclined wavy surface embedded in a porous medium. In this chapter we propose to study the mixed convection flow of a nanofluid past an inclined wavy surface embedded in a porous medium under the influence of thermal stratification. A few studies on mixed convection in a thermally stratified fluid saturated porous medium is reported in the literature. Ishak *et al.* [45] theoretically studied the similarity solutions of the mixed convection boundary layer flow over a vertical surface embedded in a thermally stratified porous medium. They have reported that the thermal stratification significantly affects the surface heat transfer as well as surface shear stress. Bansod and Jadhav [7] studied the effect

[1] Communicated to "**International Journal of Non-linear Sciences**"

of double stratification on mixed convection heat and mass transfer from a vertical surface in a fluid saturated porous medium. Ibrahim and Makinde [42] presented a boundary layer analysis for free convection flow in a doubly stratified nanofluid over a vertical plate with uniform surface heat and mass flux conditions. Mahmoud and Waheed [59] investigated the problem of steady two dimensional mixed convection flow of a micropolar fluid over stretching permeable vertical surface with radiation and thermal stratification effects. They have shown that the local Nusselt number and wall couple stress decreases with increasing thermal stratification parmeter. Srinivasacharya and Surender [102] investigated the effect of thermal and mass stratification on mixed convection boundary layer flow of a nanofluid saturated porous medium.

In this chapter we study the effect of thermal stratification on mixed convection in a nanofluid along an inclined wavy surface embedded in a porous medium. A coordinate transformation is employed to transform the complex wavy surface to a smooth surface. The governing equations are transformed into a set of partial differential equations using the non-similarity transformation and then applied the local similarity and non-similarity method to obtain coupled ordinary differential equations. Now, these equations are linearized using the Successive Linearization Method and then solved using Chebyshev spectral collocation method. The effects of pertinent parameters on physical quantities for both aiding and opposing flows are studied and displayed graphically.

7.2 Mathematical Formulation

Consider the steady mixed convection boundary layer flow over an inclined wavy surface embedded in a porous medium saturated with a nanofluid. The x coordinate is taken along the wavy plate and the y coordinate is measured normal to the plate, while the origin of the reference system is considered at the leading edge of the wavy plate. The ambient medium is assumed to be linearly stratified with respect to temperature in the form $T_\infty(x) = T_{\infty,0} + Bx$, where B is a constant which is varied to alter the intensity of stratification in the medium. The values of T_w and ϕ_w are assumed to be greater than the ambient temperature $T_{\infty,0}$ and

nanoparticle volume fraction ϕ_∞ at any arbitrary reference point in the medium (inside the boundary layer). The porous medium is assumed to be uniform and isotropic and is in local thermal equilibrium with the fluid. The fluid properties are assumed to be constant except for density variations in the buoyancy force term.

Making use of the Boussinesq and boundary layer approximations, the governing equations for the conservation of total mass, momentum, energy and nanoparticle volume fraction within the boundary layer near the wavy plate can be written as:

$$\frac{\partial u}{\partial x} + \frac{\partial v}{\partial y} = 0, \tag{7.1}$$

$$\begin{aligned}\frac{\partial u}{\partial y} - \frac{\partial v}{\partial x} = \frac{(1-\phi_\infty)\rho_{f_\infty}\beta\, K\, g}{\mu}\left(\frac{\partial T}{\partial y}\sin A - \frac{\partial T}{\partial x}\cos A\right) \\ -\frac{(\rho_p - \rho_{f_\infty})\, K\, g}{\mu}\left(\frac{\partial \phi}{\partial y}\sin A - \frac{\partial \phi}{\partial x}\cos A\right),\end{aligned} \tag{7.2}$$

$$\begin{aligned}u\frac{\partial T}{\partial x} + v\frac{\partial T}{\partial y} = \alpha\left(\frac{\partial^2 T}{\partial x^2} + \frac{\partial^2 T}{\partial y^2}\right) + \gamma\left[D_B\left(\frac{\partial \phi}{\partial x}\frac{\partial T}{\partial x} + \frac{\partial \phi}{\partial y}\frac{\partial T}{\partial y}\right)\right. \\ \left. + \frac{D_T}{T_\infty}\left(\left(\frac{\partial T}{\partial x}\right)^2 + \left(\frac{\partial T}{\partial y}\right)^2\right)\right],\end{aligned} \tag{7.3}$$

$$u\frac{\partial \phi}{\partial x} + v\frac{\partial \phi}{\partial y} = D_B\left(\frac{\partial^2 \phi}{\partial x^2} + \frac{\partial^2 \phi}{\partial y^2}\right) + \frac{D_T}{T_\infty}\left(\frac{\partial^2 T}{\partial x^2} + \frac{\partial^2 T}{\partial y^2}\right), \tag{7.4}$$

Boundary Conditions

Assume that the semi-infinite inclined wavy plate is subject to uniform wall temperature and nanoparticle volume fraction T_w and ϕ_w, respectively. Hence, the boundary conditions

are

$$v = 0,\ T = T_w,\ \phi = \phi_w \text{ at } y = 0 \tag{7.5a}$$

$$u \to U_\infty,\ T \to T_\infty(x),\ \phi \to \phi_\infty \text{ as } y \to \infty, \tag{7.5b}$$

Introducing the stream function ψ in Eqns. (7.1) - (7.4) and then using the following non-dimensional variables

$$\left.\begin{aligned} \xi = \frac{x}{l}, \quad \eta = \frac{(y/l - \delta)\, Pe^{1/2}}{\xi^{1/2}\,(1+\dot{\delta}^2)}, \quad \psi = \alpha Pe^{1/2}\xi^{1/2} f(\xi,\eta), \\ T - T_\infty(x) = (T_w - T_{\infty,0})\theta(\xi,\eta) \\ \phi - \phi_\infty = (\phi_w - \phi_\infty)\, s(\xi,\eta), \end{aligned}\right\} \tag{7.6}$$

we get the following system of nonlinear partial differential equations

$$f'' = \Delta(\sin A + \dot{\delta}\cos A)\,(\theta' - N_r s')\,, \tag{7.7}$$

$$\theta'' + \frac{1}{2} f\theta' + N_b s'\theta' + N_t \theta'^2 = \xi\left(S_T f' + f'\frac{\partial\theta}{\partial\xi} - \theta'\frac{\partial f}{\partial\xi}\right), \tag{7.8}$$

$$s'' + \frac{1}{2} Lef s' + \frac{N_t}{N_b}\theta'' = Le\xi\left(f'\frac{\partial s}{\partial\xi} - s'\frac{\partial f}{\partial\xi}\right), \tag{7.9}$$

The boundary conditions (7.5) in terms of f, θ and s becomes

$$f + 2\xi\left(\frac{\partial f}{\partial\xi}\right)_{\eta=0} = 0, \quad \theta = 1 - S_T\xi, \quad s = 1, \quad \text{at} \quad \eta = 0 \tag{7.10a}$$

$$f' \to 1, \quad \theta \to 0, \quad s \to 0 \quad \text{as} \quad \eta \to \infty \tag{7.10b}$$

The heat and nanoparticle fluxes from the wavy plate are given by

$$q_w = -kn.\nabla T, \tag{7.11a}$$

$$q_{np} = -D_B\, n.\nabla \phi. \tag{7.11b}$$

The non dimensional rate of heat transfer, called the Nusselt number $Nu_\xi = \dfrac{q_w\, x}{k\,(T_w\, -\, T_{\infty,0})}$ and the rate of nanoparticle transfer, called nanoparticle Sherwood number $NSh_\xi = \dfrac{q_{np}\, x}{D_B\,(\phi_w - \phi_\infty)}$ are given by

$$\frac{Nu_\xi}{\sqrt{Pe_\xi}} = -\frac{\theta'(\xi,0)}{(1-S_T\xi)(1+\dot{\delta}^2)^{1/2}}, \tag{7.12a}$$

$$\frac{NSh_\xi}{\sqrt{Pe_\xi}} = -\frac{s'(\xi,0)}{(1+\dot{\delta}^2)^{1/2}}. \tag{7.12b}$$

Method of Solution

A local Similarity and non-Similarity method is used to convert the non-linear boundary value problems (7.7) - (7.9) subject to the boundary conditions (7.10) to a sequence of ordinary differential equations and then the Successive Linearization Method along with Chebyshev spectral collocation method is used to solve the resulting system of equations.

$$\mathbf{A}_{i-1}\mathbf{X}_i = \mathbf{R}_{i-1}, \tag{7.13}$$

In Eqn. (7.13), $\mathbf{A}_{i-1}$ is a (6N + 6)×(6N + 6) square matrix and $\mathbf{X}_i$ and $\mathbf{R}_{i-1}$ are (6N + 6)×1 column vectors defined by

$$\mathbf{A}_{i-1} = \begin{bmatrix} A_{11} & A_{12} & A_{13} & A_{14} & A_{15} & A_{16} \\ A_{21} & A_{22} & A_{23} & A_{24} & A_{25} & A_{26} \\ A_{31} & A_{32} & A_{33} & A_{34} & A_{35} & A_{36} \\ A_{41} & A_{42} & A_{43} & A_{44} & A_{45} & A_{46} \\ A_{51} & A_{52} & A_{53} & A_{54} & A_{55} & A_{56} \\ A_{61} & A_{62} & A_{63} & A_{64} & A_{65} & A_{66} \end{bmatrix}, \quad \mathbf{X}_i = \begin{bmatrix} \mathbf{F}_i \\ \mathbf{\Theta_i} \\ \mathbf{\Phi_i} \\ \mathbf{G}_i \\ \mathbf{H}_i \\ \mathbf{K}_i \end{bmatrix}, \quad \mathbf{R}_{i-1} = \begin{bmatrix} \mathbf{r}_{1,i-1} \\ \mathbf{r}_{2,i-1} \\ \mathbf{r}_{3,i-1} \\ \mathbf{r}_{4,i-1} \\ \mathbf{r}_{5,i-1} \\ \mathbf{r}_{6,i-1} \end{bmatrix} \tag{7.14}$$

where

$\mathbf{F}_i = [f_i(\chi_0), f_i(\chi_1), ..., f_i(\chi_{N-1}), f_i(\chi_N)]^T$, $\mathbf{\Theta_i} = [\theta_i(\chi_0), \theta_i(\chi_1), ..., \theta_i(\chi_{N-1}), \theta_i(\chi_N)]^T$,
$\mathbf{\Phi_i} = [s_i(\chi_0), s_i(\chi_1), ..., s_i(\chi_{N-1}), s_i(\chi_N)]^T$, $\mathbf{G}_i = [g_i(\chi_0), g_i(\chi_1), ..., g_i(\chi_{N-1}), g_i(\chi_N)]^T$,
$\mathbf{H}_i = [h_i(\chi_0), h_i(\chi_1), ..., h_i(\chi_{N-1}), h_i(\chi_N)]^T$, $\mathbf{K}_i = [k_i(\chi_0), k_i(\chi_1), ..., k_i(\chi_{N-1}), k_i(\chi_N)]^T$,
$\mathbf{r}_{j,i-1} = [r_{j,i-1}(\chi_0), r_{j,i-1}(\chi_1), \cdots, r_{j,i-1}(\chi_{N-1}), r_{j,i-1}(\chi_N)]^T, j = 1, 2, 3, 4, 5, 6$
$A_{11} = \mathbf{D}^2,\ A_{12} = a_{1,i-1}\mathbf{D},\ A_{13} = a_{2,i-1}\mathbf{D},\ A_{14} = \mathbf{0},\ A_{15} = \mathbf{0},\ A_{16} = \mathbf{0}$
$A_{21} = b_{2,i-1}\mathbf{D} + b_{3,i-1}\mathbf{I},\ A_{22} = \mathbf{D}^2 + b_{1,i-1}\mathbf{D},\ A_{23} = b_{4,i-1}\mathbf{D},\ A_{24} = b_{5,i-1}\mathbf{I},$
$A_{25} = b_{6,i-1}\mathbf{I},\ A_{26} = \mathbf{0},\ A_{31} = c_{2,i-1}\mathbf{D} + c_{3,i-1}\mathbf{I},\ A_{32} = c_{4,i-1}\mathbf{D}^2,\ A_{33} = \mathbf{D}^2 + c_{1,i-1}\mathbf{D},$
$A_{34} = c_{5,i-1}\mathbf{I},\ A_{35} = \mathbf{0},\ A_{36} = c_{6,i-1}\mathbf{I},\ A_{41} = \mathbf{0},\ A_{42} = d_{1,i-1}\mathbf{D},\ A_{43} = d_{2,i-1}\mathbf{D},$
$A_{44} = \mathbf{D}^2,\ A_{45} = d_{3,i-1}\mathbf{D},\ A_{46} = d_{4,i-1}\mathbf{D},\ A_{51} = l_{3,i-1}\mathbf{D} + l_{4,i-1}\mathbf{I},\ A_{52} = l_{5,i-1}\mathbf{D},$
$A_{53} = l_{6,i-1}\mathbf{D},\ A_{54} = l_{7,i-1}\mathbf{D} + l_{8,i-1}\mathbf{I},\ A_{55} = \mathbf{D}^2 + l_{1,i-1}\mathbf{D} + l_{2,i-1}\mathbf{I},\ A_{56} = l_{9,i-1}\mathbf{D},$
$A_{61} = m_{3,i-1}\mathbf{D} + m_{4,i-1}\mathbf{I},\ A_{62} = \mathbf{0},\ A_{63} = m_{5,i-1}\mathbf{D},\ A_{64} = m_{6,i-1}\mathbf{D} + m_{7,i-1}\mathbf{I},$
$A_{65} = m_{8,i-1}\mathbf{D}^2,\ A_{66} = \mathbf{D}^2 + m_{1,i-1}\mathbf{D} + m_{2,i-1}\mathbf{I}$

Here $a_{k,i-1}$, $b_{k,i-1}$, $c_{k,i-1}$,$d_{k,i-1}$, $l_{k,i-1}$, $m_{k,i-1}$ are diagonal matrices of size (N+1)×(N+1) and $\mathbf{I}$ is an identity matrix of size (N +1)×(N +1). After modifying the matrix system (7.13) to incorporate boundary conditions, the solution is obtained as

$$\mathbf{X}_i = \mathbf{A}_{i-1}^{-1}\mathbf{R}_{i-1} \tag{7.15}$$

Table 7.1: Comparison of values of $-\theta'(0)$ for Aiding and Opposing flow by the present method and Cheng [23] for fixed values of for $A = \frac{\pi}{2}$, $a = 0$, $\xi = 0$, $N_r = 0$, $N_t = 0$, $N_b = 0$, $Le = 0$.

Aiding Flow			Opposing Flow		
Δ	Cheng [23]	Present	Δ	Cheng [23]	Present
0	0.5641	0.56415775	-0.2	0.5269	0.52691089
0.5	0.6473	0.64736510	-0.4	0.4865	0.48653284
1	0.7205	0.72055401	-0.6	0.442	0.44202064
3	0.9574	0.95744512	-0.8	0.3916	0.39166292
10	1.516	1.51623967	-1.0	0.332	0.33202116
20	2.066	2.066			

Results and Discussion

Numerical solutions for the dimensionless velocity, temperature and nanoparticle volume fraction functions and heat and nanoparticle mass transfer rates for aiding and opposing flows have been computed and displayed graphically in Figs. 7.1 - 7.7. The effects of thermal stratification S_T, angle of inclination A, Brownian motion parameter N_b, thermoporesis parameter N_t and amplitude a of the wavy surface have been discussed.

Table. 7.1 shows the comparison of the results of $-\theta'(0)$ for fixed values of $A = \frac{\pi}{2}$, $a = 0$, $\xi = 0$, $N_r = 0$, $N_t = 0$, $N_b = 0$, $Le = 0$, $F_c = 0$, $R = 0$ for both aiding and opposing flows with the results obtained by Cheng [23]. It is observed that these two results are in good agreement.

Figures 7.1 and 7.2 illustrate the effect of thermal stratification on velocity, temperature and nanoparticle volume fraction distributions for both aiding and opposing flows respectively. It is noticed from Fig. 7.1 that increasing the thermal stratification parameter S_T reduces the velocity for aiding flow. This is because thermal stratification reduces the effective convective potential between the heated plate and ambient fluid in the medium. Hence, the thermal stratification effect reduces velocity in the boundary layer. The temperature of the fluid decreases with an increase in the value of thermal stratification parameter. When thermal stratification is taken into consideration, the effective temperature difference be-

tween the plate and the ambient fluid will decrease; therefore, the thermal boundary layer is thickened and the temperature is reduced. The nanoparticle volume fraction of the fluid flow increases with increase in the value of thermal stratification parameter for aiding flow. In the case of opposing flow, the velocity increases but the temperature and nanoparticle volume fraction decreases with increase in the value of thermal stratification parameter as seen from Fig. 7.2.

The effect of amplitude a of the wavy surface on the velocity, temperature and nanoparticle volume fraction for both aiding and opposing flows respectively is plotted in Fig. 7.3. As a increases, velocity increases but the temperature and nanoparticle volume fraction decrease for aiding flow whereas the velocity decreases and the temperature and nanoparticle volume fraction of the fluid flow increase in the case of opposing flow as noticed in the earlier chapters.

Figure 7.4 displays the effect of angle of inclination A on the velocity, temperature and nanoparticle volume fraction for both aiding and opposing flows respectively. The equations for the limiting cases of the horizontal and vertical plates are recovered from the transformed equations by setting $A = 0^o$ and $A = 90^o$, respectively. It is noted from Fig. 7.4 that as A increases, the velocity increases near the plate but the temperature and nanoparticle volume fraction decrease within the boundary layer region for the aiding flow whereas velocity reduces but the temperature and nanoparticle volume fraction enhances for opposing flow as observed in the earlier chapters.

The effect of the wave amplitude and angle of inclination of the wavy surface on the local Nusselt number $Nu_\xi(1-S_T\xi)/{Pe_\xi}^{1/2}$ and nanoparticle Sherwood number $NSh_\xi/{Pe_\xi}^{1/2}$ is plotted in Fig. 7.5. An enhancement in wavy amplitude decreases the local heat and nanoparticle mass transfer rates for both aiding and opposing flows as shown in Figs. 7.5(a) and 7.5(b). In general, we conclude that the surface becomes more roughened for increasing values of amplitude of the wavy surface. The variation of heat and nanoparticle mass transfer rates for various values of the angle of inclination A is displayed in Figs. 7.5(c) and 7.5(d). It is seen that increase in the angle of inclination increases the buoyancy force and assists the flow, leading to an increase in the heat and nanoparticle mass transfer rates in the case

of aiding flow where as a reverse trend is seen in the case of opposing flow. The maximum values of the dimensionless heat and nanoparticle mass transfer rates are observed when the surface is vertical.

Figure 7.6 displays the effect of Brownian motion parameter N_b and thermophoresis parameter N_t on the heat and nanoparticle mass transfer rates. It is observed that the local heat transfer rate decreases with increase in the Browinian motion parameter N_b whereas the nanoparticle mass transfer rate increases with an increase in the value of Brownian motion parameter N_b for aiding flow where as a reverse pattern is observed in the case of opposing flow as shown in Figs. 7.6(a) and 7.6(b). It is seen from Figs. 7.6(c) and 7.6(d) that the heat transfer rate decreases with increase in the value of thermophoresis parameter N_t for both aiding and opposing flows and there is a negligible effect on nanoparticle mass transfer. Brownian motion is proportional to the volumetric fraction of nanoparticles in the direction from high to low concentration, whereas the thermophoresis is proportional to the temperature gradient from hot to cold. Hence, we conclude that the effect of the combination of Brownian motion and thermophoresis is to reduce the value of Nusselt number.

The streamwise distribution of the local Nusselt $Nu_\xi(1 - S_T\xi)/{Pe_\xi}^{1/2}$ and nanoparticle Sherwood numbers $NSh_\xi/{Pe_\xi}^{1/2}$ for different values of thermal stratification parameter S_T is displayed in Fig. 7.7. It is observed that both the heat and nanoparticle mass transfer rates decrease with increase in the thermal stratification parameter S_T for aiding flow whereas they are seen to decrease in the case of opposing flow.

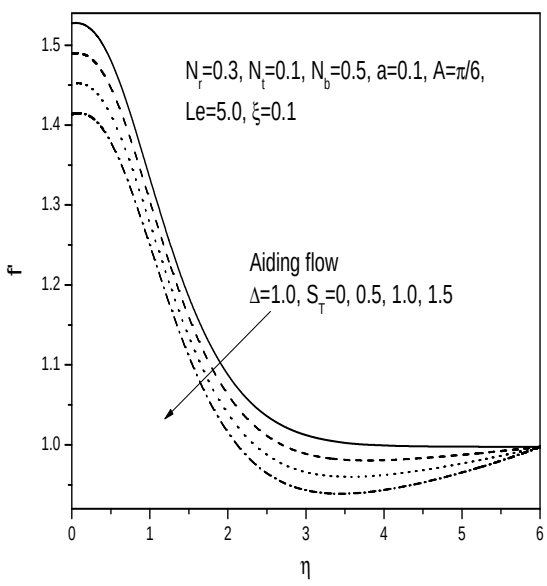

(a)

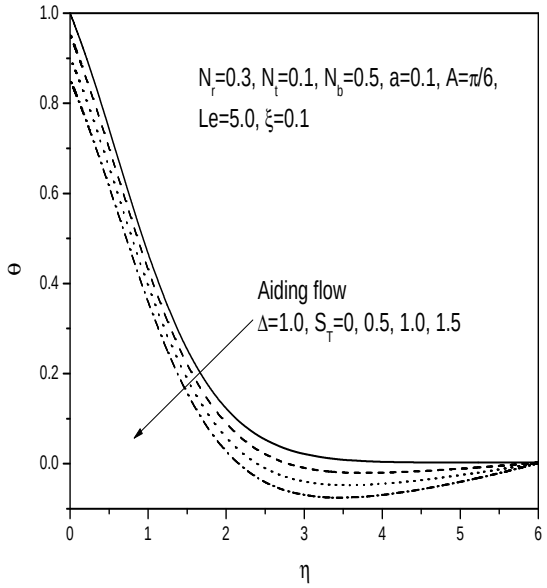

(b)

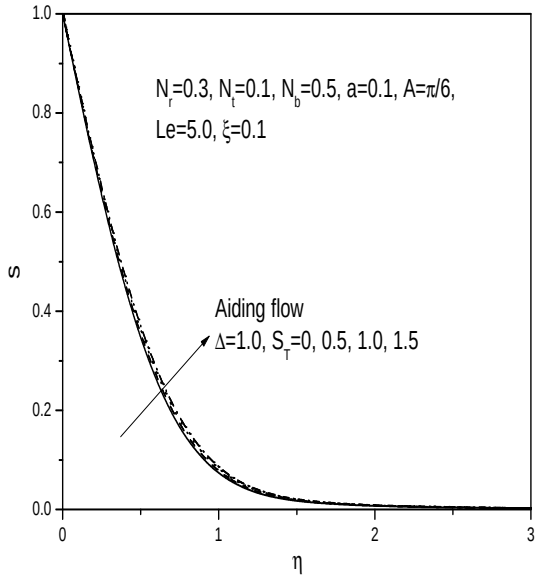

(c)

Figure 7.1: Variation of (a) velocity, (b) temperature and (c) nanoparticle volume fraction profiles with thermal Stratification parameter S_T for aiding flow.

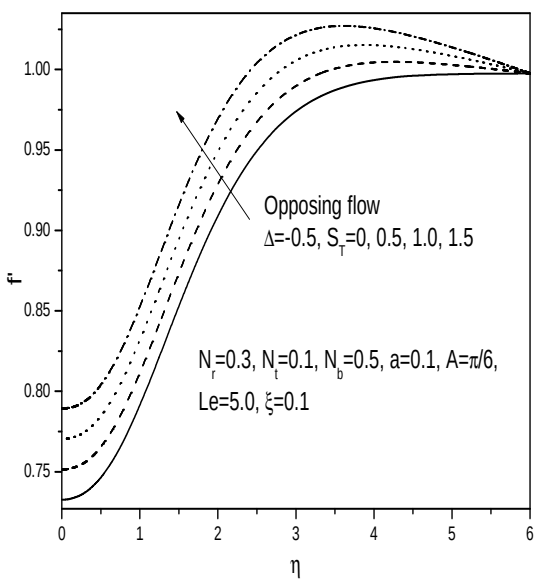

(a)

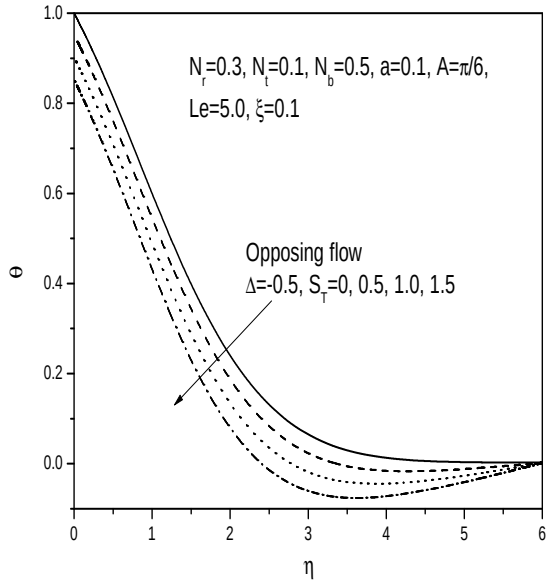

(b)

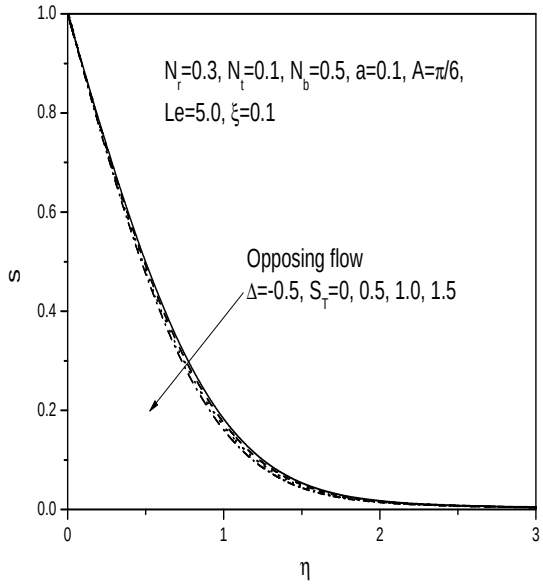

(c)

Figure 7.2: Variation of (a) velocity, (b) temperature and (c) nanoparticle volume fraction profiles with thermal Stratification parameter S_T for opposing flow.

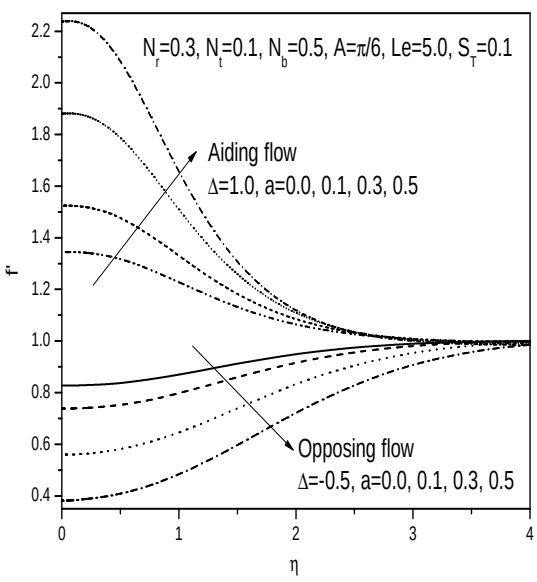

(a)

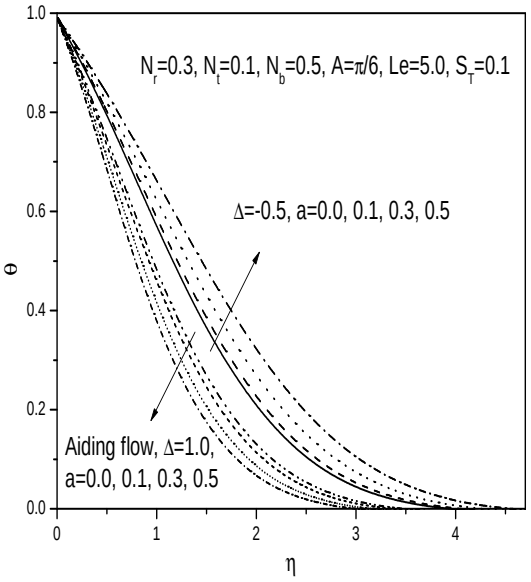

(b)

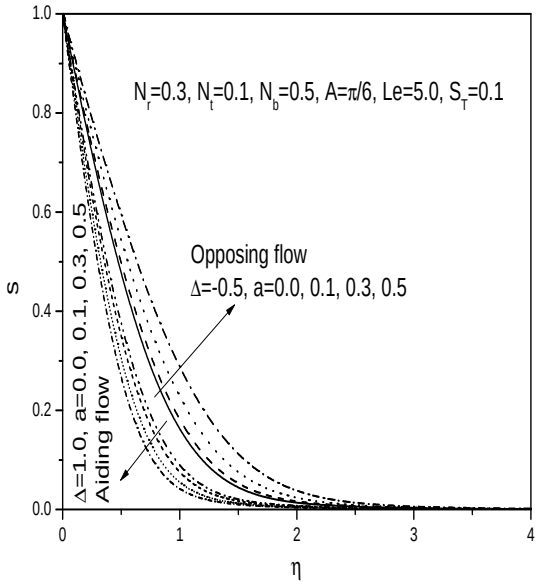

(c)

Figure 7.3: Variation of (a) velocity, (b) temperature and (c) nanoparticle volume fraction profiles with wave amplitude a for both aiding and opposing flows.

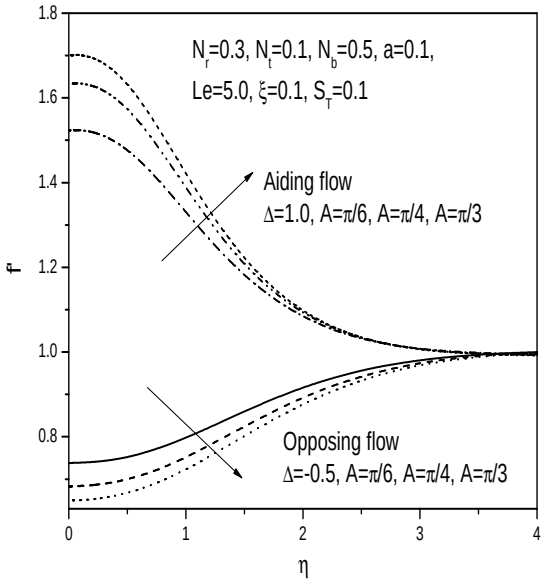

(a)

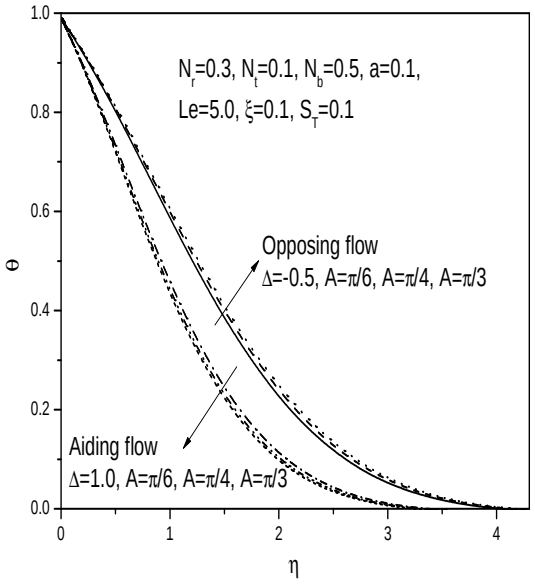

(b)

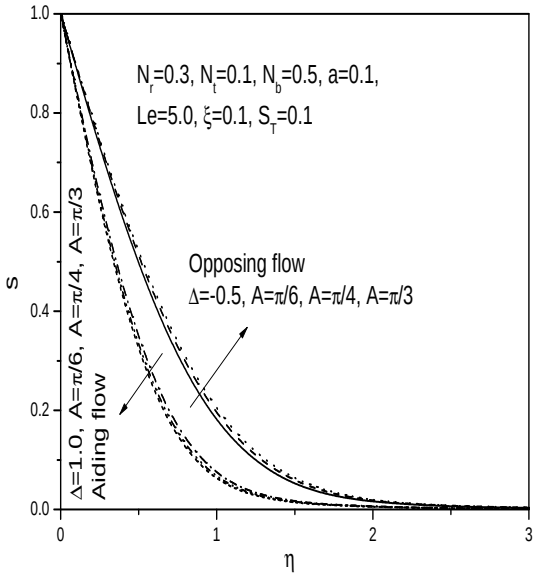

(c)

Figure 7.4: Variation of (a) velocity, (b) temperature and (c) nanoparticle volume fraction profiles with angle of inclination A for both aiding and opposing flows.

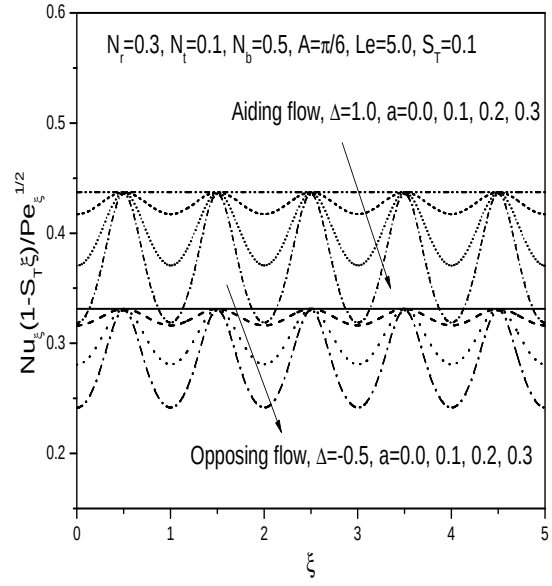

(a)

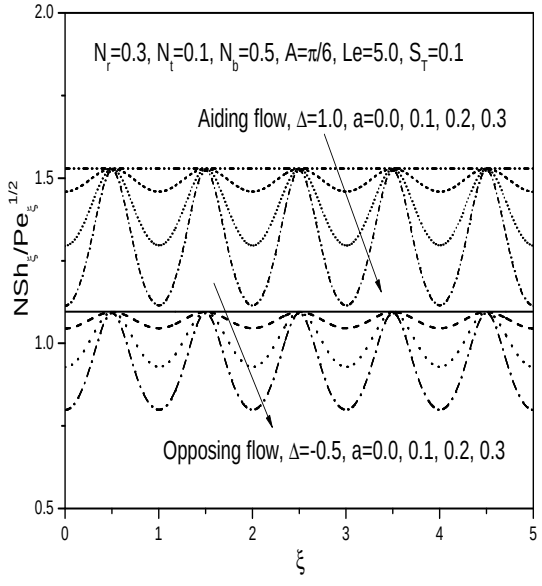

(b)

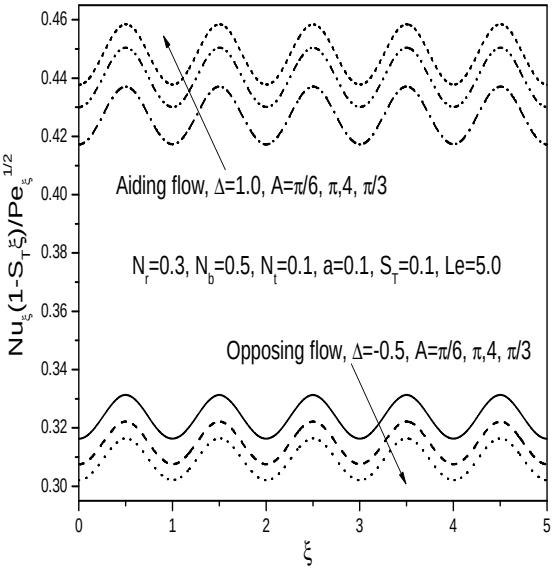

(c)

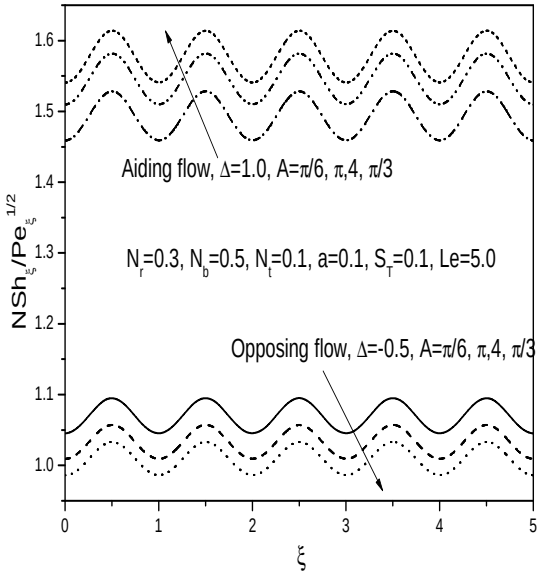

(d)

Figure 7.5: Variation of (a) heat and (b) nanoparticle mass transfer rates with wave amplitude a and (c) heat and (d) nanoparticle mass transfer rates with thermal stratification parameter S_T.

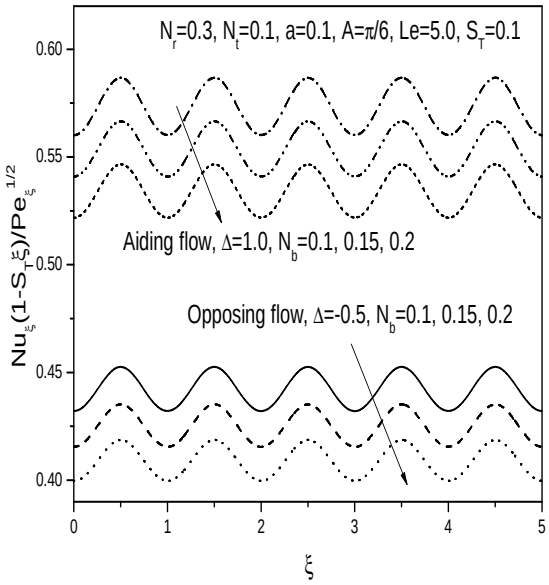

(a)

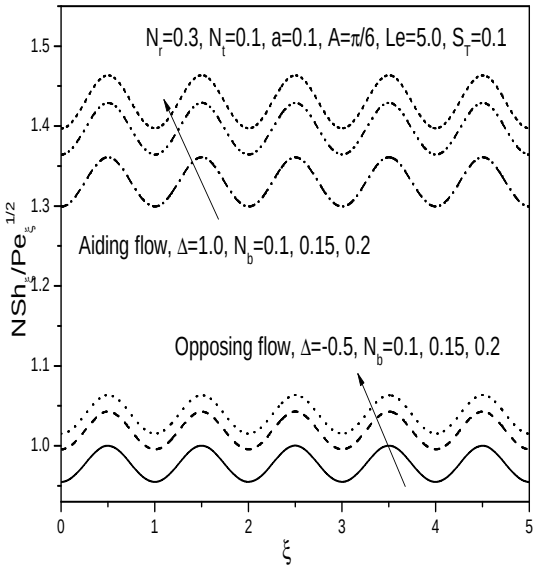

(b)

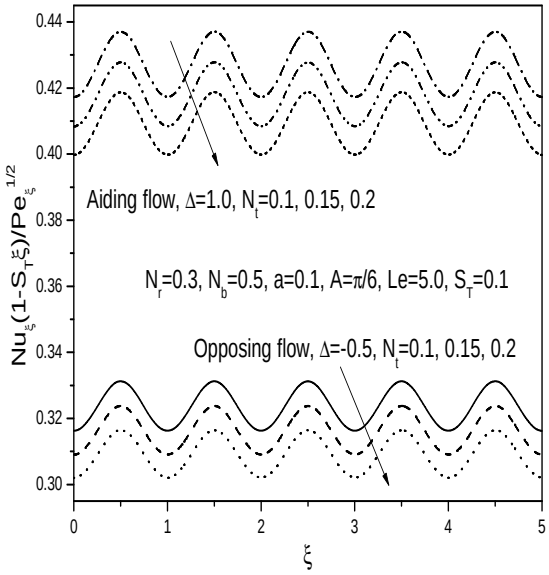

(c)

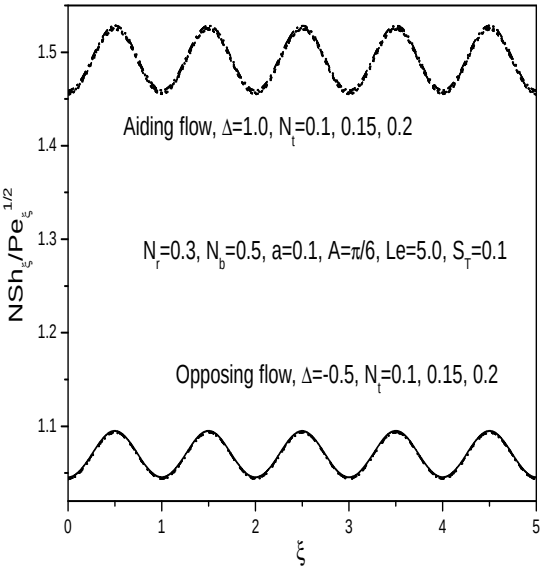

(d)

Figure 7.6: Variation of (a) heat and (b) nanoparticle mass transfer rates with Brownian motion parameter N_b and thermophoresis parameter N_t.

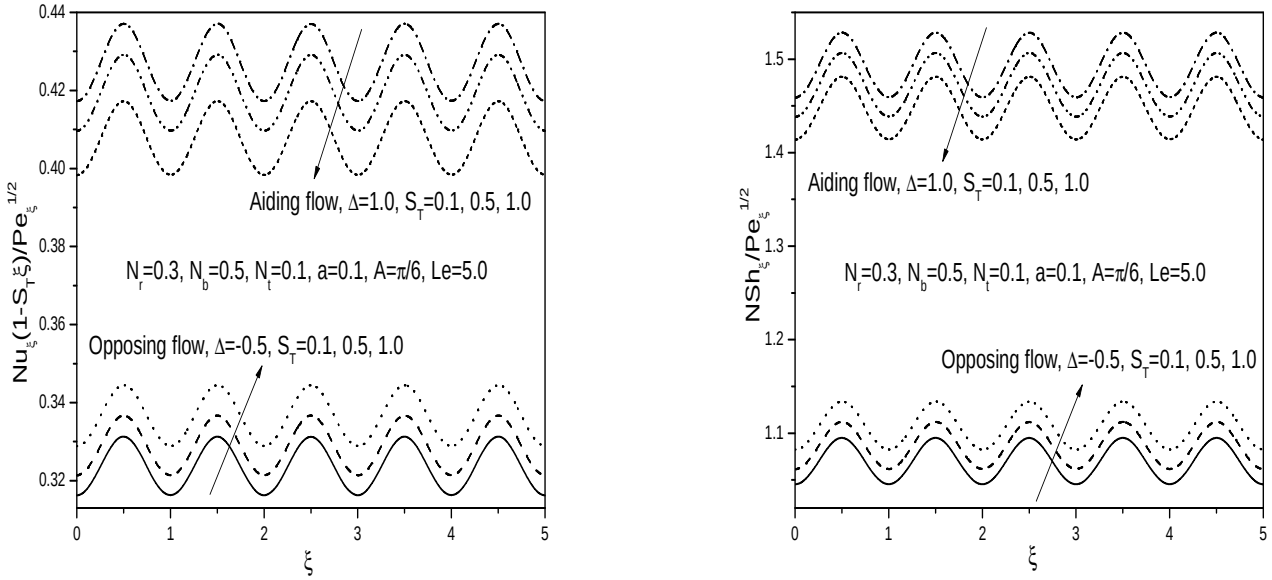

(a) (b)

Figure 7.7: Variation of (a) heat, and (b) nanoparticle mass transfer rates with thermal stratification parameter S_T.

7.3 Conclusions

In this chapter, we investigated the problem of steady, laminar mixed convection heat and nanoparticle mass transfer over an inclined wavy surface embedded in a thermally stratified porous medium saturated with nanofluid subject to uniform wall temperature and nanoparticle volume fraction conditions. From this analysis, the following conclusions can be drawn:

Increase in the thermal stratification parameter reduces the velocity, temperature, local heat and nanoparticle mass transfer rates but enhances the nanoparticle volume fraction of the fluid for aiding flow, whereas the velocity, local heat and mass transfer rates increases and the temperature and nanoparticle volume fraction decreases in the case of opposing flow. The wave amplitude a significantly effects the velocity, temperature, nanoparticle volume fraction, local heat transfer and nanoparticle mass transfer coefficients for both aiding and opposing flows. The influence of the angle of inclination A of the wavy surface to the horizontal is to enhance the velocity, local heat transfer and nanoparticle mass transfer rates, but to reduce

the temperature and nanoparticle volume fraction of the fluid flow for aiding flow and to reduce the velocity, local heat and nanoparticle mass transfer rates in the case of opposing flow.

Chapter 8

Effect of thermal radiation and thermal stratification on natural convection over an inclined wavy surface embedded in a porous medium saturated with a nanofluid [1]

8.1 Introduction

As discussed in previous chapters that natural convection flow is induced by buoyancy forces which arise from density differences in a fluid. The analysis of free convection in a thermally stratified medium is a fundamentally interesting and important problem because of its broad range of engineering applications. It has been shown by scientists that thermal stratification in energy storage may considerably increase system performance. Although the influence of stratification of the medium on the heat removal process in a porous medium is significant, very little work has been reported in the literature. Several authors [94, 48, 42, 71, 85, 87, 103]

[1] Published in "**International Journal of Mining, Metallurgy and Mechanical Engineering**"

studied convective flows in a stratified medium.

Thermal radiation plays a major role in some industrial applications such as glass production and furnace design, and also in space technology applications, such as comical flight aerodynamics rocket, propulsion systems, plasma physics and space craft reentry aerodynamics which operates at high temperatures, and also in applications involving high temperatures such as nuclear power plant, gas turbines missiles, satellites, space vehicles and aircraft etc. Hady *et al.* [40] reported that an increase in the thermal radiation parameter reduces the nanofluid temperature which leads to increase in the heat transfer rate. Kandaswamy *et al.* [48] studied the effects of thermophoresis and Brownian motion on MHD boundary layer flow of a nanofluid in the presence of thermal stratification due to solar radiation.

A survey of literature indicates that no work has been reported on natural convection of nanofluid over an inclined wavy surface in a non-Darcy porous medium under the influence of thermal radiation and thermal stratification. Hence, in this chapter we aim at exploring the effects of thermal radiation and thermal stratification on physical quantities and results are displayed through graphs.

8.2 Mathematical Formulation

A steady natural convection boundary layer flow over an inclined wavy surface embedded in a porous medium saturated with a nanofluid is considered. The x coordinate is taken along the wavy plate and the y coordinate is measured normal to the plate, while the origin of the reference system is considered at the leading edge of the wavy plate. The ambient medium is assumed to be linearly stratified with respect to temperature in the form $T_\infty(x) = T_{\infty,0} + Bx$, where B is a constant which is varied to alter the intensity of stratification in the medium. The values of T_w and ϕ_w are assumed to be greater than the ambient temperature $T_{\infty,0}$ and nanoparticle volume fraction ϕ_∞ at any arbitrary reference point in the medium. The porous medium is assumed to be uniform and isotropic and is in local thermal equilibrium with the fluid. The fluid properties are assumed to be constant except for density variations in the

buoyancy force term.

As in earlier chapters, making use of the Boussinesq and boundary layer approximations, the governing equations are:

$$\frac{\partial u}{\partial x}+\frac{\partial v}{\partial y}=0, \tag{8.1}$$

$$\left(1+\frac{\tilde{K}}{\nu}\sqrt{u^2+v^2}\right)\left[\frac{\partial u}{\partial y}-\frac{\partial v}{\partial x}\right]+\frac{\tilde{K}}{\nu\sqrt{u^2+v^2}}\left[u^2\frac{\partial u}{\partial y}+uv\left(\frac{\partial v}{\partial y}-\frac{\partial u}{\partial x}\right)-v^2\frac{\partial v}{\partial x}\right]=$$
$$\frac{(1-\phi_\infty)\rho_{f_\infty}\beta\,K\,g}{\mu}\left(\frac{\partial T}{\partial y}\sin A-\frac{\partial T}{\partial x}\cos A\right)-\frac{(\rho_p-\rho_{f_\infty})\,K\,g}{\mu}\left(\frac{\partial \phi}{\partial y}\sin A-\frac{\partial \phi}{\partial x}\cos A\right), \tag{8.2}$$

$$u\frac{\partial T}{\partial x}+v\frac{\partial T}{\partial y}=\alpha\left(\frac{\partial^2 T}{\partial x^2}+\frac{\partial^2 T}{\partial y^2}\right)+\gamma\left[D_B\left(\frac{\partial \phi}{\partial x}\frac{\partial T}{\partial x}+\frac{\partial \phi}{\partial y}\frac{\partial T}{\partial y}\right)+\frac{D_T}{T_\infty}\left(\left(\frac{\partial T}{\partial x}\right)^2+\left(\frac{\partial T}{\partial y}\right)^2\right)\right]$$
$$+\frac{16\,\sigma\,T_\infty^3}{3\,K_e}\left(\frac{\partial^2 T}{\partial x^2}+\frac{\partial^2 T}{\partial y^2}\right), \tag{8.3}$$

$$u\frac{\partial \phi}{\partial x}+v\frac{\partial \phi}{\partial y}=D_B\left(\frac{\partial^2 \phi}{\partial x^2}+\frac{\partial^2 \phi}{\partial y^2}\right)+\frac{D_T}{T_\infty}\left(\frac{\partial^2 T}{\partial x^2}+\frac{\partial^2 T}{\partial y^2}\right), \tag{8.4}$$

Boundary Conditions

Assume that the semi-infinite inclined wavy plate is subject to uniform wall temperature and nanoparticle volume fraction T_w and ϕ_w, respectively. Hence, the boundary conditions are as given by (6.5).

Introducing the stream function ψ in Eqns. (8.1) - (8.4) and making use of the non-dimensional variables given in (6.6), we get the following system of nonlinear partial differential equations

$$f''+2Gr(1+\dot{\delta}^2)^{-1/2}f'f''=(\sin A+\dot{\delta}\cos A)\,(\theta'-N_r s'), \tag{8.5}$$

$$\left(1+\frac{4R}{3}\right)\theta''+\frac{1}{2}f\theta'+N_b s'\theta'+N_t\theta'^2=\xi\left(S_T f'+f'\frac{\partial\theta}{\partial\xi}-\theta'\frac{\partial f}{\partial\xi}\right), \tag{8.6}$$

$$s''+\frac{1}{2}Lefs'+\frac{N_t}{N_b}\theta''=Le\xi\left(f'\frac{\partial s}{\partial\xi}-s'\frac{\partial f}{\partial\xi}\right), \tag{8.7}$$

The boundary conditions (6.5) in terms of f, θ and s are given by (6.10) The heat and nanoparticle fluxes from the wavy plate are given by

$$q_w=-kn.\nabla T, \tag{8.8a}$$

$$q_{np}=-D_B\, n.\nabla\phi. \tag{8.8b}$$

The non dimensional rate of heat transfer (Nusselt number Nu_ξ) and the rate of nanoparticle transfer (nanoparticle Sherwood number NSh_ξ) are given by

$$\frac{Nu_\xi}{\sqrt{Ra_\xi}}=-\frac{(1+4R/3)\theta'(\xi,0)}{(1-S_T\xi)(1+\dot{\delta}^2)^{1/2}}, \tag{8.9a}$$

$$\frac{NSh_\xi}{\sqrt{Ra_\xi}}=-\frac{s'(\xi,0)}{(1+\dot{\delta}^2)^{1/2}}. \tag{8.9b}$$

Method of Solution

A local Similarity and non-Similarity method is used to solve the non-linear boundary value problems (8.5) - (8.7) subject to the boundary conditions (6.10) to convert them to a sequence of ordinary differential equations and then the Successive Linearization Method along with Chebyshev spectral collocation method is used to solve the resulting system of equations. Proceeding same as in previous chapters we obtain the following matrix equation

$$\mathbf{A}_{i-1}\mathbf{X}_i=\mathbf{R}_{i-1}, \tag{8.10}$$

In Eqn. (8.10), $\mathbf{A}_{i-1}$ is a (6N + 6)×(6N + 6) square matrix and $\mathbf{X}_i$ and $\mathbf{R}_{i-1}$ are (6N + 6)×1 column vectors defined by

$$\mathbf{A}_{i-1} = \begin{bmatrix} A_{11} & A_{12} & A_{13} & A_{14} & A_{15} & A_{16} \\ A_{21} & A_{22} & A_{23} & A_{24} & A_{25} & A_{26} \\ A_{31} & A_{32} & A_{33} & A_{34} & A_{35} & A_{36} \\ A_{41} & A_{42} & A_{43} & A_{44} & A_{45} & A_{46} \\ A_{51} & A_{52} & A_{53} & A_{54} & A_{55} & A_{56} \\ A_{61} & A_{62} & A_{63} & A_{64} & A_{65} & A_{66} \end{bmatrix}, \quad \mathbf{X}_i = \begin{bmatrix} \mathbf{F}_i \\ \mathbf{\Theta_i} \\ \mathbf{\Phi_i} \\ \mathbf{G}_i \\ \mathbf{H}_i \\ \mathbf{K}_i \end{bmatrix}, \quad \mathbf{R}_{i-1} = \begin{bmatrix} \mathbf{r}_{1,i-1} \\ \mathbf{r}_{2,i-1} \\ \mathbf{r}_{3,i-1} \\ \mathbf{r}_{4,i-1} \\ \mathbf{r}_{5,i-1} \\ \mathbf{r}_{6,i-1} \end{bmatrix} \tag{8.11}$$

where

$\mathbf{F}_i = [f_i(\chi_0), f_i(\chi_1), ..., f_i(\chi_{N-1}), f_i(\chi_N)]^T$, $\mathbf{\Theta_i} = [\theta_i(\chi_0), \theta_i(\chi_1), ..., \theta_i(\chi_{N-1}), \theta_i(\chi_N)]^T$,
$\mathbf{\Phi_i} = [s_i(\chi_0), s_i(\chi_1), ..., s_i(\chi_{N-1}), s_i(\chi_N)]^T$, $\mathbf{G}_i = [g_i(\chi_0), g_i(\chi_1), ..., g_i(\chi_{N-1}), g_i(\chi_N)]^T$,
$\mathbf{H}_i = [h_i(\chi_0), h_i(\chi_1), ..., h_i(\chi_{N-1}), h_i(\chi_N)]^T$, $\mathbf{K}_i = [k_i(\chi_0), k_i(\chi_1), ..., k_i(\chi_{N-1}), k_i(\chi_N)]^T$,
$\mathbf{r}_{j,i-1} = [r_{j,i-1}(\chi_0), r_{j,i-1}(\chi_1), \cdots, r_{j,i-1}(\chi_{N-1}), r_{j,i-1}(\chi_N)]^T, j = 1, 2, 3, 4, 5, 6$
$A_{11} = a_{1,i-1}\mathbf{D}^2 + a_{2,i-1}\mathbf{D},\ A_{12} = a_{3,i-1}\mathbf{D},\ A_{13} = a_{4,i-1}\mathbf{D},\ A_{14} = \mathbf{0},\ A_{15} = \mathbf{0},\ A_{16} = \mathbf{0}$
$A_{21} = b_{3,i-1}\mathbf{D} + b_{4,i-1}\mathbf{I},\ A_{22} = b_{1,i-1}\mathbf{D}^2 + b_{1,i-1}\mathbf{D},\ A_{23} = b_{5,i-1}\mathbf{D},\ A_{24} = b_{6,i-1}\mathbf{I},$
$A_{25} = b_{7,i-1}\mathbf{I},\ A_{26} = \mathbf{0},\ A_{31} = c_{2,i-1}\mathbf{D} + c_{3,i-1}\mathbf{I},\ A_{32} = c_{4,i-1}\mathbf{D}^2,\ A_{33} = \mathbf{D}^2 + c_{1,i-1}\mathbf{D},$
$A_{34} = c_{5,i-1}\mathbf{I},\ A_{35} = \mathbf{0},\ A_{36} = c_{6,i-1}\mathbf{I},\ A_{41} = d_{3,i-1}\mathbf{D}^2 + d_{4,i-1}\mathbf{D},\ A_{42} = d_{5,i-1}\mathbf{D},$
$A_{43} = d_{6,i-1}\mathbf{D},\ A_{44} = d_{1,i-1}\mathbf{D}^2 + d_{2,i-1}\mathbf{D},\ A_{45} = d_{7,i-1}\mathbf{D},\ A_{46} = d_{8,i-1}\mathbf{D}$
$A_{51} = l_{4,i-1}\mathbf{D} + l_{5,i-1}\mathbf{I},\ A_{52} = l_{6,i-1}\mathbf{D},\ A_{53} = l_{7,i-1}\mathbf{D}\ A_{54} = l_{8,i-1}\mathbf{D} + l_{9,i-1}\mathbf{I},$
$A_{55} = l_{1,i-1}\mathbf{D}^2 + l_{2,i-1}\mathbf{D} + l_{3,i-1}\mathbf{I},\ A_{56} = l_{10,i-1}\mathbf{D},\ A_{61} = m_{3,i-1}\mathbf{D} + m_{4,i-1}\mathbf{I},$
$A_{62} = \mathbf{0},\ A_{63} = m_{5,i-1}\mathbf{D},\ A_{64} = m_{6,i-1}\mathbf{D} + m_{7,i-1}\mathbf{I},\ A_{65} = m_{8,i-1}\mathbf{D}^2,$
$A_{66} = \mathbf{D}^2 + m_{1,i-1}\mathbf{D} + m_{2,i-1}\mathbf{I}$

Here $a_{k,i-1}$, $b_{k,i-1}$, $c_{k,i-1}$,$d_{k,i-1}$, $l_{k,i-1}$, $m_{k,i-1}$ are diagonal matrices of size (N+1)×(N+1) and $\mathbf{I}$ is an identity matrix of size (N +1)×(N +1). After modifying the matrix system (8.10) to incorporate boundary conditions, the solution is obtained as

$$\mathbf{X}_i = \mathbf{A}_{i-1}^{-1}\mathbf{R}_{i-1} \tag{8.12}$$

Results and Discussion

Table 8.1: Comparison of $\theta'(0)$ and $f'(0)$ by the present method and Plumb and Huenefeld [83] for different values of Gr and fixed values of $A = \frac{\pi}{2}$, $a = 0$, $\xi = 0$, $S_T = 0$.

	$\theta'(0)$		$f'(0)$	
Gr	Plumb & Huenefeld[83]	Present	Plumb & Huenefeld[83]	Present
0.00	-0.4439	-0.443717	1.0000	1.0000
0.01	-0.44232	-0.442126	0.9902	0.990195
0.10	-0.42969	-0.429475	0.91608	0.916079
1.00	-0.36617	-0.365732	0.61803	0.618033
10.00	-0.25126	-0.250634	0.27016	0.270156
100.00	-0.15186	-0.151443	0.09512	0.095124

The solutions for the dimensionless velocity, temperature and nanoparticle volume fraction functions and heat and nanoparticle mass transfer rates have been computed and are displayed graphically in Figs. 8.1 - 8.7. The effects of thermal stratification S_T, thermal radiation R, Grashof number Gr, angle of inclination A, Brownian motion parameter N_b, thermoporesis parameter N_t and amplitude a of the wavy surface on the physical quantities have been discussed.

Table. 8.1 shows the comparison of the results of the values of $\theta'(0)$ and $f'(0)$ for different values of Gr and fixed values of $A = \pi/2$, $a = 0$, $S_T = 0$ with the results obtained by Plumb and Huenefeld [83]. It is shown that these two results are in good agreement.

The effect of amplitude of the wavy surface on velocity, temperature and nanoparticle volume fraction is plotted in Fig. 8.1. It is observed that as a increases, velocity increases near the plate and decreases away from the plate, whereas the temperature and nanoparticle volume fraction decreases. It is noted from Fig. 8.2 that as A increases, the velocity increases near the plate and decreases away from the plate but the temperature and nanoparticle volume fraction decrease within the boundary layer region. When the surface is vertical, the smallest temperature and nanoparticle volume fraction distributions are observed, whereas they are largest for the horizontal surface.

Figure 8.3 depicts the effect of Grashof number Gr on velocity, temperature and nanoparticle volume fraction distributions. It is clear from Fig. 8.3(a) that velocity of the fluid

decreases near the plate and then increases away from the plate with the increase of Grashof number. It is noticed from Figs. 8.3(b) and 8.3(c) that the temperature and nanoparticle volume fraction of the fluid increases with increase of the Grashof number.

Figure 8.4 presents the effect of radiation R on non dimensional velocity, temperature and nanoparticle volume fraction. It is observed from Figs. 8.4(a) and 8.4(b) that the velocity and temperature increases with increase in the value of radiation parameter. It is noticed from Fig. 8.4(c) that the nanoparticle volume fraction reduces with increase in the value of radiation parameter.

Figure 8.5 shows the effect of thermal stratification on velocity, temperature and nanoparticle volume fraction distributions. It is noticed that increase in the thermal stratification parameter S_T reduces the velocity and temperature of the fluid but increases the nanoparticle volume fraction of the fluid flow.

The effect of the wave amplitude, angle of inclination and thermal stratification on the local Nusselt number $Nu_\xi(1-S_T\xi)/{Ra_\xi}^{1/2}$ and nanoparticle Sherwood number $NSh_\xi/{Ra_\xi}^{1/2}$ is plotted in Fig. 8.6. It is revealed that an enhancement in wavy amplitude decreases the local heat and nanoparticle mass transfer rates as shown in 8.6(a) and 8.6(b). The variation of heat and nanoparticle mass transfer rates for various values of the angle of inclination A and thermal stratification parameter S_T is displayed in Figs. 8.6(c) and 8.6(d). It is shown that increase in the angle of inclination increases the heat and nanoparticle mass transfer rates but an increase in the value of thermal stratification parameter S_T reduces both the heat and nanoparticle mass transfer rates.

The effect of Brownian motion parameter N_b, thermophoresis parameter N_t, Grashof number Gr and radiation parameter R on the heat and nanoparticle mass transfer rates is presented in Fig. 8.7. It is observed that the dimensionless heat transfer rate decreases with increase in both the Browinian motion parameter and thermoporesis parameter. An increase in the value of Brownian motion parameter enhances the nanoparticle mass transfer rate and an increase in the value of thermophoresis parameter reduces the nanoparticle mass transfer rate. Figs. 8.7(c) - 8.7(d) display the streamwise distribution of Nusselt and nanoparticle

Sherwood numbers for different values of radiation parameter R and Grashof number Gr. It is seen that the heat and nanoparticle mass transfer rates enhances with increase in the radiation parameter and reduces with increase in the value of Grashof number Gr.

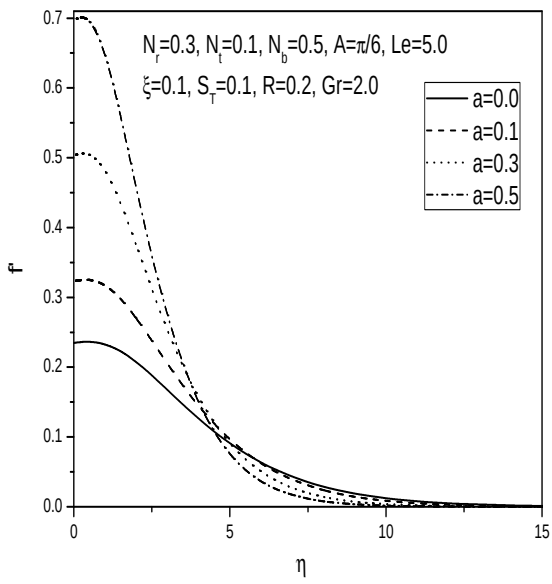

(a)

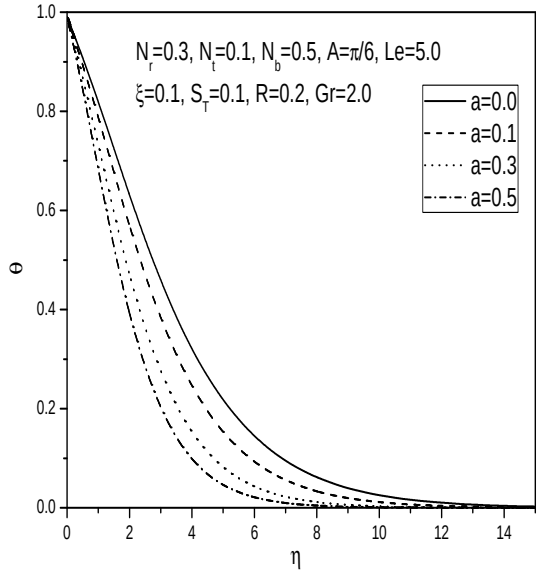

(b)

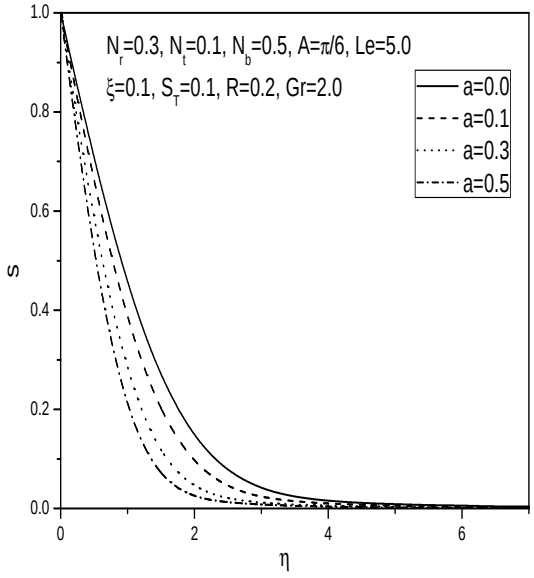

(c)

Figure 8.1: Variation of (a) velocity, (b) temperature and (c) nanoparticle volume fraction profiles with wave amplitude a.

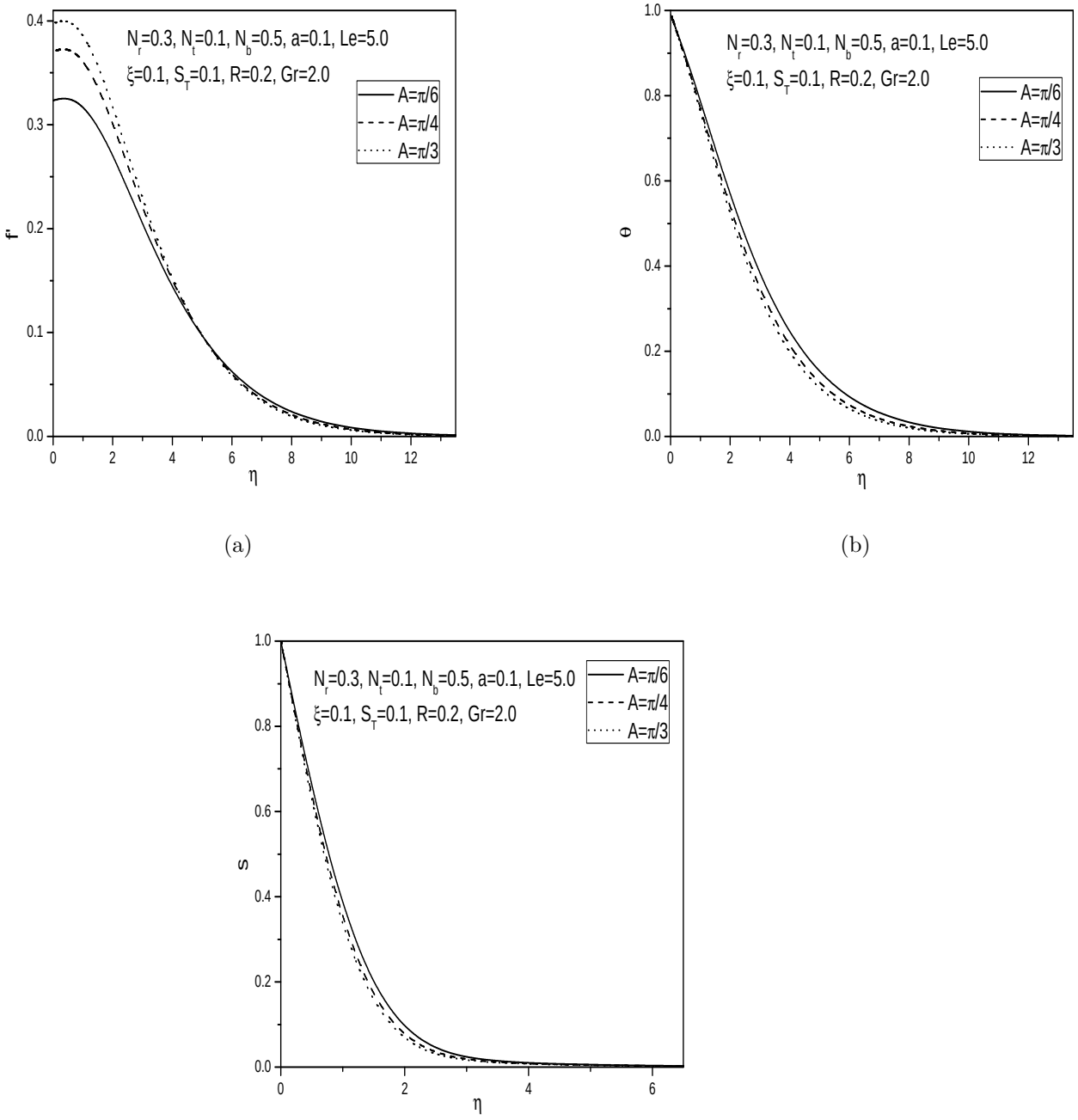

(a)

(b)

(c)

Figure 8.2: Variation of (a) velocity, (b) temperature and (c) nanoparticle volume fraction profiles with angle of inclination A.

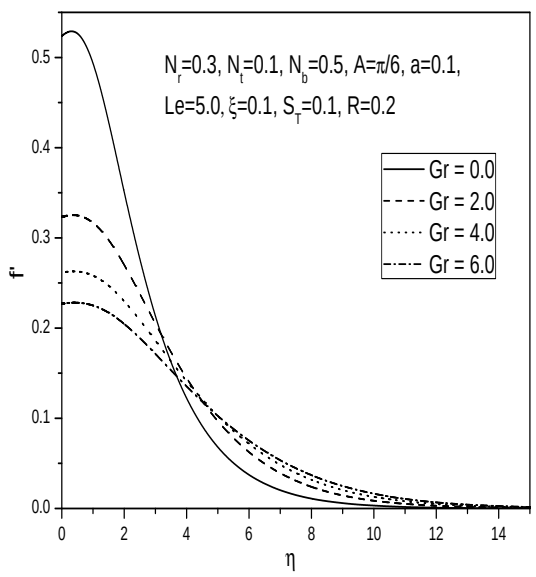

(a)

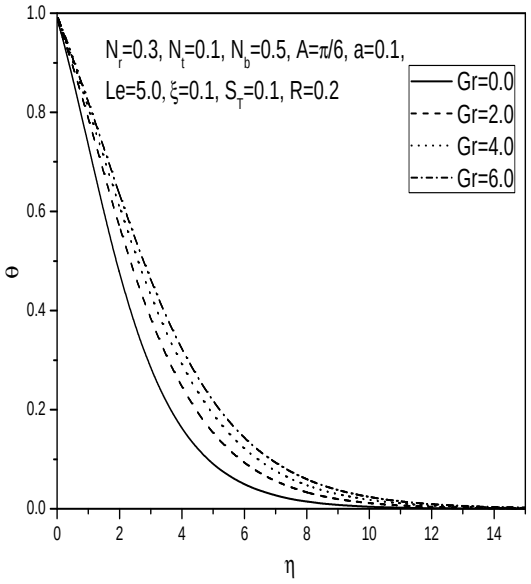

(b)

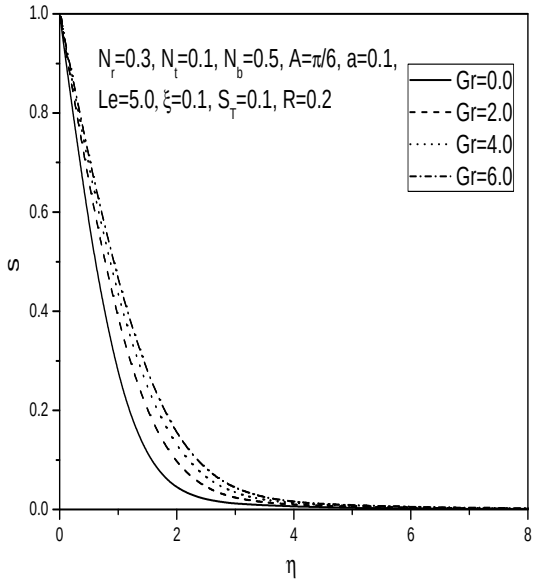

(c)

Figure 8.3: Variation of (a) velocity, (b) temperature and (c) nanoparticle volume fraction profiles with Grashof number Gr.

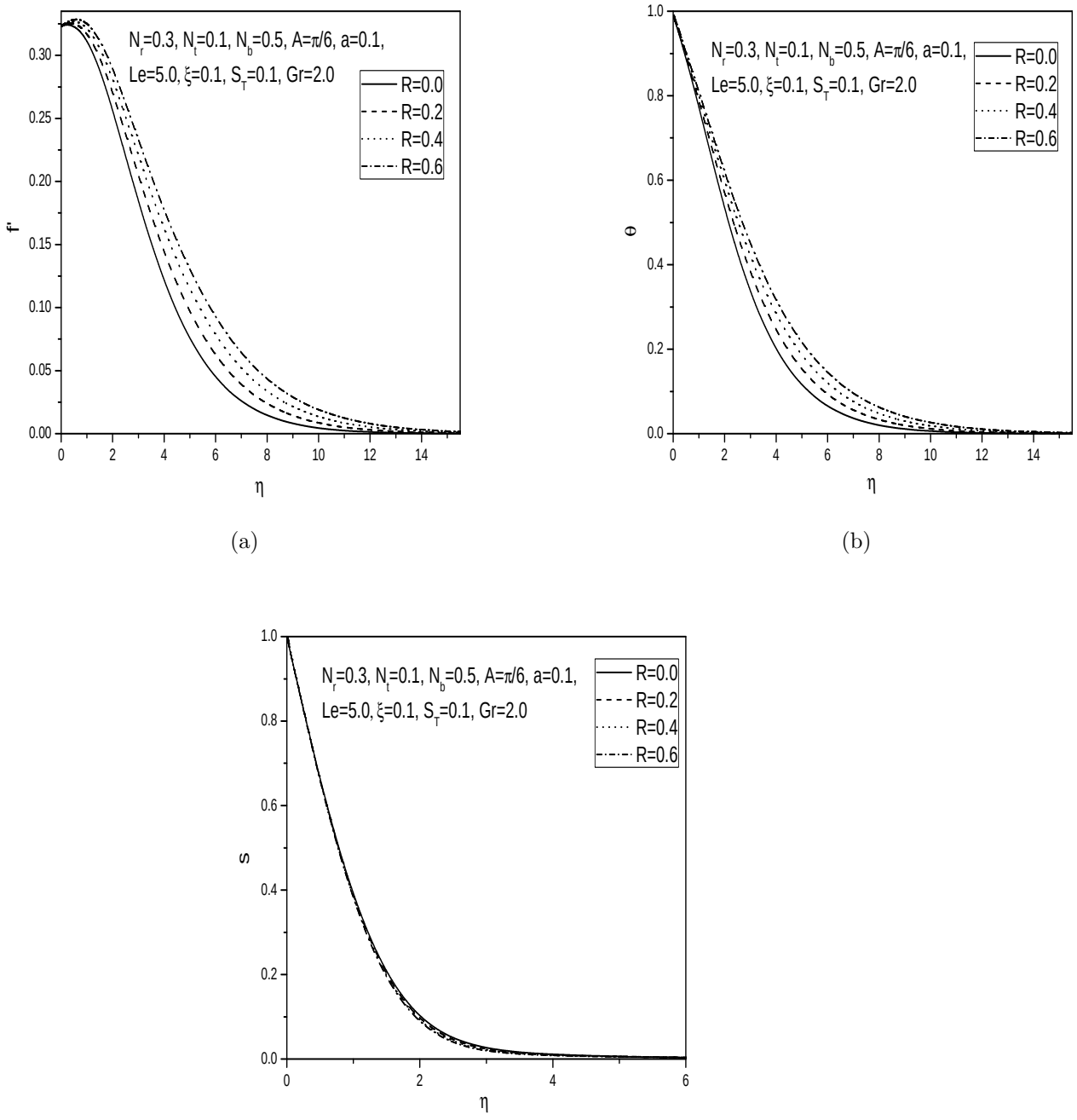

Figure 8.4: Variation of (a) velocity, (b) temperature and (c) nanoparticle volume fraction profiles with radiation parameter R.

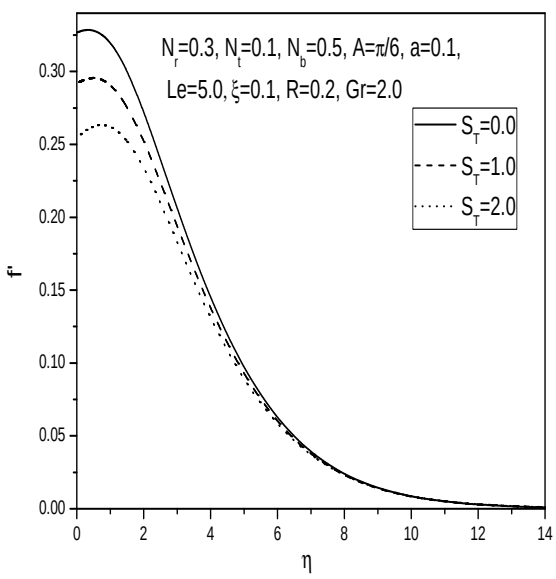

(a)

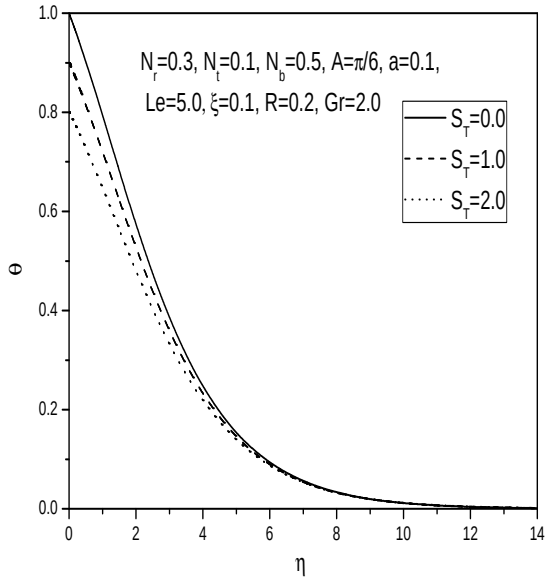

(b)

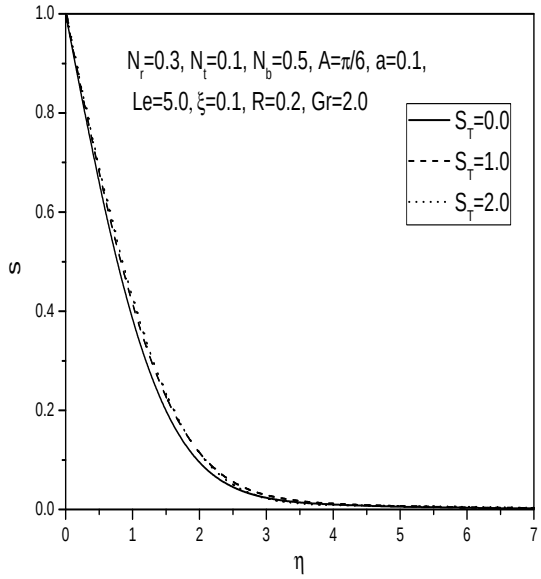

(c)

Figure 8.5: Variation of (a) velocity, (b) temperature and (c) nanoparticle volume fraction profiles with thermal Stratification parameter S_T.

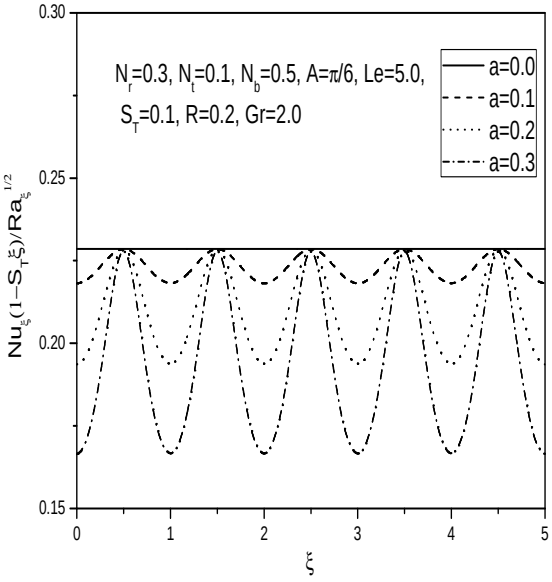

(a)

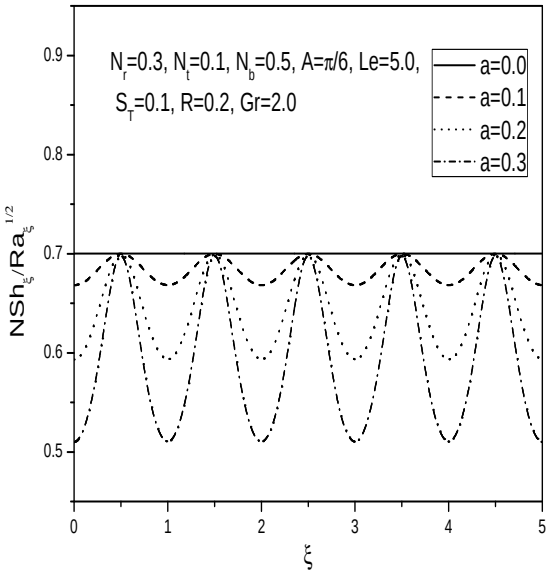

(b)

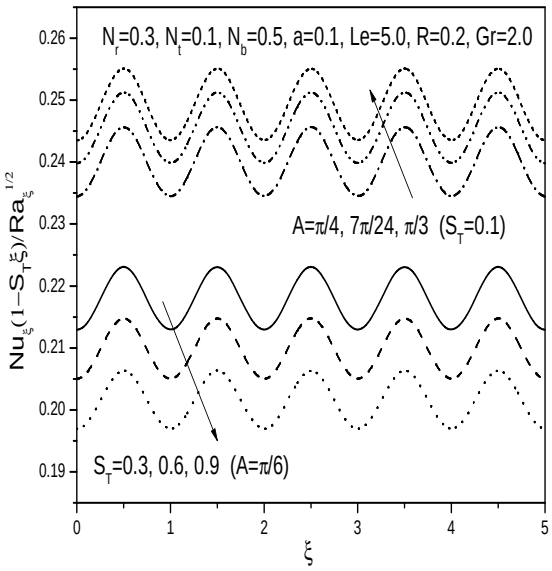

(c)

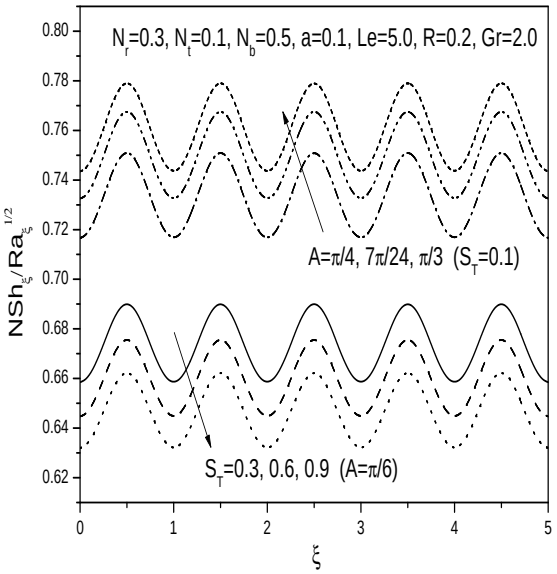

(d)

Figure 8.6: Variation of (a) heat and (b) nanoparticle mass transfer rates with wave amplitude a and (c) heat and (d) nanoparticle mass transfer rates with angle of inclination A and thermal stratification parameter S_T.

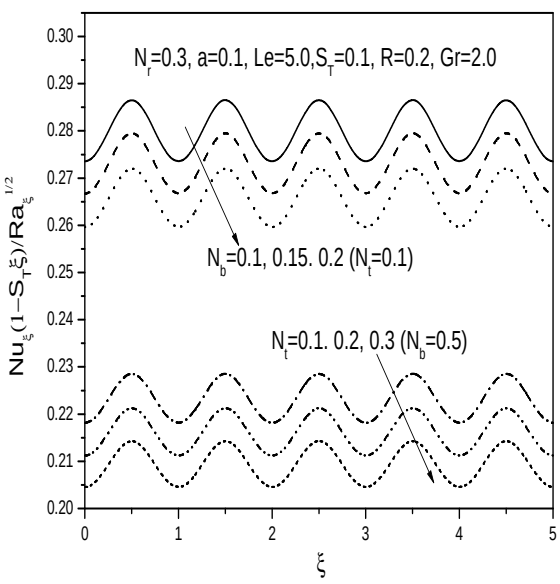

(a)

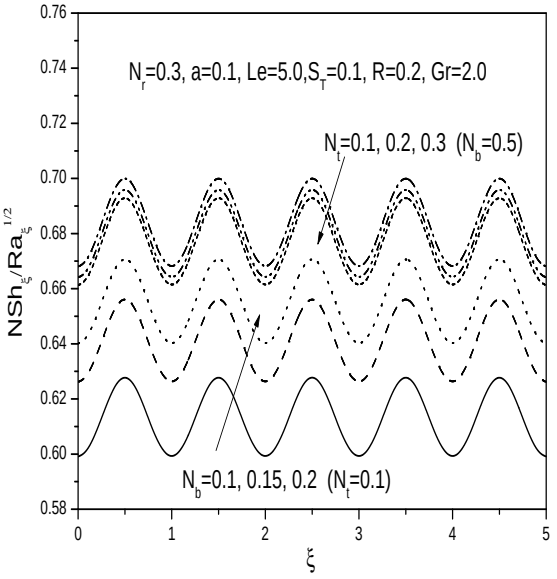

(b)

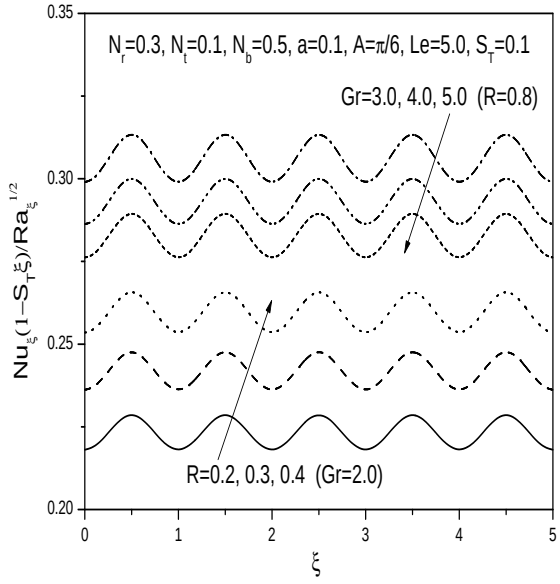

(c)

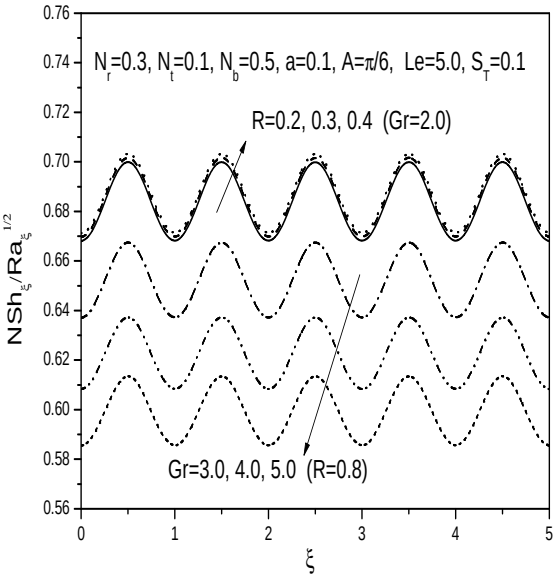

(d)

Figure 8.7: Variation of (a) heat and (b) nanoparticle mass transfer rates with Brownian motion parameter N_b and (c) heat and (d) nanoparticle mass transfer rates with thermophoresis parameter N_t.

8.3 Conclusions

In this chapter, we studied the problem of effect of thermal radiation on natural convection heat and nanoparticle mass transfer over an inclined wavy surface embedded in a thermally stratified non-Darcy porous medium saturated with nanofluid subject to uniform wall temperature and nanoparticle volume fraction conditions. From this analysis, the following conclusions can be drawn:

The effect of thermal radiation parameter R is to enhance the velocity, temperature, local heat and nanoparticle mass transfer but to decrease the nanoparticle volume fraction of the fluid. Increase in the thermal stratification parameter S_T reduces the velocity, temperature, local heat and nanoparticle mass transfer but increases the nanoparticle volume fraction of the fluid. The Grashof number significantly affects the flow field. Increase in the value of Grashof number reduces the velocity, heat and nanoparticle mass transfer rates but increase the temperature and nanoparticle volume fraction of the fluid. The effect of amplitude a of the wavy surface is found to enhance the velocity near the plate and to reduce the temperature, nanoparticle volume fraction, local heat transfer and nanoparticle mass transfer coefficients. The influence of the angle of inclination A of the wavy surface to the horizontal is to enhance the velocity, local heat transfer and nanoparticle mass transfer rates, but to reduce the temperature and nanoparticle volume fraction of the fluid flow.

Chapter 9

Mixed convection of nanofluid over an inclined wavy surface saturated non-Darcy porous medium with thermal radiation and thermal stratification effects[1]

9.1 Introduction

As mentioned in the previous chapters that the thermal stratification on mixed convection in a fluid saturated porous medium is widely accepted due to its geophysical and industrial applications such as hot dike complexes in volcanic regions for heating of ground water, development of advanced technologies for nuclear waste management, pollutant and contaminant transport in soil etc. Generally, stratification of fluid arises due to the temperature variations, concentration differences or the presence of different fluids. A survey of literature on mixed convection flow in a thermally stratified porous medium is reported. In this chapter

[1]Communicated to "**Open Engineering Journal**"

we considered the effects of radiation and thermal stratification on mixed convection flow of a nanofluid over an inclined wavy surface embedded in a non-Darcy porous medium.

The aim of the present chapter is to explore the effects of thermal stratification and thermal radiation on the physical quantities for both aiding and opposing flows and display the results graphically.

9.2 Mathematical Formulation

Consider the steady, laminar, incompressible and two-dimensional mixed convection boundary layer flow over a semi-infinite inclined wavy plate embedded in a non-Darcy porous medium saturated with a nanofluid. The plate is maintained at a uniform and constant wall temperature and nanoparticle volume fraction T_w and ϕ_w respectively. The ambient medium is assumed to be linearly stratified with respect to temperature in the form $T_\infty(x) = T_{\infty,0} + Bx$, where B is a constant which is varied to alter the intensity of stratification in the medium. $T_{\infty,0}$ and ϕ_∞ are ambient temperature and nanoparticle concentration respectively. The porous medium is assumed to be uniform and isotropic and is in local thermal equilibrium with the fluid. The effects of Brownian motion and thermophoresis are incorporated into the model for nanofluids. The fluid properties are assumed to be constant except for density variations in the buoyancy force term.

Using again the Boussinesq and boundary layer approximations, the governing equations can be written as:

$$\frac{\partial u}{\partial x} + \frac{\partial v}{\partial y} = 0, \tag{9.1}$$

$$\left(1 + \frac{\tilde{K}}{\nu}\sqrt{u^2+v^2}\right)\left[\frac{\partial u}{\partial y} - \frac{\partial v}{\partial x}\right] + \frac{\tilde{K}}{\nu\sqrt{u^2+v^2}}\left[u^2\frac{\partial u}{\partial y} + uv\left(\frac{\partial v}{\partial y} - \frac{\partial u}{\partial x}\right) - v^2\frac{\partial v}{\partial x}\right] =$$
$$\frac{(1-\phi_\infty)\rho_{f_\infty}\beta\, K\, g}{\mu}\left(\frac{\partial T}{\partial y}\sin A - \frac{\partial T}{\partial x}\cos A\right) - \frac{(\rho_p - \rho_{f_\infty})\, K\, g}{\mu}\left(\frac{\partial \phi}{\partial y}\sin A - \frac{\partial \phi}{\partial x}\cos A\right), \tag{9.2}$$

$$u\frac{\partial T}{\partial x}+v\frac{\partial T}{\partial y}=\alpha\left(\frac{\partial^2 T}{\partial x^2}+\frac{\partial^2 T}{\partial y^2}\right)+\gamma\left[D_B\left(\frac{\partial\phi}{\partial x}\frac{\partial T}{\partial x}+\frac{\partial\phi}{\partial y}\frac{\partial T}{\partial y}\right)+\frac{D_T}{T_\infty}\left(\left(\frac{\partial T}{\partial x}\right)^2+\left(\frac{\partial T}{\partial y}\right)^2\right)\right] + \frac{16\,\sigma\,T_\infty^3}{3\,K_e}\left(\frac{\partial^2 T}{\partial x^2}+\frac{\partial^2 T}{\partial y^2}\right), \tag{9.3}$$

$$u\frac{\partial\phi}{\partial x}+v\frac{\partial\phi}{\partial y}=D_B\left(\frac{\partial^2\phi}{\partial x^2}+\frac{\partial^2\phi}{\partial y^2}\right)+\frac{D_T}{T_\infty}\left(\frac{\partial^2 T}{\partial x^2}+\frac{\partial^2 T}{\partial y^2}\right), \tag{9.4}$$

Boundary Conditions

Assume that the wavy plate is subject to uniform wall temperature and nanoparticle volume fraction T_w and ϕ_w, respectively. Hence, the boundary conditions are given by (7.5)

Introducing the stream function ψ in Eqns. (9.1) - (9.4) and then using non-dimensional variables given in (7.6), we get the following system of non-linear partial differential equations

$$f''+2F_c(1+\dot{\delta}^2)^{-1/2}f'f''=\Delta(\sin A+\dot{\delta}\cos A)\left(\theta'-N_r s'\right), \tag{9.5}$$

$$\left(1+\frac{4R}{3}\right)\theta''+\frac{1}{2}f\theta'+N_b s'\theta'+N_t\theta'^2=\xi\left(S_T f'+f'\frac{\partial\theta}{\partial\xi}-\theta'\frac{\partial f}{\partial\xi}\right), \tag{9.6}$$

$$s''+\frac{1}{2}Lefs'+\frac{N_t}{N_b}\theta''=Le\xi\left(f'\frac{\partial s}{\partial\xi}-s'\frac{\partial f}{\partial\xi}\right), \tag{9.7}$$

The boundary conditions (7.5) in terms of f,θ and s are given by (7.10) The non-dimensional heat and nanoparticle mass transfer rates are respectively given by

$$\frac{Nu_\xi}{\sqrt{Pe_\xi}}=-\frac{(1+4R/3)\theta'(\xi,0)}{(1-S_T\xi)(1+\dot{\delta}^2)^{1/2}}, \tag{9.8a}$$

$$\frac{NSh_\xi}{\sqrt{Pe_\xi}}=-\frac{s'(\xi,0)}{(1+\dot{\delta}^2)^{1/2}}. \tag{9.8b}$$

Method of Solution

The transformed governing equations (9.5) to (9.7) with the boundary conditions (7.10) are solved using a local similarity and non-similarity method. The resulting boundary layer

equations are linearized using Successive Linearization Method and then solved using Chebyshev spectral collocation method as discussed in detail in the previous chapters. Proceeding same as in previous chapters, we obtain the following matrix equation

$$\mathbf{A}_{i-1}\mathbf{X}_i = \mathbf{R}_{i-1}, \tag{9.9}$$

In Eqn. (9.9), $\mathbf{A}_{i-1}$ is a (6N + 6)×(6N + 6) square matrix and $\mathbf{X}_i$ and $\mathbf{R}_{i-1}$ are (6N + 6)×1 column vectors defined by

$$\mathbf{A}_{i-1} = \begin{bmatrix} A_{11} & A_{12} & A_{13} & A_{14} & A_{15} & A_{16} \\ A_{21} & A_{22} & A_{23} & A_{24} & A_{25} & A_{26} \\ A_{31} & A_{32} & A_{33} & A_{34} & A_{35} & A_{36} \\ A_{41} & A_{42} & A_{43} & A_{44} & A_{45} & A_{46} \\ A_{51} & A_{52} & A_{53} & A_{54} & A_{55} & A_{56} \\ A_{61} & A_{62} & A_{63} & A_{64} & A_{65} & A_{66} \end{bmatrix}, \quad \mathbf{X}_i = \begin{bmatrix} \mathbf{F}_i \\ \boldsymbol{\Theta_i} \\ \boldsymbol{\Phi_i} \\ \mathbf{G}_i \\ \mathbf{H}_i \\ \mathbf{K}_i \end{bmatrix}, \quad \mathbf{R}_{i-1} = \begin{bmatrix} \mathbf{r}_{1,i-1} \\ \mathbf{r}_{2,i-1} \\ \mathbf{r}_{3,i-1} \\ \mathbf{r}_{4,i-1} \\ \mathbf{r}_{5,i-1} \\ \mathbf{r}_{6,i-1} \end{bmatrix} \tag{9.10}$$

where

$\mathbf{F}_i = [f_i(\chi_0), f_i(\chi_1), ..., f_i(\chi_{N-1}), f_i(\chi_N)]^T$, $\mathbf{\Theta_i} = [\theta_i(\chi_0), \theta_i(\chi_1), ..., \theta_i(\chi_{N-1}), \theta_i(\chi_N)]^T$,
$\mathbf{\Phi_i} = [s_i(\chi_0), s_i(\chi_1), ..., s_i(\chi_{N-1}), s_i(\chi_N)]^T$, $\mathbf{G}_i = [g_i(\chi_0), g_i(\chi_1), ..., g_i(\chi_{N-1}), g_i(\chi_N)]^T$,
$\mathbf{H}_i = [h_i(\chi_0), h_i(\chi_1), ..., h_i(\chi_{N-1}), h_i(\chi_N)]^T$, $\mathbf{K}_i = [k_i(\chi_0), k_i(\chi_1), ..., k_i(\chi_{N-1}), k_i(\chi_N)]^T$,
$\mathbf{r}_{j,i-1} = [r_{j,i-1}(\chi_0), r_{j,i-1}(\chi_1), \cdots, r_{j,i-1}(\chi_{N-1}), r_{j,i-1}(\chi_N)]^T, j = 1, 2, 3, 4, 5, 6$
$A_{11} = a_{1,i-1}\mathbf{D}^2 + a_{2,i-1}\mathbf{D}$, $A_{12} = a_{3,i-1}\mathbf{D}$, $A_{13} = a_{4,i-1}\mathbf{D}$, $A_{14} = \mathbf{0}$, $A_{15} = \mathbf{0}$, $A_{16} = \mathbf{0}$
$A_{21} = b_{3,i-1}\mathbf{D} + b_{4,i-1}\mathbf{I}$, $A_{22} = b_{1,i-1}\mathbf{D}^2 + b_{2,i-1}\mathbf{D}$, $A_{23} = b_{5,i-1}\mathbf{D}$, $A_{24} = b_{6,i-1}\mathbf{I}$,
$A_{25} = b_{7,i-1}\mathbf{I}$, $A_{26} = \mathbf{0}$, $A_{31} = c_{2,i-1}\mathbf{D} + c_{3,i-1}\mathbf{I}$, $A_{32} = c_{4,i-1}\mathbf{D}^2$, $A_{33} = \mathbf{D}^2 + c_{1,i-1}\mathbf{D}$,
$A_{34} = c_{5,i-1}\mathbf{I}$, $A_{35} = \mathbf{0}$, $A_{36} = c_{6,i-1}\mathbf{I}$, $A_{41} = d_{3,i-1}\mathbf{D}^2 + d_{4,i-1}\mathbf{D}$, $A_{42} = d_{5,i-1}\mathbf{D}$,
$A_{43} = d_{6,i-1}\mathbf{D}$, $A_{44} = d_{1,i-1}\mathbf{D}^2 + d_{2,i-1}\mathbf{D}$, $A_{45} = d_{7,i-1}\mathbf{D}$, $A_{46} = d_{8,i-1}\mathbf{D}$,
$A_{51} = l_{4,i-1}\mathbf{D} + l_{5,i-1}\mathbf{I}$, $A_{52} = l_{6,i-1}\mathbf{D}$, $A_{53} = l_{7,i-1}\mathbf{D}$, $A_{54} = l_{8,i-1}\mathbf{D} + l_{9,i-1}\mathbf{I}$,
$A_{55} = l_{1,i-1}\mathbf{D}^2 + l_{2,i-1}\mathbf{D} + l_{3,i-1}\mathbf{I}$, $A_{56} = l_{10,i-1}\mathbf{D}$, $A_{61} = m_{3,i-1}\mathbf{D} + m_{4,i-1}\mathbf{I}$,
$A_{62} = \mathbf{0}$, $A_{63} = m_{5,i-1}\mathbf{D}$, $A_{64} = m_{6,i-1}\mathbf{D} + m_{7,i-1}\mathbf{I}$, $A_{65} = m_{8,i-1}\mathbf{D}^2$,
$A_{66} = \mathbf{D}^2 + m_{1,i-1}\mathbf{D} + m_{2,i-1}\mathbf{I}$

Table 9.1: Comparison of values of $-\theta'(0)$ for aiding and opposing flows by the present method and Cheng [23] for fixed values of for $A = \frac{\pi}{2}$, $a = 0$, $\xi = 0$, $N_r = 0$, $N_t = 0$, $N_b \to 0$, $Le = 0$, $R = 0$, $S_T = 0$.

Aiding Flow			Opposing Flow		
Δ	Cheng [23]	Present	Δ	Cheng [23]	Present
0	0.5641	0.56415775	-0.2	0.5269	0.52691089
0.5	0.6473	0.64736510	-0.4	0.4865	0.48653284
1	0.7205	0.72055401	-0.6	0.442	0.44202064
3	0.9574	0.95744512	-0.8	0.3916	0.39166292
10	1.516	1.51623967	-1.0	0.332	0.33202116
20	2.066	2.066			

Here $a_{k,i-1}$, $b_{k,i-1}$, $c_{k,i-1}$,$d_{k,i-1}$, $l_{k,i-1}$, $m_{k,i-1}$ are diagonal matrices of size (N+1)×(N+1) and $\mathbf{I}$ is an identity matrix of size (N +1)×(N +1). After modifying the matrix system (9.9) to incorporate boundary conditions, the solution is obtained as

$$\mathbf{X}_i = \mathbf{A}_{i-1}^{-1}\mathbf{R}_{i-1} \tag{9.11}$$

Results and Discussion

The solutions for the dimensionless velocity, temperature and nanoparticle volume fraction functions and heat and nanoparticle mass transfer rates have been computed and are displayed graphically in Figs. 9.1 - 9.9. The effects of thermal stratification S_T, thermal radiation R, non-Darcy parameter F_c, angle of inclination A, and amplitude a of the wavy surface have been discussed.

Table. 9.1 shows the comparison of the results of the values of $\theta'(0)$ of the present problem for different values of Δ and fixed values of $A = \pi/2$, $a = 0$, $S_T = 0$ with the results obtained by Cheng [23]. It is seen that these two results are in excellent agreement.

The effect of amplitude of the wavy surface on velocity, temperature and nanoparticle volume fraction is plotted in Fig. 9.1. It is observed that as a increases, velocity increases

near the plate and decreases away from the plate, whereas the temperature and nanoparticle volume fraction decreases for aiding flow but a reverse pattern is observed in the case of opposing flow.

The variation of velocity, temperature and nanoparticle volume fraction with the angle of inclination is depicted in Fig. 9.2. It is noticed from Fig. 9.2(a) - 9.2(c) that as A increases, the velocity increases near the plate and decreases away from the plate but the temperature and nanoparticle volume fraction decrease within the boundary layer region for aiding flow whereas a reverse pattern is seen in the case of opposing flow.

Figure 9.3 depicts the effect of non-Darcy parameter F_c on velocity, temperature and nanoparticle volume fraction distributions. It is clear from Fig. 9.3(a) that increase in non-Darcy parameter reduces the velocity of the fluid in the case of aiding flow and enhances the velocity in the case of opposing flow. It is noticed from Figs. 9.3(b) and 9.3(c) that increase in the non-Darcy parameter enhances the temperature and nanoparticle volume fraction of the fluid in the case of aiding flow but reduces in the case of opposing flow.

The influence of radiation parameter R on non-dimensional velocity, temperature and nanoparticle volume fraction is presented in Fig. 9.4. It is observed from Fig. 9.4(a) that the velocity increases with increase in the value of radiation parameter for aiding flow and decreases for opposing flow. It is noticed from Fig. 9.4(b) that the temperature increases with increase in the value of radiation parameter for both aiding and opposing flows whereas a negligible effect of radiation on nanoparticle volume fraction for both aiding and opposing flows is observed as shown in Fig. 9.4(c).

The effect of thermal stratification on velocity, temperature and nanoparticle volume fraction distributions is shown in Figs. 9.5 and 9.6 for both aiding and opposing flows respectively. It is noticed from Fig. 9.5 that increase in the thermal stratification parameter S_T reduces the velocity and temperature of the fluid but increases the nanoparticle volume fraction in the case of aiding flow whereas the velocity enhances but the temperature and nanoparticle volume fraction reduce in the case of opposing flow as seen in Fig. 9.6.

The effect of the wave amplitude and angle of inclination of the wavy surface on the local

Nusselt number $Nu_\xi(1 - S_T\xi)/{Pe_\xi}^{1/2}$ and nanoparticle Sherwood number $NSh_\xi/{Pe_\xi}^{1/2}$ is plotted in Fig. 9.7. It is observed from Fig. 9.7(a) and 9.7(b) that an enhancement in wavy amplitude decreases the local heat and nanoparticle mass transfer rates for both aiding and opposing flows. From Figs. 9.7(c) and 9.7(d) it is noticed that increase in the angle of inclination increases the buoyancy force and assists the flow, leading to an increase in the heat and nanoparticle mass transfer rates in the case of aiding flow whereas a reverse trend is observed in the case of opposing flow.

Figure 9.8 displays the streamwise distribution of Nusselt and nanoparticle Sherwood numbers for different values of non-Darcy parameter F_c and radiation parameter R. It is seen that increase in the non-Darcy parameter decreases the local heat and nanoparticle mass transfer rates for aiding flow but enhances in the case of opposing flow as seen in Figs. 9.8(a) and 9.8(b). It is noticed from Fig. 9.8(c) that increase in the radiation parameter enhances the local heat transfer rate for both aiding and opposing flows whereas a negligible effect of radiation on nanoparticle mass transfer rate is seen through Fig. 9.8(d).

The effect of thermal stratification parameter S_T on the heat and nanoparticle mass transfer rates is presented in Fig. 9.9. It is observed from Fig. 9.9(a) and 9.9(b) that increase in the thermal stratification parameter reduces both the dimensionless heat and nanoparticle mass transfer rates for aiding flow but enhances in the case of opposing flow.

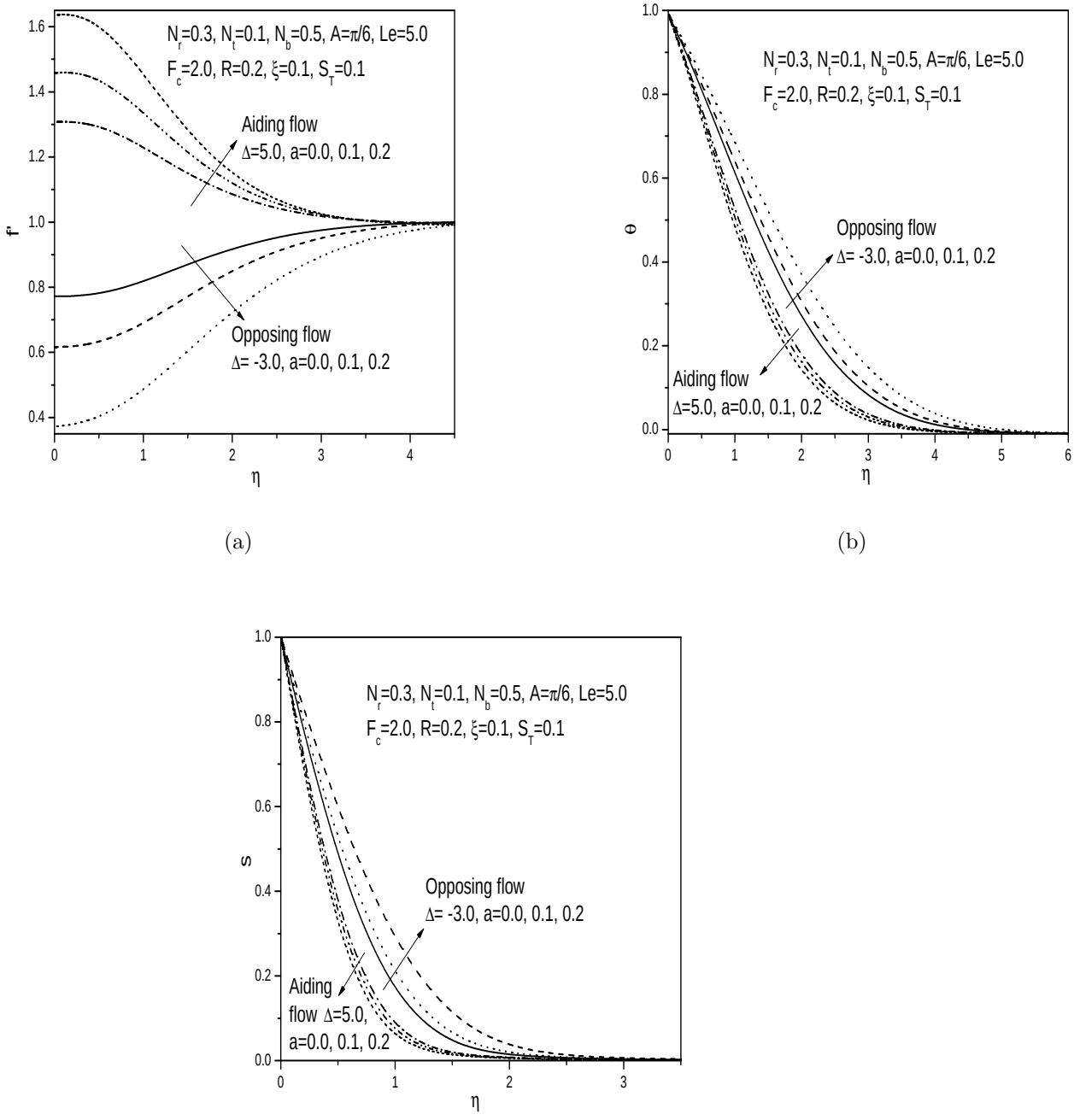

Figure 9.1: Variation of (a) velocity, (b) temperature and (c) nanoparticle volume fraction profiles with wave amplitude.

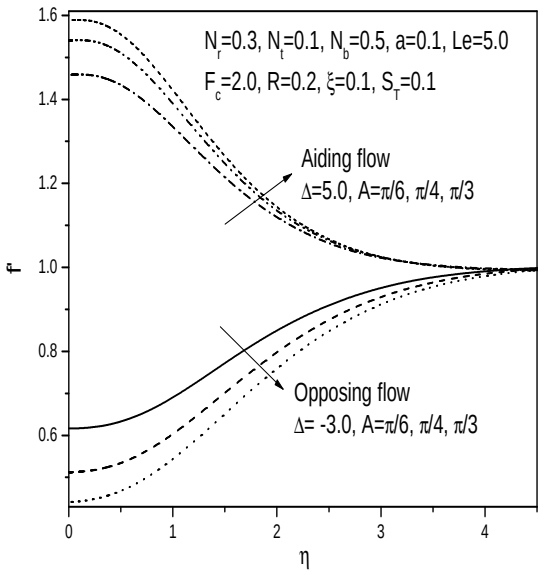

(a)

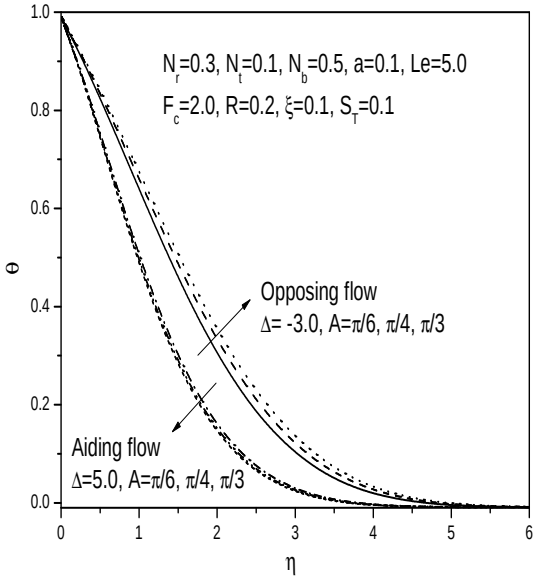

(b)

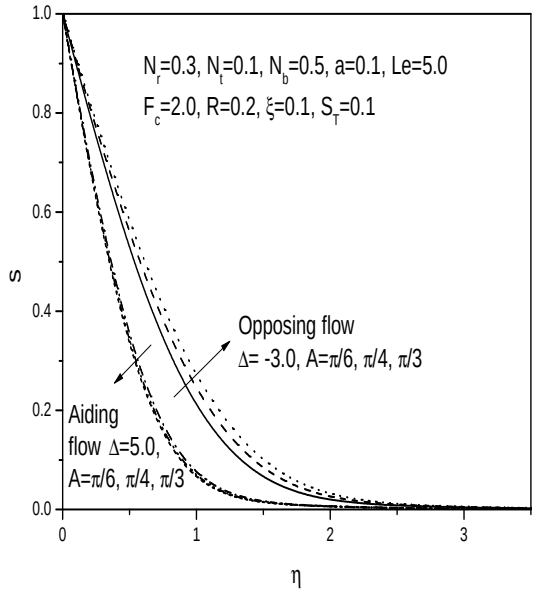

(c)

Figure 9.2: Variation of (a) velocity, (b) temperature and (c) nanoparticle volume fraction profiles with angle of inclination A.

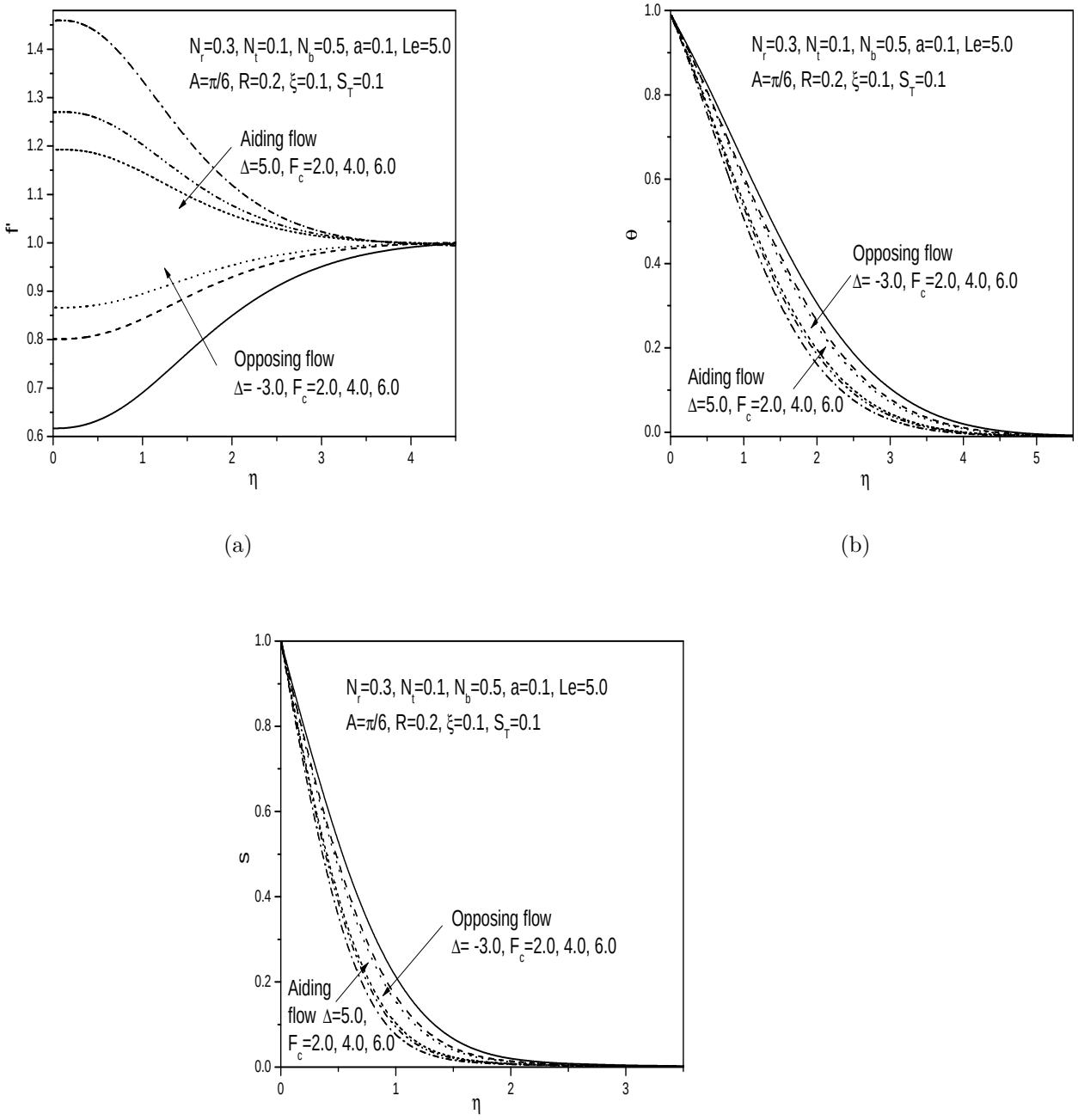

Figure 9.3: Variation of (a) velocity, (b) temperature and (c) nanoparticle volume fraction profiles with non-Darcy parameter.

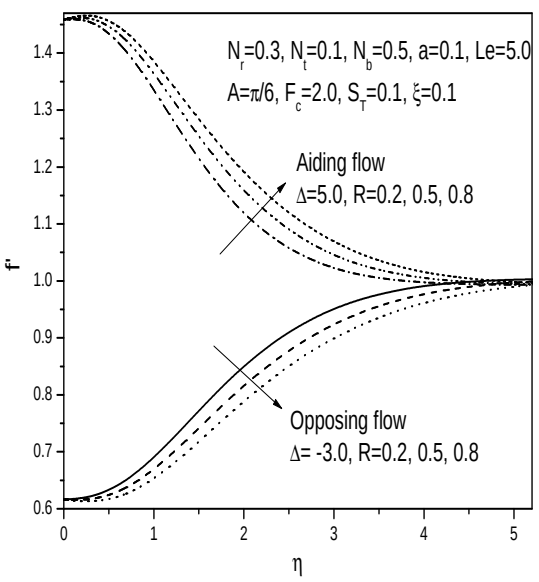

(a)

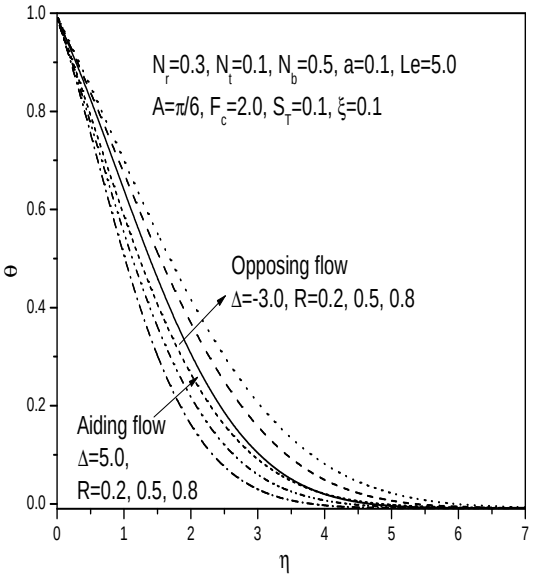

(b)

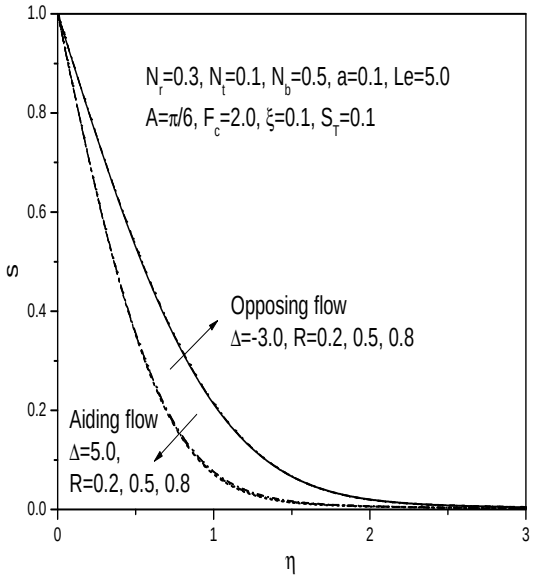

(c)

Figure 9.4: Variation of (a) velocity, (b) temperature and (c) nanoparticle volume fraction profiles with radiation parameter.

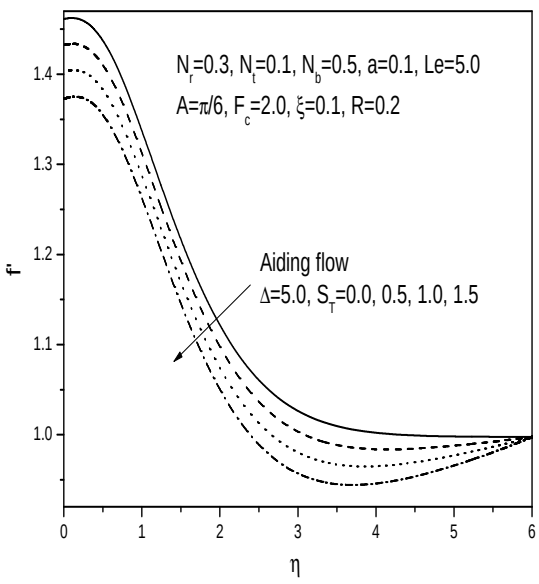

(a)

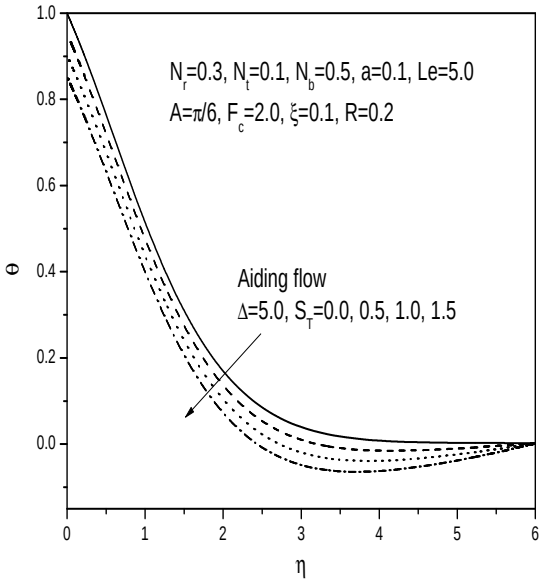

(b)

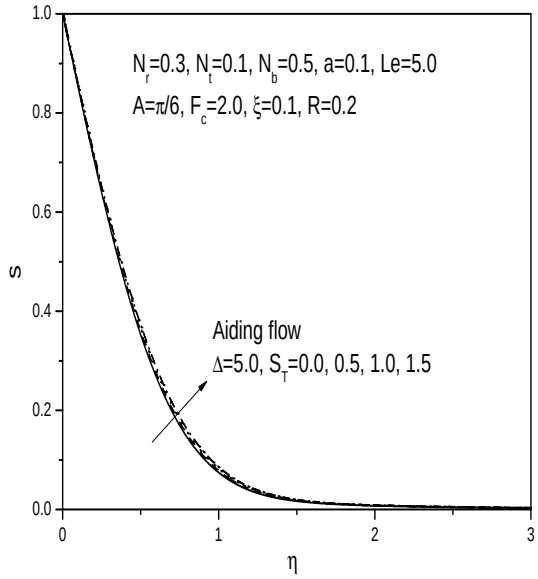

(c)

Figure 9.5: Variation of (a) velocity, (b) temperature and (c) nanoparticle volume fraction profiles with thermal stratification parameter for aiding flow.

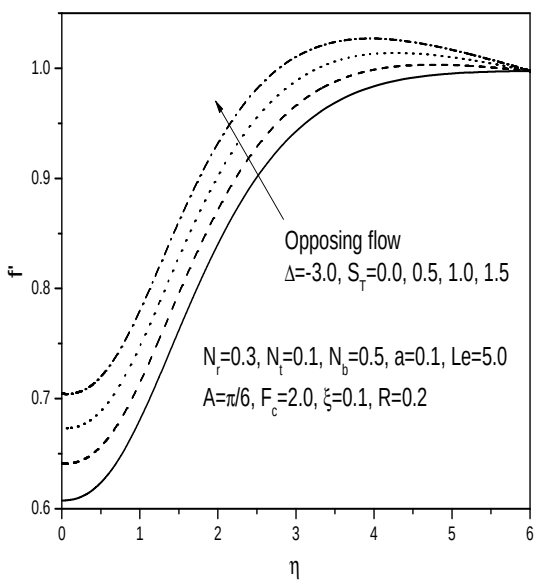

(a)

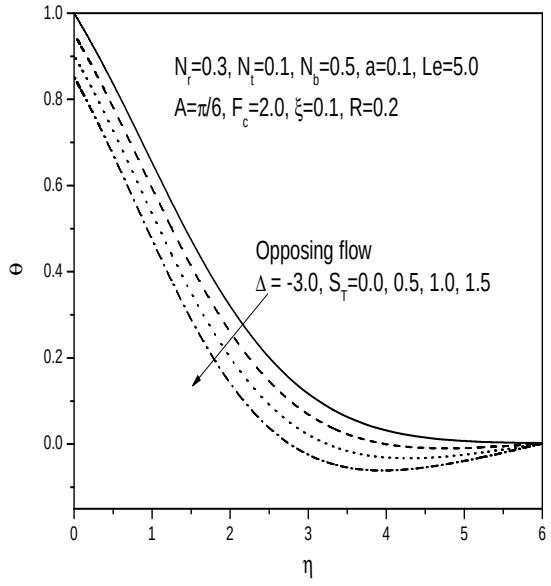

(b)

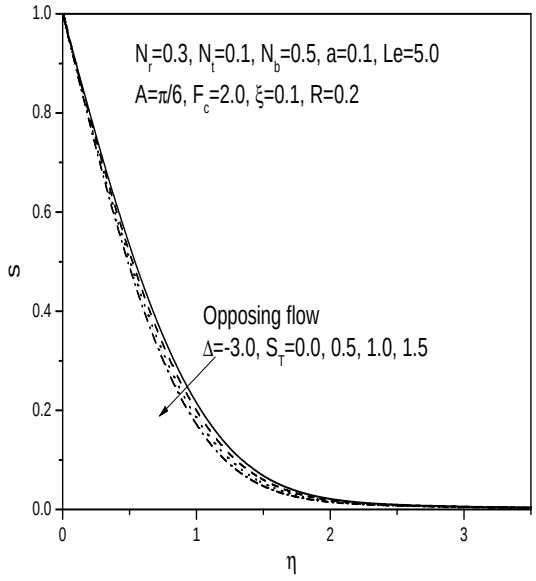

(c)

Figure 9.6: Variation of (a) velocity, (b) temperature and (c) nanoparticle volume fraction profiles with thermal stratification parameter for opposing flow.

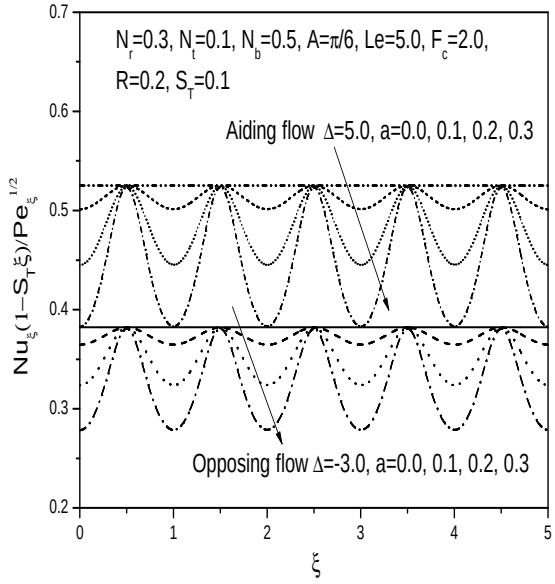

(a)

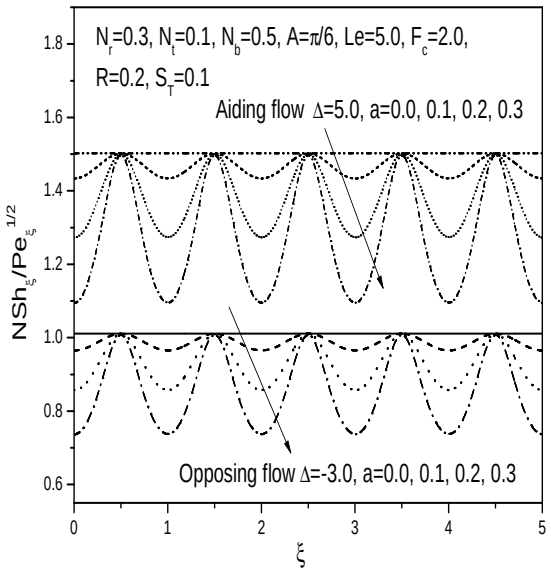

(b)

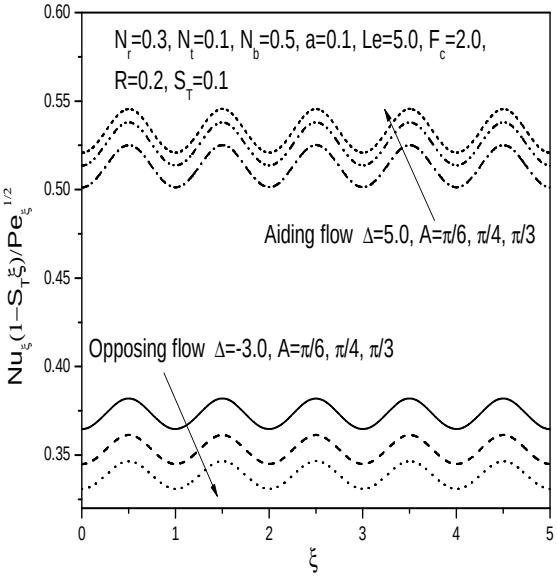

(c)

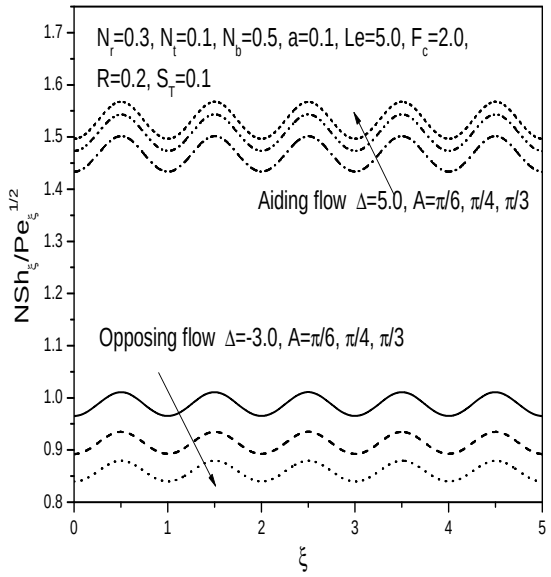

(d)

Figure 9.7: Variation of (a) heat and (b) nanoparticle transfer rates with wave amplitude and (c) heat and (d) nanoparticle transfer rates with angle of inclination.

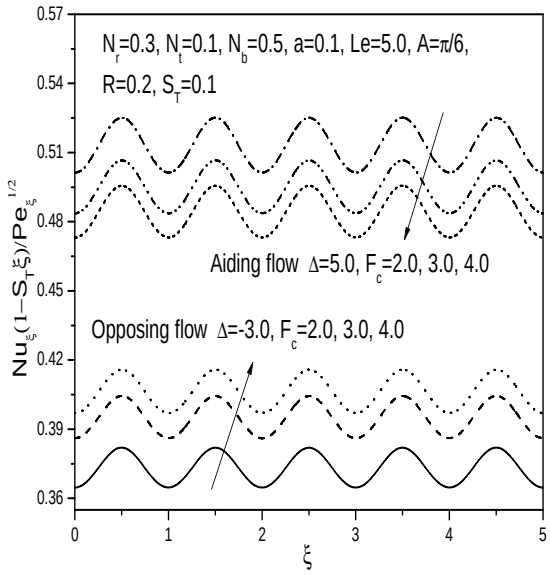

(a)

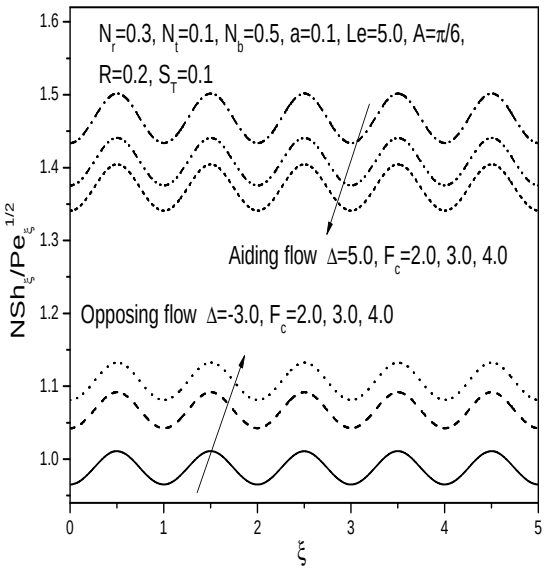

(b)

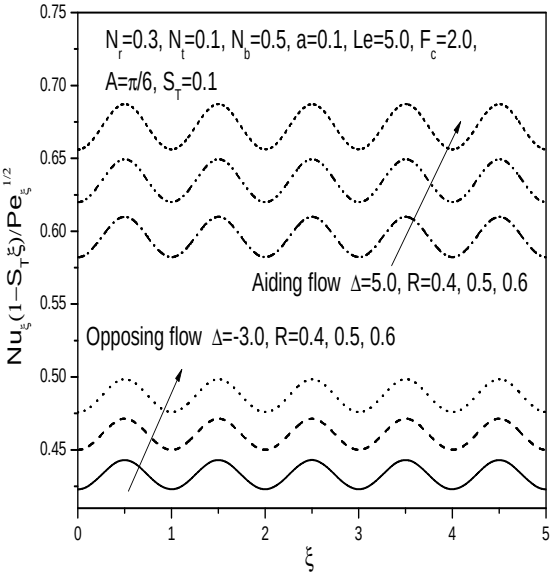

(c)

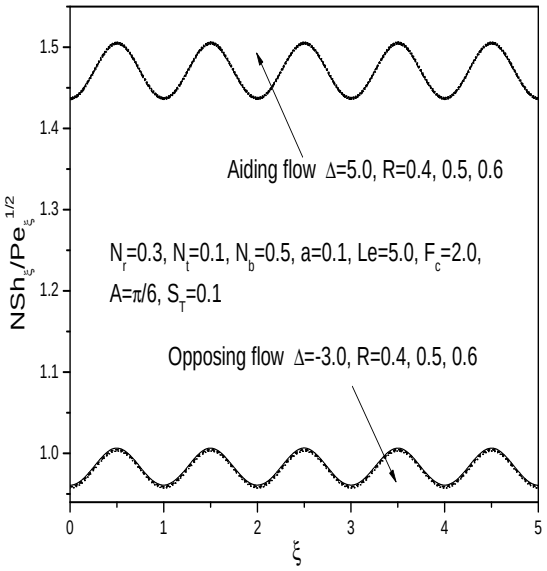

(d)

Figure 9.8: Variation of (a) heat and (b) nanoparticle transfer rates with non-Darcy parameter and (c) heat and (d) nanoparticle transfer rates with radiation parameter.

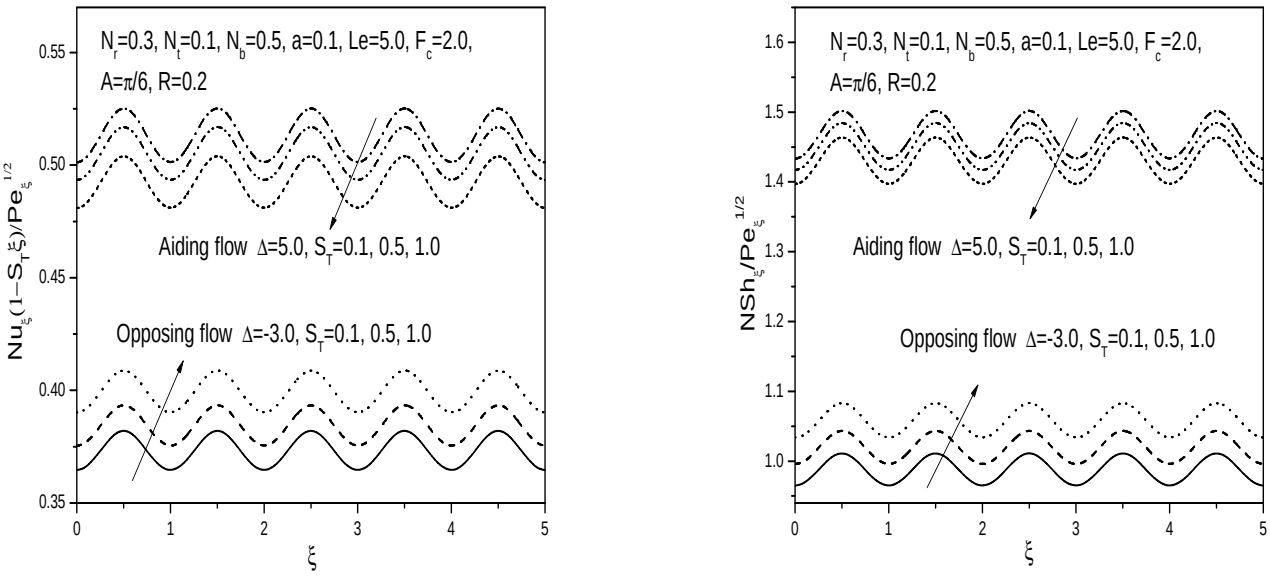

(a) (b)

Figure 9.9: Variation of (a) heat and (b) nanoparticle transfer rates with thermal stratification parameter.

9.3 Conclusions

In this chapter, we analyzed the problem of steady, laminar mixed convection heat and nanoparticle mass transfer over an inclined wavy surface embedded in a non-Darcy porous medium saturated with nanofluid with thermal stratification and thermal radiation effects, subject to uniform wall temperature and nanoparticle volume fraction conditions. From this investigation, the following conclusions can be drawn for both the cases (a) and (b):

The effect of thermal radiation parameter R is to reduce the velocity in the case of opposing flow and to enhance the temperature and local heat transfer rate for both aiding and opposing flows. Increase in the thermal stratification parameter S_T increases the velocity, local heat and nanoparticle mass transfer rates for opposing flow but reduces in the case of aiding flow whereas the temperature of the fluid reduces for both aiding and opposing flows. The non-Darcy parameter significantly affects the flow field i.e, increasing the non-Darcy parameter reduces the velocity, heat and nanoparticle mass transfer rates for aiding flow

but increases in the case of opposing flow. The effect of amplitude a of the wavy surface was found to enhance the temperature and nanoparticle volume fraction for opposing flow but to reduce the local heat transfer and nanoparticle mass transfer rates for both aiding and opposing flows. The influence of the angle of inclination A of the wavy surface to the horizontal is to reduce the velocity, local heat transfer and nanoparticle mass transfer rates but to enhance the temperature and nanoparticle volume fraction of the fluid for opposing flow.

Chapter 10

Summary and Conclusions

In this thesis an analysis of convective heat and nanoparticle mass transfer over a semi-infinite inclined wavy surface immersed in a nanofluid saturated porous medium is attempted.

The steady natural/mixed convection heat and nanoparticle mass transfer along an semi-infinite inclined wavy surface submerged in a nanofluid saturated non-Darcy porous medium has been investigated. The aim of the chapters is to present numerical solutions for the considered problems and also to investigate the effects of thermal stratification, thermal radiation, non-Darcy effect on the flow characteristics such as velocity, temperature and nanoparticle concentration along with local heat and nanoparticle mass transfer coefficients. In all the chapters (2 - 9), the non-linear governing equations and their associated boundary conditions are linearized by using Successive Linearization Method and then solved numerically by Chebyshev spectral collocation method. For the case of non-similar equations, a local similarity and non-similarity method is used for converting the partial differential equations to ordinary differential equations and then the system is solved numerically by using Successive Linearization Method. The main findings of the analysis carried are

- An increase in the Brownian motion parameter N_b, increases the velocity, temperature and local nanoparticle mass transfer coefficient for aiding flow, but reduces the nanoparticle volume fraction and local heat transfer coefficient for both aiding and

opposing flows.

- A higher value of the thermophoresis parameter N_t leads to higher temperatures and nanoparticle volume fraction for both aiding and opposing flows, but an increase in velocity for aiding flow and decrease in velocity for opposing flow is observed. Moreover, lower local heat transfer coefficient for both aiding and opposing flows and no effect on the nanoparticle mass transfer coefficient is observed.

- The effect of the amplitude a of the wavy surface is to increase the velocity and to reduce the temperature and nanoparticle volume fraction in the case of aiding flow but to reduce the velocity and to increase the temperature and nanoparticle volume fraction in the case of opposing flow. The local heat transfer and nanoparticle mass transfer coefficient reduces for both aiding and opposing flows.

- The influence of the angle of inclination A of the wavy surface to the horizontal is to enhance the velocity, local heat and nanoparticle mass transfer coefficients but to reduce the temperature and nanoparticle volume fraction of the fluid for aiding flow and a reverse trend is observed in the case of opposing flow.

- The effect of non-Darcy parameter F_c is to reduce the velocity, local heat and nanoparticle mass transfer for aiding flow and to increase the same in the case of opposing flow while the temperature and nanoparticle volume fraction increase for aiding flow and reduce for opposing flow.

- The influence of radiation parameter R is to enhance the velocity and temperature for aiding flow and reduce the same in the case of opposing flow. The local heat transfer enhances for both aiding and opposing flows and there is a negligible effect on nanoparticle volume fraction and nanoparticle mass transfer rates.

- Increase in the thermal stratification parameter S_T reduces the velocity, temperature, local heat and nanoparticle mass transfer rates but enhances the nanoparticle volume fraction of the fluid for aiding flow. The velocity, local heat and nanoparticle mass transfer rates increase and the temperature and nanoparticle volume fraction decrease in the case of opposing flow.

The work presented in the thesis can be extended to analyze the effect of Joule heating, MHD, Hall and Ion slip, double diffusion, conjugate convection, viscous dissipation etc., independently and then examining their combined effects over the complex structure. Such an exhaustive study can be a rewarding experience though it is challenging as well as time consuming.

Bibliography

[1] G. M. Abdel-Rahman. Thermal radiation and unsteady magnetohydrodynamic flow of nanofluid in stretching porous medium. *J. Thermophysics and Heat Transfer.*, 27:142–150, 2013.

[2] E. Abu-Nada. Application of nanofluids for heat transfer enhancement of separated flows encountered in a backward facing step. *Int. J. Heat Fluid Flow.*, 29:242–249, 2008.

[3] H. A. Agha, M. N. Bouaziz, and S. Hanini. Free convection boundary layer flow from a vertical flat plate embedded in a Darcy porous medium filled with a nanofluid: Effects of magnetic field and thermal radiation. *Arab. J. Sci. Eng.*, 39:8331–8340, 2014.

[4] S. Ahmad and I. Pop. Mixed convection boundary layer flow from a vertical flat plate embedded in a porous medium filled with nanofluids. *Int. Commun. Heat Mass Transfer.*, 37:987–991, 2010.

[5] F. G. Awad, P. Sibanda, S. S. Motsa, and O. D. Makinde. Convection from an inverted cone in a porous medium with cross-diffusion effects. *Computers and Mathematics with Applications.*, 61:1431–1441, 2011.

[6] A. Y. Bakier, M. A. Mansour, R. S. R. Gorla, and A. B. Ebiana. Nonsimilar solutions for free convection from a vertical plate in porous media. *Heat Mass Transfer.*, 33:145–148, 1997.

[7] V. J. Bansod and R. K. Jadhav. Effect of double stratification on mixed convection heat and mass transfer from a vertical surface in a fluid saturated porous medium. *Heat Transfer - Asian Research.*, 39:378–395, 2010.

[8] A. Bejan. *Convection Heat Transfer.* John Wiley, New York, 2004.

[9] A. Bejan and Khairy R. Khair. Heat and mass transfer by natural convection in a porous medium. *Int. J. Heat Mass Transfer.*, 28:909–918, 1985.

[10] J. Buongiorno. Convective transport in nanofluids. *ASME J. Heat Transfer.*, 128:240–250, 2006.

[11] C. Canuto, M. Y. Hussaini, A. Quarteroni, and T. A. Zang. *Spectral methods fundamentals in single domains.* Springer, Berlin, 2006.

[12] A. J. Chamkha, S. Abbasbandy, and A. M. Rashad. Non-Darcy natural convective flow for non-Newtonian nanofluid over a cone saturated in porous medium with uniform heat and volume fraction fluxes. *Int. J. Numerical Methods for Heat and Fluid Flow.*, 25:422–437, 2015.

[13] A. J. Chamkha, S. Abbasbandy, A. M. Rashad, and K. Vajravelu. Radiation effect on mixed convection over a wedge embedded in a porous medium filled with a nanofluid. *Transp. Porous Med.*, 91:261–279, 2012.

[14] A. J. Chamkha, S. Abbasbandy, A. M. Rashad, and K. Vajravelu. Radiation effect on mixed convection about a cone embedded in a porous medium filled with a nanofluid. *Meccanica.*, 48:275–285, 2013.

[15] A. J. Chamkha, M. Rashad, and R. S. R. Gorla. Non-similar solutions for mixed convection along a wedge embedded in a porous medium saturated by a non-Newtonian nanofluid: natural convection dominated regime. *Int. J. Numerical Methods for Heat & Fluid Flow.*, 24:1471–1486, 2014.

[16] R. Chand and G. C. Rana. The effects of radiation on the onset of thermal instability in a layer of nanofluid layer in a porous medium. *Int. J. Appl. Math. Mech.*, 10:76–91, 2014.

[17] C.-K. Chen, Y.-T. Yang, and K.-H. Chang. Entropy generation of radiation effect on laminar-mixed convection along a wavy surface. *Heat Mass Transfer.*, 47:385–395, 2011.

[18] C. Y. Cheng. Non-Darcy natural convection heat and mass transfer from a vertical wavy surface in saturated porous medium. *Appl. Math. Comput.*, 182:1488–1500, 2006.

[19] C. Y. Cheng. Double diffusive natural convection along a vertical wavy truncated cone in non-Newtonian fluid saturated porous media with thermal and mass stratification. *Int. Comm. Heat Mass Transfer.*, 35:985–990, 2008.

[20] C. Y. Cheng. Combined heat and mass transfer in natural convection flow from a vertical wavy surface in a power-law fluid saturated porous medium with thermal and mass stratification. *Int. Commun. Heat Mass Transfer.*, 36:351–356, 2009.

[21] C. Y. Cheng. Soret and Dufour effects on free convection boundary layers over an inclined wavy surface in a porous medium. *Int. Commun. Heat Mass Transfer.*, 38:1050–1055, 2011.

[22] C. Y. Cheng. Natural convection boundary layer flow over a truncated cone in a porous medium saturated by a nanofluid. *Int. Commun. Heat Mass Transfer.*, 39:231–235, 2012.

[23] P. Cheng. Combined free and forced convection flow about inclined surfaces in porous media. *Int. J. Heat Mass Transfer*, 20:807–814, 1977.

[24] P. Cheng and W. J. Minkowycz. Free convection about a vertical flat plate embedded in a porous medium with application to heat transfer from a dike. *J. Geophysical Research.*, 82:2040–2044, 1977.

[25] K. E. Chin, R. Nazar, N. M. Arifin, and I. Pop. Effect of variable viscosity on mixed convection boundary layer flow over a vertical surface embedded in a porous medium. *Int. Comm. Heat Mass Transfer.*, 34:464–473, 2007.

[26] S. U. S. Choi. Enhancing thermal conductivity of fluids with nanoparticles, developments and applications of non-Newtonian flows. *ASME FED.*, 231:99–103, 1995.

[27] S. U. S. Choi, Z. G. Zhang, W. Yu, F. E. Lockwood, and E.A. Grulke. Anomalously thermal conductivity enhancement in nanotube suspension. *Appl. Phys. Lett.*, 79:2252–2254, 2001.

[28] H. P. G. Darcy. Mles fontaines publiques de la ville de dijon. *Victor Dalmont*, 1856.

[29] S. K. Das, S. U. S. Choi, W. Yu, and T. Pradeep. *Nanofluids: Science and Technology.* Wiley Interscience, New Jersey, 2007.

[30] W. Daungthongsuk and S. Wongwises. A critical review of convective heat transfer nanofluids. *Renew. Sustain. Eng. Rev.*, 11:797–817, 2007.

[31] W. S. Don and A. Solomonoff. Accuracy and speed in computing the Chebyshev collocation derivative. *SIAM J. Sci. Comput.*, 16:1253–1268, 1995.

[32] J. A. Eastman, S. R. Phillpot, S. U. S. Choi, and P. Keblinski. Thermal transport in nanofluids. *Annu. Rev. Mater. Res.*, 34:219–246, 2004.

[33] M. A. El-Hakiem and M. F. El-Amin. Thermal radiation effect on non-Darcy natural convection with lateral mass transfer. *Heat Mass Transfer.*, 37:161–165, 2001.

[34] S. M. M. El-Kabeir, A. J. Chamkha, and A. M. Rashad. Effect of thermal radiation on non-Darcy natural convection from a vertical cylinder embedded in a nanofluid porous media. *J. Porous Med.*, 17:269–278, 2014.

[35] P. Gianluca, P. Samuel, and M. Sen. Nanofluids and their properties. *Appl. Mech. Reviews.*, 64:030803, 2011.

[36] R. S. R. Gorla and A. J. Chamkha. Natural convective boundary layer flow over a horizontal plate embedded in a porous medium saturated with a nanofluid. *J. Mod. Phys.*, 2:62–71, 2011.

[37] R. S. R. Gorla and A. Hossain. Mixed convective boundary layer flow over a vertical cylinder embedded in a porous medium saturated with a nanofluid. *Int. J. Numerical Methods for Heat & Fluid Flow.*, 23:1393–1405, 2013.

[38] N. Guerroudj and H. Kahalerras. Mixed convection in an inclined channel with heated porous blocks. *Int. J. Numerical Methods for Heat & Fluid Flow.*, 22:839–861, 2012.

[39] Z. Haddad, E. Abu-Nada, H. F. Oztop, and A. Mataoui. Natural convection in nanofluids: are the thermophoresis and Brownian motion effects significant in nanofluid heat transfer enhancement. *Int. J. Thermal Sci.*, 57:152–162, 2012.

[40] F. M. Hady, F. S. Ibrahim, S. M. Abdel-Gaied, and M. R. Eid. Radiation effect on viscous flow of a nanofluid and heat transfer over a nonlinearly stretching sheet. *Nanoscale Res. Lett.*, 7:1–13, 2012.

[41] P.-T. Hsu, K. Taiwan, C.-K. Chen, C.-C. Wang, and T. Taiwan. Mixed convection of micropolar fluids along a vertical wavy surface. *Acta Mechanica.*, 144:231–247, 2000.

[42] W. Ibrahim and O. D. Makinde. The effect of double stratification on boundary layer flow and heat transfer of nanofluid over a vertical plate. *Computers and Fluids.*, 86:433–441, 2013.

[43] D. B. Ingham and I. Pop. *Transport Phenomenon in Porous Media, vol.II.* Elsevier, Oxford, 2005.

[44] D.B. Ingham and I. Pop. *Transport Phenomenon in Porous Media, vol.I.* Pergamon, Oxford, 1998.

[45] R. Ishak, A. Nazar and I. Pop. Mixed convection boundary layer flow over a vertical surface embedded in a thermally stratified porous medium. *Phys. Lett. A.*, 372:2355–2358, 2008.

[46] J.-H. Jang and W.-M. Yan. Mixed convection heat and mass transfer along a vertical wavy surface. *Int. J. Heat Mass Transfer.*, 47:419–428, 2004.

[47] S. Kakac and A. Pramuanjaroenkij. Review of convective heat transfer enhancement with nanofluids. *Int. J. Heat Mass Transfer.*, 52:3187–3196, 2009.

[48] R. Kandaswamy, I. Muhaimin, and R. Mohammad. Thermophoresis and Brownian motion effects on MHD-boundary layer flow of a nanofluid in the presence of thermal stratification due to solar radiation. *Int. J. Mechanical Sciences.*, 70:146–154, 2013.

[49] W. A. Khan and A. Aziz. Double-diffusive natural convective boundary layer flow in a porous medium saturated with a nanofluid over a vertical plate: Prescribed surface heat, solute and nanoparticle fluxes. *Int. J. Thermal Sci.*, 50:2154–2160, 2011.

[50] W. A. Khan and A. Aziz. Natural convection flow of a nanofluid over a vertical plate with uniform surface heat flux. *Int. J. Thermal Sci.*, 50:1207–1214, 2011.

[51] K. Khanafer, K. Vafai, and M. Lightstone. Buoyancy-driven heat transfer enhancement in a two-dimensional enclosure utilizing nanofluids. *Int. J. Heat Mass Transf.*, 46:3639–3653, 2003.

[52] B. V. R. Kumar and Shalini. Non-Darcy free convection induced by a vertical wavy surface in a thermally stratified porous medium. *Int. J. Heat Mass Transfer.*, 47:2353–2363, 2004.

[53] A. V. Kuznetsov and D. A. Nield. Natural convective boundary-layer flow of a nanofluid past a vertical plate. *Int. J. Thermal Sci.*, 49:243–247, 2010.

[54] A. V. Kuznetsov and D. A. Nield. Double-diffusive natural convective boundary-layer flow of a nanofluid past a vertical plate. *Int. J. Thermal Sci.*, 50:712–717, 2011.

[55] F. C. Lai. Coupled heat and mass transfer by mixed convection from a vertical plate in a saturated porous medium. *Int. Comm. Heat Mass Transfer.*, 18:93–106, 1991.

[56] P. A. Lakshmi Narayana and P. Sibanda. Soret and Dufour effects on free convection along a vertical wavy surface in a fluid saturated Darcy porous medium. *Int. J. Heat Mass Transfer.*, 53:3030–3034, 2010.

[57] A. Mahdy and S. E. Ahmed. Laminar free convection over a vertical wavy surface embedded in a porous medium saturated with a nanofluid. *Transp. Porous Med.*, 90:423–435, 2012.

[58] A. Mahdy, R. A. Mohamed, and F. M. Hady. Natural convection heat and mass transfer over a vertical wavy surface with variable wall temperature and concentration in porous media. *Int. J. Appl. Math. Mech.*, 7:1–13, 2011.

[59] A. A. M. Mahmoud and S. E. Waheed. Mixed convection flow of a micropolar fluid past a vertical stretching surface in a thermally stratified porous medium with thermal radiation. *J. Mechanics.*, 29:461–470, 2013.

[60] Z. G. Makukula, S. S. Motsa, and P. Sibanda. On a new solution for the viscoelastic squeezing flow between two parallel plates. *J. of Adv. Research in Appl. Math.*, 2:31–38, 2010.

[61] Z. G. Makukula, P. Sibanda, and S. S. Motsa. A note on the solution of the Von Karman equations using series and Chebyshev spectral methods. *Boundary Value Problems*, 471793, 2010.

[62] R. B. Mansour, A. Galanis, and C. T. Nguyen. Experimental study of mixed convection with water-Al_2O_3 nanofluid in inclined tube with uniform wall heat flux. *Int. J. Thermal Sci.*, 50:403–410, 2011.

[63] J. H. Merkin. Free convetion boundary layer flow on a vertical surface in a saturated porous medium. *J. Engineering Mathematics.*, 14:301–303, 1980.

[64] S. Mirmasoumi and A. Behzadmehr. Effect of nanoparticles mean diameter on mixed convection heat transfer of a nanofluids in a horizontal tube. *Int. J. Heat Fluid Flow.*, 29:557–566, 2008.

[65] A. A. Mohammadien and M. F. El-Amin. Thermal dispersion-radiation effects on non-Darcy natural convection in a fluid saturated porous medium. *Transp. Porous Med.*, 40:153–163, 2000.

[66] M. Molla, A. Hossain, and L. S. yao. Natural convection flow along a vertical complex wavy surface with uniform surface heat flux. *ASME J. Heat Transfer.*, 129:1403–1407, 2007.

[67] M. M. Molla and M. A. Hossain. Radiation effect on mixed convection laminar flow along a vertical wavy surface. *Int. J. Thermal Sci.*, 46:926–935, 2007.

[68] S. S. Motsa and S. Shateyi. Successive linearisation solution of free convection non-Darcy flow with heat and mass transfer. *Advanced topics in mass transfer.*, 19:425–438, 2006.

[69] S. S. Motsa and P. Sibanda. A new algorithm for solving singular IVPs of Lane-Emden type. *Proceedings of the* 4^{th} *International Conference on Applied Mathematics, Simulation and Modelling. NAUN International Conferences, Corfu Island, Greece.*

[70] S. G. Moulic and L. S. Yao. Mixed convection along a wavy surface. *ASME J. Heat Transfer.*, 111:974–979, 1989.

[71] P. V. S. N. Murthy, Ch. RamReddy, A. J. Chamkha, and A. M. Rashad. Magnetic effect on thermally stratified nanofluid saturated non-Darcy porous medium under convective boundary condition. *Int. Commun. Heat Mass Transfer.*, 47:41–48, 2013.

[72] P. V. S. N. Murthy, A. Sutradhar, and Ch. RamReddy. Double-diffusive free convection flow past an inclined plate embedded in a non-Darcy porous medium saturated with a nanofluid. *Transp. Porous Med.*, 98:553–564, 2013.

[73] M. Narayana, A. A. Khidir, P. Sibanda, and P. V. S. N. Murthy. Soret effect on the natural convection from a vertical plate in a thermally stratified porous medium saturated with a non-Newtonian liquid. *ASME J. Heat Transfer.*, 135:1–10, 2013.

[74] Maria Neagu. Free convective heat and mass transfer induced by a constant heat and mass fluxes vertical wavy wall in a non-Darcy double stratified porous medium. *Int. J. Heat Mass transfer.*, 54:2310–2318, 2011.

[75] D. A. Nield. Onset of thermohaline convection in a porous medium. *Water Resour. Res.*, 4:553–560, 1968.

[76] D. A. Nield and A. Bejan. *Convection in Porous Media, 4th Edition*. Springer-Verlag, New York, 2013.

[77] D. A. Nield and A. V. Kuznetsov. Thermal instability in a porous medium layer saturated by a nanofluid. *Int. J. Heat Mass Transfer.*, 52:5796–5801, 2009.

[78] D. A. Nield and A. V. Kuznetsov. The Cheng-Minkowycz problem for natural convective boundary-layer flow in a porous medium saturated by a nanofluid. *Int. J. Heat Mass Transfer.*, 52:5792–5795, 2009.

[79] D. A. Nield and A. V. Kuznetsov. The Cheng-Minkowycz problem for the double-diffusive natural convective boundary layer flow in a porous medium saturated by a nanofluid. *Int. J. Heat Mass Transfer.*, 54:374–378, 2011.

[80] M. Nitesh, V. Manoj, D. Santosh Kumar, and A. Satheesh. Numerical simulation of mixed convection in a porous medium filled with water/Al_2O_3 nanofluid. *Heat Transfer-Asian Research.*, 42:1–14, 2013.

[81] A. Noghrehabadi, A. Behseresht, and M. Ghalambaz. Natural convection of nanofluid over vertical plate embedded in porous medium: prescribed surface heat flux. *Appl. Math. Mech. -Engl. Ed.*, 34:669–686, 2013.

[82] H. F. Oztop and E. Abu-Nada. Numerical study of natural convection in partially heated rectangular enclosures filled with nanofluids. *Int. J. Heat Fluid Flow.*, 29:1326–1336, 2008.

[83] O. A. Plumb and J. C. Huenefeld. Non-Darcy natural convection from heated surfaces in saturated porous media. *Int. J. Heat Mass Transfer.*, 24:765–768, 1981.

[84] A. Rahman, M. M. Molla, and M. M. A. Sarker. Natural convection flow along the vertical wavy cone in case of uniform surface heat flux where viscosity is an exponential function of temperature. *Int. Comm. Heat Mass Transfer.*, 38:774–780, 2011.

[85] Ch. RamReddy, P. V. S. N. Murthy, A. M. Rashad, and A. J. Chamkha. Numerical study of thermally stratified nanofluid flow in a saturated non-Darcy porous medium. *Eur. Phys. J. Plus.*, 129:1–11, 2014.

[86] A. M. Rashad, S. Abbasbandy, and A. J. Chamkha. Mixed convection flow of a micropolar fluid over a continuously moving vertical surface immersed in a thermally and solutally stratified medium with chemical reaction. *J. Taiwan Inst. Chem. Eng.*, 45:2163–2169, 2014.

[87] A. M. Rashad, S. Abbasbandy, and A. J. Chamkha. Non-Darcy natural convection from a vertical cylinder embedded in a thermally stratified and nanofluid saturated porous media. *ASME J. Heat Transfer.*, 136:1–9, 2014.

[88] A. M. Rashad, A. J Chamkha, and Abdou M. M. M. Mixed convection from a vertical surface embedded in a porous medium saturated with a non-Newtonian nanofluid. *J. Appl. Fluid Mech.*, 6:301–309, 2013.

[89] D. A. S. Rees and I. Pop. Non-Darcy natural convection from a vertical wavy surface in a porous medium. *Transp. Porous Med.*, 20:223–234, 1995.

[90] A. M. Rohni, S. Ahmad, J. H. Merkin, and I. Pop. Mixed convection boundary layer flow along a vertical cylinder embedded in a porous medium filled by a nanofluid. *Transp. Porous Med.*, 96:237–253, 2013.

[91] A. V. Rosca, N. C. Rosca, T. Grosan, and I. Pop. Mixed convection boundary layer flow past a vertical flat plate embedded in a non-Darcy porous medium saturated by a nanofluid. *Int. J. Numerical Methods for Heat & Fluid Flow.*, 24:970–987, 2014.

[92] I. Rosca, N. C.and Pop. Mixed convection stagnation point flow past a vertical flat plate with a second order slip: Heat flux case. *Int. J. Heat Mass Transfer.*, 65:102–109, 2013.

[93] A. B. Rosmila, R. Kandasamy, and I. Muhaimin. Lie symmetry group transformation for MHD natural convection flow of nanofluid over linearly porous stretching sheet in presence of thermal stratification. *Appl. Math. Mech. -Engl. Ed.*, 33:593–604, 2012.

[94] A. B. Rosmila, R. Kandaswamy, and J. Muhaimin. Lie symmetry group transformation for MHD natural conetion flow of nanofluid over linearly porous stretching sheet in the presence of thermal stratification. *Appl. Math. Mech. -Engl. Ed.*, 33:593–694, 2012.

[95] N. Rudraiah and T. P. Sasikumar. Radiation and non-Darcy effects on convection in porous media. *Chem. Eng. Commun.*, 87:53–65, 1990.

[96] M. Salari, M. Mohammadtabar, and A. Mohammadtabar. Numerical solutions to heat transfer of nanofluid flow over stretching sheet subjected to variations of nanoparticle volume fraction and wall temperature. *Appl. Math. Mech. -Engl. Ed.*, 35:63–72, 2014.

[97] S. Shateyi and S. S Motsa. Variable viscosity on magnetohydrodynamic fluid flow and heat transfer over an unsteady stretching surface with hall effect. *Boundary Value Problems.*, 2010:20 pages, 2010.

[98] S. A. Shezad, A. Qasim, A. Alsaedi, T. Hayat, and M. S. Alhothuali. Combined thermal stratified and thermal radiation effects in mixed convection flow of a thixotropic fluid. *Eur. Phys. J. Plus.*, 128:1–10, 2013.

[99] S. Siddiqa, M. A. Hossain, and S. C. Saha. Natural convection flow with surface radiation along a vertical wavy surface. *Numerical Heat Transfer.*, 64:400–415, 2013.

[100] E. M. Sparrow and H. S. Yu. Local non-similarity thermal boundary-layer solutions. *ASME J. Heat Transfer.*, 93:328–332, 1971.

[101] D. Srinivasacharya and Ch. RamReddy. Natural convection heat and mass transfer in a micropolar fluid with thermal and mass stratification. *Int. J. Comp. Methods in Engg. Science and Mechanics.*, 14:401–413, 2013.

[102] D. Srinivasacharya and O. Surender. Mixed convection boundary layer flow of a nanofluid past a vertical plate in a doubly stratified porous medium. *J. Comp. Theor. Nanosci.*, 11:1853–1862, 2014.

[103] D. Srinivasacharya and O. Surender. Nonsimilar solution for natural convective boundary layer flow of a nanofluid past a vertical plate embedded in a doubly stratified porous medium. *Int. J. Heat Mass Transf.*, 71:431–438, 2014.

[104] B. Tashtoush and M. Al-Odat. Magnetic field effect on heat and fluid flow over a wavy surface with a variable heat flux. *J. Magnetism and Magnetic Materials.*, 268:357–363, 2004.

[105] K. Tewari and P. Singh. Natural convection in a thermally stratified porous medium. *Int. J. Eng. Sci.*, 30:1003–1007, 1992.

[106] R. K. Tiwari and M. K. Das. Heat transfer augmentation in a two-sided lid-driven differentially heated square cavity utilizing nanofluids. *Int. J. Heat Mass Transf.*, 50:2002–2018, 2007.

[107] L. N. Trefethen. *Spectral methods in MATLAB.* SIAM.

[108] V. Trisaksri and S. Wongwises. Critical review of heat transfer characteristics of nanofluids. *Renew. Sustain. Eng. Rev.*, 11:512–523, 2007.

[109] M. Turkyilmazoglu and I. Pop. Heat and mass transfer of unsteady natural convection flow of some nanofluids past a vertical infinite flat plate with radiation effect. *Int. J. Heat Mass Transfer.*, 59:167–171, 2013.

[110] K. Vafai. *Handbook of Porous Media (2nd ed.).* Taylor & Francis Group, New York, 2005.

[111] K. Vafai and H. Hadim. Overview of current computational studies of heat transfer in porous media and their applications-natural convection and mixed convection. *Advances in Numerical Heat Transfer, Taylor and Francis.*, 2:331–371, 2000.

[112] C.-C. Wang and C.o.-K. Chen. Mixed convection boundary layer flow on inclined wavy plates including the magnetic field effect. *Int. J. Thermal Sci.*, 44:577–586, 2005.

[113] X. Q. Wang and A. S. Mujumdar. Heat transfer characteristics of nanofluids: a review. *Int. J. Thermal Sci.*, 46:1–19, 2007.

[114] X. Q. Wang and A. S. Mujumdar. A review on nanofluids-part i: theoretical and numerical investigations. *Brazilian J. Chem. Eng.*, 25:613–630, 2008.

[115] X. Q. Wang and A. S. Mujumdar. A review on nanofluids-part ii: theoretical and numerical investigations. *Brazilian J. Chem. Eng.*, 25:631–648, 2008.

[116] D. Wen and Y. Ding. Effect of particle migration on heat in suspensions of nanoparticles flowing through minichannels. *Microfluid Nanofluid.*, 1:183–189, 2005.

[117] M. Yasin, M. Hafizi, N. M. Arifin, R. Nazar, F. Ismail, and I. Pop. Mixed convection boundary layer ow embedded in a thermally stratified porous medium saturated by a nanofluid. *Advances in Mechanical Engineering.*, 2013:8 pages, 2013.

[118] M. E. Yazdi, A. Moradi, and S. Dinarvand. MHD mixed convection stagnation point flow over a stretching vertical plate in porous medium filled with a nanofluid in the presence of thermal radiation. *Arab. J. Sci. Eng.*, 39:2251–2261, 2014.